

# Sedimentation on tidal marshes in the Scheldt estuary

A field and numerical modelling study

Stijn Temmerman

Proefschrift ingediend tot het  
behalen van de graad van  
Doctor in de Wetenschappen

K.U. Leuven - 2003



KATHOLIEKE UNIVERSITEIT LEUVEN  
FACULTEIT WETENSCHAPPEN  
DEPARTEMENT GEOGRAFIE-GEOLOGIE

**SEDIMENTATION ON TIDAL MARSHES  
IN THE SCHELDT ESTUARY:  
A FIELD AND NUMERICAL MODELLING STUDY**

**Stijn Temmerman**

Promotor: Prof. Dr. Gerard Govers  
Co-promotoren: Prof. Dr. Patrick Meire  
Prof. Dr. Stanislas Wartel

Proefschrift ingediend tot het behalen van de graad  
van Doctor in de Wetenschappen

Academiejaar 2003-2004

Dit proefschrift werd openbaar verdedigd op 10 november 2003 om 17.30u  
in het Auditorium van het Arenbergkasteel.

Leden van de Examencommissie:

Prof. Dr. G. Govers (promotor, Departement Geografie-Geologie, K.U.Leuven)  
Prof. Dr. S. Wartel (co-promotor, Dienst Sedimentologie, K.B.I.N.)  
Prof. Dr. P. Meire (co-promotor, Departement Biologie, Universiteit Antwerpen)  
Prof. Dr. J. Poesen (Departement Geografie-Geologie, K.U.Leuven)  
Prof. Dr. G. Verstraeten (Departement Geografie-Geologie, K.U.Leuven)  
Prof. Dr. A. Van Rompaey (Departement Geografie-Geologie, K.U.Leuven)  
Prof. Dr. E. Toorman (Departement Burgerlijke Bouwkunde, K.U.Leuven)  
Dr. T. Bouma (Departement Ruimtelijke Ecologie, Nederlands Instituut voor  
Ecologie – Centrum voor Estuariene en Mariene Ecologie)







ZOEK DE VIJF GELIJKENISSEN

## Dankwoord

Waarom maak je een doctoraat over de Schelde?

Die vraag werd mij de laatste vier jaar dikwijls gesteld. En ik geef toe, het is niet zo simpel om daar een pasklaar antwoord op te geven.

Ik laat me daarom even helpen door de foto's hiernaast. Ze tonen een stukje van mijn geschiedenis, van mezelf, van mijn ouders en grootouders. Wie goed kijkt, vindt één gemeenschappelijk punt op alle foto's: niet de Schelde (dat zou te gemakkelijk zijn) maar wel een boot (of toch een stukje daarvan). Boten en de Schelde zijn twee vaste elementen die mijn afkomst bepalen. Nu ja, zelf heb ik nooit gevaren, maar mijn doctoraat mag je best vergelijken met een boottocht, die werd voortgedreven door dezelfde inspiratiebron: het varen op de Schelde, het op verkenning gaan, ontdekken, onderzoeken – de onvoorspelbare natuur van de Schelde een beetje beter leren begrijpen.

Net als het getij op de Schelde, is het werken aan een doctoraat altijd een opeenvolging van hoogte- en laagtepunten. Soms is er de inspiratie, die plotse ingeving. Dan laat je je schip meevoeren op een stroomversnelling, en dat is zalig, het geeft je kriebels. Maar er zijn ook tegenslagen, obstakels, zoals verraderlijke zandbanken, of de wind die niet goed zit, of zeker in mijn geval: modder waarin je dreigt vast te komen zitten.

Op zo'n momenten komt het er op aan de raad van een ervaren kapitein te kunnen volgen. Dat mijn schip niet vroegtijdig op de klippen is gelopen, heb ik in de eerste plaats te danken aan mijn kapitein, Gerard Govers. Van hem heb ik de knepen van het scheepmansvak geleerd. Ik heb erg genoten van zijn positieve ingesteldheid, van zijn groeiend enthousiasme voor de schorren, en misschien heb ik nog het meest geleerd door het vertrouwen dat hij me gaf om zelf het roer in handen te nemen.

Daarnaast waren er ook nog mijn twee co-kapiteins, Patrick Meire en Stan Wartel, die mee hielpen de koers uit te stippelen. Beiden behoren ze tot de meest ervaren en gedreven Schelde-vaarders die ik ken. Het was voor mij dan ook een hele eer om deel te mogen uit maken van hun crew.

Om mijn schip veilig en wel op de bestemming te krijgen, waren heel wat baggerwerken (= veldwerk) nodig. Hierbij zorgden twee 'uitvindingen' voor een belangrijke doorbraak die het baggeren heel wat makkelijker maakten. Ten eerste was er de aanlegsteiger (= de meethut op de foto's bovenaan p. 23), waar ik mijn bagger-apparatuur hoog en droog kon opbergen als het water opkwam. Het maken van die aanlegsteiger was me nooit gelukt zonder de hulp en aanwijzingen van onze handige scheepstimmerman, Jos Meersmans. Ten tweede waren er de plastic deksels van mayonaise potten, die ik te danken heb aan Davy De Gendt. Die plastic deksels kon ik ombouwen tot handige 'sediment traps' (zie foto rechtsonderaan p. 23) en hebben mij ongelooflijk veel diensten bewezen.

En dan zijn er nog de talrijke collega-schippers en matrozen, die mij een handje hielpen bij het zwaardere baggerwerk: Patriek Bleys, Ludo Cleeren, Tom De Bruyn, Frederik Francken, Daniël Jochmans, Dirk Lauwaet, Jos Meersmans, Lieven Ost, Tom Rommens, Tonny Temmerman, Michiel Vanderschaeghe, Walter Van Hoyweghen, Kristof Van Oost en Gert Verstraeten – bedankt allemaal voor jullie moed om met mij in de modder te ploeteren en voor jullie gezellige babbels tijdens de vele en lange boottochten naar de Schelde.

Tenslotte wil ik, wat mijn baggerwerk betreft, alle conservators bedanken, die mij toelieten mijn anker uit te werpen op hun schorren: Maarten Hemminga (Stichting het Zeeuwse Landschap), René Beijersbergen (conservator Paulinaschor), Jos Neve (Verdronken Land van Saeftinge), Jean Cordaro (Galgenschoor), Hendrik D'Hertefelt (schorren van de Notelaar en Branst) en François D'Hollander (Groot Schoor van Grembergen).

Verder ben ik niet de enige die baggert in de Schelde. De schippers van het NIOO-CEME uit Yerseke kunnen er ook wat van. Het lag dan ook voor de hand om onze krachten en baggermolens te bundelen. Hierbij wil ik Tjeerd Bouma en zijn collega's van harte bedanken voor het gezamenlijke werk op het Paulinaschor (zelfs bij nacht en bij ontij).

Deze samenwerking was ook de aanleiding voor mij om een tijdje in Delft aan te meren aan de kaaien van WL | Delft Hydraulics. Zij zijn heel bedreven in het spelen van zeeslag op de computer (= modelleren), wat voor mij een uitgelezen kans was om ook op dit vlak bij te leren. Ik wil in het bijzonder de volgende zeeslag-spelers bedanken die mij inwijdden in de regels van het spel: Ilka Tanczos, Mindert De Vries, Zheng Bing Wang, Arjen Luijendijk, Maarten Van Ormondt, Andries Paarlberg en Linda Kusters. Verder dank ik Andries en Wandena voor de nodige ontspanning na een dagje zeeslag, en natuurlijk Sue en Richard, die ons ondermeer meenamen op een dagje roeien in Amsterdam en een avondje Delft-in-Moulin-Rouge-stijl.

Varen doe je natuurlijk niet zonder goed geïnformeerd te zijn over de ligging van de vaargeul, over het getij, enzovoort. Gelukkig kon ik hiervoor beroep doen op diverse loodsdiensten, die mij zeer bereidwillig hun gegevens ter beschikking stelden. De volgende mensen en diensten wil ik speciaal bedanken: Erika Van den Bergh (Instituut voor Natuurbehoud, Brussel), Eric Taverniers (AWZ, afdeling Maritieme Toegang, Antwerpen), Stefan Van Damme (Universiteit Antwerpen, onderzoeksgroep Ecosysteembeheer), Dick De Jong en Bram Schouwenaar (Rijkswaterstaat, RIKZ, Middelburg), Gertjan Zwolsman (Rijkswaterstaat, RIZA, Dordrecht), Fran Dyer (Southampton Oceanography Centre, UK), en Ruth Cox (NERC Centre for Ecology and Hydrology Monks Wood, Cambridgeshire, UK).

Natuurlijk vergeet ik niet alle collega-scheepsmakkers uit de thuishaven in de Redingenstraat. Zij zorgden mee voor de gepaste werksfeer en het dagelijkse vertellen van straffe zee-verhalen 'in dat kleine café aan de haven' (= koffielokaal): bedankt An, Andreas, Anke, Anne, Annemie, Anton, Armando, Birgit, Dirk, Erika, Gerard, Gert, Greet en Kristof (met wie ik de laatste jaren met veel plezier dezelfde kajuit heb gedeeld), Gwendolyn, Ingrid, Iris, Jan, Jean, Jeroenn, Jeroenr, Johan, Jona, Jorisd, Jorisk, Jos, Katleen, Kim Chi, Kirsten, Laurent, Larry, Lieven, Liesbeth, Mary, Maude, Michiel, Miranda, Miet, Monique, Olivier, Patriek, Rafaël, Pieter, Simon, Tomr, Tomv, Veerle en Wim (en nu hoop ik niemand te zijn vergeten natuurlijk).

Tenslotte zijn er alle mensen die mij van op de wal toejuichten als ik voorbij kwam varen. Ik bedank mijn ouders, schoonouders, (schoon)broers en -zussen, familie, vrienden, burens en kennissen voor al hun aanmoedigingen en kritische vragen ('Wat steekt gij daar allemaal uit langs de Schelde?'). Zij waren voor mij de wind in mijn zeilen.

En dan is er mijn beste scheepsmaatje: Anke, het is zalig dat ik al mijn scheepsavonturen met jou kan delen. Mijn Schelde-reis zit er nu bijna op, maar onze wereldreis is nog maar pas begonnen. Nu hebben we alle tijd om samen ons schip verder uit te bouwen en uit te kijken naar de komst van ons eerste matroosje!

Leuven, 26 oktober 2003.



## Table of contents

### **Chapter 1: Introduction**

1.1. Geomorphic processes in tidal marshes .....	1
1.2. The study area: the Scheldt estuary and its tidal marshes .....	2
1.3. Social and scientific context of the research topic .....	6
1.3.1. <i>Social context</i> .....	6
1.3.2. <i>Scientific context</i> .....	9
1.4. Objectives and structure of the thesis.....	11

### **Part I: SHORT-TERM SEDIMENTATION**

### **Chapter 2: Spatial and temporal factors controlling short-term sedimentation in a salt and freshwater tidal marsh**

2.1. Introduction .....	17
2.2. The study sites .....	19
2.3. Methodology .....	19
2.3.1. <i>Field sampling sites</i> .....	19
2.3.2. <i>Measuring sediment supply and deposition</i> .....	21
2.3.3. <i>Data assessment and analyses</i> .....	24
2.4. Results .....	24
2.4.1. <i>Exploratory data representation</i> .....	24
2.4.2. <i>Temporal patterns of sediment dynamics</i> .....	26
2.4.3. <i>Spatial sedimentation patterns</i> .....	28
2.4.4. <i>An integrated spatio-temporal model</i> .....	32
2.5. Discussion and conclusions.....	36

**Chapter 3: Spatial patterns of suspended sediment transport and deposition during single tidal cycles within a small tidal marsh creek catchment**

3.1. Introduction .....	41
3.2. Study area.....	43
3.3. Methods.....	44
3.3.1. <i>General setup of the field measurements</i> .....	44
3.3.2. <i>Measuring the spatial sedimentation pattern</i> .....	46
3.3.3. <i>Modelling the spatial sedimentation pattern</i> .....	46
3.3.4. <i>Hydrodynamic measurements</i> .....	47
3.3.5. <i>Measuring suspended sediment transport</i> .....	48
3.3.6. <i>Analysing water and sediment balances</i> .....	50
3.4. Results and discussion.....	53
3.4.1. <i>Spatial and temporal variations in sedimentation rates</i> .....	53
3.4.2. <i>Modelling the spatial sedimentation pattern</i> .....	53
3.4.3. <i>Tidal creek hydrodynamics</i> .....	57
3.4.4. <i>Suspended sediment concentrations</i> .....	62
3.4.5. <i>Flow paths of water and suspended sediment</i> .....	64
3.5. Conclusions .....	67

**Chapter 4: Simulating spatial patterns of sediment transport and deposition in tidal marshes using a hydrodynamic modelling approach**

4.1. Introduction .....	69
4.2. Materials and methods .....	71
4.2.1. <i>General overview of the Delft3D model</i> .....	71
4.2.2. <i>Construction of a computational grid for the study area</i> .....	73
4.2.3. <i>Specifying input values for the model variables</i> .....	75
4.2.4. <i>Model calibration and validation</i> .....	82
4.2.5. <i>Model sensitivity analysis</i> .....	83
4.2.6. <i>Analysing the simulated spatial sedimentation patterns</i> .....	84
4.3. Results .....	85
4.3.1. <i>Validation of the hydrodynamic model</i> .....	85
4.3.2. <i>Calibration and validation of the sedimentation model</i> .....	86
4.3.3. <i>Simulating spatial sedimentation patterns under different scenarios: a model sensitivity analysis</i> .....	92
4.4. Discussion .....	93
4.4.1. <i>Some remarks on the model simulations</i> .....	93
4.4.2. <i>The influence of vegetation</i> .....	97
4.4.3. <i>Complex hydrodynamic versus simple topography-based modelling</i> .....	98
4.5. Conclusions .....	99

**Part II: LONG-TERM ACCUMULATION**

**Chapter 5: Modelling long-term tidal marsh accumulation under changing tidal conditions and suspended sediment concentrations**

5.1. Introduction .....	103
5.2. The study area .....	105
5.3. Materials and methods .....	106
5.3.1. <i>Assessment of historical long-term morphodynamics</i> .....	106
5.3.2. <i>Measurement of actual sediment dynamics</i> .....	110
5.3.3. <i>Description of the numerical model</i> .....	110
5.4. Results .....	113
5.4.1. <i>Observed long-term morphodynamics</i> .....	113
5.4.2. <i>Short-term temporal variations in suspended sediment concentration</i> .....	116
5.4.3. <i>Model implementation using empirical input data</i> .....	118
5.4.4. <i>Model results and evaluation</i> .....	121
5.5. Discussion .....	123
5.6. Conclusions .....	126

**Chapter 6: Simulating the long-term development of levee-basin topography on tidal marshes**

6.1. Introduction .....	127
6.2. Study area .....	129
6.3. Methods .....	129
6.3.1. <i>The numerical model</i> .....	129
6.3.2. <i>Model calibration</i> .....	132
6.3.3. <i>Model implementation</i> .....	135
6.4. Results .....	137
6.4.1. <i>Model calibration</i> .....	137
6.4.2. <i>Model validation</i> .....	139
6.4.3. <i>Factors influencing the long-term evolution of levees and basins</i> .....	142
6.5. Discussion .....	146
6.6. Conclusions .....	147

**Chapter 7: Long-term tidal marsh accumulation along the estuarine gradient of the Scheldt estuary: evidence from field data and numerical modelling**

7.1. Introduction .....	149
7.2. Study area.....	151
7.3. Methods.....	154
7.3.1. <i>Estimating long-term tidal marsh accumulation</i> .....	154
7.3.2. <i>Modelling long-term tidal marsh accumulation</i> .....	159
7.4. Results .....	166
7.4.1. <i>Long-term tidal marsh accumulation</i> .....	166
7.4.2. <i>Implementation and validation of the model</i> .....	169
7.5. Discussion .....	173
7.5.1. <i>Factors controlling estuarine variations in marsh accumulation</i> .....	173
7.5.2. <i>Model performance</i> .....	176
7.5.3. <i>Marsh accumulation in response to MHWL rise and incoming SSC</i> .....	177
7.6. Conclusions .....	180

**Chapter 8: General discussion and conclusions**

8.1. Short-term sedimentation patterns.....	182
8.1.1. <i>Temporal patterns</i> .....	183
8.1.2. <i>Spatial patterns</i> .....	184
8.1.3. <i>Spatial modelling</i> .....	184
8.2. Long-term tidal marsh accumulation.....	186
8.2.1. <i>Young versus old marsh surfaces</i> .....	187
8.2.2. <i>Levees versus basins</i> .....	188
8.2.3. <i>Large-scale estuarine variability</i> .....	188
8.3. Possible applications and prospects for further research.....	190

References .....	193
------------------	-----

List of symbols and abbreviations.....	205
--	-----

List of publications.....	209
---------------------------	-----

Nederlandse samenvatting.....	211
-------------------------------	-----

### **1.1. Geomorphic processes in tidal marshes**

Tidal marshes are found in temperate and high latitudes along coasts and estuaries where tidal action is significant but wave action is rather limited. Their origin is intrinsically linked to the cyclic tidal movement of the water level on oceans and seas, which act on a number of time-scales, such as semi-diurnal tidal cycles and bi-weekly spring-neap tidal cycles (Fig. 1.1). Tidal marshes are typically located high in the intertidal zone between low and high water level. As a consequence of this high elevation, they are only flooded by the highest high water levels occurring around spring tide and they are typically overgrown by specific marsh plants that can stand a certain amount of tidal inundation (Fig. 1.1). At their seaward edge, tidal marshes are generally bordered by tidal flats, which have a lower elevation and which are in principle flooded by every tidal cycle, so that no vegetation can grow on these tidal flats (Fig. 1.1).

The geomorphology of tidal marshes is characterised by a rather flat vegetated marsh surface, called the marsh platform, which is dissected by branched networks of tidal creeks that narrow and shallow inland (Fig. 1.1).

The micro-topography of marsh platforms is further characterised by the presence of higher natural levees, along the tidal creeks, and lower inner basins, at a farther distance from the creeks. The edge between the marsh and the adjacent lower lying tidal flat appears either as a gradual slope or a distinct cliff (Fig. 1.1).

As the marsh is flooded during spring tides, fine-grained suspended sediments are transported with the flooding water over the vegetated marsh platform and are partly deposited on the marsh surface. In the long-term, this sediment accumulation leads to the vertical rise of marsh platforms (e.g., Allen, 1990; French, 1993). On their turn, these elevation changes will be highly determinant for the ecological processes in tidal marshes, such as the succession of marsh plants that can stand a quite large degree of tidal inundation to tidal marsh species that are adapted to a lower degree of inundation (e.g., Leendertse *et al.*, 1997; Olf *et al.*, 1997).

In addition to these vertical elevation changes, there is also a lateral dimension of geomorphic changes in tidal marshes. On the one hand, lateral erosion of the seaward marsh edge due to tidal currents and/or wave action can result in a decrease in marsh surface area and the formation of a cliff at the marsh edge (e.g., Van Eerd, 1985; Allen, 1989; Schwimmer, 2001). On the other hand, tidal marshes can also increase in area by lateral extension of tidal marsh vegetation over adjacent bare tidal flats. Finally, the tidal creeks system within tidal marshes can change in plan, due to lateral movement of creeks, elongation and extension of the creek system or, vice versa, the silting up and reduction of the creek system. However, these processes are rather slow in tidal marshes and only effect a very small proportion of the total marsh surface area (e.g., Gabet, 1998).

This thesis deals with the first morphodynamic aspect of tidal marshes, the sedimentation and elevation change of vegetated tidal marsh platforms.

## **1.2. The study area: the Scheldt estuary and its tidal marshes**

The Scheldt estuary is situated in the southwest of the Netherlands and the northwest of Belgium (Fig. 1.2). The Dutch and Belgian parts of the Scheldt estuary are called the Western Scheldt and the Sea Scheldt, respectively. The Scheldt estuary is defined as that part of the Scheldt river that is influenced by the tide, entering the river mouth in the southern North Sea and reaching 160 km inland up to Ghent (e.g., Meire *et al.*, 1992; Baeyens *et al.*, 1998; Van Damme *et al.*, 2001). Also some tributary rivers are influenced by the tide and, in principle, need to be considered as part of the Scheldt estuary: the rivers Rupel, Grote Nete (up to Itegem), Kleine Nete (up to Grobbendonk), Dijle (up to Werchter), Zenne (up to Zemst) and Durme (up to Lokeren)

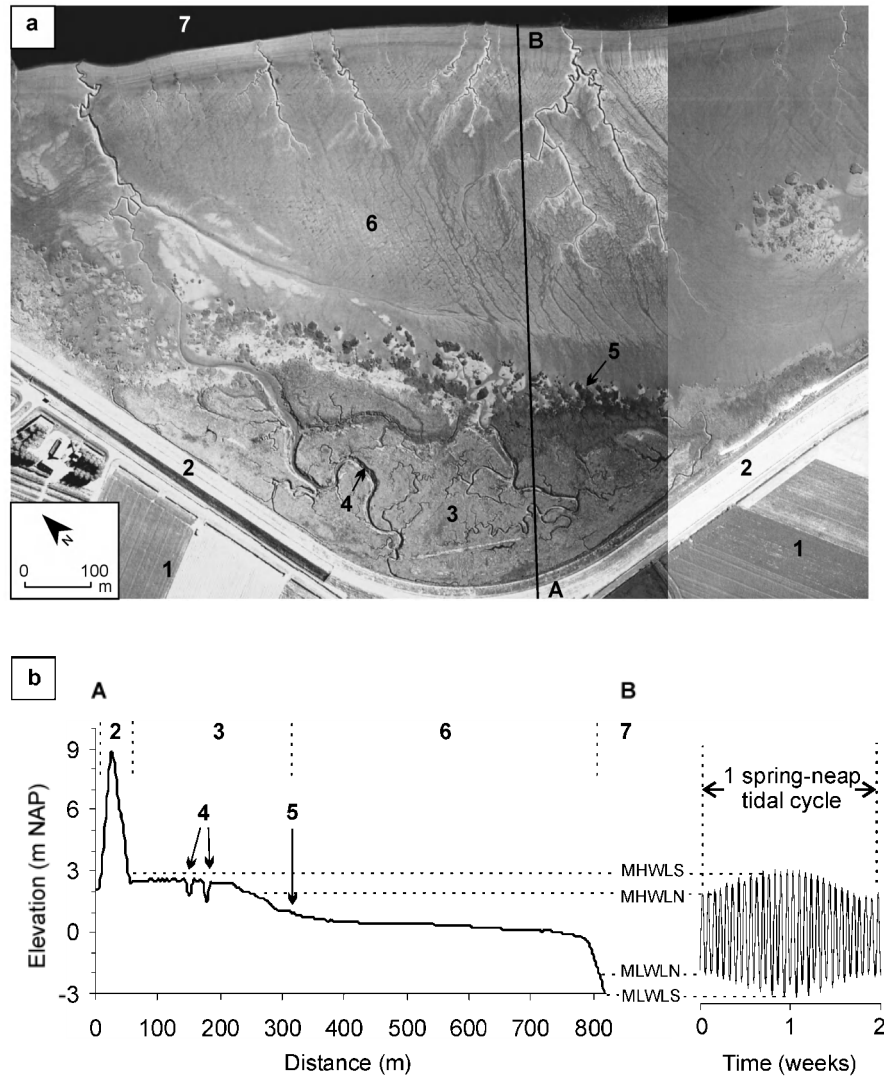


FIGURE 1.1. (a) Aerial photograph and (b) topographic cross-section of a typical tidal marsh and tidal flat environment (Paulina marsh, Western Scheldt), with indication of (1) the polder (historically embanked tidal marsh and tidal flat); (2) the present-day embankment; (3) the vegetated tidal marsh platform; (4) tidal creeks dissecting the marsh platform; (5) the marsh edge; (6) the unvegetated tidal flat; (7) the subtidal stream channel. The topographic cross-section shows the elevation (in m NAP = Nieuw Amsterdams Peil = relative to mean sea level) of the intertidal zone relative to local mean high water level at spring tides (MHWLS) and neap tides (MHWLN) and local mean low water level at spring tides (MLWLS) and neap tides (MLWLN). The aerial photographs and elevation data were placed at our disposal by Rijkswaterstaat Meetkundige Dienst.

(Claessens, 1988). Below, we describe some characteristics of the Scheldt estuary that are relevant to the dynamics of tidal marshes in the estuary.

The Scheldt estuary is characterised by a semidiurnal, meso- to macrotidal regime. The mean tidal range at the mouth in the southern North Sea ranges between 4.46 and 2.97 m during spring and neap tides, respectively (Claessens and Meyvis, 1994). As the tide enters the estuary, the tidal wave is pushed up and the mean tidal ranges increase up to 5.93 m and 4.49 m at Schelle during spring and neap tides, respectively. Further inland the tidal energy again decreases due to friction losses and the tidal ranges decrease to 2.24 m and 1.84 m near Ghent. However, strong north-westerly winds can create storm surges with resulting high water levels 2 to 3 m higher than the mean high water level (Claessens and Meyvis, 1994). The freshwater discharge of the Scheldt catchment varies between  $50 \text{ m}^3 \text{ s}^{-1}$  during dry summer and  $300 \text{ m}^3 \text{ s}^{-1}$  during wet winter months (Taverniers, 2000). Its influence on water levels is, however, only significant at the inland border of the estuary and decreases rapidly seaward. Wave action due to wind is expected to decrease landward from the mouth, as a consequence of declining fetch distances along the estuary.

The suspended sediment in the Scheldt estuary mainly consists of fine sand, silt and clay, with concentrations typically showing large spatial and temporal variations, both longitudinally along the estuary and vertically within the water column (Wartel, 1973; 1977; Wartel and Van Eck, 2000). The time-averaged suspended sediment concentration (SSC) in the upper part of the water column (which floods the tidal marshes) varies along the estuary from 30-60 mg/l between the mouth and the Dutch-Belgian border up to 100-200 mg/l between the border and Temse (e.g., Van Eck *et al.*, 1991; Van Damme *et al.*, 2001). Further upstream the suspended sediment concentrations again decrease to 50-100 mg/l (Van Damme *et al.*, 2001). Large temporal variations in SSC however occur, depending on semidiurnal, spring-neap and seasonal variations in tidal range and fresh water discharge (e.g., Fettweis *et al.*, 1998; Francken and Wartel, 2001). The origin of suspended sediments in the Scheldt estuary is partly marine and partly riverine, with a time-averaged equilibrium point near the Dutch-Belgian border (e.g., Swart, 1987; Wartel and Chen, 1998).

The morphology of the Scheldt estuary can be classified into a series of typical estuarine geomorphic units. The morphology of the Western Scheldt is characterised by multiple stream channels (flood and ebb channels) separated by tidal sand and mud flats (Fig. 1.2). In the Sea Scheldt, on the contrary, only one stream channel exists. In both zones tidal flats and marshes border the stream channel. Due to intensive embankment since medieval times, the present-day active tidal marshes are rather small and cover only 10 % of the total present-day estuarine area. Besides some smaller marshes along the Durme river, almost all tidal marshes in the Scheldt estuary can be found along the Scheldt river (Fig. 1.2). In all, 3011 ha of tidal

marshes exist along the estuary, of which 2230 ha are located in the Saeftinghe marsh, the largest marsh area within the estuary (Van Damme *et al.*, 1999).

The tidal marshes of the Scheldt estuary can be grouped into three types, according to the salinity gradient that exists along the estuary (Fig. 1.2): salt marshes in the most seaward part of the estuary, with typical halophytic plant species, brackish marshes in the middle part, with partially halophytic/helophytic plant species, and freshwater tidal marshes in the upper reaches of the estuary, which are only covered with helophytes (Fig. 1.3) (e.g., Meire *et al.*, 1992; Van den Bergh *et al.*, 2001). Between these marsh types there is a remarkable difference in vegetation height, which ranges from maximum 0.4-0.8 m on the salt marshes up to 3 m and higher on the freshwater tidal marshes.

Further relevant characteristics of particular tidal marsh sites that are studied in this thesis are described in the sections ‘Study area’ of each chapter.

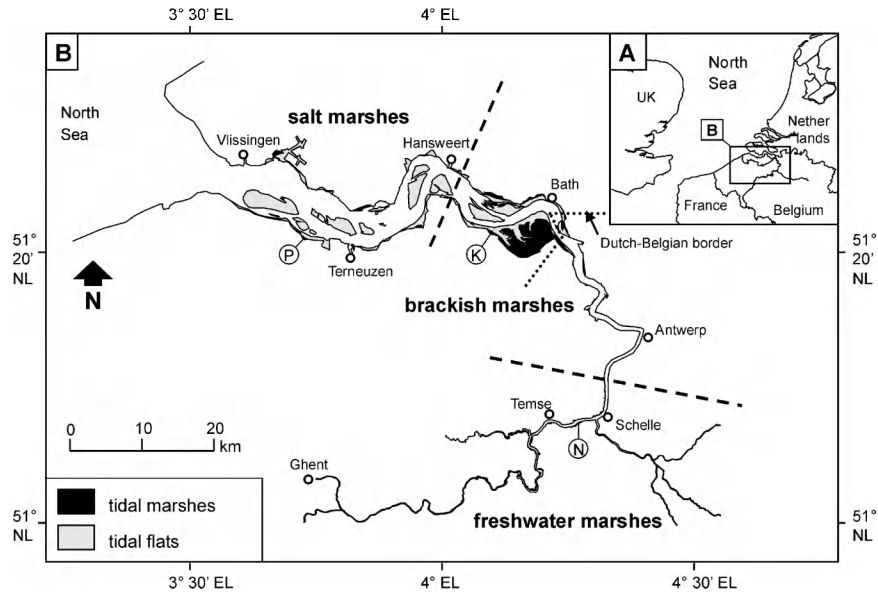


FIGURE 1.2. The Scheldt estuary: (A) location within Western Europe; (B) location of salt, brackish and freshwater tidal marshes (areas separated by heavy dashed lines). Tidal marsh sites that were used for detailed field measurements are indicated with letters: P = Paulina marsh; K = Kruispolder marsh; N = Notelaar marsh.

### 1.3. Social and scientific context of the research topic

#### 1.3.1. Social context

Tidal marshes are world-widely recognised as valuable habitats for plants and animals, such as unique salt marsh plant species and large populations of water and wading birds. Furthermore, they play an important role as sinks and/or sources for suspended sediments, pollutants and nutrients from and to the adjacent marine or estuarine ecosystem (e.g., Allen and Pye, 1992). This recognition has led to the protection of tidal marshes by several international and national regulations for the conservation of biodiversity and ecosystems, such as the international Ramsar Convention on Wetlands (<http://www.ramsar.org>), the European Community Birds Directive and Habitats Directive (<http://www.ecnc.nl>). Connected to this ecological value, tidal marshes have an economic value as breeding grounds for fish, shellfish and crustaceans. More recently, tidal marshes are increasingly recognised for their protective value against marine or estuarine flooding, by storing water and damping waves and flows during periods of extreme high water levels associated with storm surges (e.g., Möller *et al.*, 1999; 2001).

The ecological and socio-economic functions of tidal marshes sketched above are considerably affected by the deposition of suspended sediments and the resulting changes in marsh surface elevation. First, these elevation changes will cause changes in the frequency, height and duration with which tidal marshes are flooded by the tide. These changes in tidal inundation regime are determinant for changes in the ecological functioning of tidal marshes, such as the succession of vegetation and habitat change for animals. Secondly, sediment accumulation reduces the water storage capacity of tidal marshes and therefore reduces their role as inundation areas, which can protect the occupied land from flooding.

However, changes in the ecological and sea-defence value of tidal marshes will be ultimately the result of the delicate balance between the rates of sediment accumulation and the current and future rates of sea-level rise (Reed, 1995). In some places, accumulation rates were shown to be in excess of the local rate of sea-level rise, while in other places, tidal marshes were reported to be unable to accumulate with the rising sea-level, resulting in submergence and loss of large areas of tidal marsh (e.g., Baumann *et al.*, 1984; Walker *et al.*, 1987). In this respect, the question whether coastal ecosystems, such as tidal marshes, will be able to survive under future accelerated sea-level rise, is currently a major issue. Several nationally and internationally funded research programs, such as the 6<sup>th</sup> Framework Program of the European Community, emphasize on this growing demand of scientific knowledge on the impact of global climate change and sea-level rise on coastal ecosystems such as tidal marshes.



*FIGURE 1.3. (to be continued)*



FIGURE 1.3. Photographic views on (a) a salt marsh, (b) a brackish marsh, (c) a freshwater *Salix* (willow) marsh, and (d) a freshwater *Phragmites australis* (reed) marsh.

In order to maintain and enhance the ecological and sea-defence value of tidal marshes, management and restoration projects are widespread in North America and Europe. Such projects include the artificial raising or lowering of tidal marshes, the restoration of the tidal regime in formerly embanked marshes by constructing culverts or sluices through the embankment, or by complete removal of the embankment so that the embanked land becomes again part of the estuarine or coastal ecosystem (e.g., Pye and French, 1993; Pethick, 2002).

Specifically for the Scheldt estuary, the interactions between the estuarine ecosystem and human activities such as land reclamation, industrial and harbour development, and shipping are very high. Recently, the Dutch and Belgian authorities corroborated a joint long-term vision on the sustainable management of the Scheldt estuary, in which they want to maintain three main functions of the estuary (Zanting and Ten Thij, 2001): (1) the ecological function; (2) the function as safe residential and working area, protected from flooding; and (3) the function as important shipping way to the harbour of Antwerp. Within this scope, the management of the tidal marshes in the Scheldt estuary is focussed, on the one hand, on the conservation of the present-day tidal marshes. On the other hand, measures are also taken to restore or create new marsh areas. A specific example of such measures is the digging off and lowering of marshes that were formerly raised by dumping of dredged material or rubbish (e.g., Ketenissepolder, *ca.* 30 ha). Other projects include the creation of marshes through the introduction of a controlled reduced tide by use of sluices in polder areas that were selected as controlled inundation areas for flood protection (e.g., the Lippensbroek, *ca.* 8 ha; the polders of Kruikeke-Bazel-Rupelmonde, *ca.* 300 ha) (e.g., Meire *et al.*, 1997; Van den Bergh *et al.*, 1999). It is clear that such projects will result in sediment deposition and elevation changes, which on their turn will strongly determine the long-term sustainability of the restored or created marsh ecosystem. Since the present knowledge is rather limited, there is a high demand for scientific research on the sedimentation and elevation change in tidal marshes along the Scheldt estuary.

### *1.3.2. Scientific context*

During the last decades, quite a lot of research has been carried out on the morphodynamics of tidal marshes (see Allen (2000) for a recent extensive review). Numerous field studies aimed at the quantification of sedimentation rates in tidal marshes, on time scales ranging from individual tidal cycles (e.g., Reed, 1989; French *et al.*, 1995; Leonard, 1997) up to the last  $10^2$ - $10^3$  years (e.g., Armentano and Woodwell, 1975; Allen and Rae, 1988; Oenema and DeLaune, 1988; Cundy and Croudace, 1996; Shaw and Ceman, 1999). Such studies reported highly varying rates of tidal marsh accumulation, ranging from less than one up to several tens of  $\text{mm a}^{-1}$ . Much attention has

been paid to the comparison of the measured accumulation rates with local rates of mean sea-level rise, in order to evaluate the ability of the studied marshes to keep up with the rising sea-level (e.g., Roman *et al.*, 1997; Day *et al.*, 1999).

Fewer studies focussed on process-based research, in order to get insight in the mechanisms that control temporal and spatial variations in tidal marsh sedimentation. In this respect, it is important to distinguish between the spatial and temporal scales at which processes were studied. On the short term (single semi-diurnal tidal cycles up to a year), most attention was paid to the influence of the tidal inundation regime (e.g., Allen and Duffy, 1998a; Christiansen *et al.*, 2000) and wind-wave regime (e.g., Reed, 1989; Leonard *et al.*, 1995a) on temporal variations in tidal marsh sedimentation, while spatial variations in sedimentation rates within marshes are generally related to the marsh surface topography (e.g., Stoddart *et al.*, 1989; French and Spencer, 1993; Cahoon and Reed, 1995; French *et al.*, 1995; Leonard, 1997; Reed *et al.*, 1999). In long-term studies (10-10<sup>3</sup> years), spatial variations within marshes are generally neglected and instead a point-based approach is used. Most attention has been paid to the influence of sea-level rise and vertical marsh accumulation relative to the tidal frame (e.g., Pethick, 1981; Allen and Rae, 1988; Allen, 1990).

Relatively little work was done on the quantitative prediction and simulation of spatial and temporal sedimentation patterns in tidal marshes. Existing numerical simulation models for tidal marsh sedimentation, either physically-based or empirical, are all 0-dimensional time-stepping models, predicting the vertical rise of a marsh surface with time at one point in space (Krone, 1987; Allen, 1990; French, 1993; Allen, 1995; Callaway *et al.*, 1996; Allen, 1997; Day *et al.*, 1999; Van Wijnen and Bakker, 2001; Pont *et al.*, 2002; Rybczyk and Cahoon, 2002). These models were especially developed and applied to gain more insight in the long-term (10-10<sup>3</sup> years) response of tidal marshes to different scenarios of sea-level rise. However, as indicated by Allen (2000) in his extensive review article, “the models so far reported are at a rudimentary stage of development, chiefly because of a weak understanding of many components of the salt marsh environment”. Although we may say that these model approaches are qualitatively valid, until now very little attention was paid to the *quantitative* validation of model predictions against observed rates of tidal marsh sedimentation. Furthermore, 2-dimensional model studies that account for the spatial variations in sedimentation rates observed within tidal marshes are completely lacking up to now. However, in the framework of the management and restoration of tidal marshes, it is of fundamental importance to have a profound knowledge on tidal marsh morphodynamics and to have the disposal of extensively validated predictive models.

#### 1.4. Objectives and structure of the thesis

The general aim of this thesis is to gain insight in the mechanisms of tidal marsh sedimentation, using a combined field and numerical modelling approach on a number of spatial and temporal scales. As a study area the Scheldt estuary was chosen. The overall aim can be specified into the following objectives:

1. The collection of field data on spatial and temporal variations in tidal marsh sedimentation rates and elevation changes, and on the factors controlling these variations. In this respect, different temporal and spatial scales will be considered: (a) short-term ( $< 1$  year) and long-term ( $10\text{-}10^2$  years) variations; and (b) small-scale (within marshes) and large-scale (between marshes scattered along the whole estuary) variations.
2. The development and implementation of numerical models to simulate tidal marsh sedimentation and elevation changes in response to changes in the controlling factors. Also here, different model approaches will be chosen depending on the temporal and spatial scales that are considered. Especially much attention will be paid to the calibration and validation of the simulation models against the field data collected according to the previous objective.

The structure of the thesis is conceived as a compilation of scientific papers. Each paper is presented as one chapter within this thesis and, in principle, could be read individually. However, the different chapters are clearly linked to each other and special attention is given to the logical order of the chapters throughout the thesis.

Figure 1.4 shows a schematic overview of the structure of the thesis and the order of the chapters with respect to the different temporal and spatial scales that are considered. The chapters are grouped into two parts. Part I handles about the study of short-term sedimentation ( $< 1$  year), while Part II focuses on the long-term accumulation ( $10\text{-}10^2$  years).

Chapter 2 presents the results of a 1-year long field measuring campaign that was carried out to investigate the spatial and temporal factors controlling short-term sedimentation in a salt and freshwater tidal marsh in the Scheldt estuary. Special attention is given in this chapter to the identification of temporal variations in sedimentation rates on spring-neap and seasonal time-scales. In addition, spatial variations in sedimentation rates within the studied marshes could be characterised. These insights could be used to develop a first empirical topography-based model that can explain both the spatial and temporal variations in short-term sedimentation on the studied marshes.

In Chapter 3, we further focus on the detailed spatial sedimentation pattern. This chapter presents the results of an intensive field measuring campaign on the transport of suspended sediment to and the detailed spatial pattern of sediment deposition within a small tidal marsh creek catchment during single

tidal cycles. These field data allowed the further validation of the topography-based model presented in Chapter 2. Furthermore, the analysis of these field data provided insights in the role of the tidal creeks system in transporting water and sediments to and from the surrounding marsh platform.

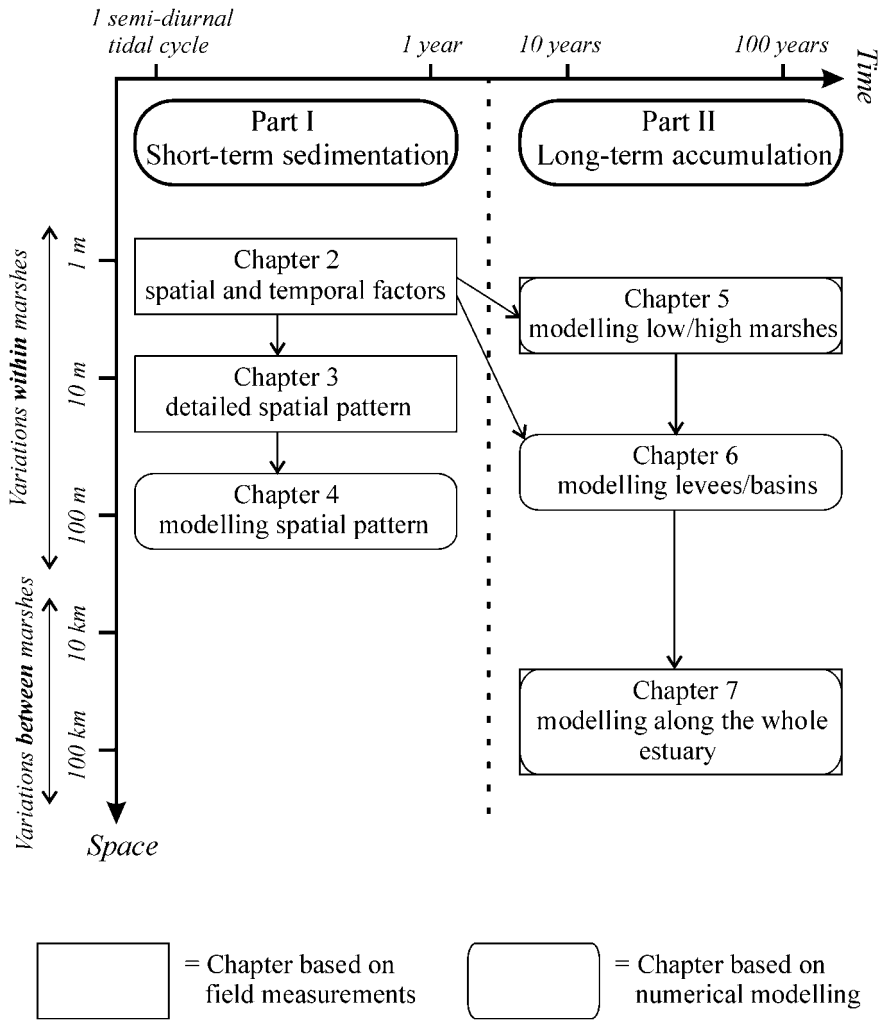


FIGURE 1.4. Schematic overview of the structure of the thesis.

In Chapter 4, the possibility is evaluated to simulate the 2-dimensional short-term sedimentation patterns on tidal marshes using a physically-based hydrodynamic and sediment transport model. An existing model (Delft3D) is implemented to the tidal creek catchment studied in Chapter 3 and the field data collected in this chapter are used to calibrate and validate the model. The model is further used to simulate spatial sedimentation patterns in response to changes in model variables that are generally thought to control tidal marsh sedimentation.

Part II of this thesis, on the long-term accumulation of tidal marshes, starts with Chapter 5. In this chapter, we develop a 0-dimensional time-stepping model to simulate the long-term vertical rise of tidal marsh surfaces. The model is based on former physically-based model approaches existing in the literature, but is innovative in terms of the modelling of suspended sediment supply to tidal marsh surfaces. The short-term field measurements performed in Chapter 2 are used to specify the model variables. In Chapter 5 field data on long-term accumulation rates are collected for a low and high marsh surface and are used to evaluate the model simulations. It is shown that the proposed model formulations to simulate the suspended sediment supply are crucial to obtain good model results.

In Chapter 6, the same model is used to simulate the long-term effects of spatial variations in sedimentation rates within marshes, by using spatially distributed values for the model input variables. The model is calibrated using the data on short-term sedimentation rates collected in Chapter 2. Next, it is evaluated whether the model is able to simulate the typical levee-basin topography within tidal marshes. Additional model runs are performed to simulate the impact of different scenarios of changing sea-level and incoming sediment concentrations on the topographic gradients within tidal marshes.

In Chapter 7, the variation in long-term accumulation rates is studied on the scale of the whole estuary. Field data on long-term tidal marsh accumulation are collected for a large number of marsh sites along the estuarine gradients in mean high water level rise and suspended sediment concentrations that exist along the Scheldt estuary. These data were used to validate the ability of the model, presented in the previous two chapters, to simulate this large-scale estuarine variability in tidal marsh accumulation. The response of the tidal marshes in the Scheldt estuary to potential future changes in mean high water level and in suspended sediment concentrations is evaluated using the simulation model.

Finally, general conclusions and some prospects for further research are presented in Chapter 8.



Part I

## SHORT-TERM SEDIMENTATION

---



## Chapter 2

### Spatial and temporal factors controlling short-term sedimentation in a salt and freshwater tidal marsh \*

---

#### 2.1. Introduction

Within the estuarine and coastal environment, tidal marshes play an important role as essential habitats for plants and animals and as sinks and/or sources for nutrients, pollutants and sediments (Allen, 2000). These functions of tidal marshes are strongly affected by sedimentation and changes in marsh surface elevation, whether this is in balance with relative sea level rise or not. Much attention has been paid to the quantification of sedimentation rates on tidal marshes, and especially to the question as to whether or not marsh sedimentation will be able to keep up with sea level rise. A wide range of measuring techniques have been used to quantify marsh sedimentation rates, over time-scales from one single tidal cycle up to several hundreds of years, including sediment traps (e.g., Allen and Duffy, 1998b; French *et al.*, 1995; Leonard, 1997; Reed, 1989), artificial or natural marker

---

\* Based on: Temmerman, S., Govers, G., Wartel, S. and Meire, P., 2003. Spatial and temporal factors controlling short-term sedimentation in a salt and freshwater tidal marsh, Scheldt estuary, Belgium, SW Netherlands. *Earth Surface Processes and Landforms*, 28(7): 739-755.

horizons (e.g., French and Spencer, 1993; Roman *et al.*, 1997), sedimentation-erosion tables (e.g., Cahoon *et al.*, 2000b), and dating of sediment cores using paleo-environmental, radiometric or geochemical techniques (e.g., Cundy and Croudace, 1996; Roman *et al.*, 1997).

Only a few studies have addressed both spatial and temporal variations in contemporary marsh sedimentation and the physical processes controlling these variations, although such studies are extremely important to understand the basic mechanisms of tidal marsh sedimentation. Furthermore, sedimentation processes were mainly studied on salt marshes. Studies on freshwater tidal marshes are very sparse and especially carried out in US marshes (e.g., Neubauer *et al.*, 2002; Orson *et al.*, 1990; Pasternack and Brush, 2001), while data from NW European freshwater tidal marshes are lacking. Some studies on salt marshes reported that temporal variations in sedimentation rates are mainly controlled by tidal inundation height (Allen and Duffy, 1998a; Christiansen *et al.*, 2000). Others indicated that wind-wave activity is the dominant controlling factor, leading in some cases to reduced sedimentation or even erosion (Pethick, 1992; Van Proosdij *et al.*, 2000), but in other places to increased sediment inputs and consequently higher sedimentation rates (Leonard *et al.*, 1995a; Reed, 1989). In addition also seasonal patterns are reported and these are often attributed to variations in biological activity (Hutchinson *et al.*, 1995; Leonard, 1997; Leonard *et al.*, 1995a; Pasternack and Brush, 2001). Spatial sedimentation patterns seem to be related to several parameters like marsh surface elevation (e.g. Cahoon and Reed, 1995; Stoddart *et al.*, 1989), the tidal creek network (e.g. French and Spencer, 1993; French *et al.*, 1995; Leonard, 1997; Reed *et al.*, 1999), and differences in vegetation structure (Leonard *et al.*, 1995a; Leonard, 1997; Boorman *et al.*, 1998). However, the relative importance and interactions between the different variables thought to control temporal and spatial variations in marsh sedimentation rates are poorly understood. As a consequence, these overall spatial and temporal variations are difficult to predict.

This paper presents a detailed study on the spatial and temporal sedimentation patterns in two contrasting marsh types within the Scheldt estuary, a salt and freshwater tidal marsh. First, field measurements are carried out to identify the relative importance of the various factors controlling spatial and temporal variations in sedimentation rates. Secondly, it was investigated to what extent both spatial and temporal variations can be correctly predicted using a relatively simple, topography-based model that integrates the effects of the different controlling variables. Finally, special attention is given to whether sedimentation patterns are different within the studied salt and freshwater marsh.

## 2.2. The study sites

Along the Scheldt estuary, large-scale estuarine gradients in tidal regime, suspended sediment regime and salinity exist (see chapter 1 paragraph 1.2). Along these estuarine gradients, two contrasting study areas were chosen: (1) the Paulina marsh, a salt marsh near the mouth where average suspended sediment concentration (SSC; *ca.* 50 mg/l near the water surface) and mean tidal range (3.9 m) are lowest; (2) the Notelaar marsh, a freshwater tidal marsh near Temse with highest average SSC (100-200 mg/l) and tidal range (5.3 m). The location of the study sites along the Scheldt estuary is shown on Figure 1.2 in chapter 1. Both study sites are similar in surface area and geomorphology, typically consisting of a vegetated marsh platform, dissected by networks of tidal creeks that narrow and shallow inland. The most visible contrasting element is the marsh vegetation. The Paulina marsh is overgrown with typical NW European salt marsh species, such as *Puccinellia maritima*, *Aster tripolium* and *Halimione portulacoides* in high interior marsh basins and mainly *Elymus pycnanthus* on the natural levees. In front of the high Paulina marsh, also a lower marsh exists which is typically dominated by *Spartina anglica* (Fig. 2.1b) (Houtekamer, 1996). On the contrary, the Notelaar marsh has a typical freshwater marsh canopy, with a community of *Phragmites australis* in the lower parts of the marsh and a community of *Salix* sp. in the higher parts (Fig. 2.1a) (Hoffmann, 1993).

## 2.3. Methodology

### 2.3.1. Field sampling sites

In order to study the impact of spatial factors on the sedimentation pattern, permanent sampling sites were established along a series of transects covering the main geomorphic units and vegetation types on the salt and freshwater marsh (Fig. 2.1 and Table 2.1). Three transects were chosen perpendicular to 3 similar first order marsh creeks, containing one measuring site on the natural levee, bordering the creek, and two sites in the lower inner marsh basin, at a distance of 20 and 40 m from the creek. One transect was established in a typical high salt marsh canopy (sites 10, 11, 12), and two transects in the two dominating freshwater vegetation types, *Phragmites australis* (sites 1, 2, 3) and *Salix* (sites 7, 8, 9). Another two transects were established over the whole width of the marsh perpendicular to the marsh edge, both on the salt marsh (sites 13 to 17) and freshwater marsh (sites 4 to 6). On the salt marsh this transect contains sampling sites on the high marsh as well as on the lower *Spartina* marsh. All transects were surveyed relative to Belgian Ordnance Level (TAW, which is approximately 2.3 m below

mean sea level at the Belgian coast), using an electronic total station (Sokkia SET5F). The sites were further described for their vegetative characteristics (plant species and, where possible, stem density and height) and grain size characteristics of surface sediments, sampled with metal rings (0.05 m in diameter and height) and analysed following the standard sieve-pipette method (Table 2.1).

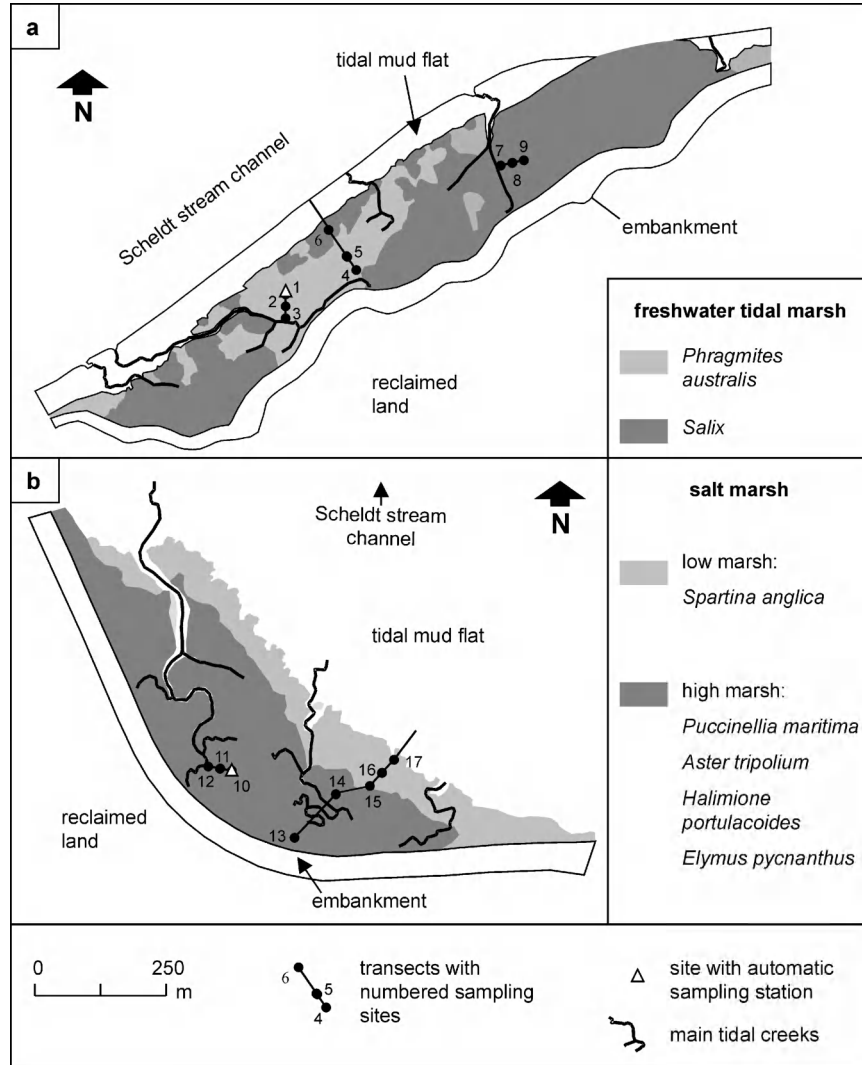


FIGURE 2.1. Maps showing the vegetative cover and sampling sites at (a) the Notelaar marsh and (b) the Paulina marsh.

TABLE 2.1. Description of measuring sites for geomorphic situation, mean sand (>63 µm) and clay (<2 µm) content of surface sediment, dominant plant species, stem density and height (at the end of the growing season).

Site	Geomorphology*	Sand (%)	Clay (%)	Vegetation†	Stem density‡ (m <sup>-2</sup> )	Stem height (m)
1,2,4,5	Ba	1.2	28.9	<i>P.a.</i>	90-140	3.7-4.0
3	Le	1.1	32.9	<i>I.g.</i>	60-90	2.2-2.9
6,7	Le	25.6	26.7	<i>S.sp.</i>	-	> 4.0
8,9	Ba	1.4	44.	<i>S.sp.</i>	-	> 4.0
10,11,14	Ba	2.5	31.2	<i>P.m.</i>	-	0.1-0.3
				<i>H.p.</i>	-	0.2-0.5
12	Le	51.4	17.0	<i>E.p.</i>	-	0.3-0.7
13	Ba	1.7	26.2	<i>E.p.</i>	-	0.3-0.7
15	Lo	16.5	23.4	<i>A.t.</i>	40-50	0.4-0.7
				<i>S.sp.</i>	180-240	0.1-0.3
16,17	Lo	11.4	31.5	<i>S.a.</i>	400-600	0.4-0.6

\* geomorphic units: Ba = inner basin; Le = levee; Lo = low marsh without basin-levee morphology.

† dominant plant species: *P.a.* = *Phragmites australis*; *I.m.* = *Impatiens glandulifera*; *S.sp.* = *Salix* species; *P.m.* = *Puccinellia maritima*; *H.p.* = *Halimione portulacoides*; *E.p.* = *Elymus pycnanthus*; *A.t.* = *Aster tripolium*; *S.sp.* = *Salicornia* species; *S.a.* = *Spartina anglica*.

‡ - stem density was not estimated given the nature of vegetation cover (grass, trees).

### 2.3.2. Measuring sediment supply and deposition

We measured suspended sediment concentrations and deposition rates in both studied marshes during a 1-year period (from April 2000 until May 2001). The frequency distribution of high water levels was for both marsh sites during this 1-year period very comparable to the long-term frequency distribution of high water levels for the period 1981-1990, so that we can say that the measuring period is representative (Fig. 2.2).

Temporal variations in suspended sediment concentrations were measured from an automatic sampling platform located in a central marsh basin in both studied marshes (site 1, 10, Fig. 2.1 and Fig. 2.3). For every tidal inundation, the water level above the marsh surface was recorded every 5 minutes, using an ISCO flowmeter 4220, and 1 litre water samples were pumped up from 0.15 m above the marsh surface, using an ISCO sampler 6700. For each inundation cycle a first sample was automatically taken once the inundation height exceeded 0.15 m. Subsequent samples were taken every 30 minutes, until the marsh was no longer submerged. Every 15 days (at every neap tide) the filled bottles were collected and new empty ones were placed in the sampler. To determine the suspended sediment concentration (SSC in g/l), the water samples were filtered in the lab with preweighed filter papers (pore diameter = 0.45 µm), which were subsequently washed through with de-ionized water to remove salts. Samples of only 4 or 5 inundation events were

analysed for each spring-neap cycle, so that the full range of low to maximum inundation events during that spring-neap cycle was covered. In all, 245 samples were analysed, covering 27 % of all inundation events during the measuring period.

During the same 1-year period, we also sampled the sediment that settled out from suspension on the marsh surface using on all sampling sites circular plastic sediment traps (diameter = 0.233 m) (Fig. 2.3). The traps were attached to the marsh surface using steel claws and were constructed with a floatable cover to protect the deposited sediment from splash by raindrops during low tides. Every 15 days (at neap tide after each spring-neap cycle) the traps were collected and replaced by clean ones. In the laboratory, the deposited sediment was washed from the traps and rinsed with de-ionized water, to remove salts, and sieved at 707  $\mu\text{m}$ , to remove macroscopic plant and/or shell material that floated and deposited on the traps. The remaining sediment was then oven-dried at 105° C and weighed to determine the deposition rate of suspended sediment (in  $\text{g}\cdot\text{m}^{-2}$ ). In all, 425 samples were analysed, covering all 25 spring-neap cycles during the year and all 17 sampling sites.

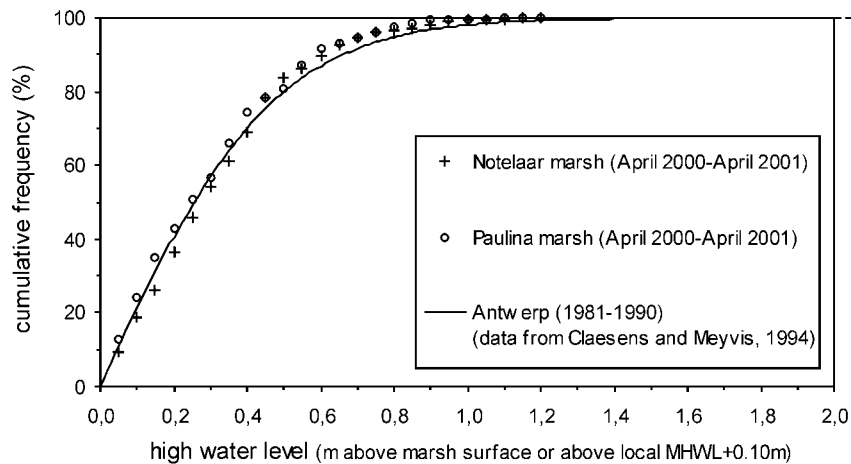


FIGURE 2.2. Cumulative frequency distribution of high water levels (in m): (1) above the Notelaar and Paulina marsh surface (own data recorded for all tidal cycles that flooded the marsh surface from April 2000 until May 2001) and (2) at Antwerp (long-term tide-gauge data for the period 1981-1990 for all high water levels higher than local mean high water level (MHWL) + 0.10 m; data from Claessens and Meyvis, 1994).

The reference level for the Antwerp tidal data (local MHWL + 0.10 m) was chosen to make the Antwerp data comparable with the measured high water levels above the Notelaar and Paulina marsh surfaces, which are 0.7 and 0.10 m above local MHWL respectively. Local MHWL's are all calculated for the period 1981-1990 (Claessens & Meyvis, 1994).



FIGURE 2.3. Photographs illustrating the field sampling methods: (a) measuring platform at the Paulina marsh (site 10) equipped with ISCO instruments for automated water level measurements and water sampling; (b) similar measuring platform at the Notelaar marsh (site 1); (c) detail of water sampling probe, at 15 cm above the marsh surface, connected to the measuring platform; (d) plastic sediment trap to sample deposited sediments, constructed with a floatable cover, which moves up and down with the tides and which protects the deposited sediment from splash by raindrops during low tides.

### 2.3.3. Data assessment and analyses

The water surface was assumed to be horizontal at high tide, so that for each inundation event and every sampling site the maximum inundation height was calculated based on the water level measurements at sites 1 and 10 on the Paulina and Notelaar marsh respectively, and considering the elevation differences between the sites. The corresponding inundation time was calculated using the observed relationship between maximum inundation height and time ( $R^2=0.89$  and  $0.96$  for the Paulina and Notelaar marsh respectively). By adding up inundation times of individual inundation events, cumulative inundation times were calculated for each spring-neap cycle. Since cumulative inundation time both reflects the magnitude and frequency of inundations during a spring-neap cycle, this parameter was found to be the best to characterise tidal marsh inundation during this time period, over which sedimentation rates were measured.

Daily mean wind velocities and directions at Vlissingen (Royal Dutch Meteorological Institute, KNMI) and Deurne near Antwerp (Royal Meteorological Institute of Belgium, KMI) were used as proxy data for wave activity near the Paulina and Notelaar marsh respectively (Fig. 1.1).

These time-series of wind-wave and tidal activity, together with data on spatial factors like topographic situation and vegetation cover, were analysed for influence on measured SSC and sedimentation rates, using t-test procedures, one-way analysis of variance (ANOVA) and regression analysis. All statistical analyses were performed using SAS/STAT software (SAS Institute Inc., 1989). Based on regression models, maps of the spatial sedimentation pattern were computed in IDRISI (Eastman, 1994).

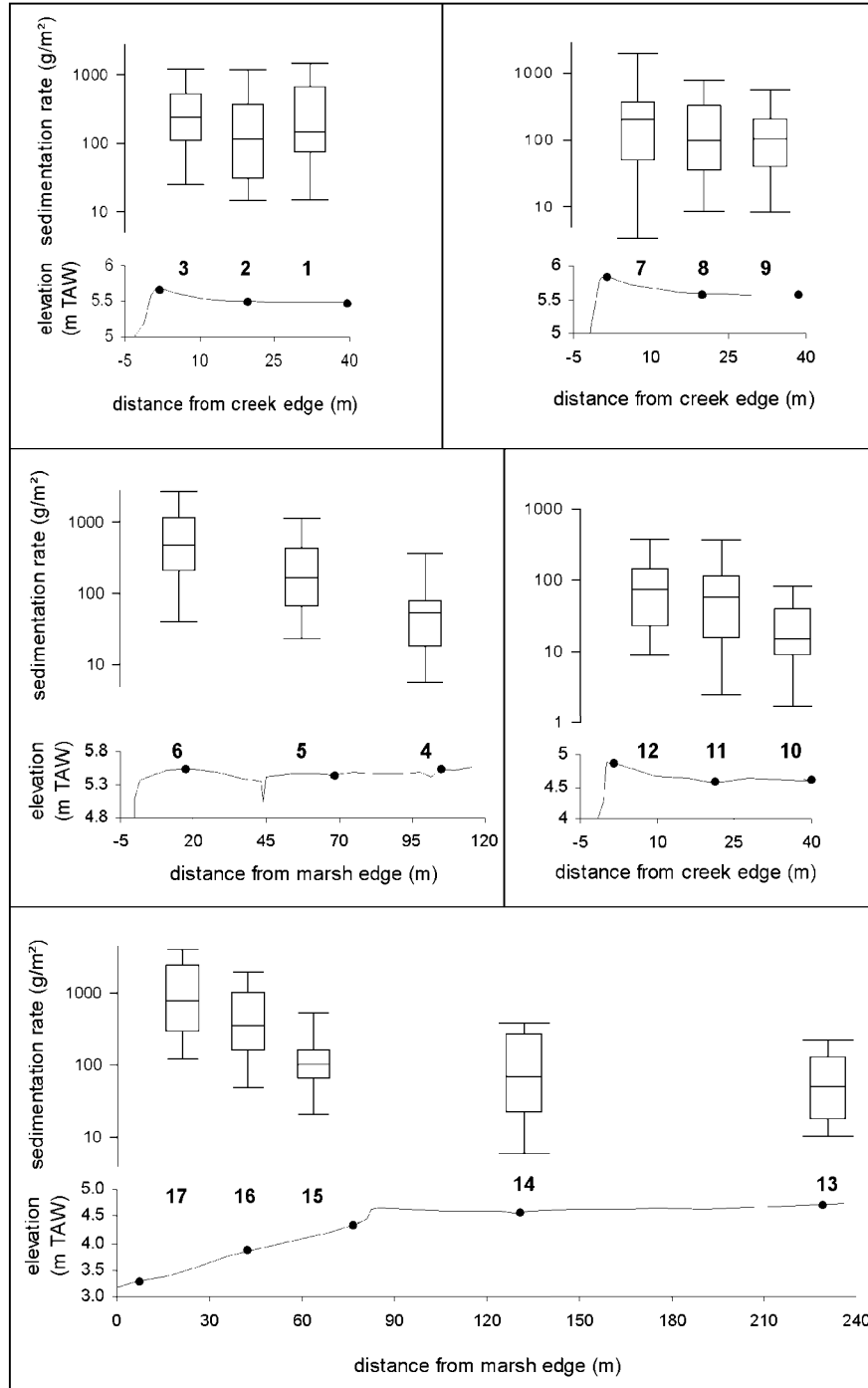
## 2.4. Results

### 2.4.1. Exploratory data representation

In Figure 2.4 the distribution of sedimentation rates is summarised by boxplots, representing both the spatial variations between the sampling sites and temporal variations between spring neap cycles. Time-averaged sedimentation rates spatially ranged from 40 to 1650  $\text{g.m}^{-2}$  per spring-neap cycle, while at each sampling site temporal variations were high, ranging in the order of 1 to  $10^3$   $\text{g.m}^{-2}$  per spring-neap cycle. The sedimentation data sets are typified by skewed distributions, and are therefore first log transformed for each sampling site to enhance normality for further t-tests and ANOVA.

---

FIGURE 2.4. Whisker boxplots of sedimentation datasets, obtained by measurements over 25 spring-tidal cycles at 17 sampling sites. The boxplots are plotted with respect to the position of sampling sites along the topographic transects, situated on Figure 2.1.



#### 2.4.2. Temporal patterns of sediment dynamics

During all sampled inundation cycles SSC is found to decrease with time, indicating that the suspended sediment is continuously settling during the whole duration of inundation and that no resuspension occurs during ebb tide (e.g., Fig. 2.5). However the initial SSC (or ISSC), measured at the beginning of marsh flooding, varies considerably from one tide to another. Figure 2.6 shows that the ISSC linearly increases with maximum inundation height, recorded at high tide, for all sampled inundation events, both at the Notelaar and Paulina marsh. This relationship between ISSC and inundation height must be interpreted as follows: as the marsh is inundated by higher tides, the flooding water has a higher capacity to transport suspended sediment, so that the ISSC is higher.

In addition, this increase of ISSC with inundation height is greater during the winter period (October-March) than during the summer period (April-September). An unpaired t-test showed that the difference in ISSC between winter and summer is significant for both studied marshes (Table 2.2). This is in accordance with the seasonal variations in SSC observed in the stream channel of the Scheldt, which are generally related to seasonal variations in biological activity, in wind-wave activity and in fluvial water and sediment discharge (Fettweis *et al.*, 1998).

The measured sedimentation rates vary between spring-neap cycles following a similar temporal pattern. Figure 2.7 shows that sedimentation rates increase exponentially with cumulative inundation time. Especially for inner marsh sites sedimentation rates are significantly higher during winter than during summer for a same inundation time, while for sites situated next to creeks or marsh edges this seasonal difference is not always significant (Fig. 2.7, Table 2.2).

Apart from tidal and seasonal influence, the role of wind-wave activity was examined. Table 2.3 shows that for most sampling sites no significant relationship could be found between ISSC or sedimentation rates on the one hand and average wind speeds on the other hand (see columns (b)). The relationship with tidal inundation height or time is on the contrary highly significant for most sites (columns (a)). For these sites the remaining variation, expressed by the residuals resulting from regression between ISSC/SR and inundation height/time, is also not significantly related to average wind velocity (columns (c)). Only for sites 15-17, situated on the *Spartina* marsh, sedimentation rate is not significantly related to inundation time and better related to average wind velocity, especially for the winter period. This may be an indication that these marsh sites, situated on the lower *Spartina* marsh bordering the marsh edge, are more sensitive to wind-wave activity.

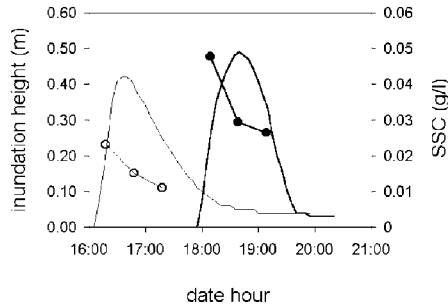


FIGURE 2.5. Typical example of the temporal evolution of the inundation height above the marsh surface (in solid line) and suspended sediment concentration (SSC; in dots and line) during a tidal inundation at the Notelaar marsh (thick lines and black dots) and Paulina marsh (thin lines and white dots).

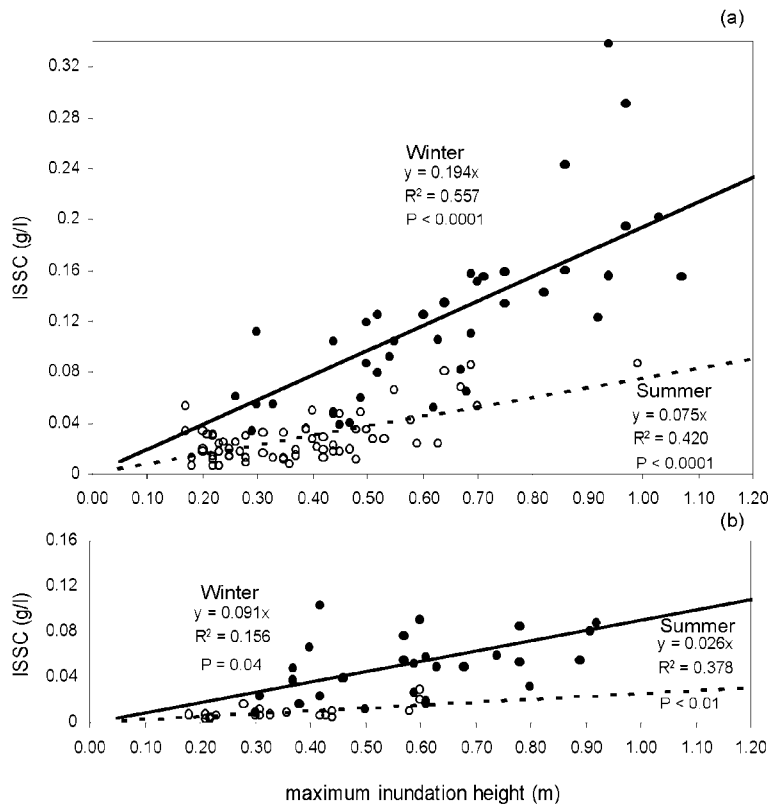


FIGURE 2.6. Linear relationship between initial suspended sediment concentration (ISSC) and maximum inundation height observed at (a) the Notelaar marsh (site 1) and (b) the Paulina marsh (site 10). Note the difference between summer (Apr-Sept; indicated in white symbols and broken line) and winter (Oct-Mar; in black symbols and solid line) observations.

TABLE 2.2. P-values resulting from unpaired t-tests comparing initial suspended sediment concentration (ISSC) and sedimentation rate data (logSR) between winter and summer period at each measuring site (since variances of summer and winter data sets are unequal, P-values using Satterthwaite's computational method are presented here (SAS Institute Inc., 1989)). P-values in bold indicate that the difference between winter and summer period is not significant ( $\alpha = 0.01$ ) at these sites. For all other sites there is a significant difference between winter and summer data.

data	site	P-value	data	site	P-value	data	site	P-value
ISSC	1	<0.0001	logSR	6	<b>0.0393</b>	logSR	12	<b>0.0235</b>
	10	<0.0001		7	0.0027		13	<b>0.0525</b>
logSR	1	0.0002	8	0.0003	14	0.0037		
	2	<0.0001	9	0.0009	15	0.0051		
	3	0.0082	10	0.0054	16	<b>0.0400</b>		
	4	0.0008	11	0.0020	17	<b>0.0561</b>		
	5	0.0041						

### 2.4.3. Spatial sedimentation patterns

Figure 2.4 illustrates well that the spatial sedimentation pattern is influenced by the marsh surface topography. A first topographic control is exerted by marsh surface elevation: low lying marshes, such as the *Spartina* marsh (sites 15, 16, 17), are characterised by much higher sedimentation rates than high marshes (sites 10 to 14), due to more frequent, higher and longer inundations during a same spring-neap cycle (Fig. 2.8a). However, measuring sites, which are situated next to tidal creeks or marsh edges, do not follow this relationship. Only when these sites are omitted from Figure 2.8a, a strong relationship is found between sedimentation rate and elevation.

A second topographic control is exerted by distance from the sediment source: along each sampling transect sedimentation rates decrease with increasing distance from the creek or marsh edge (Fig. 2.4). ANOVA confirms that sedimentation rates in inner marsh basins are not significantly different from each other, while they are significantly higher on the levees (Table 2.4). Figure 2.8b shows that for all sampling transects the time-averaged sedimentation rate, expressed relative to its value next to the creek or marsh edge, decreases exponentially with increasing distance from the creek or marsh edge. However, sampling sites 16 and 17 do not fit in this model and are omitted, because sedimentation is here strongly influenced by the much lower marsh elevation. Our data further suggest that absolute sedimentation rates are highest at the marsh edge and decrease along marsh creeks with increasing distance from the marsh edge (Fig. 2.8c).

Spatial and temporal factors controlling short-term sedimentation

TABLE 2.3.  $R^2$  and  $P$ -values resulting from linear regression analyses (a) between initial suspended sediment concentration (ISSC) and inundation height at high tide ( $I_h$ ); (b) between ISSC and daily mean wind velocity ( $W_d$ ); (c) between the residuals from regression (a) ( $ISSC_{Res}$ ) and  $W_d$ ; (d) between sedimentation rate per spring-neap cycle ( $\log SR$ ) and cumulative tidal inundation time ( $I_t$ ); (e) between  $SR$  and daily mean wind velocity averaged over the whole spring-neap cycle  $W_{sn}$ ; (f) between the residuals from regression (d) ( $SR_{Res}$ ) and  $W_{sn}$ . All regression analyses (a to f) are carried out for winter and summer data separately. Notice that for most sampling sites significant relationships ( $P$ -value  $< 0.05$ ) are only found between ISSC/ $\log SR$  and tidal inundation height/time (indicated in bold). Only for sites 15-17, situated on the low *Spartina* marsh near the marsh edge, sedimentation rate is better related to mean wind velocity.

Site	ISSC summer data						ISSC winter data					
	(a)		(b)		(c)		(a)		(b)		(c)	
	$ISSC \times I_h$		$ISSC \times W_d$		$ISSC_{Res} \times W_d$		$ISSC \times I_h$		$ISSC \times W_d$		$ISSC_{Res} \times W_d$	
	$R^2$	P	$R^2$	P	$R^2$	P	$R^2$	P	$R^2$	P	$R^2$	P
1	<b>.42</b>	<b>&lt;.01</b>	<.01	.75	.03	.21	<b>.56</b>	<b>&lt;.01</b>	.04	.20	<.01	.70
10	<b>.38</b>	<b>&lt;.01</b>	.07	.34	.14	.15	<b>.16</b>	<b>.04</b>	.02	.43	<.01	.79
Site	SR summer data						SR winter data					
	(d)		(e)		(f)		(d)		(e)		(f)	
	$\log SR \times I_t$		$SR \times W_{sn}$		$SR_{Res} \times W_{sn}$		$\log SR \times I_t$		$SR \times W_{sn}$		$SR_{Res} \times W_{sn}$	
	$R^2$	P	$R^2$	P	$R^2$	P	$R^2$	P	$R^2$	P	$R^2$	P
1	.35	.07	.02	.78	.03	.73	<b>.54</b>	<b>&lt;.01</b>	.09	.36	.05	.51
2	<b>.41</b>	<b>.04</b>	.15	.40	.03	.71	<b>.58</b>	<b>&lt;.01</b>	.09	.36	.01	.74
3	<b>.71</b>	<b>&lt;.01</b>	.39	.13	.44	.11	<b>.76</b>	<b>&lt;.01</b>	.18	.19	<.01	.78
4	<b>.67</b>	<b>&lt;.01</b>	.13	.42	<.01	.88	<b>.59</b>	<b>&lt;.01</b>	.28	.10	.06	.48
5	<b>.59</b>	<b>&lt;.01</b>	.42	.12	.28	.22	<b>.82</b>	<b>&lt;.01</b>	.20	.16	.10	.36
6	<b>.77</b>	<b>&lt;.01</b>	.08	.53	.20	.31	<b>.64</b>	<b>&lt;.01</b>	.19	.18	.02	.67
7	<b>.85</b>	<b>&lt;.01</b>	.07	.58	.09	.51	<b>.87</b>	<b>&lt;.01</b>	.16	.23	.02	.65
8	<b>.70</b>	<b>&lt;.01</b>	.33	.17	.20	.31	<b>.60</b>	<b>&lt;.01</b>	.05	.51	.13	.29
9	<b>.84</b>	<b>&lt;.01</b>	.11	.47	<.01	.86	<b>.76</b>	<b>&lt;.01</b>	.21	.15	<.01	.81
10	.23	.20	.02	.74	.03	.68	.12	.30	.16	.22	.33	.07
11	<b>.46</b>	<b>.04</b>	<.01	.93	.03	.66	<b>.64</b>	<b>&lt;.01</b>	.02	.64	.17	.19
12	<b>.60</b>	<b>.01</b>	<.01	.98	<.01	.83	<b>.97</b>	<b>&lt;.01</b>	<.01	.85	.13	.25
13	.28	.15	.21	.22	.18	.26	<b>.86</b>	<b>&lt;.01</b>	.03	.61	.12	.27
14	<b>.59</b>	<b>.01</b>	<.01	.82	.04	.61	.10	.33	.03	.62	.07	.41
15	.43	.05	.41	.07	<b>.55</b>	<b>.02</b>	.08	.37	<b>.47</b>	<b>.01</b>	<b>.34</b>	<b>.05</b>
16	.16	.29	<.01	.89	.01	.77	.07	.44	.18	.19	.21	.15
17	.07	.52	<.01	.88	.07	.48	.06	.46	<b>.39</b>	<b>.03</b>	.24	.10

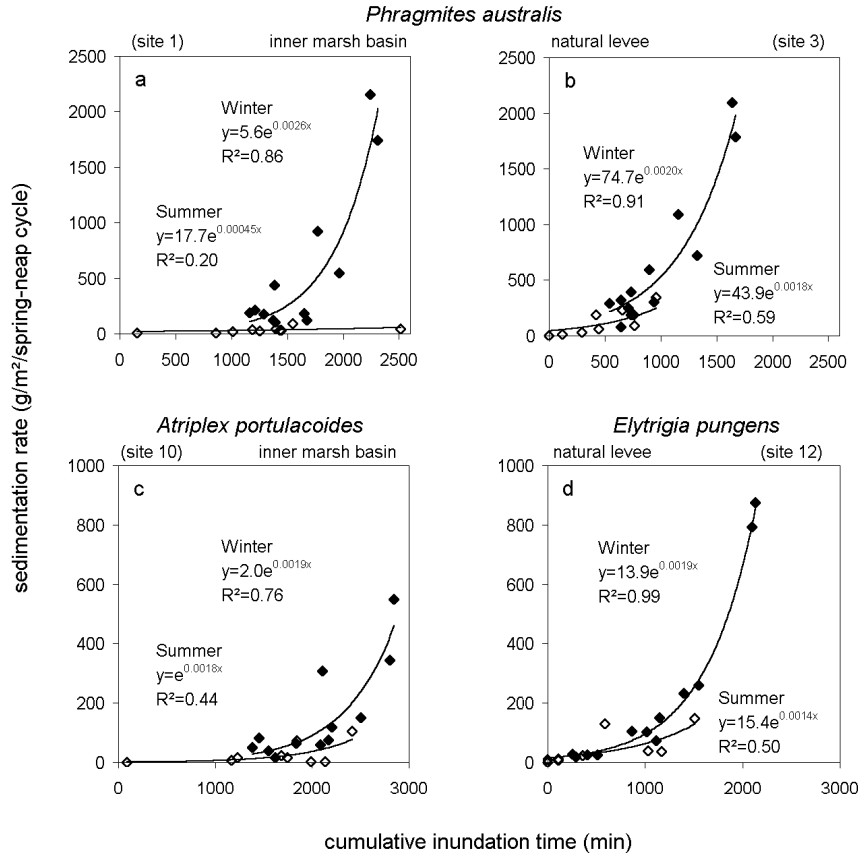


FIGURE 2.7. Exponential relationship between sedimentation rate (per spring-neap cycle) and cumulative inundation time. Examples are shown for (a) a freshwater *Phragmites australis* marsh basin (site 1), (b) the adjoining natural levee (site 3), (c) a high salt marsh basin (site 10) and (d) the adjoining levee (site 12). Note the differences in axis. Summer (Apr-Sept) and winter (Oct-Mar) observations are plotted in white and black symbols respectively. The sampling sites are situated on Figures 2.1 and 2.3.

FIGURE 2.8. (a) Mean sedimentation rate per spring-neap cycle in relation to marsh surface elevation (expressed relative to local mean high water level) for all sampling sites. White dots indicate data points from levees (sites 3, 6, 7, 12) and are incorporated in the construction of the broken regression line but omitted in the construction of the solid regression line. (b) Relative mean sedimentation rate in relation to distance from the creek or marsh edge for all sampling transects situated within different vegetation types (see Fig. 2.1 for location of the transects). (c) Absolute mean sedimentation rate next to creek or marsh edges in relation to distance from the marsh edge, measured along the creeks system.

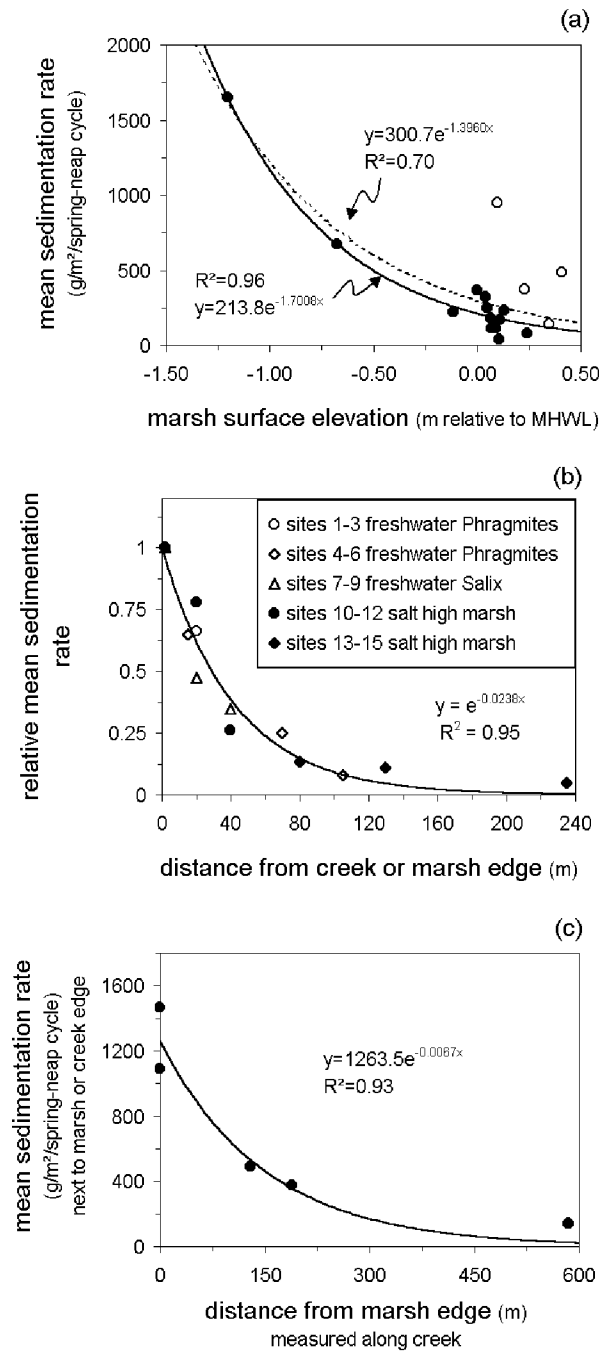


TABLE 2.4. One-way ANOVA results for intercomparison between measuring sites during the winter, summer and whole 1-year measuring period.  $Pr>F$ -values in bold indicate that the difference in ISSC or sedimentation rate (SR) between compared sites is not significant ( $\alpha = 0.05$ ). In all other cases there is a significant difference between sites.

data type	intercomparison between	compared sites	Pr>F		
			winter	summer	year
SR	fresh basins	1,2,5,8,9	<b>0.3733</b>	<b>0.3074</b>	<b>0.4236</b>
	fresh basins & levee	1,2,5,8,9,3,6,7	<b>0.0739</b>	0.0160	0.0278
	salt basins	10,11,13,14	<b>0.1904</b>	<b>0.6411</b>	<b>0.6881</b>
	salt basins & levees	10,11,13,14,12	0.0042	<b>0.2853</b>	0.0236
	salt high & low marsh	10 to 17	<0.0001	<0.0001	<0.0001
	fresh & salt basins	1,2,5,8,9, 10,11,13,14	<0.0001	0.0165	<0.0001
ISSC	fresh & salt basin	1,10	<0.0001	<0.0001	0.0028

#### 2.4.4. An integrated spatio-temporal model

The above-described analyses showed that spatial variations in sedimentation rates are partly explained by elevation differences. These spatial differences in elevation are in fact equivalent to temporal differences in tidal inundation height and duration, which are the main factors controlling temporal variations in sedimentation. It is then worthwhile to investigate to what extent both spatial and temporal sedimentation patterns can be described in terms of a limited number of controlling parameters, which interrelate and act synergistically.

A multiple non-linear regression model of the following form is proposed:

$$SR = k \cdot e^{lH} \cdot e^{mD_c} \cdot e^{nD_e} \quad (2.1)$$

where  $SR$  = the sedimentation rate ( $\text{g.m}^{-2}$  per spring-neap cycle),  $H$  = the intensity of tidal inundation (this parameter will be further specified below),  $D_c$  = the distance to the nearest creek or marsh edge (m) and  $D_e$  = the distance to the marsh edge (m), measured along the nearest creek. For sampling transects perpendicular to the marsh edge,  $D_e$  is set to zero. The model parameters  $k$ ,  $l$ ,  $m$  and  $n$  are determined using a non-linear regression procedure in SAS/STAT (SAS Institute Inc., 1989).

TABLE 2.5. Correlation coefficients resulting from correlation between  $H$  (marsh surface elevation relative to local mean high water level),  $D_c$  (distance to the nearest creek or marsh edge) and  $D_e$  (distance to the marsh edge, measured along the nearest creek) for the 17 measuring locations used in this study.

	$H$	$D_c$	$D_e$
$H$	1	0.13	0.33
$D_c$	0.13	1	-0.40
$D_e$	0.33	-0.40	1

First, regression analysis was carried out with sedimentation rates averaged over the 1-year measuring period as the dependent variable and incorporating the spatial variation between all 17 salt and freshwater marsh sites. In this case  $H$  is estimated by the surface elevation relative to the local mean high water level. Table 2.5 shows that the correlation between the variables  $H$ ,  $D_c$  and  $D_e$  is very weak so that they can be regarded as independent variables. Figure 2.9a compares sedimentation rates as observed and estimated by the regression model. It can be seen that the model is able to predict almost all of the observed spatial variability ( $R^2 = 0.95$ ).

Secondly, a similar regression analysis was carried out, taking the distinction between winter and summer sedimentation into account. Again observations and model predictions are in good agreement (Fig. 2.9a;  $R^2 = 0.93$  and  $0.98$  for winter and summer respectively). The model parameter  $k$  is larger for the winter than for the summer period, indicating that sediment input is larger during winter (Table 2.6). The parameter  $l$  is more negative during winter, which means that elevation differences have then a more pronounced effect on spatial variations in sedimentation rate. Seasonal differences in  $m$  and  $n$  values suggest that sedimentation gradients along and perpendicular to tidal creek edges are less pronounced during winter than during summer. This confirms that sediment trapping during flooding from the creeks to the inner marshes is greater during summer and consequently less sediment reaches the inner marsh basins (see also Fig. 2.7).

Finally, it was also investigated whether both temporal and spatial variations between spring-neap cycles and between sampling sites can be modelled using equation 2.1. In this case  $H$  is estimated by cumulative inundation height and is both time- and space-dependent. Figure 2.9b shows that the presented model structure can partly explain the observed spatio-temporal sedimentation pattern ( $R^2 = 0.68$  and  $0.56$  for winter and summer, respectively).

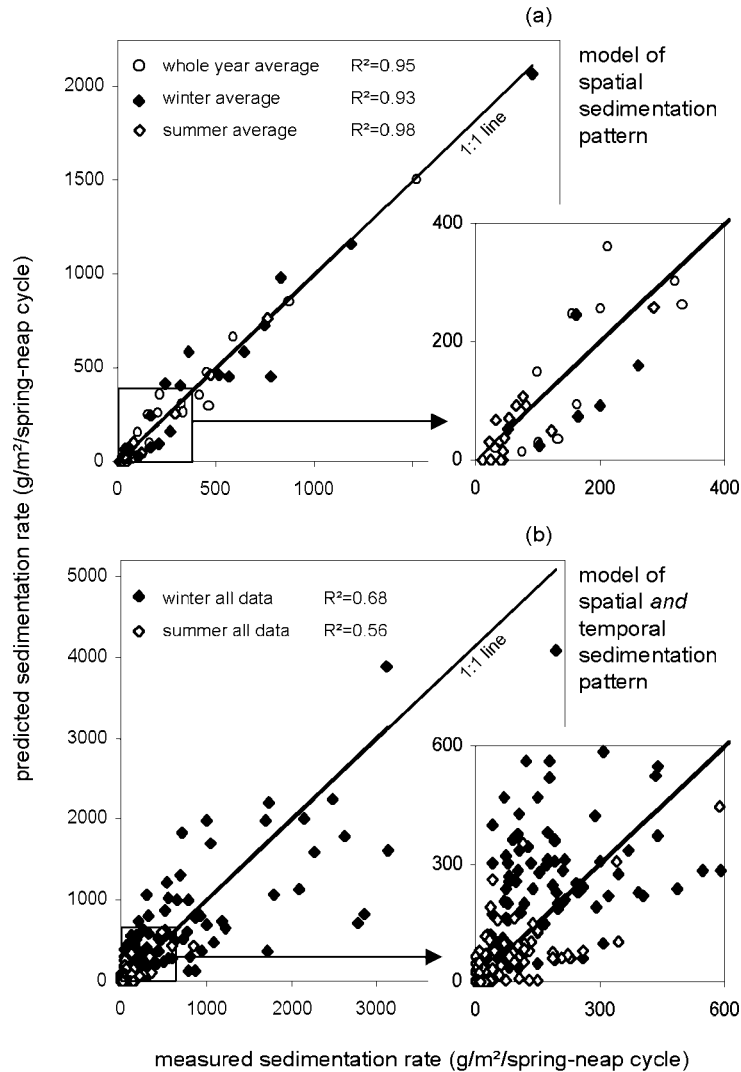


FIGURE 2.9. Comparison of sedimentation rates per spring-neap cycle as measured and predicted using multiple non-linear regression (see text). (a) The model incorporates only the spatial sedimentation pattern by using for all sampling sites sedimentation rates averaged over the whole 1-year measuring period, over the winter and over the summer period. (b) The model incorporates both the spatial and temporal sedimentation pattern by using sedimentation rates as measured at each sampling site and for each individual spring-neap cycle during the year. Regression was carried out separately for all winter and all summer data.

TABLE 2.6. Model parameters ( $k, l, m, n$ ) and  $R^2$ -values resulting from multiple non-linear regression analyses using equation 1 (see text).

SR data	$k$	$l$	$m$	$n$	$R^2$
whole year average per site	1174.9	-0.3165	-0.0195	-0.0058	0.95
winter average per site	1565.5	-0.3352	-0.0174	-0.0046	0.93
summer average per site	737.3	-0.2036	-0.0298	-0.0137	0.98
winter all data	275.8	0.3006	-0.0216	-0.0043	0.68
summer all data	129.6	0.3943	-0.0392	-0.0075	0.56

TABLE 2.7.  $R^2$  values resulting from regression analyses using simplified versions of eq. 2.1, using as the independent variable: (1) only  $H$  ( $m, n = 0$ ); (2) only  $D_c$  ( $l, n = 0$ ); (3) only  $D_e$  ( $l, m = 0$ ); (4) only  $H$  and  $D_c$  ( $n=0$ ); (5) only  $H$  and  $D_e$  ( $m=0$ ); (6) only  $D_c$  and  $D_e$  ( $l=0$ ); (7)  $H, D_c$  and  $D_e$  (the original model).

	(1) $H$	(2) $D_c$	(3) $D_e$	(4) $H, D_c$	(5) $H, D_e$	(6) $D_c, D_e$	(7) $H, D_c, D_e$
whole year average per site	.70	.19	.16	.75	.70	.92	.95
winter average per site	.63	.18	.16	.72	.66	.88	.93
summer average per site	.72	.13	.15	.75	.73	.96	.98
winter all data	.37	.01	.08	.45	.41	.17	.68
summer all data	.06	.03	.07	.22	.12	.28	.56

In order to evaluate the relative importance of each of the three variables  $H$ ,  $D_c$  and  $D_e$ , it was also investigated to what extent the spatial variations in sedimentation rates  $SR$  can be predicted based on only one or two of these three variables. This was done by regression analysis using eq. 2.1 but: (1) only using  $H$  as an independent variable (by setting  $m, n=0$ ); (2) only using  $D_c$  ( $l, n=0$ ); (3) only using  $D_e$  ( $l, m=0$ ); (4) using  $H$  and  $D_c$  ( $n=0$ ); (5) using  $H$  and  $D_e$  ( $m=0$ ); and (6) using  $D_c$  and  $D_e$  ( $l=0$ ). The  $R^2$  values resulting from these regression analyses are listed in Table 2.7. It can be seen from this table that generally higher  $R^2$  values are obtained when using only  $H$  than when using only  $D_c$  or  $D_e$  as an independent variable. However, when looking at the combination of two independent variables, the use of  $D_c$  and  $D_e$  (and thus omitting  $H$ ) as independent variables results in the highest  $R^2$  values. It has to be noticed that these  $R^2$  values are very close to the  $R^2$  values resulting from regression analysis using the original model, based on  $H, D_c$  and  $D_e$  (Table 2.7). Thus,  $D_c$  and  $D_e$  together explain the largest proportion of the variability in sedimentation rates observed between the 17 measuring sites.

Based on the regression models it is now possible to generate maps of the fully 2-dimensional sedimentation pattern in a raster based Geographical Information System (GIS). For each raster cell that represents the marsh surface a value of  $H$ ,  $D_c$  and  $D_e$  has to be calculated. This was done for a raster image with 1 by 1 m cells of the Paulina marsh, where elevation data are available from airborne laser altimetry conducted by the Dutch Rijkswaterstaat Meetkundige Dienst (1 point/9 m<sup>2</sup>, guaranteed minimal vertical accuracy of 0.20 m) (Van Heerd and Van 't Zand, 1999). From these elevation points a digital elevation model was computed using a triangulation with linear interpolation method. The tidal creek network was digitised based on geo-referenced recent aerial photographs and converted to a raster image. For each marsh surface cell, the distance to the nearest tidal creek cell ( $D_c$  in eq. 2.1) and the distance of this nearest tidal creek cell to the creek mouth at the marsh edge, measured along the creek ( $D_e$  in eq. 2.1), was calculated using the program modules DISTANCE, COST and ALLOCATE in IDRISI (Eastman, 1994). Finally the sedimentation rate in every marsh surface cell was calculated by solving equation 2.1 and using the calculated values of  $H$ ,  $D_c$  and  $D_e$ . Maps of the whole year averaged and summer and winter averaged sedimentation rate per spring-neap cycle were made using the appropriate model parameters in Table 2.6. Figure 2.10a clearly shows that the calculated sedimentation pattern is the result of the combined influence of surface elevation, the creek network, and distance to the marsh edge. Measured and calculated sedimentation rates at the measuring sites are in very good agreement (Fig. 2.10b), indicating that the proposed method is very useful to compute 2-dimensional patterns of tidal marsh sedimentation.

## 2.5. Discussion and conclusions

As reported from earlier studies, short-term temporal sedimentation patterns are in some tidal marshes mainly controlled by wind-wave activity (Reed, 1989; Leonard *et al.*, 1995a; Van Proosdij *et al.*, 2000), while other studies indicate that tidal influence is more dominant (Allen and Duffy, 1998a; Christiansen *et al.*, 2000). In the meso- to macro-tidal Scheldt estuary the tide is the most important factor that governs temporal patterns of tidal marsh sedimentation.

For almost all sampling sites we observed an exponential increase of marsh sedimentation with increasing inundation time. The exponential nature of this relationship can be explained as a consequence of a linear increase in ISSC with maximum inundation height. Based on numerical modelling, Temmerman *et al.* (2003a) showed that the relationship between sedimentation rate and inundation time is exponential when ISSC increases

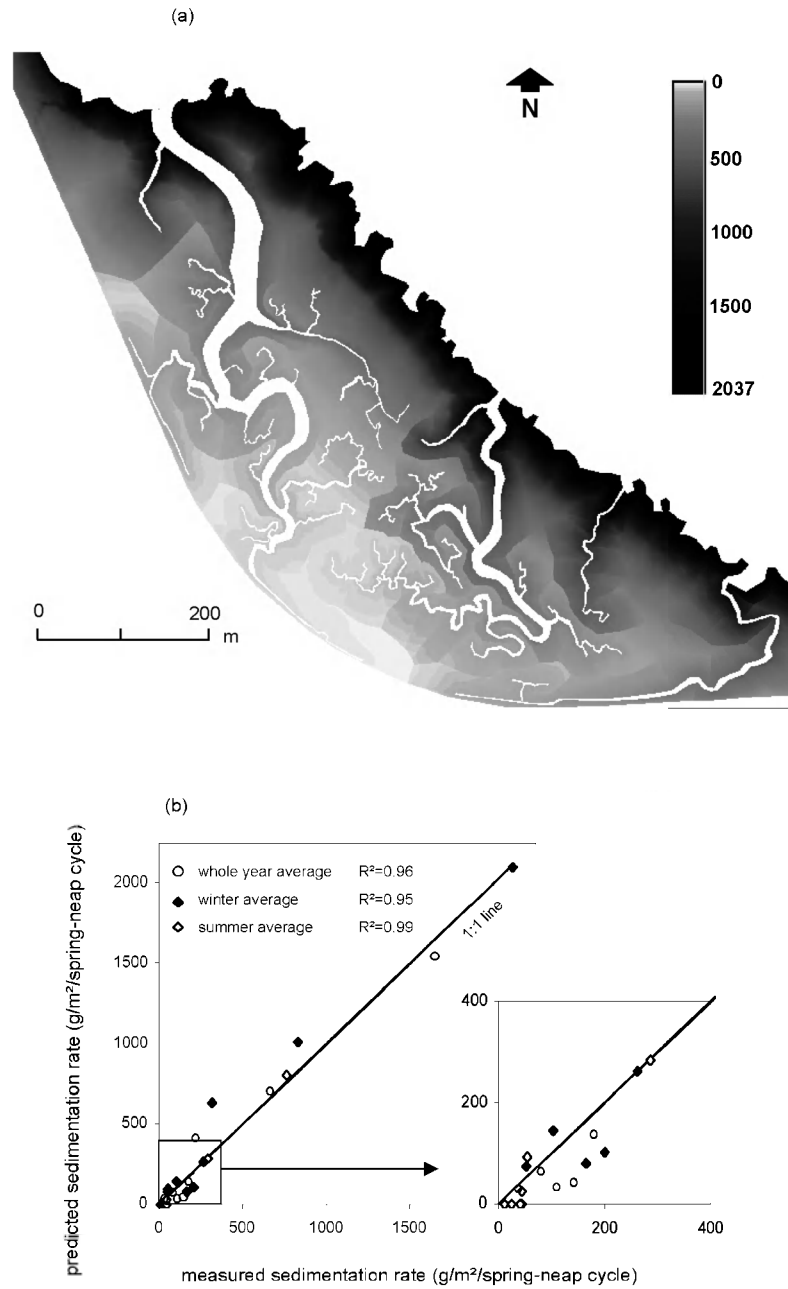


FIGURE 2.10. (a) Simulated spatial sedimentation pattern at the Paulina marsh averaged over 1 year (in  $g\ m^{-2}$ /spring-neap cycle). (b) Comparison between measured and predicted sedimentation rates per spring-neap cycle, for sedimentation rates averaged over 1 year, over the winter and over the summer period.

linearly with inundation height, while the relationship between sedimentation rate and inundation time is linear when ISSC is assumed to be constant (see later in chapter 5). The fact that an exponential relationship between sedimentation rate and inundation time is found for most sampling sites suggests that the linear increase of ISSC with increasing inundation height is a general mechanism that controls suspended sediment supply to the marsh surface.

Seasonal variations in sedimentation rates on tidal marshes are reported by several authors (e.g. Hutchinson *et al.*, 1995; Leonard, 1997; Leonard *et al.*, 1995a). Higher sedimentation rates are often found during the summer period, which is explained by higher bioturbation of bottom sediments, leading to higher SSC and tidal marsh sedimentation rates. However, we observed higher overmarsh SSC and sedimentation rates during the winter period than during the summer period for a same inundation height or time. This is in accordance with the seasonal variations in SSC observed in the stream channel of the Scheldt, which are generally related to seasonal variations in biological activity, in wind-wave activity and in fluvial water and sediment discharge (Fettweis *et al.*, 1998).

The difference between winter and summer sedimentation rates is most important in inner marsh basins, while this seasonal difference is not significant near creek and marsh edges. One possible explanation could be that sediment trapping along flow paths from creeks to inner marshes is enhanced during the summer period, as a consequence of higher growing densities and hydraulic resistance by marsh plants during summer (see also Boorman *et al.*, 1998) or by higher settling velocities of the suspended sediment during summer, for example due to enhanced bioflocculation. Consequently less sediment is reaching the inner marsh basins during the summer period. At this moment, however, quantitative data are lacking and further research is needed to fully understand this seasonal sedimentation pattern.

Our study shows that the spatial depositional pattern on the tidal marshes along the Scheldt estuary can be predicted from three morphometric variables only. As has been widely reported from other salt marshes, sedimentation rates decrease with increasing surface elevation (e.g. Cahoon and Reed, 1995; Stoddart *et al.*, 1989) and with increasing distance from tidal creeks (e.g. French and Spencer, 1993; French *et al.*, 1995; Leonard, 1997; Reed *et al.*, 1999). Our study further shows that sedimentation rates along creek edges decrease with increasing distance from the marsh edge, measured along the creeks system. While former studies focussed on the identification of the different possible controlling variables, our study clearly shows that both spatial and temporal sedimentation patterns can be well predicted using a single multiple regression model that only incorporates the three controlling variables discussed above.

The fact that the same model very well predicts the sedimentation patterns and rates on a salt and freshwater marsh, located at the extremes of the estuarine gradient, suggests that the physical-sedimentological processes controlling tidal marsh sedimentation are similar over the whole estuarine gradient of the Scheldt estuary. The differences in vegetation characteristics, which strongly vary between and within the studied salt and freshwater marshes, seem to have no detectable influence on the spatial sedimentation pattern. It is often stated that marsh vegetation reduces tidal currents and therefore promotes sediment deposition (Leonard *et al.*, 1995a; Leonard and Luther, 1995). However, it seems that very high and dense vegetation, which is typical for a freshwater *Phragmites australis* or *Salix* marsh, is not more effective in tempering flow speeds and trapping sediments than typically lower salt marsh plants such as *Puccinellia maritima* and *Halimione portulacoides*.

In former studies, 2D sedimentation patterns were calculated from a spatial network of measuring sites, using conventional spatial interpolation techniques like kriging (Leonard, 1997; French and Spencer, 1993) and bilinear interpolation (French *et al.*, 1995). Especially French *et al.* (1995) emphasised the difficulties of calculating sedimentation rates based on interpolation of spatially distributed measurements. In this regard, this paper presents an alternative method to calculate 2D spatial sedimentation patterns, by spatially implementing an empirical model that takes into account the physical variables that determine the spatial distribution of sediment over the marsh surface. Inundation frequency, height and duration are reflected in the model by surface elevation, while the transport pathways of the sediment are reflected by the distance from the creeks and the distance from the marsh edge measured within the creeks system. Although the combined influence of surface elevation and the creek network is successfully modelled, our approach has also certain limitations. Especially where creek basins with an important difference in distance from the creek mouth are adjacent, strong discontinuities in sedimentation rates may appear (Fig. 2.10a). In order to handle such difficulties a more hydrodynamically based model has to be used, which takes into account the complex flow of water and suspended matter over the marsh surface topography and through the marsh vegetation cover.



## Chapter 3

# Spatial patterns of suspended sediment transport and deposition during single tidal cycles within a small tidal marsh creek catchment

---

### 3.1. Introduction

During high tides, tidal marshes are flooded and suspended sediments, nutrients and pollutants, are transported to and partly deposited on the marsh surface. The transport pathways of sediments and nutrients during flooding and draining of the marsh surface are the result of the water flow over the complex micro-topography and through the marsh vegetation cover. These patterns of water flow and sediment and nutrient transport are the key factors determining the geomorphic and ecological evolution of tidal marshes.

Recently, a number of field studies was undertaken to study the flow fields and suspended sediment transport over tidal marsh surfaces at the time-scale of single tidal cycles (Wang *et al.*, 1993; Leonard *et al.*, 1995a; Leonard and Luther, 1995; Leonard, 1997; Christiansen *et al.*, 2000; Van Proosdij *et al.*, 2000; Davidson-Arnott *et al.*, 2002; Leonard *et al.*, 2002). These studies were typically carried out along transects of a few to some tens of metres perpendicular to tidal marsh creeks or to the seaward marsh edge, which are considered as the sources of water and suspended sediment supply. Wang *et al.* (1993) and Leonard (1997) reported that at the beginning of flooding and

at the end of draining of the marsh platform, flow directions are more or less perpendicular to tidal creeks, while landward sheet flow parallel to tidal creeks occurred during peak flood and seaward sheet flow occurred during peak ebb. Furthermore, flow velocity, turbulent kinetic energy, shear velocity and suspended sediment concentration were found to decrease with increasing distance from tidal creeks (Leonard *et al.*, 1995a; Leonard and Luther, 1995; Christiansen *et al.*, 2000; Leonard *et al.*, 2002). Recently, vertical flow profiles were also characterised in tidal marsh vegetation canopies, both in laboratory flume experiments (Pethick *et al.*, 1990; Shi *et al.*, 1995; Shi *et al.*, 1996) and in the field (Leonard and Luther, 1995; Christiansen *et al.*, 2000).

Although these studies provided important insights, Allen (2000) states in his extensive review article of tidal marsh research that “the movement of water and suspended particles across a marsh platform yet remains perhaps the worst understood aspect of marsh morphodynamics”. Indeed, two-dimensional spatial patterns of flow and sediment transport through tidal marsh creeks and over marsh surfaces are not documented. The major problem here is, undoubtedly, the spatial resolution. Existing field studies were based on a rather limited number of measuring sites, because of the restricted availability of measuring equipment and manpower, and it will be nearly impossible to obtain ever a sufficiently dense network of measuring sites to cover the full spatio-temporal pattern of flow hydrodynamics and sediment transport over a marsh surface.

In this respect, current developments in numerical modelling of fluid flows, grouped under the term ‘Computational Fluid Dynamics’ (CFD), offer interesting perspectives. Recent years have witnessed the growing application of CFD models to study water flow and sediment transport processes in a wide range of aquatic environments (Lane, 1998). These hydrodynamic modelling studies allowed the representation of flow and sediment transport processes in two or three dimensions and at spatial and temporal resolutions that can never be reached in field studies. In this respect, hydrodynamic models offer the potential to improve our understanding of complex flow and sediment transport processes in tidal marshes. However, before a hydrodynamic model can be implemented for a specific marsh area, a large number of field data need to be collected for model input and for model calibration and validation.

This study presents the collection and analysis of high-resolution field data on hydrodynamics and suspended sediment transport and deposition during single tidal cycles within a small tidal marsh creek catchment. First, field measurements of the detailed spatial sedimentation pattern are used to test and refine a formerly presented topography-based model, which enables the prediction of spatial variations in tidal marsh sedimentation. Secondly, a method is presented to calculate and analyse water and sediment balances over single tidal cycles, based on digital elevation modelling, spatial

interpolation of sedimentation rate measurements and hydrodynamic and sediment transport measurements within the tidal creeks system entering the studied marsh. The presented analysis allows to gain insight in the role of the tidal creeks system in supplying water and sediments to the marsh surface, for different tidal cycles with different inundation heights and for high and low marshes with or without a well-developed creeks system.

Finally, the calibration and validation of a hydrodynamic model, using the collected field data, is described in the following chapter (chapter 4).

### 3.2. Study area

The study was carried out for the Paulina marsh, a typical salt marsh situated in the Western Scheldt (see Fig. 1.2 in chapter 1). At this point in the Scheldt estuary, the mean tidal range is about 3.9 m (Claessens and Meyvis, 1994) and the time-averaged suspended sediment concentration is in the order of 30 mg/l near the water surface (Van Eck *et al.*, 1991; Van Damme *et al.*, 2001). The Paulina marsh was found to be appropriate for this study, because all successional stages from young (low) to old (high) salt marsh can be found here. Concerning the geomorphology of the Paulina marsh, a clear distinction can be made between two parts (Fig. 3.1): (1) a high marsh, which is characterised by a relatively flat topography and a well-developed tidal creek system and levee-basin topography between the creeks; and (2) a low marsh, which gradually slopes down to the edge of the marsh and with only few tidal creeks and no levee-basin topography. In front of the marsh a large tidal flat exists. The vegetation of the Paulina marsh also reflects this difference between high and low marsh. The high marsh is covered by a climax vegetation of NW European salt marsh species, such as *Puccinellia maritima*, *Aster tripolium*, *Halimione portulacoides* and *Elymus pycnanthus*. In contrast, the low marsh is dominated by a pioneer vegetation of *Spartina anglica*.

### 3.3. Methods

#### 3.3.1. General setup of the field measurements

The most evident geomorphic unit, used to study sediment transport and deposition in tidal marshes, is the catchment of a tidal creek system. A tidal creek catchment is defined as the marsh area that is flooded and drained by one tidal creek beginning at the marsh edge and branching into a dendritic creek system. A tidal creek catchment can then be considered as a quasi-closed system in which water and sediments circulate. However no real interfluves are present between adjacent creek catchments, so that minor fluxes of water and sediment may occur between adjacent catchments. The tidal creek catchment that was used for this study is situated on Figure 3.1. It has a surface area of 5.6 ha.

On the time-scale of single tidal cycles, the suspended sediment transport to and from a tidal marsh area has been estimated traditionally by measuring

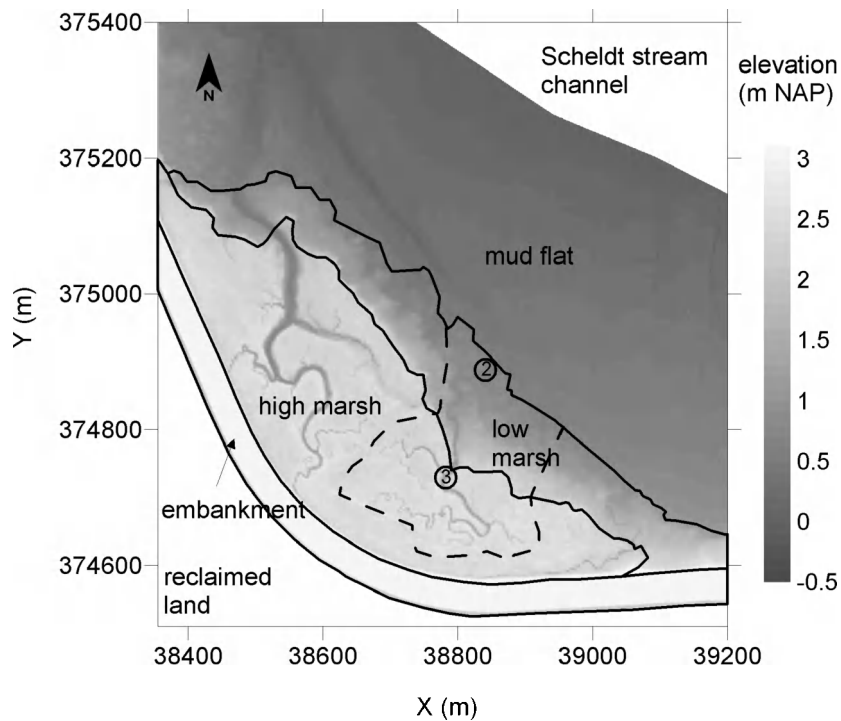


FIGURE 3.1. Digital elevation model (DEM) of the study area, the Paulina marsh, with indication of the high and low marsh. The broken line indicates the studied tidal marsh creek catchment. The automated measuring frames are indicated with the numbers 2 (for Frame 2) and 3 (for Frame 3).

suspended sediment discharges through the main tidal creek that floods and drains a tidal creek catchment (Settlemyre and Gardner, 1977; Boon, 1978; Ward, 1981; Reed *et al.*, 1985; Reed, 1987; 1988; French and Stoddart, 1992; Leonard *et al.*, 1995b). More recently, studies concentrated on the direct measurement of sediment deposition rates over single tidal cycles using sediment traps that were installed on the vegetated marsh platform (Reed, 1989; French *et al.*, 1995; Hutchinson *et al.*, 1995; Leonard, 1997; Christiansen *et al.*, 2000; Van Proosdij *et al.*, 2000). In this study, we used a combination of both methods within the same tidal creek catchment.

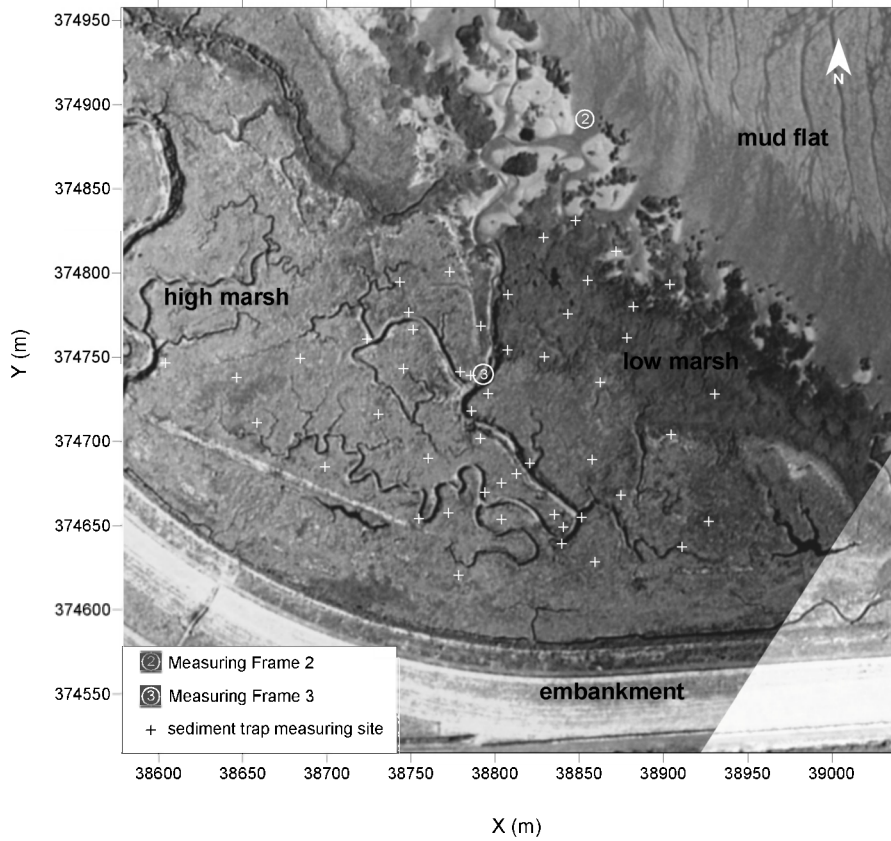


FIGURE 3.2. Aerial photograph of the studied tidal creek catchment, with indication of the location of measuring frames and the sediment trap measuring sites (aerial photograph provided by Rijkswaterstaat Meetkundige Dienst).

### 3.3.2. Measuring the spatial sedimentation pattern\*

Sedimentation rates were measured at 50 measuring sites well-distributed within the studied tidal creek catchment (see Fig. 3.2) using two methods depending on the time-scale of the measurements. First, sedimentation rates were measured over two spring-neap tidal cycles, the first from 05/08/2002 to 20/08/2002 and the second from 02/09/2002 to 16/09/2002, using plastic circular sediment traps. These traps were installed at each of the 50 measuring locations during neap tide and collected again at the following neap tide (15 days later) to determine the amount of deposited sediment. This method is described in detail in Temmerman *et al.* (2003b) (chapter 2).

Secondly, sedimentation rates were measured at the same 50 locations during four semi-diurnal inundation cycles (11 and 12/08/2002, and 10 and 11/09/2002). For this, filter paper traps were used, which were shown to be most accurate for measurements on the time-scale of one semi-diurnal tidal cycle (e.g. Reed, 1989; French *et al.*, 1995; Leonard, 1997). The filter papers (paper diameter = 15 cm) were first oven-dried for 24 h at 50° C and weighed without sediment. Next, they were attached to aluminium plates, which were on their turn fixed to the marsh surface just before and collected just after high tide. The filter papers were subsequently washed through to remove salts and again oven-dried for 24 h at 50° C and weighed to determine the amount of deposited sediment.

### 3.3.3. Modelling the spatial sedimentation pattern

In chapter 2, we showed that the spatial variations in sedimentation rates can be described by a relatively simple topography-based model (Temmerman *et al.*, 2003b):

$$SR = k \cdot e^{lH} \cdot e^{mD_c} \cdot e^{nD_e} \quad (3.1)$$

where  $SR$  = sedimentation rate ( $\text{g}/\text{m}^2$ ),  $H$  = elevation of the marsh surface (m relative to a certain reference level),  $D_c$  = distance from the nearest tidal creek (m) and  $D_e$  = distance from the marsh edge, measured along the nearest creek (m). The validity of this model, which was originally based on field data from 17 measuring sites (see chapter 2), is further tested here against the sedimentation measurements resulting from a network of 50 measuring sites. For each of the 50 sites, values for the model parameters  $H$ ,  $D_c$  and  $D_e$  were determined as follows. The elevation of the marsh surface  $H$  was surveyed in the field relative to local benchmarks (in m NAP) using an electronic total station (Sokkia SET5F). In this way, also the xy co-ordinates of each measuring site were surveyed relative to the Dutch xy co-ordinates system.

---

\* This work was done as part of the master thesis of Dirk Lauwaet (2003).

The parameters  $D_c$  and  $D_e$  were determined in a raster-based geographical information system (Idrisi) based on the xy polygon of the tidal creeks system, which was digitised from a geo-referenced aerial photograph, and using the nearest distance algorithms DISTANCE, COST and ALLOCATE in Idrisi (Eastman, 1994).

The observed sedimentation rates were used then to calibrate the model parameters  $k$ ,  $l$ ,  $m$  and  $n$ . First, in order to reduce the temporal variation between the different monitoring periods and to concentrate on the spatial variation between the 50 measuring sites, time-averaged sedimentation rates were calculated for the two spring-neap cycles, on the one hand, and for the four semi-diurnal cycles, on the other hand. Next, for both datasets a calibration and validation procedure was carried out. Each dataset, containing 50 sedimentation rate observations, was sorted from the lowest up to the highest measured sedimentation rate. Measuring locations with an even ranking number were used for calibration, locations with an uneven ranking number were used for validation. The calibration dataset was used to determine the appropriate values for the parameters  $k$ ,  $l$ ,  $m$  and  $n$  in eq. 3.1, using a multiple non-linear regression procedure in SAS (SAS Institute Inc., 1989). The resulting  $k$ ,  $l$ ,  $m$  and  $n$  values and the  $H$ ,  $D_c$  and  $D_e$  values for the measuring sites of the validation dataset were used then to calculate the sedimentation rates for each measuring site in the validation data set. Finally, these calculated sedimentation rates were compared with the observed sedimentation rates for model validation.

#### 3.3.4. Hydrodynamic measurements

As an essential input to run a hydrodynamic model, the vertical tidal movement of the water level has to be known for the study area. Furthermore, it is recommended to have data on the hydrodynamics in the study area, such as flow velocities and directions, to validate the model.

These field data were provided by an intensive field measuring campaign using a series of hydrodynamic measuring frames that were installed in the study area from 11 June to 2 October 2002 by the Netherlands Institute of Ecology – Centre for Marine and Estuarine Ecology (NIOO-CEME) in collaboration with WL | Delft Hydraulics (see Bouma *et al.* (submitted) for an overview of this measuring campaign). A distinction can be made between measuring frames that were installed in the tidal creeks entering the salt marsh and frames that were placed in the salt marsh vegetation. The first were used to monitor the movement of water and suspended sediments into and out of the tidal creeks system, while the latter set of measuring frames was installed to study the detailed hydrodynamics (tidal currents and wave propagation and damping) along transects within the submerged vegetation. In this study, the data gathered from the first set of measuring frames was processed and analysed with emphasis to the transport of suspended

sediments through the tidal creeks system in relation to the spatial sedimentation patterns we measured.

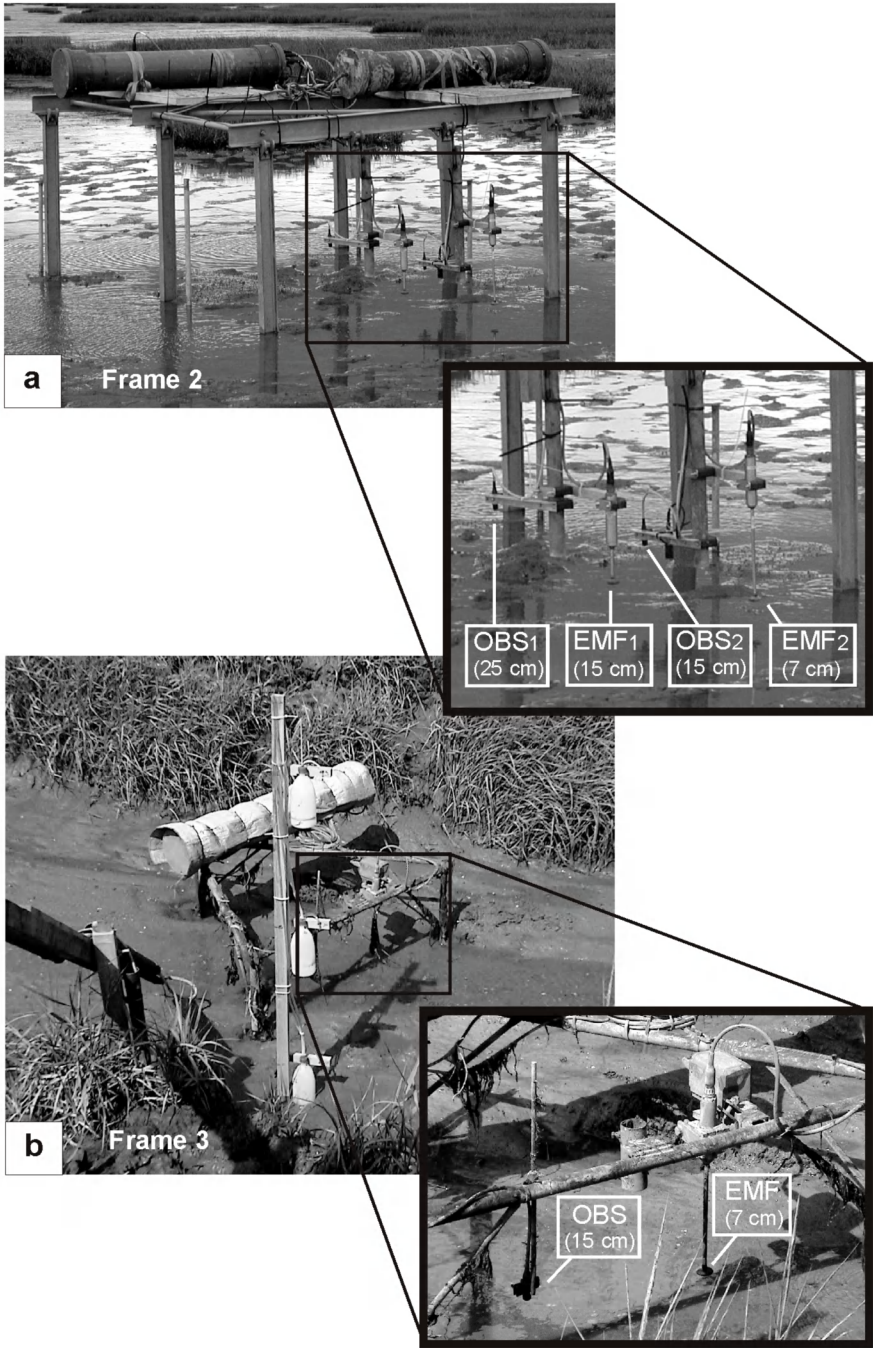
Figure 3.2 shows the location of these measuring frames (further named Frame 2 and 3) within the studied tidal creek catchment. Frame 2 was installed at the mouth of the main tidal creek at the edge between the tidal flat and the salt marsh, while Frame 3 was placed deeper into the creeks system at the border between the low and high marsh (Fig. 3.2). Both frames were equipped with (1) a pressure sensor, to measure the water level fluctuations due to the tide, (2) electro-magnetic flow meters (EMF), to measure variations in tidal currents, and (3) optical backscatter sensors (OBS), to measure turbidity (Fig. 3.3). The height of the different sensors above the local sediment surface is indicated on Figure 3.3. The frames were programmed so that data were sampled with a frequency of 4 Hz during 6 hours around high water (i.e. the time that the frames were submerged around high water) for the semi-diurnal tidal cycles from 11 June to 2 October 2002. The 4 Hz data files were processed to time-series of 1-minute averages and 15-minutes averages.

### 3.3.5. Measuring suspended sediment transport

Frames 2 and 3 were equipped with an OBS (Optical Back Scatter) sensor measuring the turbidity of the water column in FTU (Formazine Turbidity Units) with a frequency of 4 Hz. In order to calibrate the OBS data (in FTU) to suspended sediment concentrations (SSC; in  $\text{g l}^{-1}$ ), we installed an automatic water sampling station just next to Frame 3 (see e.g. Fig. 2.3 in chapter 2). The sampling station was equipped with an automatic water sampler (ISCO 6700) that pumped up 1 litre water samples near the OBS sensor of Frame 3 from 0.15 m above the bottom. The sampler was programmed so that for every semi-diurnal tidal cycle, one sample was taken at flood tide when the water level exceeded the level of 0.5 m above the creek bottom. For the four semi-diurnal cycles, that were sampled in detail with the filter paper sediment traps (see above), additional water samples were taken during the whole inundation cycle with a time interval of 30 minutes until the study area was no longer submerged.

---

*FIGURE 3.3. Photographs showing the automatic measuring frames operated by the Netherlands Institute of Ecology and WL | Delft Hydraulics at low tide: (a) Frame 2 at the creek mouth and (b) Frame 3 within the creek. In the insets, details of the EMF (Electro Magnetic Flowmeter) and OBS (Optical Back Scatter) sensors are shown, with indication of their height above the bottom. For Frame 2, only data of EMF2 and OBS2 were used in this study.*



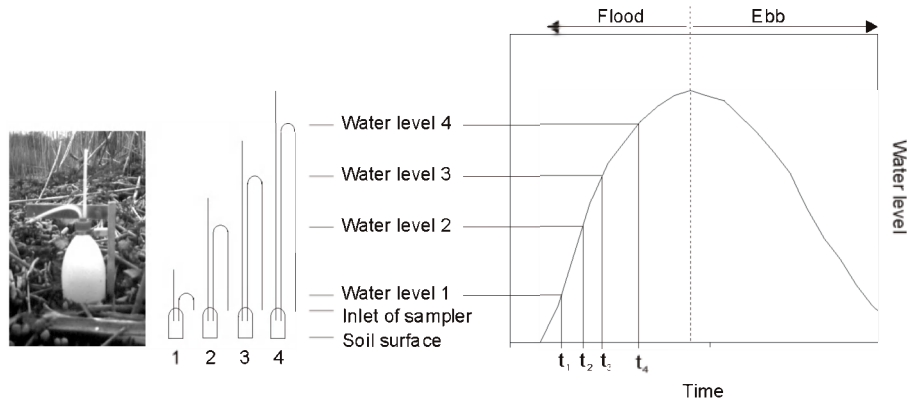


FIGURE 3.4. Schematic illustration of setup of siphon samplers used to sample water at different points in time during flood at Frame 2. Bottle 1 is filled at time  $t_1$ , when the water level exceeds level 1; bottle 2 is filled at time  $t_2$ , when the water level exceeds level 2; etc.

For Frame 2, no automatic water sampling station, such as placed next to Frame 3, could be installed for practical reasons. Instead, siphon samplers were used here. These are 1 litre bottles with siphon tubes as inlets: during each of the four semi-diurnal tidal cycles, a set of four siphon samplers was installed so that the samplers filled at different points in time during the flood (see Fig. 3.4).

The SSC in all collected water samples was determined by filtering the samples with pre-weighted filter papers (pore diameter =  $0.45 \mu\text{m}$ ), which were subsequently washed through with de-ionized water to remove salts and then oven-dried for 24 h at  $50^\circ \text{C}$  and reweighed. The resulting SSC data (in  $\text{g l}^{-1}$ ) were then correlated to the 1-minute averaged OBS data (in FTU) gathered from the measuring frames. In this way, the OBS data could be calibrated from FTU to  $\text{g l}^{-1}$ .

### 3.3.6. Analysing water and sediment balances

Although no direct field observations of the two-dimensional flow and sediment transport pattern are available, the following analysis of the field data allows to gain some insight in the transport pathways of water and suspended sediment and especially in the role of the tidal creeks system in supplying water and sediments to the marsh surface. Based on the flow velocity ( $u$  in  $\text{m s}^{-1}$ ) and water level ( $h$  in m) measurements, the total water volumes discharged through the creeks system during flood ( $V_F$ ) and ebb ( $V_E$ ) (in  $\text{m}^3$ ) were calculated as:

$$V_F = \int_F u \cdot A(h) \cdot dt \quad (3.2)$$

and

$$V_E = \int_E u \cdot A(h) \cdot dt \quad (3.3)$$

where  $A(h)$  is the wet cross-section (in  $m^2$ ) at time  $t$ , which is a function of the water level  $h$  at time  $t$ . For Frame 3 a detailed survey of the creek cross-section was carried out, so that the wet cross-section  $A(h)$  could be calculated at any time  $t$  from the water level  $h$ . At Frame 3, the creek has a wet cross-section of *ca.*  $4.5 m^2$  at the moment of bankfull water level. At the location of Frame 2, however, no clear incised creek is present (see Fig. 3.1 and Fig. 3.2). Therefore, for Frame 2 the wet cross-section was calculated as:  $A(h) = 7h$ . A factor 7 was used, since this is the width (in m) of the creek where it becomes more and more incised at a few tens of meters behind the creek mouth at Frame 2 (see Fig. 3.1 and 3.2).

Next, the calculated  $V_F$  and  $V_E$  values were compared with the total water volume  $V_{HW}$  stored at high tide above the marsh surface. This water volume  $V_{HW}$  was calculated in a raster-based Geographical Information System (Idrisi) based on a 1 by 1 m resolution Digital Elevation Model of the study area that was computed from laser altimetry data of Rijkswaterstaat Meetkundige Dienst (Fig. 3.1; see chapter 4 for more details on these elevation data). It was assumed that the water surface was horizontal at high tide, which is a realistic assumption for such a small study area. For Frame 2, which is situated at the seaward marsh edge,  $V_F$  and  $V_E$  were compared with  $V_{HW}$  calculated for the whole tidal creek catchment, while for Frame 3, which is situated at the edge between the low and high marsh surface,  $V_{HW}$  was calculated only for the high marsh surface situated within the studied tidal creek catchment (see Fig. 3.1).

A similar exercise was done for the total amount of suspended sediment transported through the creeks system and deposited on the marsh platform. The first was calculated as follows:

$$TSS_F = \int_F u \cdot A(h) \cdot C \cdot dt \quad (3.4)$$

and

$$TSS_E = \int_E u \cdot A(h) \cdot C \cdot dt \quad (3.5)$$

where  $TSS_F$  and  $TSS_E$  are the total suspended sediment mass transported through the creek during flood and ebb respectively, and  $C$  is the suspended sediment concentration (SSC in  $\text{g l}^{-1}$ ) at time  $t$  measured at both measuring frames. The net import or export of suspended sediment over one semi-diurnal tidal cycle was then calculated as:

$$TSS_{net} = TSS_F + TSS_E \quad (3.6)$$

For Frame 2, reliable SSC data were only available for the semi-diurnal tidal cycles of 11 and 12/08/2002 (see above), so that  $TSS_{net}$  values could be calculated only for these two tidal cycles.

Next, the total suspended sediment mass that was deposited on the marsh surface ( $TSS_{dep}$ ) was calculated from the 50 sedimentation rate measuring sites using three methods: (1) by calculation of the arithmetic mean sedimentation rate and multiplying it with the surface area; (2) by spatial interpolation using conventional 2-dimensional kriging (see also French *et al.*, 1995); (3) by spatial implementation of the topography-based regression model (eq. 3.1) (see also chapter 2 Fig. 2.10). For all three methods, the surface area occupied by tidal marsh creeks was excluded so that the calculated  $TSS_{dep}$  values only apply for the vegetated marsh platform. The calculations were performed separately for the high and low marsh part of the tidal creek catchment, so that the calculated  $TSS_{dep}$  values could be compared with the  $TSS_{net}$  values calculated for Frame 2 (at the marsh edge, so to be compared with  $TSS_{dep}$  for the whole catchment) and Frame 3 (at the border between low and high marsh, so to be compared with  $TSS_{dep}$  for the high marsh part of the catchment).

TABLE 3.1. *P*-values resulting from *t*-tests comparing (1) sedimentation rates on the high marsh versus sedimentation rates on the low marsh; (2) sedimentation rates on natural levees versus sedimentation rates in basins.

	monitoring period					
	spring-neap cycles		semi-diurnal cycles			
	05-20/08	02-16/09	11/08	12/08	10/09	11/09
(1) high versus low marsh	<0.01	<0.01	<0.01	<0.01	<0.01	<0.01
(2) levees versus basins	<0.01	<0.01	0.16	<0.01	<0.01	0.26

TABLE 3.2. P-values resulting from (1) a t-test comparing sedimentation rates measured during the two spring-neap cycles and (2) ANOVA comparing sedimentation rates measured during the four semi-diurnal cycles.

	P-value
(1) comparison of two spring-neap cycles	0.06
(2) comparison of four semi-diurnal cycles	0.77

### 3.4. Results and discussion

#### 3.4.1. Spatial and temporal variations in sedimentation rates

The results of the sedimentation rate measurements on the 50 measuring sites are shown in Figure 3.5. The spatial sedimentation pattern is primarily determined by much higher sedimentation rates on the low than on the high marsh, both for the two spring-neap tidal cycles and for the four semi-diurnal tidal cycles. In addition, on the high marsh, sedimentation rates were generally higher on levees just next to the tidal creeks compared to basins at a farther distance from the creeks (Fig. 3.5). Statistical t-tests on the log-transformed data showed that this difference between the high and low marsh, on the one hand, and between the levees and basins, on the other hand, is significant for most measuring periods (Table 3.1).

Figure 3.5 further indicates that temporal variations in sedimentation rates exist between the measuring periods. However, t-tests and ANOVA on the log-transformed data showed that these temporal differences between the two spring-neap tidal cycles and between the four semi-diurnal tidal cycles are not significant at a significance level of 5 % (Table 3.2). Variations in tidal inundation height and duration are the most important factors that determine temporal variations in tidal marsh sedimentation rates in the Scheldt estuary (Temmerman *et al.*, 2003b; see chapter 2). However, for this study we chose measuring periods that were very comparable in terms of tidal inundation regime (see below, Fig. 3.8), since it was not our aim to gather data on *temporal* variations in sedimentation but on the detailed *spatial* sedimentation pattern.

#### 3.4.2. Modelling the spatial sedimentation pattern

Table 3.3 presents the results of the calibration of the topography-based model (eq. 3.1) using the observed spatial sedimentation patterns. Both for the spring-neap cycles and for the semi-diurnal cycles, the calibration resulted in a very good agreement between observed and predicted

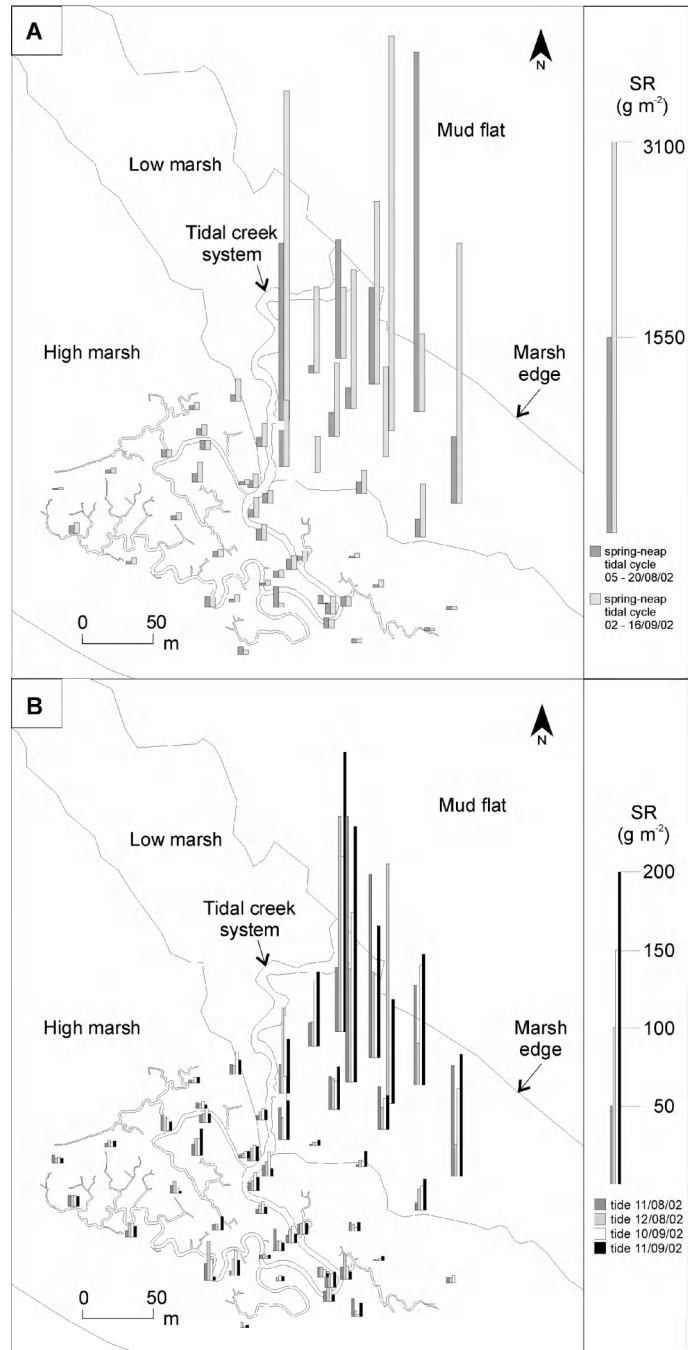


FIGURE 3.5. The spatial sedimentation pattern measured over (a) two spring-neap cycles and (b) four semi-diurnal tidal cycles.

TABLE 3.3. Model parameters ( $k, l, m, n$ ) and  $R^2$ -values resulting from calibration of the topography-based model (eq. 1). Calibration run 1:  $H, D_c$  and  $D_e$  determined from GIS analyses; Calibration run 2: *idem*, but  $D_c$  and  $D_e$  are set to zero for measuring sites for which  $D_c > 40$  m (see text for more details).

calibra- tion run	data set	$k$	$l$	$m$	$n$	$R^2$
1	spring-neap	301.4	-0.4935	0.0344	-0.0023	0.94
	semi-diurnal	1609.5	-3.7115	0.0026	0.0086	
2	spring-neap	1067.0	-0.2174	-0.0102	-0.0080	0.69
	semi-diurnal	281.1	-1.2659	-0.0417	-0.0022	

sedimentation rates ( $R^2 = 0.94$  in both cases; see calibration run 1 in Table 3.3). However, for the validation dataset the correspondence between observed and predicted sedimentation rates is very poor ( $R^2 = 0.51$  and  $<0.01$ , respectively). Furthermore, the calibration resulted, illogically, in a positive  $m$  value for the spring-neap calibration dataset and in positive  $m$  and  $n$  values for the semi-diurnal dataset (Table 3.3). These positive values indicate that sedimentation rates would increase with increasing distance  $D_c$  from the tidal marsh creeks and increasing distance  $D_e$  from the marsh edge. This is in contradiction with Figure 3.5 and the statistical t-tests summarised in Table 3.1, which indicated that sedimentation rates on the high marsh are significantly higher on measuring sites just next to tidal creeks than on sites farther away from creeks. The reason why the regression analysis resulted in positive  $m$  and  $n$  values is because the highest sedimentation rates were observed for measuring sites on the low marsh, although these sites are located at the largest distance from tidal creeks (see Fig. 3.5). However, the high sedimentation rates on the low marsh are due to the low surface elevation. On the low marsh no dense tidal creek system has developed as on the high marsh and therefore the influence of surface elevation on the sedimentation rates is more important than the influence of the tidal creeks system.

Therefore a threshold distance  $D_c$  was introduced: once  $D_c > 40$  m we can say that the influence of the tidal creeks and the marsh edge is negligible relative to the influence of the marsh surface elevation. This was modelled by setting  $D_c$  and  $D_e$  to zero for measuring sites for which  $D_c$  was larger than 40 m. This resulted in positive  $m$  and  $n$  values, both for the spring-neap and semi-diurnal dataset (Table 3.3). Predicted versus observed sedimentation rates are plotted in Figure 3.6. Both for the spring-neap and semi-diurnal calibration and validation datasets, an acceptable match between predicted and observed sedimentation rates is obtained ( $R^2$  values ranging from 0.87 to 0.62). It can be concluded then that the relatively simple topography-based regression model is able to reproduce quite well the observed spatial sedimentation pattern at the Paulina marsh.

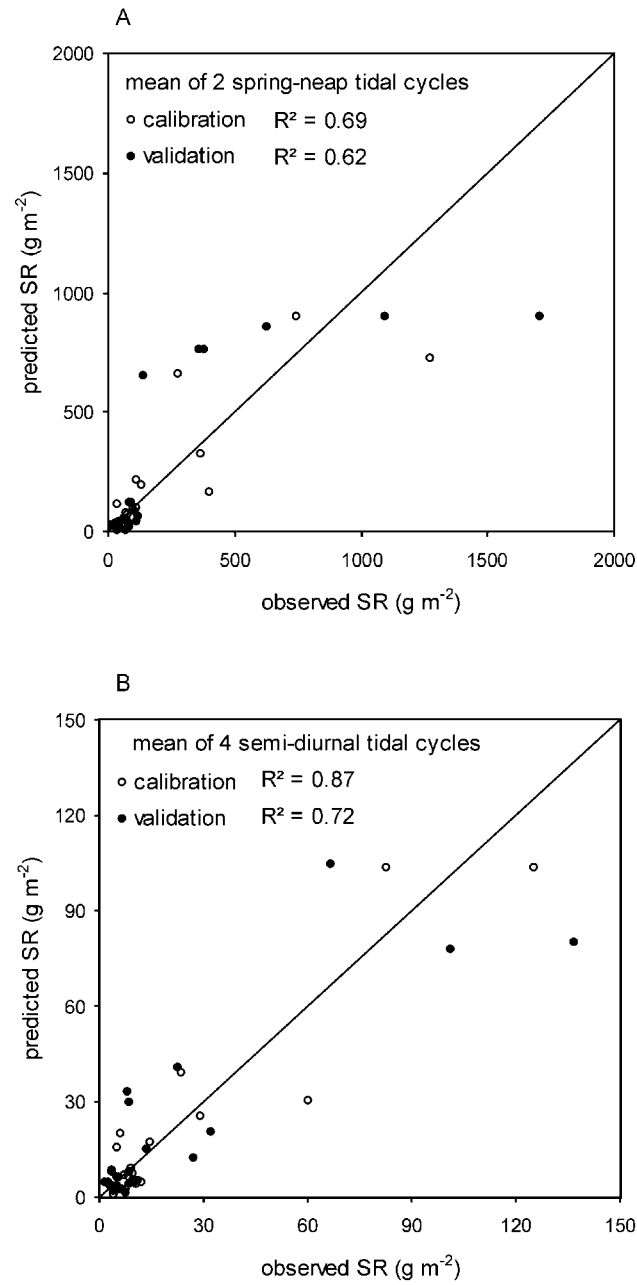


FIGURE 3.6. Observed versus predicted sedimentation rates (SR) using the topography-based model (eq. 3.1). Calibration and validation results are presented (a) for the mean dataset of the two spring-neap tidal cycles, and (b) for the mean dataset of the four semi-diurnal tidal cycles.

### 3.4.3. Tidal creek hydrodynamics

The results of the hydrodynamic measurements at Frame 2 and 3 are presented in the Figures 3.7 and 3.8 for the two spring-neap tidal cycles that were sampled in detail. Figure 3.8 shows that for both measuring periods the tidal inundation regime was very comparable. A number of characteristic flow patterns can be determined, which are very typical for tidal marshes and which should be simulated properly when applying a hydrodynamic model for the study area.

First, at the time-scale of one semi-diurnal tidal cycle, the tidal water movement in the study area is characterised by a clear tidal asymmetry both in the water level and in the flow velocity fluctuations (Fig. 3.7): the rising tide is considerably shorter than the falling tide, the first with faster vertical change of the water level and higher maximum flow velocities. When looking at the time-scale of a spring-neap tidal cycle, this pattern of tidal asymmetry is repeated systematically for every semi-diurnal tidal cycle, although maximum flow velocities are highest during spring tides and lowest during neap tides (Fig. 3.8).

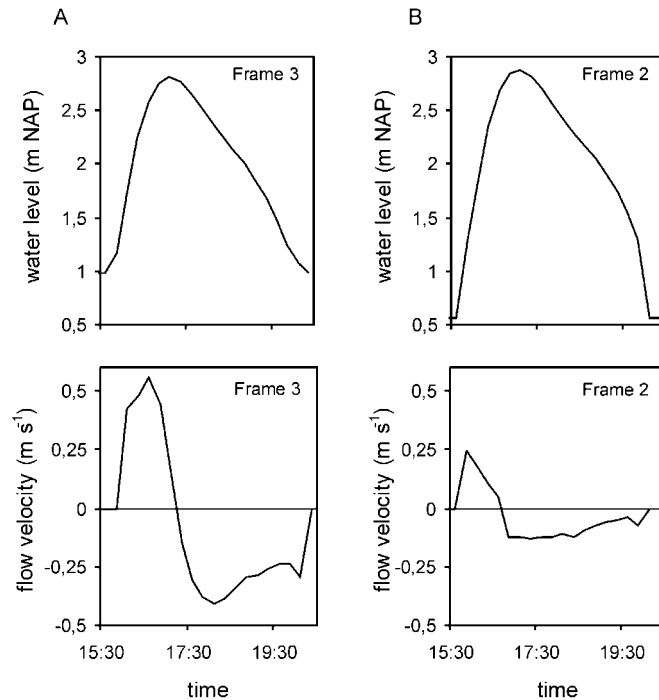


Figure 3.7. Example of the temporal variation in water level and flow velocity measured during one semi-diurnal tidal inundation cycle (11/08/2002) at (a) Frame 3 and (b) Frame 2.

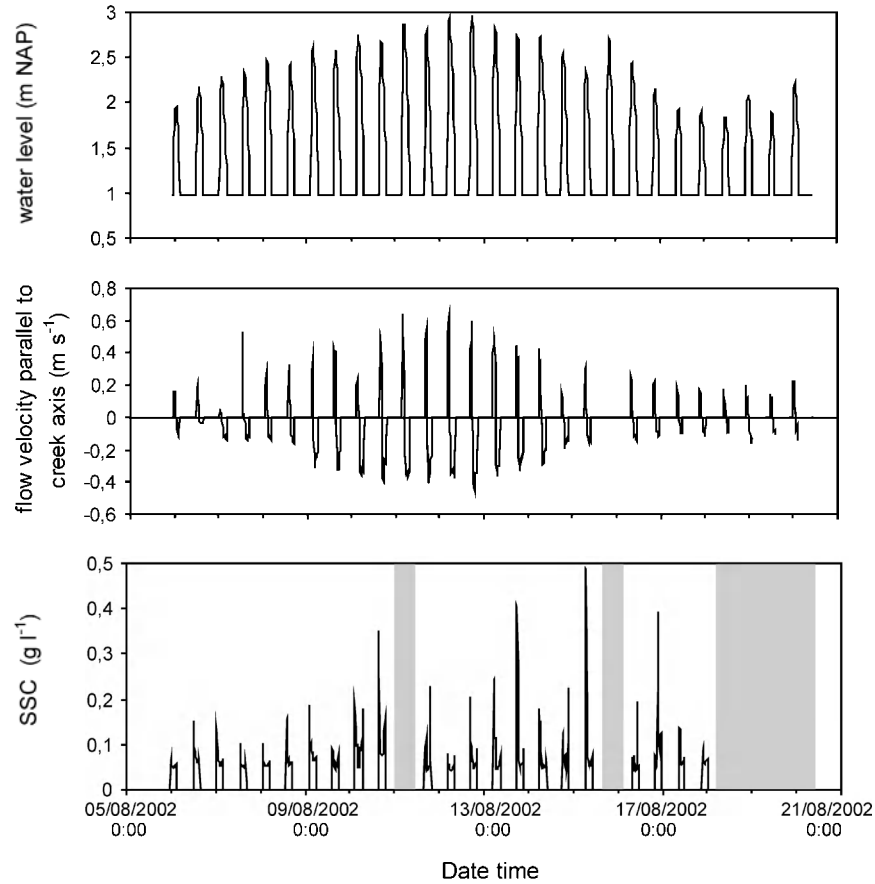


FIGURE 3.8a (to be continued)

For Frame 3 a clear distinction can be made between neap tides, which do not overtop the creek banks at the high marsh (these are called under-marsh tides; Allen, 2000), and spring tides, which largely overtop and flood the high marsh surface (called over-marsh tides). During over-marsh (spring) tides, marked flow velocity pulses were observed at the moment of flooding and draining of the marsh platform, while these velocity pulses were absent during under-marsh (neap) tides (Fig. 3.9; see also Bouma *et al.*, submitted). Such over-marsh velocity pulses are widely reported from tidal flow studies in salt marsh creeks (e.g. Bayliss-Smith *et al.*, 1979; Healey *et al.*, 1981; Dankers *et al.*, 1985; Reed *et al.*, 1985; Reed, 1989; Stoddart *et al.*, 1989;

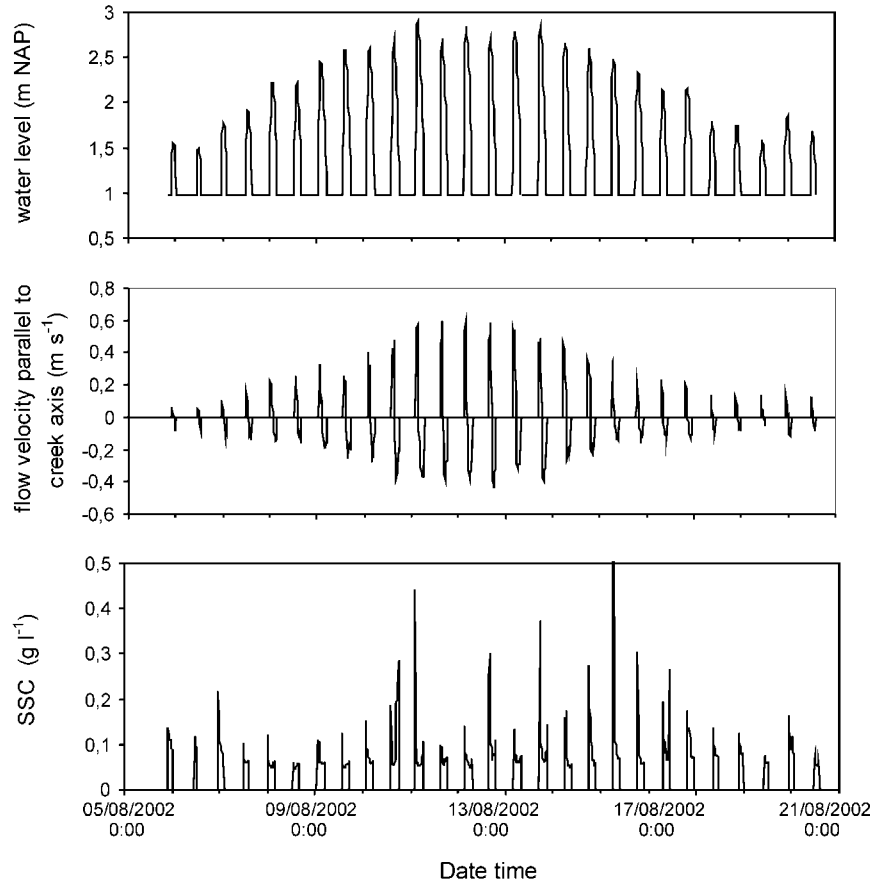


FIGURE 3.8b (to be continued)

French and Stoddart, 1992) and are explained by the sudden increase in the volume of water that needs to be transported through the tidal marsh creeks, at the moment that the water level changes from under-marsh to over-marsh water levels and consequently the whole marsh platform is flooded (Pethick, 1980; Allen, 1994). For Frame 2 at the marsh edge, these velocity pulses were not observed, because no clear incised creek is present here (see Fig. 3.1 and Fig. 3.2). As a consequence, the surrounding marsh platform is not flooded from a creek and no velocity pulses occur.

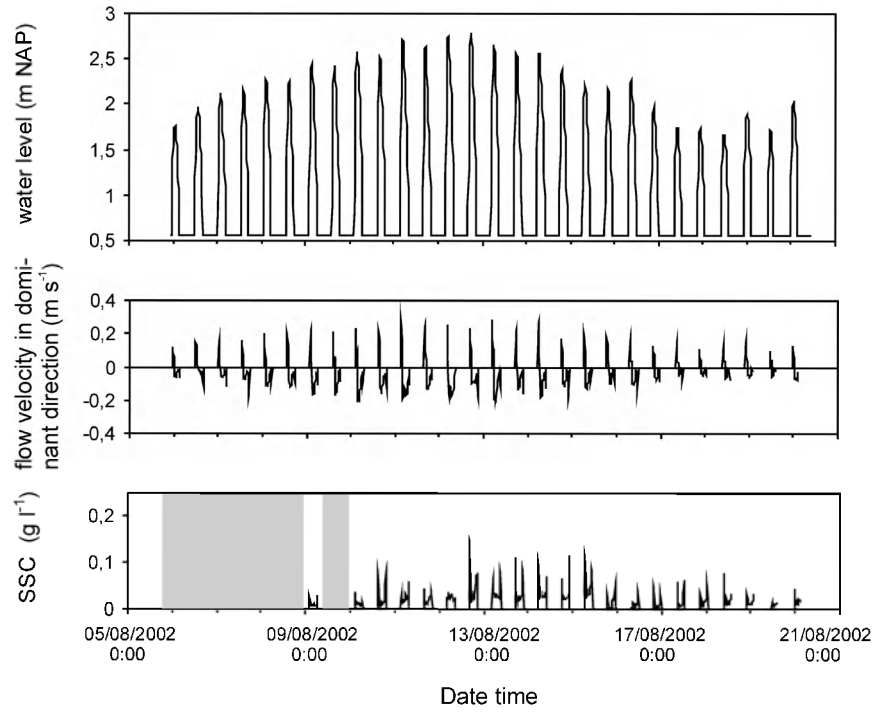


FIGURE 3.8c (to be continued)

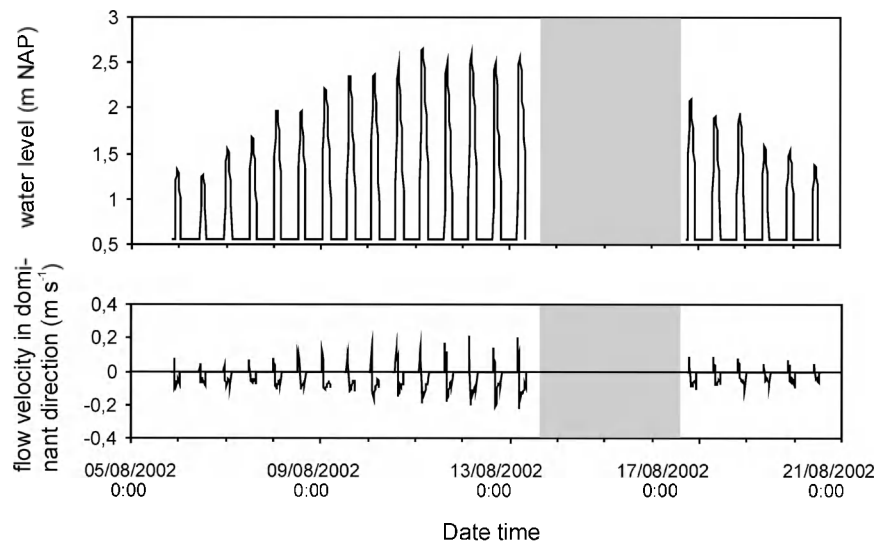


FIGURE 3.8d (to be continued)

FIGURE 3.8. Time-series of water level, flow velocity, and suspended sediment concentration (SSC), recorded at (a,b) Frame 3 and (c,d) Frame 2 during two spring-neap tidal cycles (the first from 5 to 20/08/2002 and the second from 2 to 16/09/2002). Time periods during which the measuring equipment failed are indicated in grey (see text for details).

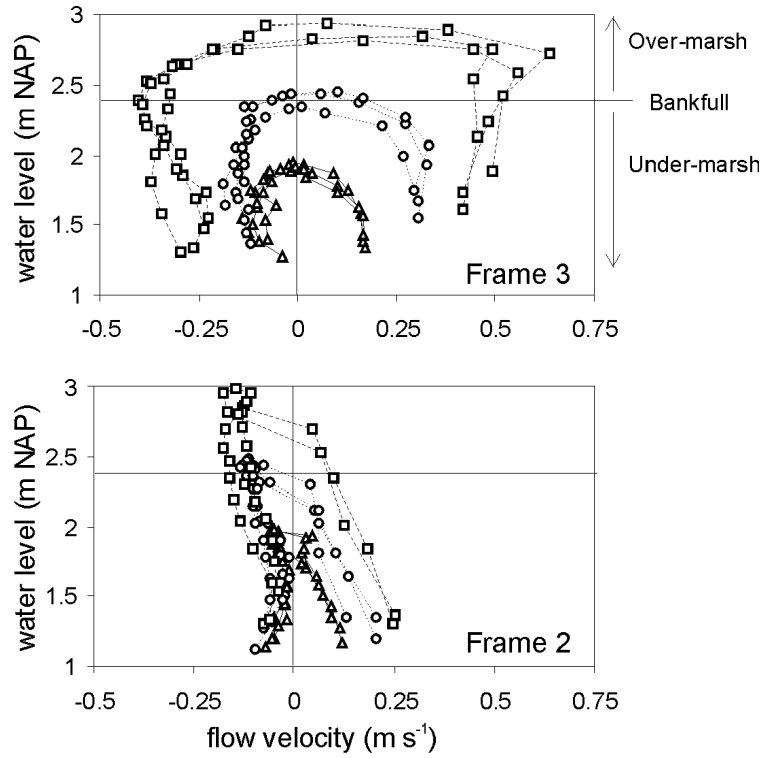


FIGURE 3.9. Water level-flow velocity curves for (a) Frame 2 and (b) Frame 3 for a number of under-marsh, bankfull and over-marsh tides. Bankfull level is defined as the level of the high marsh surface.

### 3.4.4. Suspended sediment concentrations

The results of the correlation between the OBS data (in FTU) and the SSC data (in  $\text{g l}^{-1}$ ) measured at Frame 2 and 3 are presented in Figure 3.10. For Frame 3 a large number of suspended sediment samples was available from the ISCO sampler, so that a series of samples could be selected that covered the whole measuring period from August to September and that ranged from the lowest ( $0.03 \text{ g l}^{-1}$ ) to the highest ( $0.97 \text{ g l}^{-1}$ ) measured SSC values. In this way, a good calibration curve could be obtained for Frame 3 (Fig. 3.10). However, for Frame 2, only 16 sediment samples could be taken with the siphon samplers, four samples during each of the four semi-diurnal tidal cycles that were sampled in detail. Furthermore, the measuring equipment of Frame 2 failed during the last two semi-diurnal cycles (10 and 11/09/2002), so that no OBS data were recorded for this period and only 8 samples remained for the calibration. Figure 3.10 shows that no good spreading of SSC values could be obtained, which makes the calibration of the OBS data of Frame 2 more uncertain.

Figure 3.8 shows the resulting SSC time-series at Frame 2 and 3. Gaps in the time-series are frequently occurring. For Frame 3, this is due to algae growth on the OBS sensor during certain periods, which resulted in incorrect extremely high OBS signals and SSC values. These erroneous SSC values ( $> 1.5 \text{ g l}^{-1}$ ) were filtered out of the data series. For Frame 2, algae growth was not the major problem, but the inaccurate calibration of the OBS sensor resulted for some periods in negative or unrealistically high SSC values.

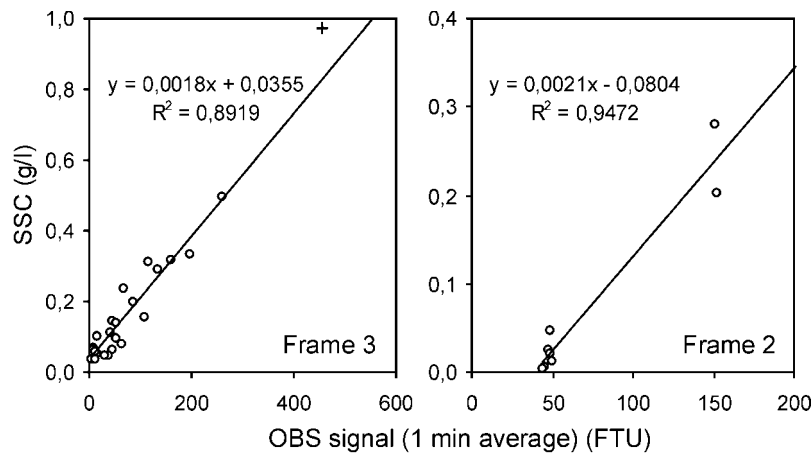


FIGURE 3.10. Correlation between suspended sediment concentration (SSC in  $\text{g/l}$ ) and Optical Back Scatter (OBS) signal (in FTU) measured at 0.15 m above the bottom at Frame 3 and Frame 2. (The outlier data point for Frame 3, indicated with a cross, was not taken into account for the regression analysis.)



### 3.4.5. Flow paths of water and suspended sediment

A general insight in the flow paths within the study area is provided by comparing the calculated water volumes  $V_F$  and  $V_E$  (eqs. 3.2 en 3.3) and net sediment mass  $TSS_{net}$  (eqs. 3.4; 3.5 and 3.6) discharged through the creeks system with the total water volume  $V_{HW}$  stored at high tide above the marsh surface and total sediment mass  $TSS_{dep}$  deposited on the marsh surface.

The comparison between  $V_F$  and  $V_E$ , on the one hand, and  $V_{HW}$ , on the other hand, is presented for Frame 2 and 3 in Figure 3.12a and b, respectively. For Frame 3,  $V_F$  and  $V_E$  are very comparable to  $V_{HW}$  for under-marsh tides and also for over-marsh tides, which flood the high marsh platform to a maximum inundation height of about 0.2 m. This means that for these tidal cycles the tidal creeks system accounts for *ca.* 100 % of the total water volume transported to and from the high marsh surface. Once this “threshold” inundation height of 0.2 m is exceeded, the percentage of water supplied through the creeks system progressively decreases with increasing high water level and the exchange of water across the marsh edge becomes more and more important. Furthermore,  $V_F$  and  $V_E$  are for all tidal cycles in the same order of magnitude, indicating that for the high marsh the water follows the same transport pathways during flood and ebb.

For Frame 2 this is not the case. For all tidal cycles,  $V_F$  is considerably lower than  $V_E$ , suggesting that there is a net export of water over single tidal cycles. Furthermore, both  $V_F$  and  $V_E$  differ from  $V_{HW}$ . It is clear then that the supply of water to and from the low marsh surface does not take place at Frame 2 only, but since no clear incised creek is present at the marsh edge, the exchange of water will take place through the entire length of the marsh edge.

The results of the sediment flux calculations are presented in Tables 3.4 and 3.5. The total deposited sediment masses  $TSS_{dep}$  are in the same order of magnitude for the three calculation methods that were used, although kriging resulted in a slightly higher estimation of  $TSS_{dep}$  than the other two methods (spatial implementation of the topography-based model (eq. 3.1) and calculation of the product of the mean sedimentation rate and the surface area) (Table 3.4). During the four semi-diurnal cycles that were monitored, 1.09 to 1.69 tonnes of dry sediment were deposited per semi-diurnal cycle

---

FIGURE 3.12. (a) Comparison of calculated water volumes discharged through the creeks system during flood ( $V_F$ ) and ebb ( $V_E$ ) at Frame 2 and calculated water volume stored at high tide ( $V_{HW}$ ) above the entire studied tidal creek catchment. (b) Comparison of  $V_F$  and  $V_E$  calculated for Frame 3 and  $V_{HW}$  calculated for the high marsh surface.

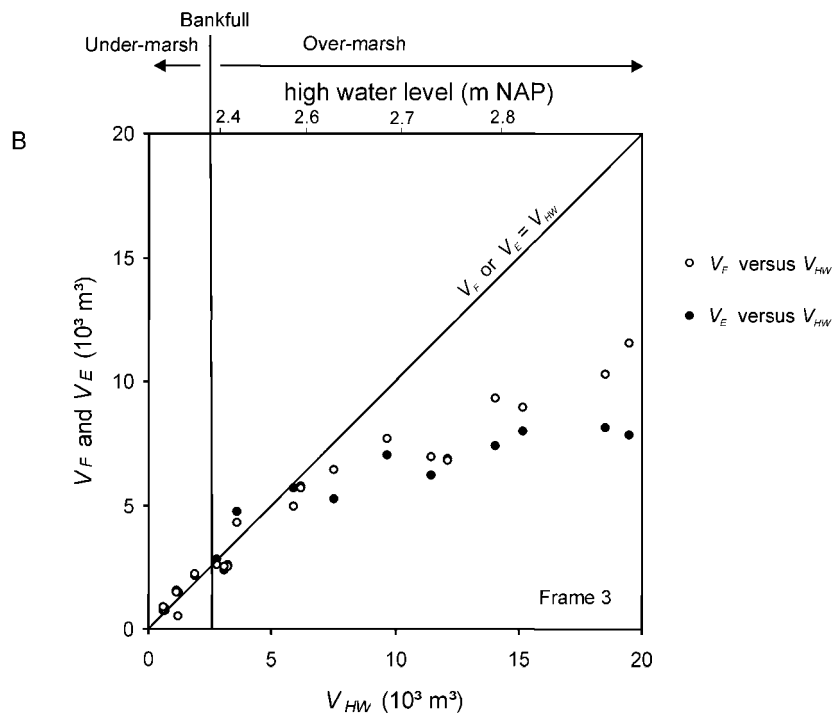
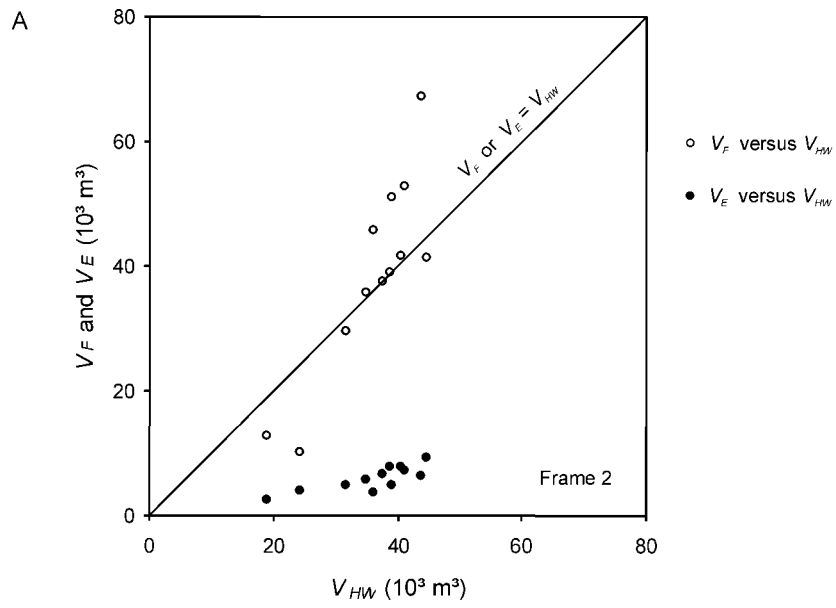


TABLE 3.4. Total suspended sediment mass ( $TSS_{dep}$  in tonnes dry weight) deposited in the studied tidal creek catchment (surface area = 5.6 ha), calculated using three methods: (1) mean = calculated as the arithmetic mean of the 50 measuring sites multiplied with surface area; (2) kriging = calculated by kriging based on the 50 measuring sites; (3) model = calculated by spatial implementation of the topography-based model (eq. 3.1).

		monitoring period					
		spring-neap cycles		semi-diurnal cycles			
method	marsh area*	05-20/08	02-16/09	11/08	12/08	10/09	11/09
mean	L	13.74	21.36	1.06	0.84	1.02	1.44
	H	1.70	2.24	0.19	0.25	0.26	0.19
	L+H	15.44	23.60	1.25	1.09	1.28	1.64
kriging	L	22.91	22.24	1.21	1.10	1.43	1.98
	H	1.72	2.83	0.21	0.25	0.27	0.26
	L+H	24.63	25.07	1.43	1.36	1.69	2.23
		mean of spring-neap cycles		mean of semi-diurnal cycles			
model	L	19.52		1.23			
	H	1.29		0.11			
	L+H	20.82		1.34			

\* L = low marsh; H = high marsh; L+H = low + high marsh.

TABLE 3.5. Total suspended sediment mass (in tonnes dry weight) transported through the tidal creeks system during flood ( $TSS_F$ ), ebb ( $TSS_E$ ) and net ( $TSS_{net}=TSS_F+TSS_E$ ), calculated for Frame 3 (for the high marsh only) and Frame 2 (for the low and high marsh). Positive values indicate an import of suspended sediments, while negative values indicate that suspended sediments are exported. The creek cross-section at Frame 3 is ca. 4.5 m<sup>2</sup> at bankfull water level. At Frame 2 there is no clear creek incision.

			monitoring period					
			spring-neap cycles		semi-diurnal cycles			
frame	area*	$TSS$	05-20/08	02-16/09	11/08	12/08	10/09	11/09
3	H	$TSS_F$	8.150	8.400	0.785	0.772	0.989	0.541
		$TSS_E$	-5.605	-5.853	-0.542	-0.481	-0.626	-0.287
		$TSS_{net}$	2.545	2.546	0.243	0.291	0.363	0.254
2	L+H	$TSS_F$			0.007	0.007		
		$TSS_E$			-0.033	-0.087		
		$TSS_{net}$			-0.026	-0.080		

\* H = high marsh; L+H = low + high marsh.

within the studied tidal creek catchment, while during each of the two spring-neap cycles, 15 to 25 tonnes dry sediment were deposited. For frame 3, a net import of suspended sediments  $TSS_{net}$  through the creeks system was calculated for all monitoring periods (Table 3.5). Comparison of Tables 3.4 and 3.5 shows that the  $TSS_{net}$  values at Frame 3 are higher than the  $TSS_{dep}$  values for the high marsh platform, both for the two spring-neap cycles and for the four semi-diurnal cycles. This difference between  $TSS_{net}$  and  $TSS_{dep}$  may to some extent reflect deposition within the creek system (e.g. French and Stoddart, 1992). However, measuring errors may also be involved:  $TSS_{net}$  was estimated using SSC measurements at 0.15 m above the creek bottom. Sediment concentrations at this level are probably higher than sediment concentrations in the water actually flooding the marsh surface. Nevertheless, the fact that  $TSS_{net}$  values are not lower but higher than  $TSS_{dep}$  values in all cases, seems to suggest that the creeks system serves as an important sediment transport pathway to the high marsh platform.

For Frame 2, again a different situation is observed. Here, a net export of suspended sediments from the marsh was measured (Table 3.5). However, the exported sediment masses are small (0.026 and 0.080 tonnes per semi-diurnal cycle) compared to the total sediment masses deposited in the tidal creek catchment (1.09 to 1.43 tons per semi-diurnal cycle). This indicates again that tidal exchange of suspended sediments takes place through the entire length of the marsh edge and not only at Frame 2.

### 3.5. Conclusions

This study presented the collection of high-resolution field data on hydrodynamics and suspended sediment transport and deposition during single tidal cycles within a small tidal marsh creek catchment:

(1) Measurements of the detailed spatial sedimentation pattern showed that sedimentation rates decrease with increasing marsh surface elevation and increasing distance from the seaward marsh edge and from tidal creeks. Based on these three topographic variables, the spatial variations in sedimentation rates can be explained by a relatively simple topography-based multiple regression model. However, on the young marsh surface, sedimentation rates are primarily controlled by surface elevation alone.

(2) Hydrodynamic measurements in the main tidal creek that enters the studied marsh showed that the tidal flow through the creeks system is characterised by a marked flood-ebb asymmetry and the occurrence of flow velocity pulses associated with over-marsh tides, which flood the surrounding marsh platform. At the mouth of the creeks system, no such velocity pulses were observed since no clear creek incision is present at the marsh edge where the creek spreads out over the adjacent tidal flat.

(3) For the low marsh near the seaward marsh edge, the exchange of water and suspended sediments during tidal inundation takes place through the entire length of the marsh edge, since no clear incised tidal creeks system is present on the low marsh. On the high marsh a dense tidal creeks system has developed, which serves as the primary transport pathway of water and suspended sediments to and from the high marsh platform. For tidal cycles that exceed an inundation height of 0.2 m at the high marsh, the supply of water through the marsh edge and over the marsh surface becomes more and more important with increasing high water level of the tidal cycles.

The presented dataset further allows the calibration and validation of hydrodynamic models to simulate and improve our understanding of the transport and deposition of suspended sediments in tidal marshes. This is done in the following chapter.

## Chapter 4

# Simulating spatial patterns of sediment transport and deposition in tidal marshes using a hydrodynamic modelling approach

---

### 4.1. Introduction

Over the last few decades, we have seen the development of sophisticated hydrodynamic models that allow to compute the movement of water over complex surfaces (see e.g. Hervouet and Van Haren, 1996 for a review). These models were originally developed for engineering studies, in order to simulate for example water flow around constructions such as bridges and jetties or through pipes. Recent years have witnessed the growing application of commercial and academic hydrodynamic modelling software in environmental sciences such as geomorphology (Lane, 1998). Hydrodynamic modelling has been used to study flow and sediment transport processes in a large range of geomorphic systems such as river channels (e.g., Lane and Richards, 1998; Booker *et al.*, 2001) and estuaries (e.g., French and Clifford, 2000). It has been shown to be a useful tool since complex flow and sediment transport patterns can be studied in two or three dimensions and at high spatial and temporal resolutions that can hardly be reached in field studies.

In this respect, hydrodynamic modelling offers a high potential to improve our understanding of key processes that determine the transport and deposition of suspended sediments during tidal inundation of tidal marshes. Although until present hydrodynamic models were not applied to tidal marshes, they were recently quite extensively implemented to simulate inundation and sedimentation processes in alluvial floodplains (e.g. Gee *et al.*, 1990; Bates *et al.*, 1992; 1996; 1998; Hardy *et al.*, 2000). Given the geomorphic analogy between alluvial floodplains and tidal marshes (the latter can actually be considered as floodplains periodically flooded by the tide), the results of these floodplain modelling studies provide an interesting basis for the application of hydrodynamic models in tidal marsh environments. Analogous to the hydrodynamic modelling of floodplain inundation and sedimentation processes, suitable hydrodynamic models need to represent tidal marsh processes in an appropriate way and therefore need to fulfil a number of criteria:

- (1) Flow and transport processes need to be modelled in two or three dimensions, to capture the spatial variability of tidal marsh processes.
- (2) Temporal changes in flow fields have to be simulated dynamically with a high temporal resolution. Special attention should be given to the fact that tidal marshes are periodically flooded and drained over semi-diurnal tidal cycles. Therefore, numerical algorithms for flooding and drying should be able to simulate a dynamically moving flow field boundary.
- (3) Field studies in tidal marshes demonstrated that the spatial pattern of sediment transport and deposition is strongly related to the marsh surface topography (e.g. Stoddart *et al.*, 1989; French *et al.*, 1995; Leonard, 1997; Temmerman *et al.*, 2003b); chapters 2 and 3 of this thesis). In this respect, the model must account for the effect of the complex micro-topography on the flow of water and sediments over tidal marshes and should be able to represent the marsh surface topography with a high spatial resolution.
- (4) The model should incorporate the effect of the tidal marsh vegetation, since it is widely assumed in the literature that the flow through and over the submerged vegetation cover will have a considerable impact on flow and sediment transport processes (e.g. Pethick *et al.*, 1990; Leonard and Luther, 1995; Shi *et al.*, 1995; 1996; Christiansen *et al.*, 2000).

This study presents the first attempt to apply an existing hydrodynamic and sediment transport model to simulate sedimentation processes in a tidal marsh. The Delft3D model, which was developed at WL | Delft Hydraulics (The Netherlands), was used for this study since it satisfies all the criteria mentioned above. More importantly, research is already being carried out by WL | Delft Hydraulics on the modelling of tidal marsh hydrodynamics (e.g., Mol, 2003). Furthermore, a large effort has been devoted to the incorporation of the effect of plant-flow interactions in the Delft3D model (e.g. Uittenbogaard, 2003), which is an aspect that hardly received any attention in other hydrodynamic modelling software.

The aim of this study is, first, to calibrate and validate the Delft3D model using an extensive field data set on hydrodynamics and suspended sediment transport and deposition that was collected at the Paulina marsh. The collection and analysis of these field data is described in detail in the previous chapter (chapter 3). Secondly, once the model is calibrated and validated, further model simulations are carried out in order to gain more insight in the impact of different factors, such as the vegetation cover, suspended sediment characteristics and tidal inundation height, on the spatial sedimentation pattern within the studied tidal marsh.

## 4.2. Materials and methods

### 4.2.1. General overview of the Delft3D model

Delft3D is an integrated numerical hydrodynamic and transport modelling system that is developed by WL | Delft Hydraulics (The Netherlands) and that is widely used to simulate flow and transport phenomena in coastal seas, estuaries, rivers and lakes (e.g., Stelling and Van Kester, 1994; Winterwerp and Uittenbogaard, 1997). Given the high numerical complexity of the modelling system, we will not discuss the numerical details and will restrict this section to a brief overview to situate the general modelling approach that was used. For a full description of the mathematical formulations and numerical methods, we refer to WL | Delft Hydraulics (2003).

The complete Delft3D modelling system comprises a whole range of sub-models. For this study, we used the hydrodynamic model Delft3D-FLOW to compute the water movement over the study area. These hydrodynamic computations were used then as input for a sediment transport model, Delft3D-SED.

The hydrodynamic model Delft3D-FLOW solves the three-dimensional Navier Stokes equations for incompressible free surface flow. The Navier-Stokes equations describe the movement of water based on the physical laws of conservation of mass and conservation of momentum. The Navier-Stokes equations are solved under the Shallow Water and Boussinesq assumptions. This means that in the vertical momentum equation the vertical accelerations are neglected, which leads to the hydrostatic pressure equation. The vertical velocities are computed then from the continuity equation. The resulting system of equations consists of the continuity equation, the horizontal momentum equations and the hydrostatic pressure equation. Bottom friction is modelled using the Chézy coefficient and turbulence is modelled using a so-called k- $\epsilon$  turbulence model, which is generally used in hydrodynamic modelling (e.g., Hervouet and Van Haren, 1996).

In order to simulate the effect of vegetation on the hydrodynamics, additional formulations for flow through plants were recently added to the Delft3D-FLOW model. These additional formulations account for the effects of plants, which are modelled as rigid vertical cylinders, on the momentum and turbulence equations of Delft3D-FLOW. The effect of the vegetation on the momentum equations is incorporated by calculating the friction forces exerted by the cylindrical structures on the flow, while the influence on the turbulence equations is modelled as an extra source term of turbulence caused by the plants. These plant-flow interaction formulations are mathematically described in Uittenbogaard (2003). Model simulations were extensively validated against laboratory flume experiments on flow through plant canopies (e.g. Houwing *et al.*, 2000; Baptist, 2003; Uittenbogaard, 2003).

The sediment transport model is based on the three-dimensional advection-diffusion (mass balance) equation for suspended sediment:

$$\begin{aligned} \frac{\partial C}{\partial t} + \frac{\partial uC}{\partial x} + \frac{\partial vC}{\partial y} + \frac{\partial (w - w_s)C}{\partial z} \\ = \frac{\partial}{\partial x} \left( \varepsilon_{s,x} \frac{\partial C}{\partial x} \right) + \frac{\partial}{\partial y} \left( \varepsilon_{s,y} \frac{\partial C}{\partial y} \right) + \frac{\partial}{\partial z} \left( \varepsilon_{s,z} \frac{\partial C}{\partial z} \right) \end{aligned} \quad (4.1)$$

where  $C$  = suspended sediment concentration ( $\text{kg m}^{-3}$ );  $u$ ,  $v$  and  $w$  = flow velocity components ( $\text{m s}^{-1}$ ) in  $x$ ,  $y$  and  $z$  directions respectively;  $\varepsilon_{s,x}$ ,  $\varepsilon_{s,y}$  and  $\varepsilon_{s,z}$  = eddy diffusivities ( $\text{m}^2 \text{s}^{-1}$ ) in  $x$ ,  $y$  and  $z$  directions;  $w_s$  = settling velocity ( $\text{m s}^{-1}$ ) of suspended sediment. The local flow velocities and eddy diffusivities are based on the results of the hydrodynamic computations. The settling velocity of suspended sediment is user-specified.

For this particular model application, only cohesive sediment (i.e. clay and silt  $< 63 \mu\text{m}$  and no sand  $> 63 \mu\text{m}$ ) and no erosion but only sedimentation is considered, which are acceptable assumptions for vegetated tidal marsh surfaces. For cohesive sediment the sedimentation rate  $SR$  ( $\text{kg m}^{-2} \text{s}^{-1}$ ) is then calculated using the Partheniades-Krone formula (Partheniades, 1965):

$$\begin{aligned} SR = w_s C_b \left( 1 - \frac{\tau}{\tau_{cr,d}} \right), & \quad \text{when } \tau < \tau_{cr,d} \\ = 0, & \quad \text{when } \tau \geq \tau_{cr,d} \end{aligned} \quad (4.2)$$

where  $C_b$  = the suspended sediment concentration ( $\text{kg m}^{-3}$ ) in the near bottom computational layer;  $\tau$  = the bed shear stress computed by the

hydrodynamic model;  $\tau_{cr,d}$  = the user-specified critical shear stress for sediment deposition ( $\text{N m}^{-2}$ ).

The set of partial differential equations described above are numerically solved over the study area and over a certain time period by space and time discretisation using a finite difference approach. In the horizontal direction, a rectangular finite difference grid is used with (m,n) co-ordinates, while in the vertical direction different layers are used in a so-called  $\sigma$  co-ordinate system (Philips, 1957). For each (m,n, $\sigma$ ) point of the computational grid, the Delft3D model dynamically computes hydrodynamic and sediment transport parameters such as water depth, flow velocity in horizontal and vertical directions, bottom shear stress, suspended sediment concentration and sedimentation rate. Since for this tidal marsh application flooding and drying of the computational grid need to be simulated, adapted flooding and drying algorithms, provided within the Delft3D model, were used. In order to prevent numerical instability, which is a major problem in hydrodynamic applications including flooding and drying of the computational grid, a minimum threshold water depth of 0.05 m was used to start the sediment transport computations.

#### *4.2.2. Construction of a computational grid for the study area*

In order to calibrate and validate the model, it was applied to the tidal creek catchment within the Paulina marsh, which was studied in chapter 3. More details about the study area can be found in that chapter.

An orthogonal rectangular grid was constructed for the studied tidal creek catchment using the grid-generating program Delft-RGFGRID (Fig. 4.1). The resolution of the computational grid was chosen considering both the desired level of detail of topographic representation of the marsh surface and the computing time needed to perform the model simulations. A horizontal grid resolution of 4 by 4 m and the use of four vertical layers was found to be consistent and necessitates a corresponding time step of 6 seconds, in order to meet the Courant criterion to obtain a numerically stable solution. Corresponding computation times were *ca.* 2 h 15 min to simulate one tidal inundation cycle (5 h real time) on a Pentium 4 2.4 GHz.

It is assumed that the tidal exchange of water and suspended sediment between the modelled area and the rest of the estuary is taking place through the edge of the marsh, i.e. the north-eastern boundary of the computational grid (see Fig. 4.1). This boundary is therefore defined as a so-called open boundary, where the tidal water level fluctuations and the concentration of the suspended sediment in the water column have to be specified to run the Delft3D model. The north-western and south-eastern boundaries can be regarded as the edges of the marsh area that is flooded via the studied tidal creeks system during flood tide and drained via the same creeks system

during ebb tide. We can assume that these boundaries act as interfluges between the studied creeks system and adjacent creeks systems, so that the net exchange of water and sediment is assumed here to equal zero. Therefore, both boundaries are defined as closed boundaries. However, it is not excluded that in reality minor fluxes of water and sediment occur between adjacent catchments, especially during high inundation events. Finally, the south-western boundary is located along the embankment bordering the tidal marsh and is therefore also defined as a closed boundary (Fig. 4.1).

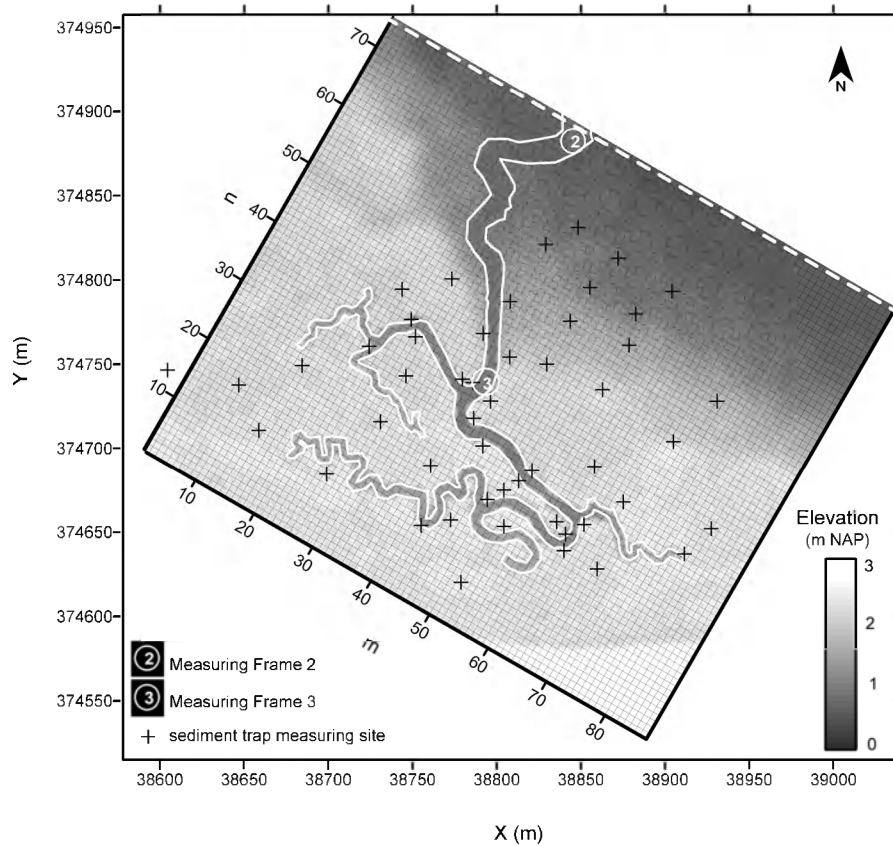


FIGURE 4.1. The computational grid of the studied tidal marsh creek catchment: in foreground the grid in thin black lines, in background a contour map of the elevation of the marsh surface specified for every grid cell. The closed boundaries of the grid are indicated in thick black lines, the open boundary at the marsh edge in broken white line. The grid co-ordinates (m,n) are shown relative to the Dutch (x,y) co-ordinate system. The (x,y) polygon of the tidal creeks system, used for the representation of the creek topography into the grid (see text), is shown in thin white line. The location of measuring frames and the sediment trap measuring sites are indicated in white symbols and black crosses, respectively.

#### 4.2.3. Specifying input values for the model variables

In order to simulate the water flow and sediment transport over the computational grid, we need to specify a number of model input variables.

To run the hydrodynamic model, we need information on:

- (1) the elevation of the marsh surface for every grid cell
- (2) the vegetation type for every grid cell and a number of vegetation characteristics (height, density, stem diameter) per vegetation type
- (3) the vertical tidal movement of the water level at the open boundary of the grid, in order to force the tidal inflow and outflow over the grid.

For the sediment transport model, we need information on:

- (1) the temporal fluctuations in suspended sediment concentration at the open boundary
- (2) the characteristic settling velocity  $w_s$  of the suspended sediment and the critical shear stress for sediment deposition  $\tau_{cr,d}$ .

##### 4.2.3.1. Topographic representation

For the study area, elevation data are available from airborne laser altimetry or LiDAR (light-induced direction and ranging), which is a recent technique through which high-resolution topographic data can be obtained for large areas by laser scanning of the earth surface from an airplane (Measures, 1991). LiDAR measurements are currently carried out for the whole surface area of The Netherlands by Rijkswaterstaat Meetkundige Dienst. For the study area, this resulted in an extensive data set of elevation points with a resolution of 3 by 3 m and a vertical and horizontal accuracy of 0.20 and 0.30 m respectively, as specified by Rijkswaterstaat (Van Heerd and Van 't Zand, 1999). For this model application, vertical accuracy is of high importance, since spatio-temporal variations in tidal marsh sedimentation were shown to be very sensitive to variations in surface elevation and tidal inundation height (Temmerman *et al.*, 2003b; chapter 2).

Therefore, an additional quality control on the vertical accuracy of the LiDAR data was performed. A digital elevation model (DEM) with a resolution of 1 by 1 m was computed from the LiDAR data using a triangulation with linear interpolation method. In the field, the elevation of the vegetated marsh surface was surveyed with an electronic total station (Sokkia SET5F) at 76 locations well-distributed within the studied tidal creek catchment. Both the field survey and LiDAR measurements were referenced relative to the Dutch xy co-ordinate system, while the z co-ordinate is expressed relative to the Dutch ordnance level NAP (= Nieuw Amsterdams Peil). The elevation of the 76 field survey points ( $z_{\text{survey}}$ ) was compared then with the DEM generated from the LiDAR data ( $z_{\text{LiDAR}}$ ). Figure 4.2 shows that a good correlation was found between  $z_{\text{survey}}$  and  $z_{\text{LiDAR}}$  ( $R^2=0.95$ ) and that the mean elevation difference  $z_{\text{LiDAR}} - z_{\text{survey}}$  was 0.15 m

with a standard deviation of 0.13 m. Since the vertical errors on the total station measurements are very small (in the order of millimetres only), quasi all of this difference must be related to the LiDAR measurements. On the one hand, the mean difference of 0.15 m may be interpreted as a systematic over-estimation of the surface elevation by the LiDAR measurements as a consequence of laser reflection on the marsh vegetation cover instead of on the earth surface. On the other hand, the standard deviation of 0.13 m may be interpreted as vertical inaccuracy related to the LiDAR technology (see e.g. Baltasvias (1999) for an overview). All LiDAR elevations were therefore lowered by 0.15 m and interpolated to the Delft3D computational grid of the study area.

The resulting computational grid represents the marsh topography very well, except for the tidal marsh creeks. A very discontinuous and irregular representation of the creek bottom elevations was obtained, because both the resolution of the LiDAR measurements (3 by 3 m) and of the computational grid (4 by 4 m) is too low to fully capture the creek topography. This was especially the case for the smallest creeks near the head of the dendritic creek system, as the creeks typically shallow and narrow inland from about 7 m width at the creek mouth to only 0.30 m at the head of the creeks system (Fig. 4.1).

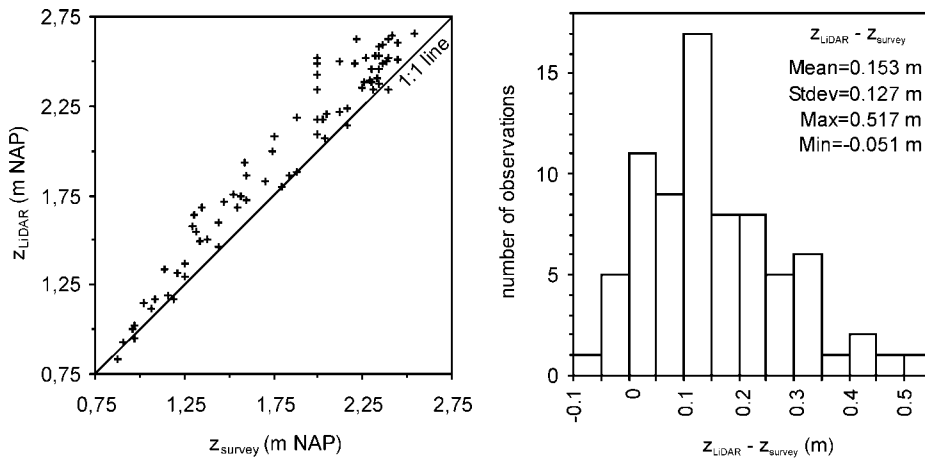


FIGURE 4.2. Comparison between elevations determined from field surveys ( $z_{\text{survey}}$ ) and from LiDAR measurements ( $z_{\text{LiDAR}}$ ) for 76 control points.

To solve this problem, the elevation data points of the computational grid were modified as follows. First, the tidal creek edges were mapped as an xy polygon from geo-referenced aerial photographs. All elevation points of the computational grid, situated within this tidal creek polygon, were deleted from the grid. Next, a second polygon was defined, incorporating only the creeks with a bottom elevation below 1.70 m NAP (i.e. more than 0.50 m below the mean elevation of the high marsh) and thus omitting the smallest creeks at the head of the creeks system. The width of this polygon was then manually adjusted so that at least one grid cell of 4 by 4 m was contained within every cross section along the creeks system (Fig. 4.1). Finally, a linear interpolation algorithm was applied within this polygon to interpolate new elevation values to the grid based on detailed field survey data of the thalweg of the creeks. In this way the gradual increase of the elevation of the tidal creek bottom with increasing distance from the marsh edge was continuously and smoothly represented in the computational grid (Fig. 4.1). For the grid points falling within the first creek polygon but outside of the second creek polygon (i.e. grid points falling within the smallest creeks at the head of the creek system), a new elevation value was interpolated based on the elevation values of the nearby marsh surface grid cells. Thus, in the model these locations were considered as being part of the marsh surface and not of the creek system.

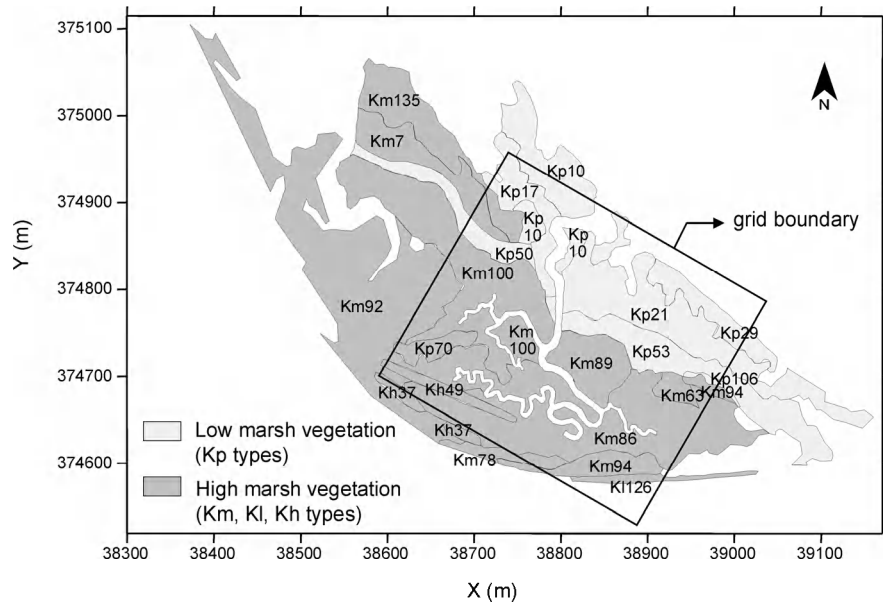


FIGURE 4.3. Vegetation map used as input for the Delft3D model, based on the vegetation map of Rijkswaterstaat (after Koppejan, 2000). The vegetation composition of each of the vegetation types is described in Table 4.1.

#### 4.2.3.2. Vegetation

The different vegetation types that are present in the study area need to be specified for each grid cell of the computational grid so that the Delft3D model can account for the effect of the vegetation structure on the flow. For each vegetation type, both the horizontal spatial distribution and the vertical distribution of the plant morphology have to be defined.

The specification of the horizontal distribution of different vegetation types was based on the vegetation classification system of Rijkswaterstaat Meetkundige Dienst for vegetation mapping of Dutch salt marshes (Koppejan, 2000). The most recent vegetation map (1998) of the study area was used as input polygon file to assign a vegetation type to each grid point of the computational grid (Fig. 4.3). The plant species composition of each vegetation type is summarised in Table 4.1. The vegetation types were further grouped into two main vegetation types with contrasting plant morphology: (1) a low marsh vegetation type (Kp types; *Spartina anglica* dominant) and (2) a high marsh vegetation type (Km, Kl and Kh types; *Puccinellia maritima*; *Halimione portulacoides* and *Aster tripolium* dominant) (Fig. 4.3 and Table 4.1).

For both vegetation types a number of input parameters has to be specified to describe the vertical distribution of plant structures. With plant structures we mean stems, branches and leaves, which are all modeled as vertical rigid cylindrical structures. The input parameters are a characteristic diameter of structures and the number of cross sections of structures per m<sup>2</sup> of horizontal plane. Both parameters can vary in the vertical direction and, therefore, have to be defined for each vertical layer of the model. It is clear that a real life representation of the vegetation structure in the model is impossible. Therefore, a best estimate for these model input parameters was determined as follows.

For the Kp vegetation types (*Spartina anglica* dominant), large differences in vegetation cover (in %) between the Kp subtypes were apparent from the vegetation mapping by Rijkswaterstaat (Table 4.1). For each of these Kp subtypes the plant density (plants per m<sup>2</sup>) was determined as follows. The number of plants per m<sup>2</sup> was counted on a series of 0.5 by 0.5 m plots situated in *Spartina* fields with a 100 % cover \*. Next, the plant density was calculated for each Kp subtype by multiplying the plant density, measured on the 100 % cover plots, with the fractional vegetation cover, as reported by Rijkswaterstaat for each Kp subtype (Table 4.2). For all Km, Kl and Kh vegetation types, a 100 % vegetation cover was observed (see Table 4.1) and, therefore, plant densities were assumed here to be homogeneous in space. For *Puccinellia maritima* (a grass) and *Halimione portulacoides* (a small

---

\* This field work was done by the Centre for Estuarine and Marine Ecology (NIOO-CEME) (see Bouma *et al.*, submitted).

TABLE 4.1. Percentage of plant species in each vegetation type in the study area, based on vegetation mapping by Rijkswaterstaat (see Fig. 4.3). The vegetation types are listed in the left column. Plant species are considered as dominant (Dom.) when covering >50% of the surface area, co-dominant (Co-dom.) species cover <50%. Plant species names are abbreviated as: n.v.= no vegetation; S.a.=*Spartina anglica*; S.sp.=*Salicornia* species; P.m.=*Puccinellia maritima*; A.t.=*Aster trololium*; H.m.=*Halimione portulacoides*; L.v.=*Limonium vulgare*; T.m.=*Triglochin maritima*; A.m.=*Artemisia maritima*; E.p.=*Elymus pycnanthus*.

Dom.:	n.v.	S.a.	S.sp.	P.m.	P.m.	P.m.	H.p.	P.m.	P.m.	A.m.	E.p.
Co-dom.:					A.t.		H.p.		L.v.	T.m.	
Kp29	95	5									
Kp10	80	20									
Kp26	60	40									
Kp17	10	90									
Kp21	10	90									
Kp53		80	10					10			
Kp106			100								
Kp50		90					10				
Kp70		60					30	10			
K1126				100							
Km78		20					60	20			
Km7		20			60				20		
Km63				20		60	20				
Km135								30		70	
Km100			5					70	20		5
Km92		10					90				
Km89						20	75			5	
Km86		10		15			70				5
Km94							100				
Kh37							30				70
Kh49											100

shrub-like plant species) no field data on plant densities were directly available. The number of plant structures per m<sup>2</sup> is for both species typically very high and therefore high densities of 4000 and 2000 structures per m<sup>2</sup> were assumed for *Puccinellia maritima* and *Halimione portulacoides*, respectively.

The vertical distribution of stem diameters and plant structures per m<sup>2</sup> was specified based on available field measurements of plant morphology\*. *Spartina anglica* plants were harvested on six plots of 0.5 by 0.5 m and for each plot a representative sub-sample of ca. 30 individual plants was described for plant height, vertical distribution of stem diameter, the height

\* This field work was done by the Centre for Estuarine and Marine Ecology (NIOO-CEME) (see Bouma *et al.*, submitted).

TABLE 4.2. Plant densities and characteristic stem diameters used in the Delft3D-FLOW model for each vegetation type. Plant species names are abbreviated as: *S.a.*=*Spartina anglica*; *P.m.*=*Puccinellia maritima*; *H.p.*=*Halimione portulacoides*; *A.t.*=*Aster tripolium*.

vegetation type	% cover	plant species	plant density (m <sup>-2</sup> )	stem diameter (m)
Kp29	5	<i>S.a.</i>	63	0.004
Kp10	20	<i>S.a.</i>	250	0.004
Kp26	40	<i>S.a.</i>	500	0.004
Kp17, Kp21	90	<i>S.a.</i>	1125	0.004
Kp53, Kp106, Kp50, Kp70	100	<i>S.a.</i>	1250	0.004
All Kl, Km, Kh types	100	<i>P.m.</i>	4000*	0.002
		<i>H.p.</i>	2000*	0.005
		<i>A.t.</i>	20	0.010

\*Plant densities could not be measured because of the complex morphology of the plant species but are estimated (see text).

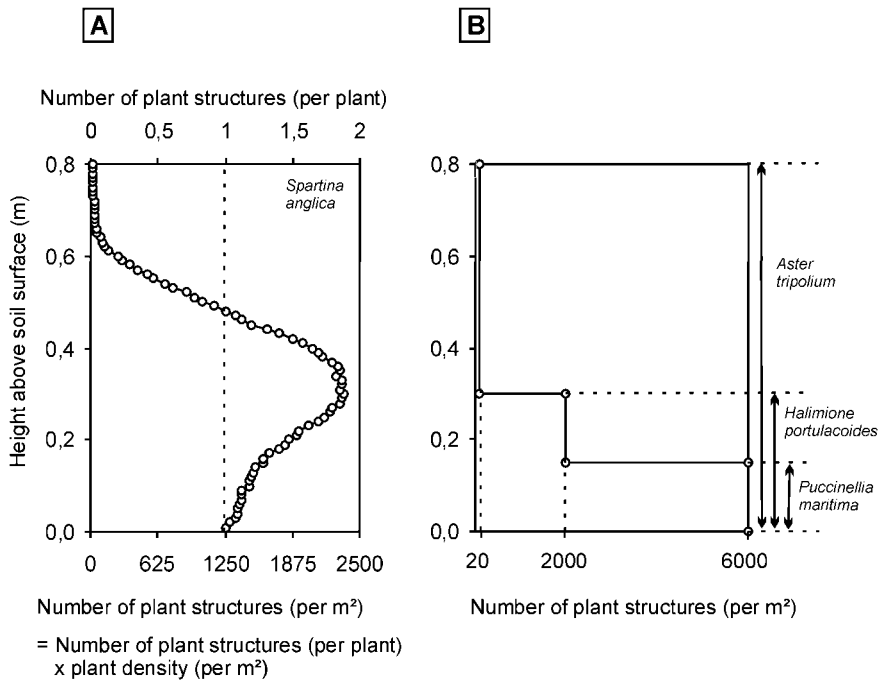


FIGURE 4.4. Vertical distribution of plant structures used as input in the Delft3D model for (a) the low marsh vegetation type (Kp types; *Spartina anglica* dominant) and (b) the high marsh vegetation type (Kl, Km, Kh types; *Puccinellia maritima*, *Halimione portulacoides* and *Aster tripolium* dominant).

were leaves are growing on the stem, and the length of each of these leaves. Based on these data and considering an average angle of  $45^\circ$  between the stem and its leaves, a detailed vertical distribution of plant structures could be calculated (Mol, 2003) (Fig. 4.4a). This vertical plant structure distribution was then used as model input for the low marsh (Kp) vegetation types, assuming that both stems and leaves can be modelled as cylindrical structures, which is a reasonable assumption for the small needle-shaped leaves of *Spartina anglica*. For the high marsh (Km, Kl, Kh) vegetation types, no such detailed measurements of vertical plant structure were available. Instead, the vertical plant structure was schematically modelled here, as the combined vertical structure of *Puccinellia maritima*, *Halimione portulacoides* and *Aster tripolium*, in three vertical layers, as presented in Figure 4.4b. In the lowest layer (from 0-0.15 m above the soil surface) the density of plant structures is related to all three of these plant species, in the middle layer (0.15-0.30 m) only to plant structures of *Halimione portulacoides* and *Aster tripolium*, and in the highest layer (0.30-0.80 m) only to *Aster tripolium*.

#### 4.2.3.3. Open boundary conditions

The model was applied using the field data obtained for the semi-diurnal inundation cycle of 11/08/2002, with high water around 17 h. During this semi-diurnal cycle, the study area was completely inundated during the flood tide and completely drained again during the subsequent ebb tide (see Fig. 3.7 in chapter 3)

In order to run the Delft3D model the temporal evolution of the water level and of the suspended sediment concentration (SSC) have to be specified at the open boundary of the grid. These time-series of water level and SSC were provided by the field data recorded at the automatic measuring Frames 2 and 3. These field data are described and analysed in detail in chapter 3. The data from Frame 2, which was installed at the mouth of the creeks system at the open boundary of the grid, were used to specify the open boundary conditions (Fig. 4.1). The 4 Hz raw data were processed to time-series of 1-minute averages. From these input time-series, the model computes water levels and SSC at every time step of 6 seconds using a linear interpolation method. The model simulation was started during flood tide at a water level of 1.60 m NAP, which corresponds with a water depth of *ca.* 0.10 m at the open boundary, and was ended during the subsequent ebb tide, when water level had fallen again to 1.60 m NAP.

#### 4.2.4. Model calibration and validation

In order to solve the sediment transport equations (eqs. 4.1 and 4.2), yet the sediment settling velocity  $w_s$  (in  $\text{m s}^{-1}$ ) and the critical shear stress for sedimentation  $\tau_{cr,d}$  (in  $\text{N m}^{-2}$ ) need to be known. For both model variables, no field data were available. These parameters were therefore used to calibrate the sedimentation model against the field measurements of spatial variations in sedimentation rates that were measured at 50 measuring sites during the semi-diurnal tidal cycle of 11/08/2002 (see chapter 3).

The following calibration and validation procedure was used. First, the dataset of 50 sedimentation rate observations was sorted from the lowest up to the highest measured sedimentation rate and a ranking number from 1 to 50 was given to each measuring location. Next, the measuring locations with an even ranking number were used for calibration, the locations with an uneven ranking number for validation. In this way, both the calibration and validation dataset cover the whole range of observed sedimentation rates and both datasets contain measuring sites well-distributed over the study area.

The Delft3D model was run then using a number of combinations of input values for  $w_s$  and  $\tau_{cr,d}$ . No different sediment classes with different settling velocities  $w_s$  were used, so that only one characteristic settling velocity needed to be specified. Different model runs were carried out with input values for  $w_s$  ranging from 1 to  $7 \times 10^{-4} \text{ m s}^{-1}$  in steps of  $0.5 \times 10^{-4} \text{ m s}^{-1}$ , which corresponds with realistic median grain sizes ranging from 10 to 26  $\mu\text{m}$ . For  $\tau_{cr,d}$  input values ranging from 0.1 to  $0.6 \text{ N m}^{-2}$  in steps of  $0.1 \text{ N m}^{-2}$  were used, which are representative values for mud (WL | Delft Hydraulics, 2003). For each combination of  $w_s$  and  $\tau_{cr,d}$ , the model was run and the simulated sedimentation rates were compared with the calibration dataset of observed sedimentation rates. In order to determine the optimal values for  $w_s$  and  $\tau_{cr,d}$ , for which the spatial sedimentation pattern predicted by the model best agrees with the observed pattern, the model efficiency coefficient ( $ME$ ), as proposed by Nash and Sutcliffe (1970), was calculated for each model run with a certain  $w_s$  and  $\tau_{cr,d}$  combination:

$$ME = 1 - \frac{\sum (SR_{obs} - SR_{pred})^2}{\sum (SR_{obs} - SR_{mean})^2} \quad (4.3)$$

where  $SR_{obs}$  is the observed sedimentation rate,  $SR_{pred}$  is the predicted sedimentation rate, and  $SR_{mean}$  is the mean of the observed calibration dataset of sedimentation rates. Values for  $ME$  range from  $-\infty$  to 1. The closer  $ME$  approximates 1, the better the model predicts individual sedimentation rates.

In order to validate the model, the predicted spatial variations in sedimentation rates, calculated by the model using the optimal values for  $w_s$  and  $\tau_{cr,db}$  were compared with the validation dataset of observed sedimentation rates.

#### 4.2.5. Model sensitivity analysis

After model calibration and validation, additional model simulations were carried out to evaluate the sensitivity of the model predictions to different input values for a number of model variables that are generally supposed to control variations in sedimentation rates on tidal marshes.

First, in order to investigate the effect of the vegetation cover, ten model runs were carried out, one without any vegetation on the marsh surface, and nine runs with different combinations of plant densities (250, 750 and 2000 stems  $m^{-2}$ ) and plant heights (0.2, 0.6 and 3.0 m) (Table 4.3). All vegetation runs were done assuming an idealised horizontally and vertically homogeneous vegetation cover. This means that only one vegetation type, with one specified plant density, was considered for the whole vegetated marsh area, and that plants were simulated as one vertical cylindrical structure, with a certain diameter and height and without branches or leaves. The chosen plant heights can be regarded as representative for low grass-like vegetation types (0.2 m) like *Puccinellia maritima* typical for salt marshes, medium high vegetation types (0.6 m) like *Spartina anglica* and *Scirpus maritimus* on brackish marshes, and high vegetation types (3.0 m) like *Phragmites australis* on freshwater tidal marshes.

Secondly, the impact of the incoming suspended sediment concentration (SSC) in the water that floods the marsh surface is simulated using different input values for SSC at the open boundary of the computational grid (0.06, 0.1 and 0.2 g/l) (Table 4.3). These SSC values are representative for the spatial and temporal variations in SSC occurring in the Scheldt estuary. Also the influence of the settling velocity of the suspended sediment was evaluated by using different values of 1, 2, 4 and 7.  $10^{-4}$  m  $s^{-1}$  (Table 4.3).

Finally, we know that temporal variations in sedimentation rates are related to variations in high water level between single tidal cycles. Furthermore, in Temmerman *et al.* (2003b) we showed that the incoming SSC, at the beginning of marsh flooding, is higher for tidal cycles with a higher high water level (see Fig. 2.6 in chapter 2). In order to identify the impact of tidal marsh inundations with a different high water level on the spatial sedimentation pattern, two series of model runs were carried out. In the first series, the high water level was varied but the incoming SSC was kept constant (Table 4.3; hw\_run\_01 up to 03). In the second series, the high water level was varied and the incoming SSC was assumed to be positively related to the high water level (Table 4.3; hw\_run\_04 up to 06).

TABLE 4.3. Summary of additional model runs. All runs were performed using the same input values as for the model calibration and validation, except for the input parameters specified in this table. SSC=suspended sediment concentration;  $w_s$ =settling velocity; HW=high water level.

model run	stem density ( $m^{-2}$ )	stem height (m)	stem diameter (m)	SSC (g/l)	$w_s$ ( $10^{-4}$ $m s^{-1}$ )	HW (m NAP)
vege_run_01	no vegetation cover					
vege_run_02	250	0.2	0.002			
vege_run_03	750	0.2	0.002			
vege_run_04	2000	0.2	0.002			
vege_run_05	250	0.6	0.004			
vege_run_06	750	0.6	0.004			
vege_run_07	2000	0.6	0.004			
vege_run_08	250	3.0	0.010			
vege_run_09	750	3.0	0.010			
vege_run_10	2000	3.0	0.010			
ssc_run_01				0.060		
ssc_run_02				0.100		
ssc_run_03				0.200		
ws_run_01					1	
ws_run_02					2	
ws_run_03					4	
ws_run_04					7	
hw_run_01				0.030		2.45
hw_run_02				0.030		2.80
hw_run_03				0.030		3.40
hw_run_04				0.030		2.45
hw_run_05				0.060		2.80
hw_run_06				0.100		3.40

#### 4.2.6. Analysing the simulated spatial sedimentation patterns

In Temmerman *et al.* (2003b), we showed that spatial variations in tidal marsh sedimentation can be modelled using a simple topography-based multiple regression model of the following form:

$$SR = k \cdot e^{lH} \cdot e^{mD_c} \cdot e^{nD_e} \quad (4.4)$$

where  $SR$  = sedimentation rate ( $g m^{-2}$ ),  $H$  = elevation of the marsh surface (m relative to a certain reference level),  $D_c$  = distance from the nearest tidal

creek (m) and  $D_e$  = distance from the marsh edge, measured along the nearest creek (m).

It is interesting then to see to what extent the spatial sedimentation pattern, simulated with Delft3D, corresponds to the topography-based relationship of eq. 4.4. This was investigated by multiple regression analysis using eq. 4.4 and using the sedimentation rates simulated at each of the 50 measuring locations as the dependent variable. For the independent variables  $H$ ,  $D_c$  and  $D_e$ , the same values were used as explained in chapter 3. As was done in chapter 3,  $D_c$  and  $D_e$  were set to zero for marsh sites for which  $D_c > 40$  m (see paragraph 3.3.3. for more details).

This regression procedure further offers an interesting tool to analyse the spatial sedimentation patterns that were simulated with the Delft3D model using different input values for vegetation parameters, suspended sediment characteristics and high water levels (see paragraph 3.2.5 above). In order to analyse the impact of the different scenarios, the simulated spatial sedimentation patterns needed to be compared. The sedimentation patterns show a strong spatial autocorrelation so that it is difficult to decide whether or not observed differences are statistically significant. Therefore, for each model run a multiple regression analysis was carried out using eq. 4.4 and the resulting regression parameters  $k$ ,  $l$ ,  $m$  and  $n$  were compared between the different simulations. In order to define whether the difference between the regression parameters was significant or not, the 95 % confidence intervals were computed for each regression parameter.

### 4.3. Results

#### 4.3.1. Validation of the hydrodynamic model

The performance of the hydrodynamic model was validated by comparison of the simulated and observed temporal variation of the water level and flow velocities at Frame 3. Figure 4.5a shows that the observed variation in water level is very well reproduced by the model for the entire simulated tidal inundation cycle. Figure 4.5b shows that the flow velocities are much harder to predict. The model simulates the flood and ebb asymmetry in the flow velocity but predicted absolute flow velocities differ considerably from measured flow velocities (Fig. 4.5b). The model further simulates well the complete flooding and draining of the tidal marsh during the simulated inundation cycle, as is illustrated in Figure 4.6. In correspondence with field observations, the simulated flow velocities are highest in the main tidal creek during the flood and ebb tide and lowest on the vegetated marsh platform around high water (Fig. 4.6).

### 4.3.2. Calibration and validation of the sedimentation model

The results of the calibration of the sedimentation model are presented in Figure 4.7. The calibration curves show an optimum value of  $2 \cdot 10^{-4} \text{ m s}^{-1}$  for  $w_s$  and  $0.4 \text{ N m}^{-2}$  for  $\tau_{cr,d}$ , for which the highest model efficiency ( $ME$ ) value of 0.74 was obtained. In Figure 4.8, observed versus predicted sedimentation rates, calculated by the model using the optimal values for  $w_s$  and  $\tau_{cr,d}$ , are plotted. A good agreement is obtained between the predicted and observed sedimentation rates, both for the calibration and validation dataset ( $R^2=0.82$  and 0.67, respectively). However, it can be noticed that for most measuring locations the model overestimates the observed sedimentation rates, while it underestimates the highest observed sedimentation rates.

Figure 4.9 shows the spatial sedimentation pattern that was simulated with the Delft3D model superimposed on an isometric projection of the topography of the study area. A clear sedimentation gradient is simulated in relation to the elevation gradient on the low marsh, while on the high marsh,

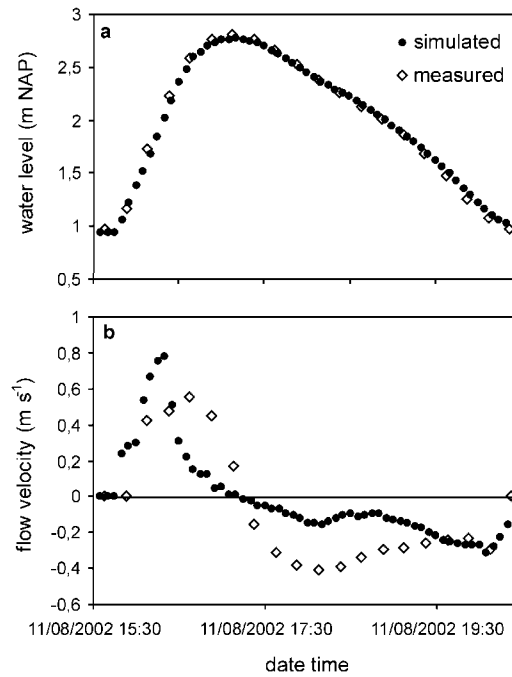


FIGURE 4.5. Comparison of hydrodynamic variables measured at Frame 3 and simulated with the Delft3D model for one semi-diurnal tidal cycle (11/08/2002): (a) water level (m NAP) fluctuation during the simulated tidal cycle; (b) flow velocity in the dominant flow direction parallel to creek axis. Since the observed flow velocities were measured near the creek bottom (0.07 m above it), they are compared with the velocities computed for the bottom computational layer of the model.

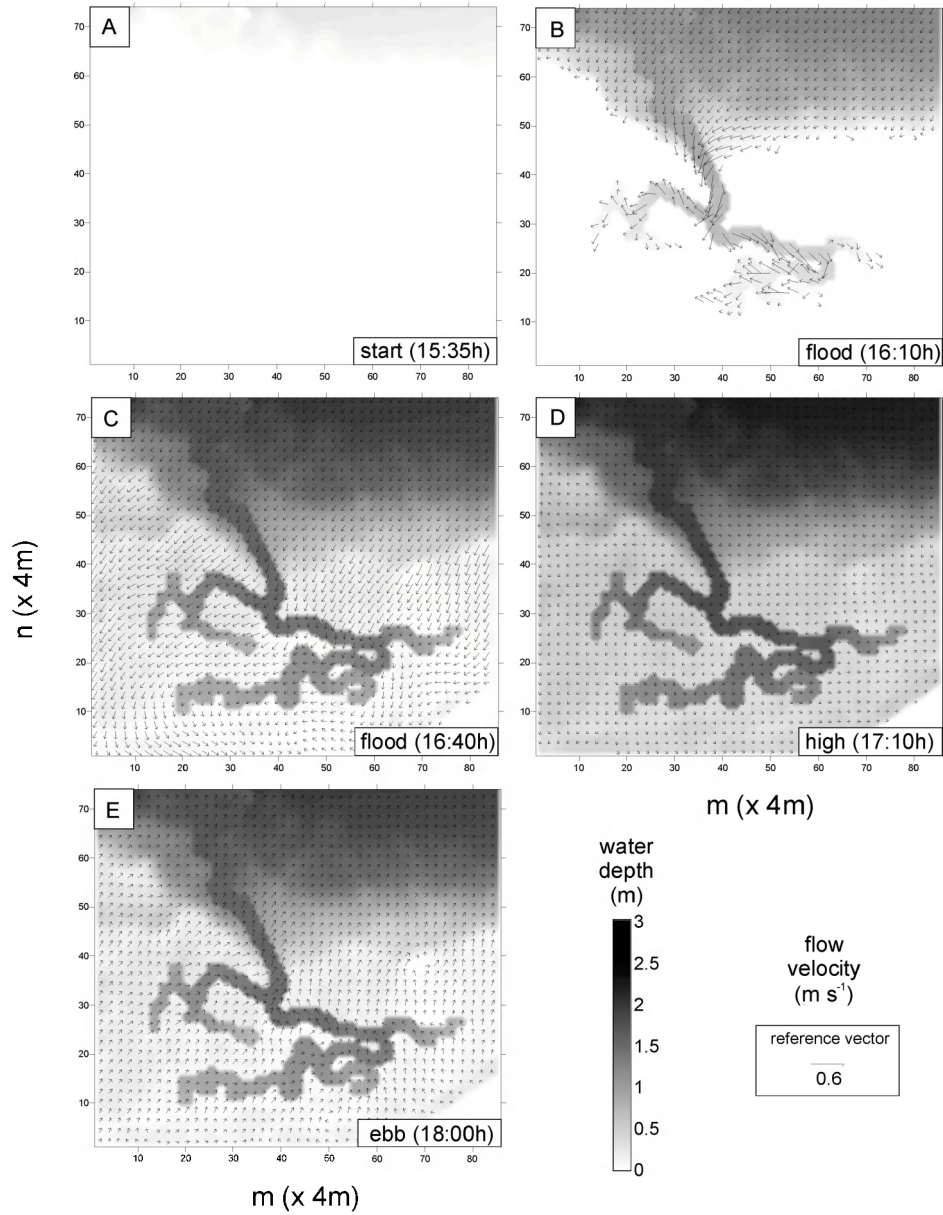


FIGURE 4.6. Contour plots of water depth and vector plots of flow directions and velocities simulated over the computational grid at different time steps of the simulated inundation cycle: (a) start of simulation (only 0.10 m water depth at the open boundary, the rest of the grid is dry); (b) the low marsh and tidal creeks are flooded; (c) beginning of flooding of the high marsh surface; (d) high tide; (e) just before draining of the high marsh surface.



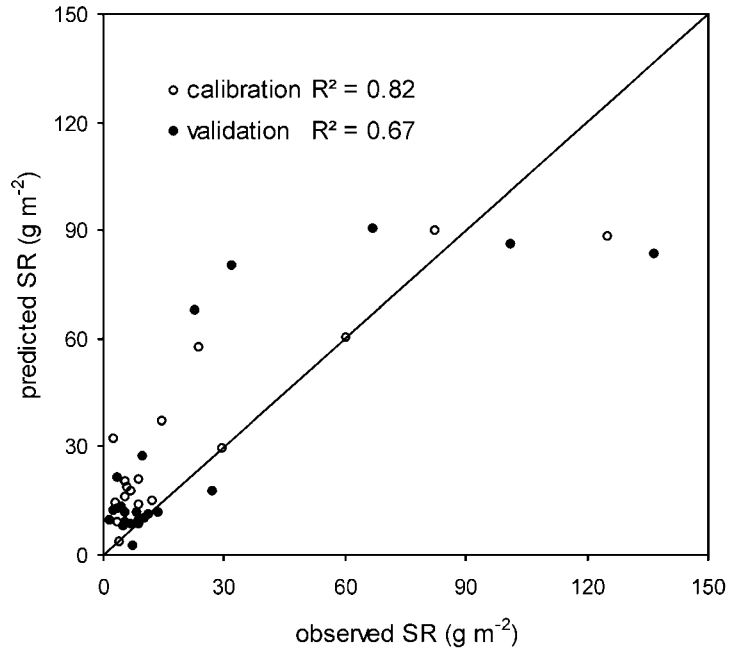


FIGURE 4.8. Observed versus predicted sedimentation rates (SR in  $\text{g m}^{-2}$ ), using optimal  $w_s$  and  $\tau_{cr,d}$  values, for the calibration and validation dataset.

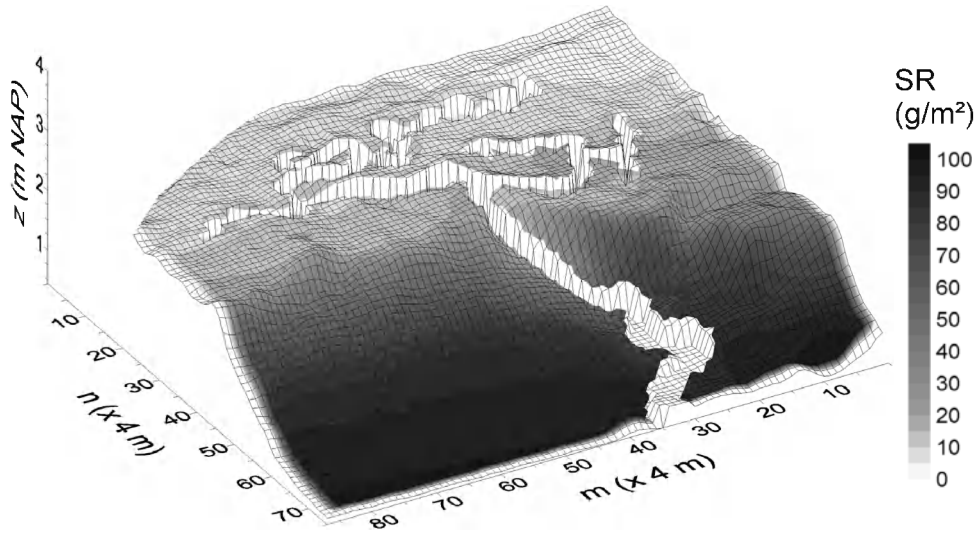


FIGURE 4.9. The simulated spatial pattern of sedimentation rates (SR) superimposed on an isometric projection of the marsh surface topography. The tidal creeks are left blank.

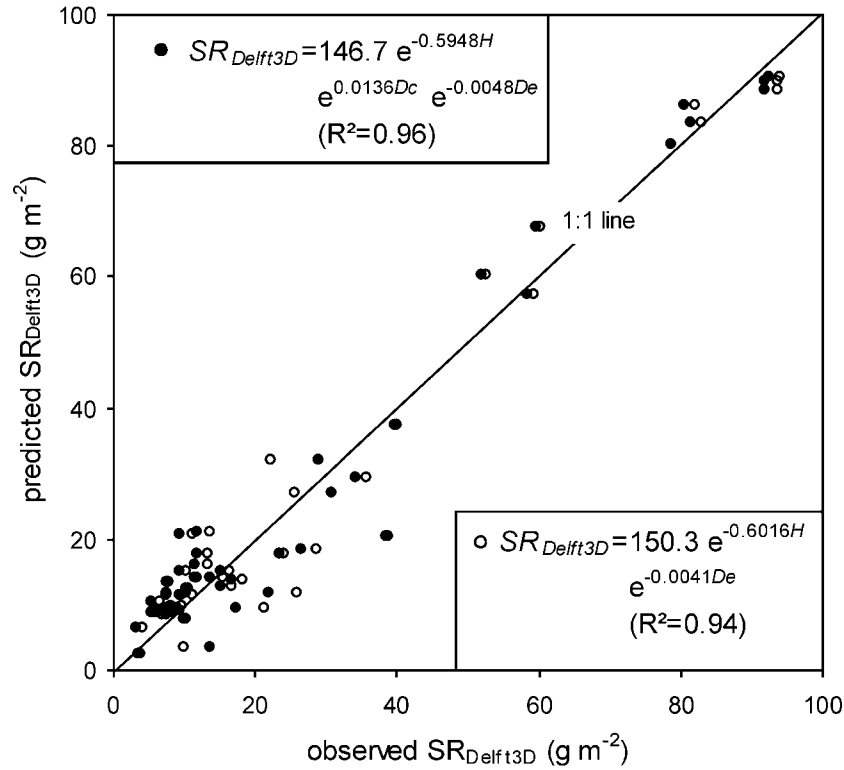
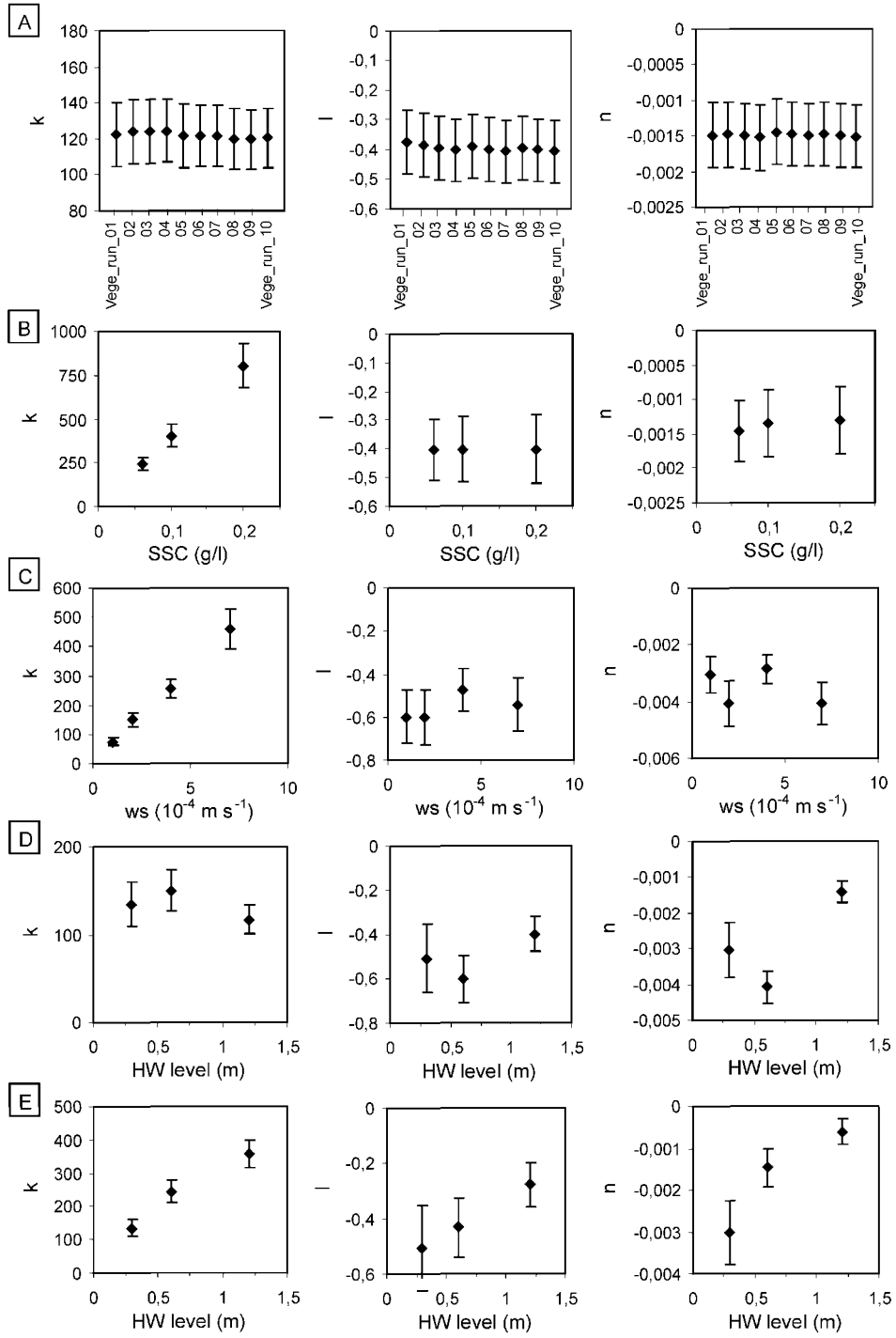


FIGURE 4.10. The spatial pattern of sedimentation rates, that was simulated with Delft3D (see Fig. 4.9), was analysed with the topography-based regression model (eq. 4.4). The “observed” Delft3D sedimentation rates (*y*-axis: observed  $SR_{Delft3D}$ ) are plotted here against the Delft3D sedimentation rates, “predicted” or reproduced by the topography-based regression model (*x*-axis: predicted  $SR_{Delft3D}$ ). The regression procedure was carried out twice: (1) incorporating all three topographic parameters  $H$ ,  $D_c$  and  $D_e$  in the regression analysis (black dots); (2) incorporating only  $H$  and  $D_e$  in the regression analysis (white dots).

FIGURE 4.11: Regression parameters  $k$ ,  $l$ ,  $m$  and  $n$  resulting from multiple regression analyses (using eq. 4.4) of the spatial sedimentation patterns simulated with Delft3D under different scenarios of (a) vegetation cover (see *vege\_run\_01* up to 10 in Table 4.3), (b) suspended sediment concentration (SSC), (c) settling velocity ( $w_s$ ), and (d,e) high water (HW) level. Error bars indicate 95 % confidence intervals for each estimated regression parameter.



#### 4.3.3. Simulating spatial sedimentation patterns under different scenarios: a model sensitivity analysis

Additional model runs were carried out to evaluate the impact of different input values for vegetation parameters, suspended sediment concentrations, settling velocities and high water levels, on the simulated spatial sedimentation pattern (Table 4.3). Figure 4.11 shows the variation of the regression parameters, resulting from regression analysis of the spatial sedimentation patterns simulated with Delft3D, using the topography-based regression model in eq. 4.4. Notice that for all model runs, the regression parameter  $m$  was found to be not significantly different from zero and is therefore not shown in Figure 4.11. In paragraph 4.3.2 above it was already discussed that the distance from the creeks  $D_c$  can be ignored as a variable controlling the spatial sedimentation pattern simulated with the Delft3D model.

The results for the vegetation runs are shown in Figure 4.11a. Although these simulations were run using highly different input plant densities and heights (Table 4.3), no significant differences between the vegetation runs were found for all regression parameters. Even for vegetation run one, without any vegetation cover, the simulated spatial sedimentation pattern is not significantly different from the sedimentation pattern simulated in vegetation run ten, with an extremely dense and high vegetation cover.

On the contrary, the concentration and settling velocity of the incoming suspended sediment at the open boundary of the model have a strong influence. Figures 11b and 11c clearly show that the regression parameter  $k$  linearly increases with increasing SSC or increasing settling velocity. The parameters  $l$  and  $n$ , however, do not show a significant trend with changing SSC or settling velocity. This means that the relative decrease of sedimentation rates with increasing surface elevation  $H$  or distance from the marsh edge  $D_e$  is independent of changes in SSC or settling velocity. Or otherwise formulated, the spatial pattern of sediment deposition stays more or less the same (in relative terms), but (in absolute terms) has to be multiplied with a certain factor if SSC or settling velocity increase.

The results of the model runs, for tidal cycles with a different high water level, are presented in Figures 11d and 11e. The model runs, using a constant incoming SSC, lead to unrealistic predictions (Fig. 4.11d). For the model run simulating the highest high water level, the lowest value for  $k$  is obtained. This is in contradiction with field measurements, which showed that tidal inundation cycles with higher high water levels result in higher sedimentation rates (see Fig. 2.7 in chapter 2). However, Temmerman *et al.* (2003b) observed that the incoming SSC, at the beginning of an inundation cycle, is linearly increasing with the high water level, occurring during that inundation cycle (see Fig. 2.6 in chapter 2). For the model runs, for which incoming SSC was specified as a positive function of high water level, a positive relationship was found between  $k$  and the high water level (Fig.

4.11e). So this means that higher sedimentation rates are simulated for inundation cycles with higher high water levels, which is indeed in accordance with the field measurements. This suggests then that the incorporation of the positive linear relationship between incoming SSC and high water level is crucial to obtain model results that realistically predict the increase of sedimentation rates with increasing high water levels. The model simulations further show that the regression parameters  $l$  and  $n$  become less negative when high water level increases (Fig. 4.11e). This indicates that during inundation cycles with higher inundation heights, the suspended sediment is transported higher onto the marsh and farther away from the marsh edge before it is deposited.

#### 4.4. Discussion

##### 4.4.1. Some remarks on the model simulations

This modelling study showed that the spatial variations in sedimentation rates that were observed in the study area can be simulated reasonably well using the hydrodynamic and sediment transport model Delft3D. Yet some remarks can be made.

In the previous chapter, we compared field data on water volumes and sediment masses discharged through the creeks system with water volumes stored at high tide and sediment masses deposited on the marsh surface, which provided general insights in the flow paths within the study area (see paragraph 3.4.4 in chapter 3). The same analysis procedure, as was carried out in chapter 3 for the field data, was also performed for the simulated data, in order to investigate whether the simulated pathways of water and sediment supply correspond with the field data. These analyses of the simulated data were only carried out for Frame 3, since Frame 2 is located at the open boundary of the model grid (see Fig. 4.1).

First, the total water volumes discharged through the creeks system at Frame 3 during flood ( $V_F$ ) and ebb ( $V_E$ ) (in  $m^3$ ) were calculated as:

$$V_F = \int_F u \cdot A(h) \cdot dt \quad (4.5)$$

and

$$V_E = \int_E u \cdot A(h) \cdot dt \quad (4.6)$$

where  $A(h)$  is the wet cross-section (in  $m^2$ ) at time  $t$ , which is a function of the water level  $h$  at time  $t$ . The simulated  $V_F$  and  $V_E$  values were calculated

for every computational layer of the model and subsequently summed over all four layers of the model. The resulting  $V_F$  and  $V_E$  values were compared with the total water volume  $V_{HW}$  stored at high tide above the marsh surface. Table 4.4 shows that for the simulated semi-diurnal cycle of 11/08/2002, the observed water volumes discharged during flood ( $V_F$ ) and ebb ( $V_E$ ) through the creeks system, determined from the field data, accounted for 53 and 66 % of  $V_{HW}$ , respectively. However, the simulated  $V_F$  and  $V_E$  values only accounted for 26 and 31 % of  $V_{HW}$  and are very close to the bankfull water volume that can be stored within the creeks system. The remaining percentages of  $V_{HW}$  must then be regarded as the water volume that is supplied across the high marsh edge. It is clear then that the model simulates that, once the creeks are at bankfull level, most water is supplied across the high marsh edge and simply overflows the creeks (see Fig. 4.6). This is in contradiction with the field data, which suggest that the creeks system serves as an important transport pathway of water to and from the high marsh surface.

The same exercise was done for the total amount of suspended sediment transported through the creeks system at Frame 3 during flood ( $TSS_F$ ) and ebb ( $TSS_E$ ):

$$TSS_F = \int_F u \cdot A(h) \cdot C \cdot dt \quad (4.7)$$

and

$$TSS_E = \int_E u \cdot A(h) \cdot C \cdot dt \quad (4.8)$$

where  $C$  is the suspended sediment concentration (in  $\text{g l}^{-1}$ ) at time  $t$ . Also here eqs. 4.7 and 4.8 were solved for each computational layer of the model and the resulting  $TSS_F$  and  $TSS_E$  values were summed over the whole depth of the water column. The net import or export of suspended sediment was then calculated as:  $TSS_{net} = TSS_F + TSS_E$ . This  $TSS_{net}$  was compared to the simulated total sediment mass deposited on the high marsh surface ( $TSS_{dep}$ ). Table 4.5 shows that  $TSS_{net}$  and  $TSS_{dep}$ , calculated from the field measurements, are in the same order of magnitude, which indicated that the creeks system serves as the primary sediment transport pathway to the high marsh surface (see chapter 3). However, the  $TSS$  values calculated from the simulations show that the simulated  $TSS_F$ ,  $TSS_E$  and  $TSS_{net}$  are much lower than the simulated  $TSS_{dep}$  (Table 4.5). This indicates that the model simulations clearly underestimate the role of the tidal creeks system in supplying suspended sediment to the high marsh surface. As a consequence,

TABLE 4.4. Summary of water balance calculations for the high marsh surface for the semi-diurnal tidal cycle of 11/08/2002, based on the field measurements and simulations:  $V_{HW}$  = total water volume stored at high tide above the high marsh surface;  $V_F$  and  $V_E$  = total water volumes discharged through the creeks system at Frame 3 during flood ( $V_F$ ) and ebb ( $V_E$ ).

$V_{HW}$ (m <sup>3</sup> )	measured				simulated			
	$V_F$ (m <sup>3</sup> )	$V_F$ (%)*	$V_E$ (m <sup>3</sup> )	$V_E$ (%)*	$V_F$ (m <sup>3</sup> )	$V_F$ (%)*	$V_E$ (m <sup>3</sup> )	$V_E$ (%)*
14055	7419	53	9337	66	3679	26	4323	31

\* % relative to  $V_{HW}$

TABLE 4.5. Summary of sediment balance calculations for the high marsh surface for the semi-diurnal tidal cycle of 11/08/2002, based on the field measurements and simulations:  $TSS_{dep}$  = total sediment mass deposited on the high marsh surface;  $TSS_F$  and  $TSS_E$  = total sediment mass discharged through the creeks system at Frame 3 during flood ( $V_F$ ), ebb ( $V_E$ ), and net ( $TSS_{net}=TSS_F+TSS_E$ ). All values are in tonnes dry weight. Positive values indicate an import of suspended sediments, while negative values indicate that suspended sediments are exported.

$TSS_{dep}$	measured			simulated			
	$TSS_F$	$TSS_E$	$TSS_{net}$	$TSS_{dep}$	$TSS_F$	$TSS_E$	$TSS_{net}$
0.20	0.79	-0.54	0.24	0.38	0.10	-0.07	0.03

the model simulates that the major part of the suspended sediment is transported to the high marsh through the high marsh edge and not via the creeks system, which is in contradiction with the field data.

A number of other contradictions between the model simulations and the field data can be attributed to the same fact that the model simulates the flooding and draining of the high marsh platform from the high marsh edge and not from the creeks. Figure 4.12 shows that the velocity pulses, that were observed at Frame 3 in the main creek at the moment of flooding and draining of the surrounding marsh platform (see chapter 3), were not simulated properly by the model. Instead a decrease in the creek flow velocity was simulated once the high marsh surface was flooded (Fig. 4.12). The velocity pulses, which are widely reported from tidal marsh creeks (e.g. Bayliss-Smith *et al.*, 1979; Healey *et al.*, 1981; Dankers *et al.*, 1985; Stoddart *et al.*, 1989), are explained by the sudden increase in the creek

discharges, at the moment of flooding and draining of the surrounding marsh platform *from* and *to* the tidal creeks (Pethick, 1980; Allen, 1994). However, the model predicts that progressive flooding of the high marsh platform starts from the high marsh edge and *not* from the tidal creeks (Fig. 4.6). As a consequence, the flow velocity pulses, that are typically observed in tidal marsh creeks, are not simulated by the model.

In addition, flow directions perpendicular to the tidal creeks, as observed at the beginning of flooding and at the end of draining of tidal marsh platforms (e.g. Wang *et al.*, 1993; Leonard, 1997), were not simulated here. Instead flow directions were simulated to be more or less perpendicular to the marsh edge (Fig. 4.6). Furthermore, the decrease of flow velocities and SSC with increasing distance from tidal creeks (e.g. Leonard *et al.*, 1995a; Leonard and Luther, 1995; Christiansen *et al.*, 2000; Leonard *et al.*, 2002) is also not simulated by the model, but the model simulations show a clear decrease of SSC with increasing distance from the marsh edge. As a result, the simulated spatial sedimentation pattern also indicates a decrease in sedimentation rates with increasing distance from the marsh edge (Fig. 4.9), which is in accordance with the field measurements. However, the decrease of sedimentation rates with increasing distance from the tidal creeks was not simulated properly by the model. We can conclude then that the overall spatial sedimentation pattern is reasonably well simulated, although the model underestimates the role of the tidal creeks system in supplying water and sediments to the high marsh platform.

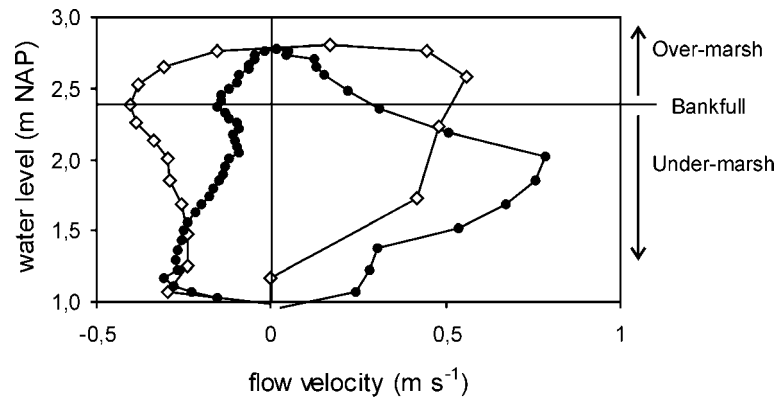


FIGURE 4.12. Water level-flow velocity curve observed (in white symbols) and simulated (in black symbols) for the semi-diurnal cycle of 11/08/2002 at Frame 3 in the main tidal creek.

#### 4.4.2. The influence of vegetation

The model simulations indicated that the vegetation cover on tidal marshes does not have a significant influence on the spatial sedimentation pattern. This conclusion is remarkable, since it is widely assumed that vegetation on tidal marshes plays a crucial role in reducing flow velocities and shear stresses and promoting the deposition of suspended sediments (e.g. Leonard *et al.*, 1995; Leonard and Luther, 1995; Shi *et al.*, 1996; Boorman *et al.*, 1998; Yang, 1999). However, the impact of different vegetation types and the relative importance of the presence of a vegetation cover on the spatial sedimentation pattern are unclear.

On the one hand, the model simulated that strong differences in vegetation structure, ranging from a vegetation cover typical for NW European salt marshes (rather low stands of e.g. *Puccinellia maritima*, *Halimione portulacoides*, *Spartina anglica*) and freshwater marshes (high and dense stands of *Phragmites australis*), do not result in significantly different spatial sedimentation patterns. In agreement with these simulations, field measurements showed that the same spatial sedimentation patterns are found on salt and freshwater marshes in the Scheldt estuary (Temmerman *et al.*, 2003b; see chapter 2). Furthermore, Leonard *et al.* (2002) showed that the detailed flow dynamics, suspended sediment concentrations and deposition rates were not significantly different within a *Spartina* and *Phragmites* marsh in the Chesapeake Bay (USA). They attributed their findings to the low water levels and very low flow velocities (less than  $5 \text{ cm s}^{-1}$ ) encountered in tidal marshes, which limits the interaction between the flow and the vegetation. In accordance with these findings, both our field studies and the model simulations suggest that differences in vegetation structure, ranging from salt to freshwater marsh vegetation, are not strong enough to have a significant effect on flow hydrodynamics and sediment transport and deposition on tidal marshes.

On the other hand, the model simulations indicated that even the presence or absence of a vegetation cover makes no significant difference for the simulated spatial sedimentation pattern. However, field studies comparing vegetated marshes and adjacent unvegetated tidal flats illustrated that flow velocities are typically lower, while sedimentation rates are higher within the vegetation than on the unvegetated tidal flat (e.g. Yang, 1998; 1999; Shi *et al.*, 2000). Nevertheless, in this respect, the question may be raised whether the difference in flow and sedimentation processes on vegetated marshes and unvegetated tidal flats reflects the influence of vegetation rather than the influence of the higher elevation of tidal marshes within the intertidal zone. As a consequence of this higher elevation, tidal marshes are typically inundated by the uppermost portion of the tidal curve, very close to high water when the rate of vertical water level change and consequently horizontal flow velocities are smallest during a tidal cycle. Furthermore, the typically flat topography of vegetated tidal marsh platforms creates no

important hydraulic gradients or divergence of water, which prevents the formation of concentrated flow and higher flow velocities. The high elevation and flat topography of tidal marshes may then be an explanation why the model simulates very low flow velocities and bottom shear stresses even without a vegetation cover and why the simulated sedimentation pattern is not significantly different with or without a vegetation cover. This may be especially the case for high inner marshes, which are under normal conditions only inundated with an inundation height of 0.2 to 0.5 m.

However, a number of uncertainties related to the model simulations may also be identified. First, questions may be raised concerning the plausibility of the simplified model representation of vegetation by rigid cylindrical structures. In reality, vegetation has a much more complex morphology and can bend under flow conditions. Secondly, during extremely high inundation events, accompanied with higher flow velocities and bed shear stresses, the presence of a vegetation cover may play a more significant role in reducing flow velocities and promoting sediment deposition. However, such scenarios were not investigated here with the model. Finally, other mechanisms, such as wave damping by marsh vegetation, were not incorporated in this model application. Especially for low marsh parts near the seaward marsh edge, vegetation has a considerable influence on the attenuation of waves (Möller *et al.*, 1999) and therefore may impact the spatial pattern of sediment transport and deposition near the marsh edge.

#### *4.4.3. Complex hydrodynamic versus simple topography-based modelling*

Compared with the complex hydrodynamic Delft3D model, the rather simple topography-based model is able to predict very well the spatial sedimentation pattern observed at the study site. Comparison of Figure 3.7b (in chapter 3) and Figure 4.8 (in this chapter) shows that for the topography-based model, the resulting  $R^2$  values were 0.87 for the calibration dataset and 0.72 for the validation dataset. For the hydrodynamic model  $R^2$  values amounted 0.82 and 0.67 for the calibration and validation dataset, respectively. It is clear then that the performance of both model approaches is very comparable.

Physically-based hydrodynamic and sediment transport models, like the Delft3D model, have the advantage that they incorporate in detail the physical processes of water flow and sediment transport over an area with complex topography. As a result, such models can be used to improve our understanding of flow and sediment transport processes in, in principal, any aquatic environment and, as this study suggests, also in tidal marshes. However, a major disadvantage of hydrodynamic models is that they are very data-demanding. They can only be applied after that large datasets are gathered on time-series of tidal water level, flow velocities and suspended sediment concentrations and high-resolution spatial data on marsh surface elevation and vegetation characteristics. Furthermore, a large number of

additional parameter values need to be estimated (e.g. sediment settling velocities, critical shear stresses for erosion/sedimentation etc.), which makes the model very sensitive to errors on these parameter estimates and which implies careful calibration and validation of the model against field data. Another disadvantage of hydrodynamic models is that large computation times are needed to solve the complex numerical schemes. For this application for example, where every model run simulated one tidal inundation cycle (5 h real time), it took about 2 h 15 min to carry out one model run on a Pentium 4 2.4 GHz. It is obvious then that for the study of the long-term (10-100 years) geomorphic evolution of tidal marshes, which is of major importance in tidal marsh research, such a hydrodynamic modelling approach is not appropriate.

In this respect, a simplified modelling approach like the topography-based regression model (eq. 4.4) has a number of advantages since it requires a limited amount of input parameter values and it is very simple in terms of numerical complexity. On the other hand, the model is not physically-based but empirical: the regression parameters  $k$ ,  $l$ ,  $m$  and  $n$  in eq. 4.4 are determined from field data. As a consequence, the topography-based regression model is probably much more area-specific than the physically-based hydrodynamic model and it may be questioned whether the regression model is applicable to other tidal marshes. Furthermore, the topography-based approach does not allow to predict the impact of changing environmental conditions, such as changes in incoming sediment concentrations. In this respect, a more physically-based approach has to be used. It may then be concluded that both model types have advantages and disadvantages: as shown in this study, the combined use of both model types therefore allows for a better understanding of marsh sedimentation dynamics.

#### 4.5. Conclusions

This study presented the calibration and validation of a state-of-the-art hydrodynamic and sediment transport model, Delft3D, to simulate the two-dimensional spatial pattern of sediment deposition over a marsh surface. The simulated spatial variations in sedimentation rates were shown to correspond well with observed spatial variations. However, the role of tidal creeks in determining flow and sediment transport pathways within tidal marshes is underestimated by the model. This leads to the conclusion that hydrodynamic models offer clear potential for use as a predictive tool, but need to be applied with caution. Further work is needed to enhance the representation of hydrodynamic and sediment transport phenomena that are typical for tidal marshes.

Further, this study investigated the role of different factors that are generally thought to control tidal marsh sedimentation. First, model simulations showed that the vegetation covering the marsh surface has no important effect on the deposition of suspended sediments. Especially the topography of the marsh surface determines the simulated spatial sedimentation pattern, while the influence of the vegetation cover is negligible. Secondly, the model simulations indicated that higher concentrations and settling velocities of the incoming suspended sediment result in higher sedimentation rates, without any systematic change in the spatial differences in sedimentation rate. Finally, during tidal inundation cycles with higher high water levels, more sediment is deposited on the marsh surface and the suspended sediment is transported relatively higher on the marsh and farther away from the marsh edge before it is deposited.

## Part II

### LONG-TERM ACCUMULATION

---



## Chapter 5

# Modelling long-term tidal marsh accumulation under changing tidal conditions and suspended sediment concentrations \*

---

### 5.1. Introduction

Tidal marshes are widely recognised as net sinks of sediment, which leads, in the long-term, to vertical rise or accumulation of tidal marsh platforms and which is the major factor that controls changes in the ecological and economic functions of tidal marshes (Allen and Pye, 1992; Reed, 1993). Numerous field studies have been conducted on sediment accretion in tidal marshes on time-scales of less than 100 years, using a wide range of measuring techniques (see Allen (1990), French and Spencer (1993) and Allen (2000) for an overview). An important insight in the accumulation of tidal marshes on time-scales of the order of  $10^2$  to  $10^3$  years comes from the study of Pethick (1981). He observed an asymptotic relationship between marsh surface elevation and age for the salt marshes of north Norfolk (U.K.), from which he concluded that young tidal marshes are rapidly built up. As

---

\* Based on: Temmerman, S., Govers, G., Meire, P. and Wartel, S., 2003. Modelling long-term tidal marsh growth under changing tidal conditions and suspended sediment concentrations, Scheldt estuary, Belgium. *Marine Geology*, 193(1-2): 151-169.

the marsh surface rises higher within the tidal frame and is consequently less flooded, the accumulation rate decreases and the marsh surface finally tends to an equilibrium level high in the tidal frame (Pethick, 1981). This negative feedback mechanism between elevation and accumulation rate is widely assumed to be the most important mechanism controlling the long-term vertical accumulation of tidal marshes (e.g., Letzsch and Frey, 1980; Allen, 1990; 2000; French, 1993). When the marsh surface is in equilibrium with the tidal frame and continues to aggrade under rising sea-level, the accumulation rate is assumed to be equal to the rate of sea-level rise (e.g., Allen, 1990; Shi, 1993; Orson *et al.*, 1998). In many places however, it was found that tidal marshes are not able to keep up with rising sea-level (Reed, 1995; Ward *et al.*, 1998), resulting in submergence and major losses of tidal marsh areas (Baumann *et al.*, 1984; Walker *et al.*, 1987; Kearney and Stevenson, 1991).

A relatively small number of physically-based numerical models were developed to simulate and to help understand long-term ( $10\text{-}10^3$  years) vertical marsh dynamics. These models are based on a 0-dimensional time-stepping modelling approach, to simulate the vertical accumulation of marsh platforms with time at one point in space that is considered representative for the whole platform (Krone, 1987; Allen, 1990; 1995; 1997; French, 1993). On shorter time-scales ( $< 1$  year) spatial variations in sedimentation rates within a marsh are significant (French and Spencer, 1993; French *et al.*, 1995; Leonard, 1997; Temmerman *et al.*, 2003b; see chapters 2, 3 and 4 of this thesis) and a 1- or 2-dimensional spatially distributed modelling approach has to be used (Allen, 1994; Woolnough *et al.*, 1995). For longer time-scales ( $10\text{-}10^3$  years), however, the general flat topography of marsh platforms suggests that the 0-dimensional approach is acceptable.

The existing models of Krone (1987), Allen (1990), and French (1993) are all based on the same basic principle of a negative feedback between marsh surface elevation and frequency of tidal inundation. A simple mass balance approach is used, since the complex flow structure in and over the marsh vegetation and complex variations in suspended sediment supply and settling velocity are still poorly understood (e.g., Pethick *et al.*, 1990; Leonard and Luther, 1995; Shi *et al.*, 2000). Krone (1987) proposed a 0-dimensional mass balance model, which was used to simulate the response of tidal marshes in San Francisco Bay to historical sea-level change. These simulations showed that marsh surfaces only attain a relative equilibrium level after the rate of sea-level rise becomes constant. French (1993) followed a similar modelling approach to simulate marsh response to regional subsidence and to several scenarios of future sea-level rise along the barrier-coast of north Norfolk (U.K.). Allen (1990) conducted a series of numerical experiments on the long-term vertical accumulation of Holocene salt marshes in the Severn estuary (U.K.), under different rates of sea-level change and of organic sediment deposition. With a similar modelling scheme Allen (1995; 1997)

also simulated the succession of minerogenic to organogenic marshes and the expansion and shrinkage of marsh creek networks, when sea-level fluctuates about an underlying upward trend.

However, as indicated by Allen (1997), the model applications described above are rather exploratory and were especially conducted to investigate the general long-term behaviour of tidal marshes. They were only to a very limited degree validated using observed data, so that the results are only qualitatively valid. This paper aims to evaluate a refined 0-dimensional time-stepping model for vertical marsh accumulation. First, the historical accumulation at two locations within a specific minerogenic tidal marsh is reconstructed using field data and is used as an independent data set for model testing. Second, the input variables for the model are obtained by extensive short-term field measurements of the suspended sediment regime at the actual marsh surface. The implementation and evaluation of the model shows that an important modification of the existing models is necessary to obtain model predictions that are in good agreement with long-term field observations.

## 5.2. The study area

For a description of the Scheldt estuary we refer to paragraph 1.2 in chapter 1. The marsh studied in this chapter, the Notelaar marsh, is located in the most seaward part of the fresh water zone of the Scheldt estuary, nearly 4 km downstream from Temse (see Fig. 1.2 in chapter 1). The Notelaar marsh has a total area of 27 ha and covers a length of 2 km along the stream channel of the Scheldt estuary. It typically consists of a vegetated marsh platform, with elevation differences never greater than 0.30 to 0.40 m, and is dissected by tidal creeks that branch, narrow and shallow inland. The marsh is situated in the zone where the tidal range and suspended sediment concentrations attain their largest values along the Scheldt estuary. Local tidal water levels are represented in Figure 5.1, in relation to the marsh surface elevation. The vegetated marsh platform is only flooded during spring tides, while the unvegetated tidal flat, which borders the marsh, is flooded during every high tide. The vegetation at the Notelaar marsh consists of typical freshwater tidal marsh plants, consisting of *Phragmites australis* in the lower elevations of the marsh and a community of *Salix* sp. in the higher elevations (Fig. 5.2d). Both plant communities are abundant producing a very dense vegetation cover. In these freshwater tidal marshes, *Phragmites australis* reaches exceptional heights of up to 4 m.

### 5.3. Materials and methods

#### 5.3.1. Assessment of historical long-term morphodynamics

The morphodynamics at the Notelaar marsh during the past five decades were reconstructed using a combination of two methods: (1) the interpretation of aerial photographs of different ages, and (2) sampling and analysis of undisturbed sediment cores.

The Notelaar marsh is covered by 10 aerial photograph series, which date from 1944 to 1998. These photos of successive age clearly illustrate how the geomorphology, land use, and vegetation cover changed during the past five decades. Four maps were made based on four aerial photograph series (1944, scale 1:16.800; 1951, 1:18.000; 1965, 1:10.000; and 1998, 1:10.000) that illustrate all changes in land use or vegetation cover that occurred at the Notelaar marsh over this time period (Fig. 5.2).

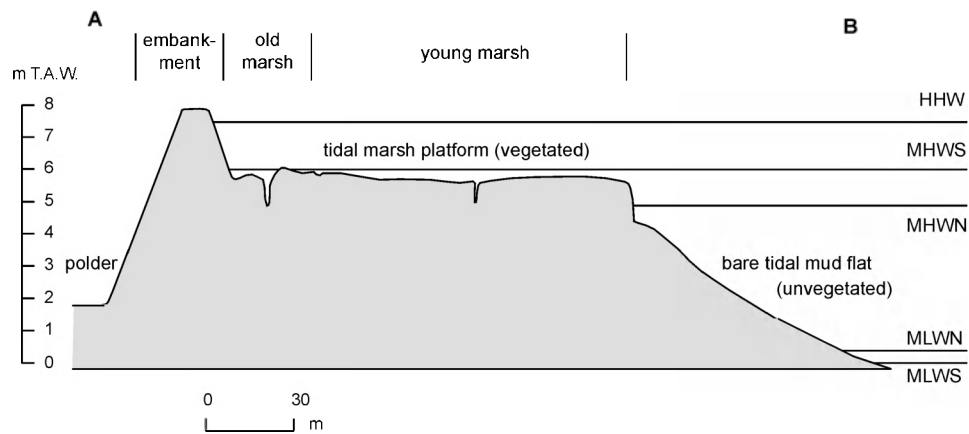
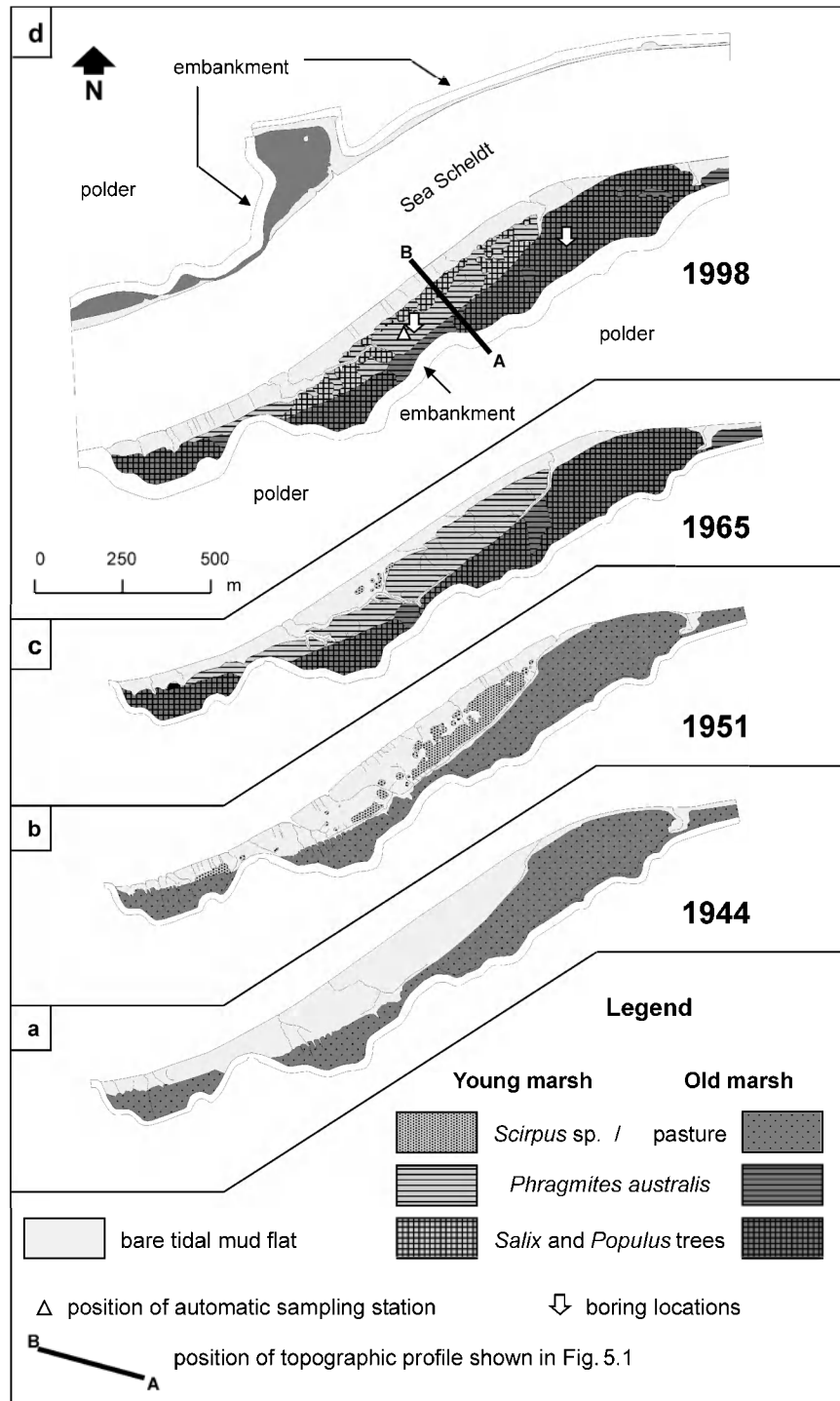


FIGURE 5.1. Topographic profile across the Notelaar marsh (see Fig. 5.2d for location of profile A-B). Local tidal water levels are indicated relative to Belgian Ordnance Level (TAW) HHW = highest high water level; MHWLS and MHWLN = mean high water level at spring and neap tide resp.; MLWLN and MLWLS = mean low water level at neap and spring tide, respectively).

Based on vegetative changes observed from aerial photographs, two marsh sections can be distinguished, which are further referred to as the young and old marsh (Temmerman, 1999). From both marsh sections undisturbed sediment cores were collected with a “Beeker-sampler”, a piston corer with thin-walled tubes of 5.7 cm in diameter and 150 cm in length and an inflatable valve at the bottom that prevents sediment loss while raising the corer to the surface. Both at the young and old marsh, a series of 5 replicate cores was collected within a small boring area of no more than 10 by 10 m (Fig. 5.2d). The marsh surface elevation at both boring locations was measured, relative to the fixed datum of the Belgian levelling network (TAW or Tweede Algemene Waterpassing). All sediment cores were analysed in 1 cm sections to identify the plant debris that was preserved within the deposited sediment. Only plant debris of above-ground origin was considered (i.e., no roots, but only leaves and stems). This plant debris was assumed to be deposited in situ. The floating in of debris originating from distant marsh sections with a different vegetation cover, is very unlikely, because the dense and 2 to 4 m high vegetation cover prevents large displacement of plant detritus during tidal inundations, which are only exceptionally higher than 1.5 m. In this way, we identified for each boring location sediment layers containing different plant debris, which could be related to the different land use or vegetation cover types that succeeded in time at the specific boring location.

The contact elevation between sediment layers with different plant debris corresponds in time to the historic marsh surface elevation at the moment of land use/vegetation cover change. This change was then dated using the aerial photographs. In this way, a series of time-elevation points was determined. The error on the contact elevations was estimated by the standard deviation, as determined from the five replicate cores, and was found to be low (between 3.3 cm and 6.4 cm). The error on the dating of the historic land use/vegetation cover change, with which a contact elevation is associated, is determined by the time interval between successive aerial photos before and after the land use or vegetation cover change (see also Fig. 5.3). Finally, from these time-elevation points a long-term historical accumulation rate of the marsh surface was calculated.

For comparison, recent accumulation rates were measured at four locations (two close to each of both boring locations) using white feldspar marker horizons of 60 by 60 cm, placed on the marsh surface on 30/03/2000. Thickness of sediment deposits was estimated after 2 years by the mean and standard deviation of 6 measurements above each marker horizon, using a small gouge (diameter = 1.5 cm).



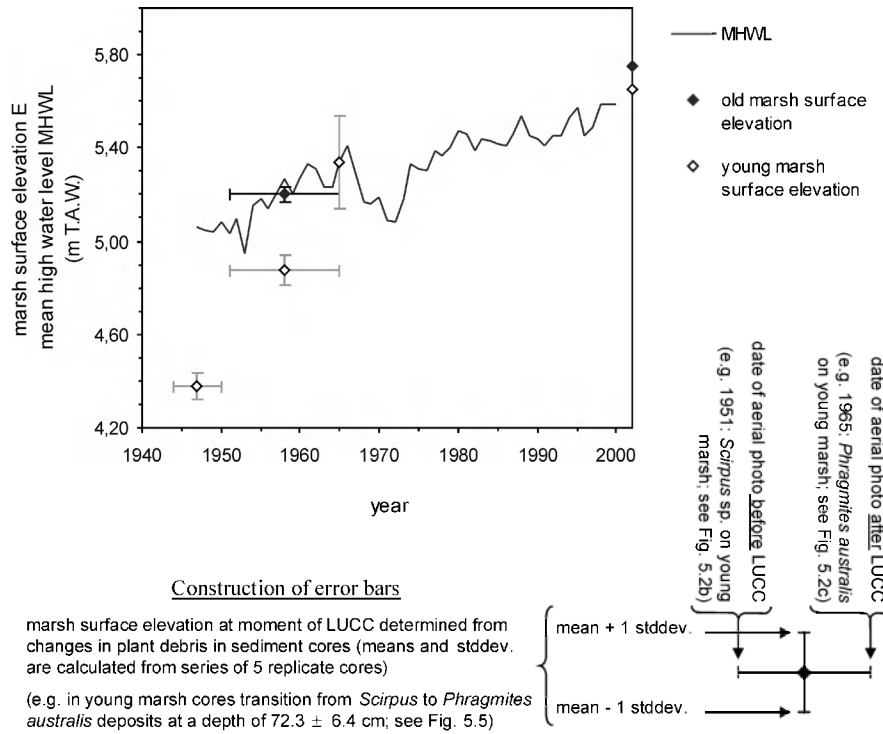


FIGURE 5.3. Observed vertical accumulation of the old and young marsh of the Notelaar. Construction of time-elevation points is based on land use or vegetation cover changes (LUCC), which could be dated using aerial photos (see Fig. 5.2) and the marsh surface elevation at that moment was derived from sediment cores (see Fig. 5.5). The construction of error bars is explained in the lower part of this figure (error bars for the 2002 data points, which are the measured present-day marsh elevations, are  $< 0.01$  m and are therefore not shown). MHWL = yearly mean high water level (Waterways and Maritime Affairs Administration of the Flemish Community).

FIGURE 5.2. Reconstruction of the land use and vegetation cover types that succeeded in time at the Notelaar marsh, based on aerial photographs dating back to (a) 1944, (b) 1951, (c) 1965 and (d) 1998; on this last map the position of the automatic sampling station, the cross-section in Figure 5.1 and the boring locations at the young and old marsh are also indicated.

### 5.3.2. Measurement of actual sediment dynamics

During a one-year period (April 2000 - April 2001), temporal variations of suspended sediment concentration in the flooding water were measured, using an automatic sampling station, located at the boring location on the young marsh (see Fig. 5.2d). For every tidal inundation during the year, the water level above the marsh surface was measured automatically every 5 minutes with an ISCO flowmeter 4220 and saved as digital time-inundation height data. At the same time, samples from the flooding water were automatically pumped up from a sampling point, located at 0.15 m above the marsh surface, and stored in 1 litre bottles with an ISCO sampler 6700. The sampler and flowmeter were programmed in such a way that, once the inundation height was higher than 0.15 m, a first sample was taken. Subsequent samples were collected every 30 minutes, until the water level was again below 0.15 m above the marsh surface. This sampling routine was repeated for each inundation cycle during the 1-year measuring period. Every 15 days (at every neap tide) the filled bottles were collected and replaced by empty ones. In the laboratory, water samples were filtered with filter papers (pore diameter = 0.45  $\mu\text{m}$ ) to determine the suspended sediment concentration (SSC in g/l). In order to reduce the laboratory work, samples of only 4 or 5 tidal inundation events were analysed for each spring-neap cycle so that the full range of low to maximum inundation events during that spring-neap cycle was covered. In all, 194 samples were analysed, covering 102 tidal inundations spread over 25 spring-neap cycles or 27 % of the total number of inundation events during the 1-year measuring period.

### 5.3.3. Description of the numerical model

Following the 0-dimensional time-stepping model approaches of Allen (1990; 1995; 1997) and French (1993), the rate of change in marsh surface elevation  $E$  (in m relative to a fixed datum) at a certain point may be written as:

$$dE/dt = dS_{\text{min}}/dt + dS_{\text{org}}/dt + dP/dt \quad (5.1)$$

where  $dS_{\text{min}}/dt$  is the rate of mineral sediment deposition,  $dS_{\text{org}}/dt$  the rate of organic sediment deposition and  $dP/dt$  is the rate of compaction of the deposited sediment, after dewatering, under younger sediment load. All terms are in m/year.

The yearly rate of mineral sediment deposition  $dS_{min}/dt$  is further specified as (after Krone, 1987):

$$dS_{min}/dt = \int_{year} \int_T \frac{w_s \cdot C(t) \cdot dt}{\rho} \quad (5.2)$$

Sediment deposition is here classically modelled as the product of a characteristic settling velocity  $w_s$  (in m/s) and the depth-averaged concentration  $C$  (in g/l or kg/m<sup>3</sup>) of the suspended sediment above the marsh surface. During one tidal inundation,  $C$  varies with time  $t$ . In order to obtain the thickness of the deposited sediment layer, this product is divided by the dry bulk density  $\rho$  (in kg/m<sup>3</sup>) of the inorganic surface sediment, after dewatering over spring-neap and seasonal time-scales. This deposition term is first integrated over the total duration  $T$  of one tidal inundation and then over all inundations during a year. Equation 5.2 ignores the existence of a vertical sediment concentration gradient in the water column overlying the marsh surface, and assumes that there is no resuspension of sediment, once it has settled to the marsh surface. These assumptions are acceptable, because the inundation heights and flow velocities above the marsh surface are typically low, due to the very flat topography and hydraulic resistance by the dense and high marsh vegetation.

The temporal variation  $C(t)$  during one inundation is modelled using the following mass balance equation:

$$\frac{d[h(t) - E] \cdot C(t)}{dt} = -w_s \cdot C(t) + C(0) \cdot \frac{dh}{dt} \quad (5.3)$$

where  $h(t)$  is the time-dependent water surface elevation,  $E$  is the elevation of the marsh surface for a given year and  $C(0)$  is the sediment concentration (in kg/m<sup>3</sup>) in the flooding water.  $h(t)$  and  $E$  are expressed in m relative to a fixed datum. Equation 5.3 describes the change in suspended sediment mass above a unit area of the marsh surface (first term), as a result of the vertical settling of suspended sediment (second term) and lateral flux of water with a suspended sediment concentration  $C(0)$  (third term).  $C(0)$  will have a specific value during the flood tide (when  $dh/dt > 0$ ), while during the ebb tide (when  $dh/dt < 0$ )  $C(0)$  is set to equal  $C(t)$ . This equation also assumes that there is no resuspension after sediment deposition. Further derivation of eq. 5.3 leads to the mass balance equation that was proposed by Krone (1987) and also used by French (1993):

$$[h(t) - E] \cdot \frac{dC}{dt} = -w_s \cdot C(t) + [C(0) - C(t)] \cdot \frac{dh}{dt} \quad (5.4)$$

The function  $h(t)$ , describing the temporal variation of the water level within one semidiurnal tidal cycle, is modelled using the average tidal curve at Temse (Fig. 5.4a), where the nearest tide-gauge station of the Flemish Waterways and Maritime Affairs Administration is located (nearly 4 km upstream from the Notelaar marsh). We suppose that this mean tidal curve simply moves up or down as the high water level is higher or lower. This simplification is acceptable because only the uppermost portion of the tidal curve floods the marsh surface.  $h(t)$  can then be calculated for any tidal inundation with a high water level  $h(t_{HW})$  as:

$$h(t) = a \cdot \frac{1}{1 + \left(\frac{t - x_0}{b}\right)^2} + h(t_{HW}) - h(t_{MHW}) \quad (5.5)$$

where  $a$ ,  $b$  and  $x_0$  are constants ( $a = 5.3787$ ;  $b = 10837.0147$ ;  $x_0 = 220.2821$ ) and  $h(t_{MHW})$  = the mean high water level (= 5.44 m TAW at Temse; Claessens and Meyvis, 1994).

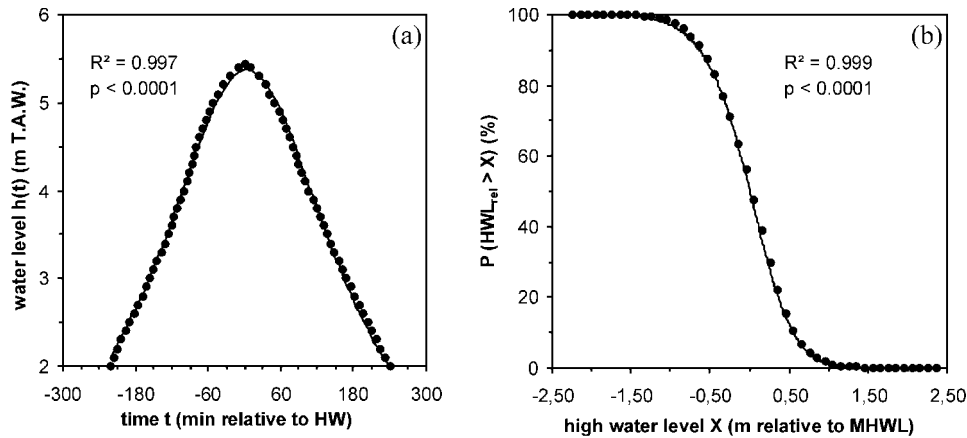


Figure 5.4. (a) Observed (dots) and modelled (line) mean tidal curve at Temse for the period 1981-1990; (b) observed (dots) and modelled (line) high water frequency distribution at Antwerp for the period 1981-1990. All observed tidal data were provided by the Waterways and Maritime Affairs Administration of the Flemish Community.

From eqs. 5.5, 5.3 and 5.2,  $dS_{\min}/dt$  can now be computed for single tidal inundations with a certain high water level  $h(t_{\text{HW}})$ . To calculate the total sedimentation rate  $dS_{\min}/dt$  for every year in the simulation period, the frequency distribution of high water levels has to be simulated for every year. To do this we used the observed evolution of yearly mean high water level (MHWL) at Temse and the yearly-averaged frequency distribution of high water levels around MHWL at Antwerp, which is the nearest tide-gauge station where these data are available (Claessens and Meyvis, 1994). This frequency distribution is modelled as (Fig. 5.4b):

$$P(HWL_{rel} > X) = y_0 + \frac{a}{\left(1 + e^{\frac{(X-x_0)}{b}}\right)^c} \quad (5.6)$$

where  $HWL_{rel}$  is the high water level relative to mean high water level (in m) and  $a$ ,  $b$ ,  $c$ ,  $x_0$  and  $y_0$  are constants (here  $a = 100.5877$ ,  $b = -0.3160$ ,  $c = 1.7014$ ,  $x_0 = 0.2414$  and  $y_0 = -0.0017$ ).  $P$  is expressed in per cent.

The above described simulation model was programmed in Matlab, solving eqs. 5.5, 5.3 and 5.2 in time-steps of 300 s and eq. 5.1 in time-steps of 1 year. In this modelling study, the observed long-term vertical accumulation of the Notelaar marsh was simulated in order to test the model. The assessment of representative values for the model input variables was based on the results of the short-term field measurements.

## 5.4. Results

### 5.4.1. Observed long-term morphodynamics

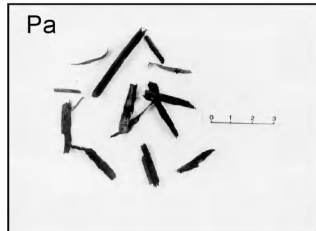
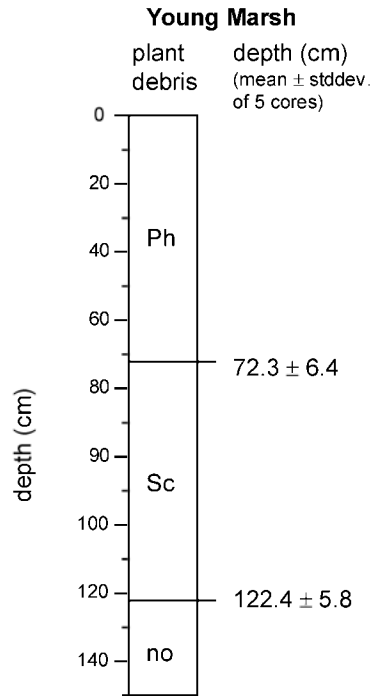
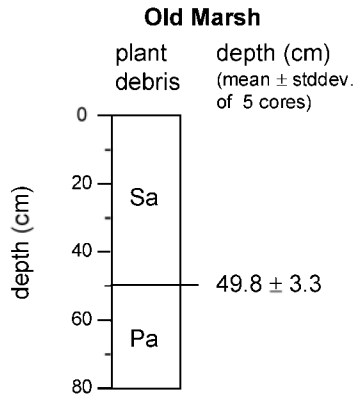
The aerial photographs of the Notelaar marsh show that the present-day marsh consists of two sections: an old marsh, which is already present on the photographs of 1944, and a young marsh, which started to form between 1944 and 1951 (Fig. 5.2). As the old marsh is already shown on the topographic maps of De Ferraris (1774-1777) and Vandermaelen (1846-1854), it must have formed before the end of the 18<sup>th</sup> century. These maps indicate that the old marsh was then used as a pasture. The aerial photographs of 1944 and 1951 show that the old marsh surface was then divided into lots and covered by low grassy vegetation, which leads to the conclusion that the old marsh was still used as a pasture (Fig. 5.2a and b). By 1965, the pasture had disappeared and was replaced by trees, mainly *Salix* and possibly also *Populus* sp. (Fig. 5.2c). The rectilinear growing pattern of these trees indicates that they were planted for the cultivation of willow

withes, which was very common along the Sea Scheldt until the end of the 1960s (Durinck, 1981). Since then an abandoned *Salix* and *Populus* vegetation cover developed at the old marsh (Fig. 5.2d).

In contrast, the young marsh has a different history. Comparison of aerial photos shows that the young marsh was not yet formed in 1944, but instead an unvegetated tidal flat existed (Fig. 5.2a). By 1951, a large part of this tidal flat was colonised by *Scirpus* sp., typically growing in concentric patterns (Fig. 5.2b), which forms the initial stage of the natural vegetation succession of freshwater tidal marshes within the Scheldt estuary (Hoffmann, 1993). By 1965, almost all of the *Scirpus* plants were replaced by a dense, closed *Phragmites australis* cover, the next phase of the natural vegetation succession (Fig. 5.2c). Between 1965 and 1998, some *Salix* trees expanded from the old marsh to the young marsh, especially on the natural levees that developed along the streamside border of the young marsh and along the main tidal creeks. However, at present, *Phragmites australis* remains the dominant plant species over a large portion of the young marsh (Fig. 5.2d).

Both at the young and old marsh, five undisturbed sediment cores were collected, and the macroscopic plant debris in the cores was identified (Fig. 5.5). For the old marsh, the upper sediment layer (to a depth of  $49.8 \pm 3.3$  cm) contains woody plant debris and oblong leafs as a consequence of accumulation under the *Salix* vegetation. Deposits below this level contain no woody plant debris but only small remains of grasses (Fig. 5.5), indicating that these sediments were deposited while the old marsh was still under pasture. For the young marsh, the recent *Phragmites australis* phase is characterised by remains of cylindrical hollow stems (Fig. 5.5). Below  $72.3 \pm 6.4$  cm, the macroscopic plant debris is totally different and consists of large amounts of dark coloured tubers and remains of three-cornered stems, typical for *Scirpus maritimus*. This sharp boundary between *Phragmites australis* and *Scirpus* deposits is also observed at the same elevation in the cliffs that border the young marsh platform. Finally, below  $122.4 \pm 5.8$  cm depth no plant remains are found anymore, indicating that this sediment was deposited when the young marsh was not yet formed, and instead, an unvegetated tidal flat existed.

→  
 FIGURE 5.5. Schematic core logs, presenting the plant debris found in sediment cores taken at the Notelaar marsh: Sa = remains of *Salix* sp. (oblong leafs and wooden debris); Pa = pasture (remains of grasses); Ph = *Phragmites australis* (hollow stems); Sc = *Scirpus* sp. (three-cornered stems and tubers); no = no plant remains (unvegetated tidal flat deposits). The contact elevations, between sediment layers containing different plant debris, are presented here as the arithmetic mean  $\pm$  the standard deviation (stddev.) of 2 series of 5 cores, one series taken at the old marsh and one at the young marsh. The scale bar on the photographs is subdivided in cm.



Each contact level between these sediment layers was dated using the aerial photographs, resulting in a set of time-elevation points for the young and old marsh (Fig. 5.3). One additional point was added to Figure 5.3: extensive vegetation surveys on the freshwater marshes of the Sea Scheldt showed that *Phragmites australis* occurs at MHWL  $\pm$  0.2 m (mean  $\pm$  standard deviation of 50 observations; Criel *et al.*, 1999). On the young marsh of the Notelaar, *Phragmites australis* was first observed on the aerial photographs of 1965. This allows to construct an additional time-elevation point on Figure 5.3.

Figure 5.3 shows that the young marsh started to grow between 1944 and 1951 at an elevation clearly below that of the old marsh. The first colonisation of the bare tidal flat by *Scirpus* sp. was situated at a level of 68.4  $\pm$  5.8 cm below mean high water level at that time (MHWL in black line on Fig. 5.3). This is in agreement with the present day observed appearance of *Scirpus* along the freshwater zone of the Scheldt estuary at a level of 0.6 to 1.7 m below MHWL (Hoffmann *et al.*, 1997). After this *Scirpus* colonisation, the young marsh quickly accumulated to a level only about 0.3 m below MHWL, at a mean accumulation rate of 4.6  $\pm$  3.2 cm/year between 1947 and 1958. During the period 1958-2002, the young marsh aggraded slower (1.8  $\pm$  0.3 cm/year), at a rate only slightly higher than that of the old marsh (1.2  $\pm$  0.2 cm/year), which is in equilibrium with MHWL rise (on average 1.0 cm/year; Fig. 5.3). The actual accumulation rates, measured with feldspar marker horizons, are 1.6  $\pm$  0.1 cm a<sup>-1</sup> and 1.6  $\pm$  0.2 cm a<sup>-1</sup> for the young marsh and 1.5  $\pm$  0.4 cm a<sup>-1</sup> and 1.3  $\pm$  0.2 cm a<sup>-1</sup> for the old marsh. Although these accumulation rates were measured over only 2 years, they are in good agreement with the above-mentioned long-term accumulation rates.

#### 5.4.2. Short-term temporal variations in suspended sediment concentration

Field measurements of the temporal variation in suspended sediment concentration (SSC) above the marsh surface show that the SSC generally decreases with time during a tidal inundation cycle (Fig. 5.6), which is a consequence of settling of the suspended sediment. The initial SSC (i.e., the SSC at the beginning of an inundation cycle at the moment that the inundation height exceeds 0.15 m) varies, however, from one tide to another. Figure 5.7 shows this variation of the initial SSC (ISSC) as a function of the maximum inundation height at high water for every inundation cycle that was sampled. A positive linear relationship is observed between ISSC and maximum inundation height: as the marsh is submerged by higher tides, the flooding water apparently has a higher capacity to transport suspended sediment, so that the ISSC is higher.

In addition, this increase of ISSC with maximum inundation height is much greater during the winter (Oct-Mar) than during the summer period (Apr-Sept). This observation appears to be consistent with observed seasonal variations in SSC in the stream channel of the Scheldt estuary, which are generally attributed to seasonal variations in fresh water discharge, biological activity, wind regime, and terrestrial erosion (e.g., Fettweis *et al.*, 1998). Allen (2000) also indicates that seasonal changes in water viscosity, due to changes in water temperature, can partly explain seasonal variations in SSC in British estuaries.

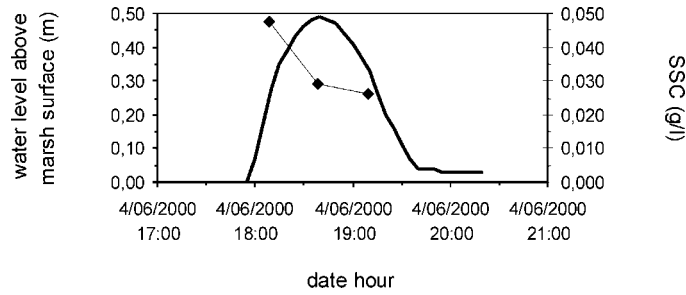


FIGURE 5.6. Example of the temporal variation of the water level above the marsh surface (thick line) and suspended sediment concentration (SSC; symbols and thin line) during 1 tidal inundation of the Notelaar marsh.

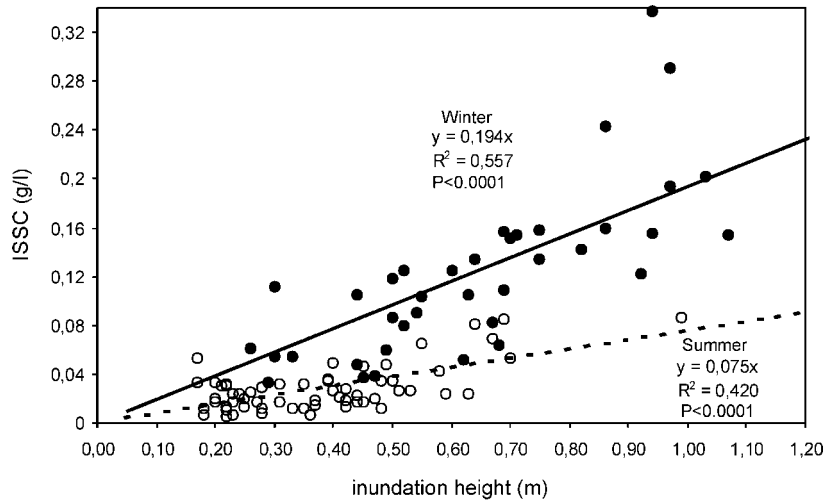


FIGURE 5.7. Linear relationship between initial suspended sediment concentration (ISSC) and inundation height observed at the Notelaar marsh during a 1-year period (Apr-2000 to Apr-2001). Note the difference between summer (Apr-Sept; indicated in white symbols and broken line) and winter (Oct-Mar; black symbols and solid line) observations.

### 5.4.3. Model implementation using empirical input data

The numerical model was applied to the young and old marsh of the Notelaar, using empirical field data as input values for the model variables (Table 5.1: model runs 1 to 4). For both the young and old marsh, the simulation started from the earliest time-elevation point that was reconstructed from the aerial photos and sediment cores: an initial marsh surface elevation  $E(0)$  of 4.35 m TAW in 1947 was taken for the young marsh, and 5.20 m TAW in 1958 for the old marsh. In order to solve the model equations, we further needed input values for the rate of organic sediment deposition  $dS_{org}/dt$ , the compaction rate  $dP/dt$  and the sediment parameters  $w_s$ ,  $C(0)$  and  $\rho$ .

$dS_{org}/dt$  incorporates the deposition of organic matter from below-ground roots as well as from above-ground litter.  $dS_{org}/dt$  varies in response to the succession of tidal marsh plant communities and to complex variations in their biomass productivity and decay processes, so that at present  $dS_{org}/dt$  can not be modelled in a simple way (Allen, 2000). Following the model applications of Allen (1990) and French (1993) we assume as a first approximation that  $dS_{org}/dt$  is constant, which is acceptable for mineral-dominated marshes like the Notelaar marsh. Based on a mean organic matter content of nearly 6 %, measured in the sediment cores, and based on the estimated actual accumulation rate of 0.015 m/year (averaged for the old and young marsh),  $dS_{org}/dt$  is set to  $9 \cdot 10^{-4}$  m/year. Because the value of  $dS_{org}/dt$  is very low, compared to values of  $dS_{min}/dt$ ,  $dS_{org}/dt$  will not have an important influence on the vertical accumulation rate  $dE/dt$ .

The compaction rate  $dP/dt$  is simulated on a yearly basis, so that compaction of recently deposited sediment, primarily due to sediment dewatering over spring-neap and seasonal cycles, is not included. This effect is in fact already included in the value for the dry bulk density  $\rho$  in eq. 5.2, which is estimated at 350 kg/m<sup>3</sup>, based on field measurements at the boring locations. The compaction term  $dP/dt$  only includes the compaction of the deposited sediment, after dewatering, under younger sediment load. Both Allen (1990) and French (1993) assume in their model applications that the compaction rate  $dP/dt$  after dewatering can be set to zero. For the Notelaar marsh, no significant increase in dry bulk density was observed with increasing depth beneath the marsh surface, indicating that compaction is not an important process. Therefore  $dP/dt$  is here set to zero. Cahoon *et al.* (2000a) also showed a close correspondence between sediment accretion and actual elevation change for UK marshes, confirming that compaction in such minerogenic marsh types is not significant. However, on longer time-scales and in more organogenic marsh types compaction can play an important role (Pizzuto and Schwendt, 1997; Allen, 1999; 2000).

TABLE 5.1. Summary of model runs and input parameter values.

Run	Marsh	$C(0)$	$E(0)$ (m TAW)	period	MHWL change
1	Old	$C(0)=cte=0.040$ g/l	5.20	1958-2000	} observed time series
2	Old	$C(0)=k.[h(t_{HW})-E]$	5.20	1958-2000	
3	Young	$C(0)=cte=0.040$ g/l	4.35	1947-2000	} (see Fig. 5.10)
4	Young	$C(0)=k.[h(t_{HW})-E]$	4.35	1947-2000	
5	Young	$C(0)=cte=0.040$ g/l	5.60	2000-2100	} exponential increase (see Fig. 5.11)
6	Young	$C(0)=k.[h(t_{HW})-E]$	5.60	2000-2100	

For every model run:  $w_s = 10^{-4}$  m/s;  $\rho = 350$  kg/m<sup>3</sup>;  $dS_{org}/dt = 6.10^{-4}$  m/yr;  $dP/dt = 0$  m/yr.

To determine the settling velocity  $w_s$  of the suspended sediment, we did not carry out direct measurements on the collected suspended sediment samples, partly because of the low sediment concentrations, which would lead to unreliable measurements of  $w_s$ . Furthermore, such measurements are very difficult for fine-grained estuarine sediments as a consequence of aggregation and formation of flocs, which easily break up when sampled (e.g., Eisma *et al.*, 1997). However, from our measurements, we made an estimation of the *in-situ* settling velocity by inverse modelling. For 44 inundation events, the temporal evolution of the inundation height ( $[h(t)-E]$  in eq. 5.3) and of the suspended sediment concentration ( $C(0)$  and  $C(t)$  in eq. 5.3) were measured, so that the equivalent  $w_s$  can be calculated from eq. 5.3 as:

$$w_s = \left[ \frac{C(0)}{C(t)} - 1 \right] \cdot \frac{dh}{dt} - \frac{[h(t)-E]}{C(t)} \cdot \frac{dC}{dt} \quad (5.7)$$

For all these inundation events  $w_s$  was computed in time-steps of 300 s and averaged over the whole inundation period. The settling velocity of suspended sediment in estuaries is generally found to increase exponentially with suspended sediment concentration, as a consequence of increased interparticle collisions and flocculation processes (e.g., Krone, 1962; Van Leussen, 1988; Eisma *et al.*, 1997). Krone (1987) also uses this exponential relationship between  $w_s$  and  $C(t)$  in his salt marsh accumulation model.

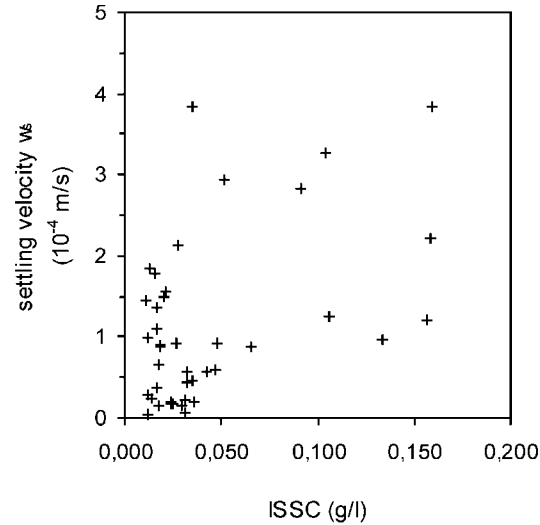


FIGURE 5.8. Variation of settling velocity  $w_s$  at the Notelaar marsh as a function of initial suspended sediment concentration (ISSC).

However, Figure 5.8 shows that there is no clear relationship between the calculated  $w_s$  and the initial SSC at the Notelaar marsh. Teeter (2001) also indicates that this relationship disappears for sediment concentrations smaller than 0.100 g/l. Allen (1990) and French (1993) indicate that complex variations in  $w_s$  exist in the field, but since the knowledge is at present rather limited, they do not model these variations and instead use a constant median settling velocity  $w_s$ . Because no detailed data for the Notelaar marsh are available and this study focuses only on long-term suspended sediment modelling,  $w_s$  is treated here also as a constant, and is estimated from Figure 5.8 to be  $10^{-4}$  m/s.

In eqs. 5.3 and 5.4, the suspended sediment concentration  $C(0)$  in the flooding water is set to equal  $C(t)$  during the ebb tide. During the flood tide, Krone (1987) and French (1993) assume that  $C(0)$  has a constant value for all inundation cycles. They both derive a value for  $C(0)$  by calibrating their model against an observed record of long-term salt marsh accumulation. The obtained  $C(0)$  value is then used as a constant in all subsequent simulations. Allen (1990) does not model the temporal variation of  $C(t)$  during a tidal cycle, like in eqs. 5.3 and 5.4, but only uses eq. 5.2 with a sediment concentration  $C$ , which is assumed to be constant during a tidal cycle. Our field data, however, clearly indicate that  $C(t)$ , as well as  $C(0)$ , are not time-independent.  $C(t)$  decreases with time during a tidal inundation (Fig. 5.6) and

the initial SSC, at the beginning of marsh inundation, varies linearly with maximum inundation height (Fig. 5.7). Therefore,  $C(0)$  can not be considered as a constant, but has to be specified as:

$$C(0) = k \cdot [h(t_{HW}) - E] \quad (5.8)$$

where  $k$  is a constant,  $E$  is the marsh surface elevation and  $h(t_{HW})$  is the water level at high tide (both relative to a fixed datum). In order to evaluate the influence of a linear increase of  $C(0)$  with inundation height on the modelling results, the model simulations were carried out twice. First a constant value for  $C(0)$  was used, following Krone (1987) and French (1993). Based on the field measurements, a constant time-averaged  $C(0)$  value of 0.040 g/l was used, which corresponds with an observed median inundation height of 0.30 m above the surface of the Notelaar marsh (Fig. 5.7). Secondly, eq. 5.8 was incorporated in the model by substitution in eqs. 5.3 and 5.4. Since the deposition rate  $dS_{min}/dt$  is calculated by the model on a yearly basis, the observed seasonal variation of  $k$  is not modelled but a constant value, averaged over the year, of 0.1345 was derived from the field data (Fig. 5.7).

#### 5.4.4. Model results and evaluation

For individual inundation events, a continuous decrease of SSC is predicted, which is in good agreement with the field observations (compare Fig. 5.9a with Fig. 5.6). Furthermore, the simulated sedimentation rate  $dS_{min}/dt$ , summed over the whole period of an inundation cycle, increases linearly with maximum inundation height, when  $C(0)$  is treated as a constant, while an exponential increase is observed, when  $C(0)$  is defined as a function of inundation height (Fig. 5.9b). In the latter case, much greater sedimentation rates are predicted, especially for tidal cycles that result in high inundations. The final modelling results for the young and old marsh of the Notelaar are shown in Figure 5.10. The implementation of Krone's model, using a constant  $C(0)$ -value, results in an important underestimation of the observed accumulation at the Notelaar marsh, both for the young and for the old marsh. However, when the relationship between  $C(0)$  and inundation height is incorporated in the model, the observed vertical accumulation is very well predicted. The original model of Krone (1987) strongly underestimates the sedimentation rate  $dS_{min}/dt$ , especially for young marsh surfaces which have a lower elevation and which are consequently flooded by more and higher tidal inundations (Fig. 5.9b and Fig. 5.10). His model produces somewhat better results with a constant  $C(0)$  value which is about twice the measured mean value of 0.040 g/l, but also in this case his model does not simulate

well the strongly asymptotic decrease of the vertical accumulation rate of the young marsh. This leads to the conclusion that the use of a constant  $C(0)$  value results in biased predictions and that the relationship between  $C(0)$  and inundation height has to be incorporated in the existing simulation models to predict successfully the vertical accumulation rate of tidal marshes.

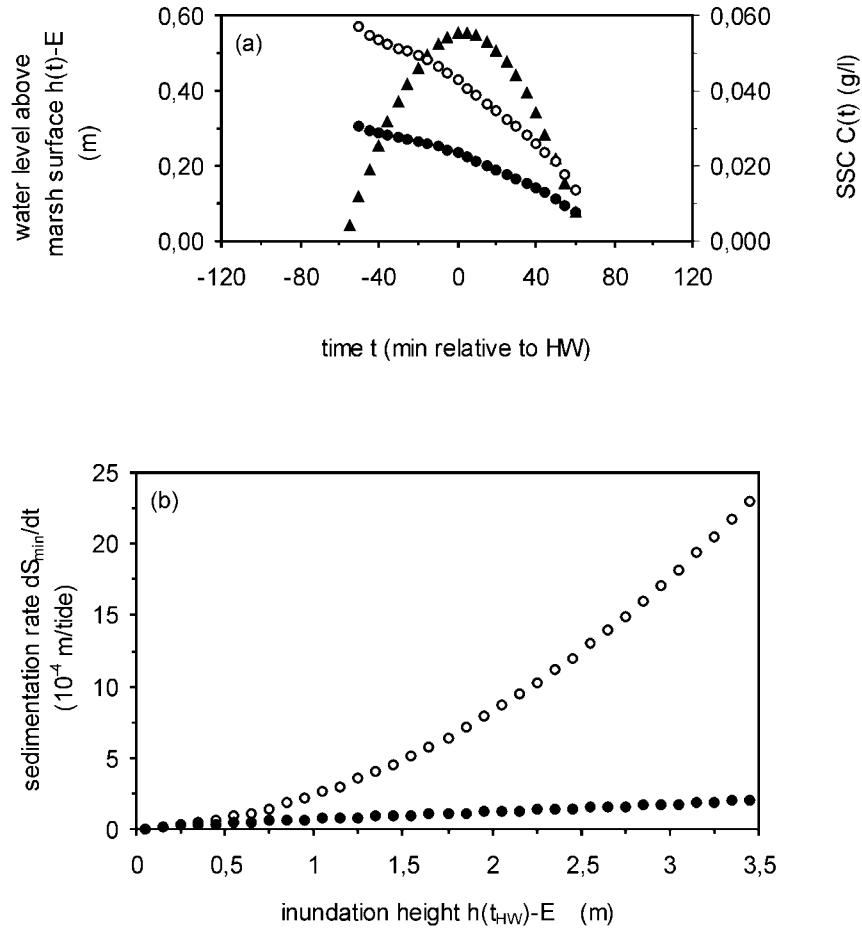


FIGURE 5.9. Comparison of modelling results using a constant  $C(0)$  (of 0.040 g/l) (black dots) or  $C(0) = k \cdot [h(t_{HW}) - E]$  ( $k = 0.1345$ ) (white dots): (a) example of predicted tidal curve (triangles) and temporal evolution of suspended sediment concentration  $SSC$  (dots) during 1 tidal inundation with inundation height = 0.55 m above the marsh surface; (b) predicted sedimentation rate as a function of inundation height for individual tidal inundations with an inundation height ranging from 0.05 to 3.45 m above the marsh surface.

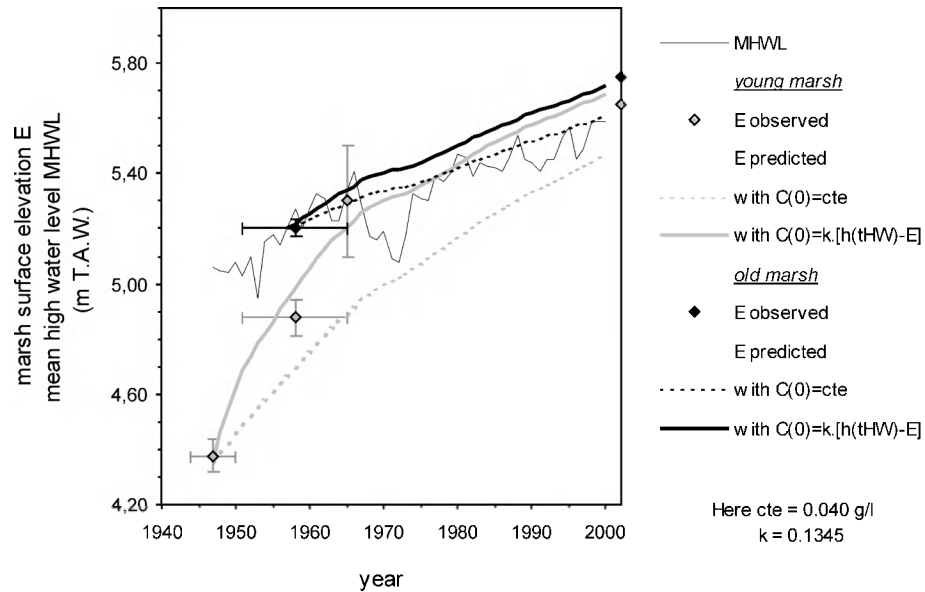


FIGURE 5.10. Observed (symbols) and predicted (lines) vertical accumulation of the young marsh (in grey) and old marsh (in black) of the Notelaar. Model predictions, with  $C(0)=constant (=0.040$  g/l) are indicated with broken lines, while predictions with  $C(0)=k[h(t_{HW})-E]$  ( $k = 0.1345$ ) are indicated with solid lines.

## 5.5. Discussion

The observed vertical accumulation of the Notelaar freshwater tidal marsh corresponds very well with the widely expressed idea that low young salt marshes are characterised by a higher accumulation rate than high old marshes. As the marsh surface rises, the accumulation rate will progressively decrease as a consequence of decreasing frequency and period of tidal inundation (e.g., Steers, 1977; Letzsch and Frey, 1980; Pethick, 1981; Allen and Rae, 1988). The old marsh of the Notelaar has reached an equilibrium level relative to the tidal frame, at an average elevation of 0.1 m to 0.2 m above MHWL, and accumulates as fast as MHWL rises. The young marsh started to grow at a lower elevation. Since then it accumulated very quickly and asymptotically almost up to the equilibrium level of the old marsh (Fig. 5.10). This is in accordance with the findings of Pethick (1981), who showed that a strongly asymptotic relationship exists between age and elevation of salt marshes in north Norfolk (U.K.). Also, a negative correlation between

marsh elevation and sedimentation rate was found in other salt marshes, both from long-term observations (e.g., Allen, 1990; French, 1996) and from short-term measurements (e.g., French, 1993; Allen and Duffy, 1998a).

The very fast accumulation of young freshwater tidal marshes in the Scheldt estuary implies that the inundation frequency and height quickly decreases, and that the initial phase in the vegetation succession with *Scirpus* sp. is consequently rapidly followed by the next phase with *Phragmites australis*. The *Scirpus* phase at the young marsh of the Notelaar had already come to an end at most 15 years after the marsh was formed (Fig. 5.2). The fast accumulation of young marshes is one possible explanation why the area of freshwater *Scirpus* marshes is at present so small along the Sea Scheldt, while the older phases with *Phragmites australis* and *Salix* are very common. The implementation of the model, using Krone's (1987) original mass balance equation with a constant  $C(0)$  value, resulted in a clear underestimation of the observed accumulation of both the young and old marsh of the Notelaar (Fig. 5.10). We found that the use of a constant value for  $C(0)$  is responsible for the failure of the model. Reed (1995), for example, noticed that not only long-term changes in marsh inundation but also changes in suspended sediment concentrations will have an important influence on the long-term response of tidal marsh surfaces. Until now, however, it was found to be very difficult to predict the long-term response of over-marsh suspended sediment concentrations to any changes in marsh inundation height and frequency (Reed, 1995). However, we observed an increase of initial SSC with inundation height from short-term field measurements and considered this increase to be the main mechanism controlling long-term changes in ISSC, when tidal marsh inundation is changing.

A similar positive linear relationship between ISSC and inundation height was observed by Christiansen *et al.* (2000) on a coastal salt marsh in Virginia (U.S.A.), indicating that this modelling approach is possibly also applicable to other tidal marshes in the world. Furthermore, as discussed above, the long-term asymptotic accumulation of the Notelaar marsh corresponds very well with long-term accretionary mechanisms reported from other more marine salt marshes (e.g. Pethick, 1981; Allen, 1990; French, 1996), which further supports the applicability of the model. However, further research is needed to test the possibilities of the presented model structure, to predict observed tidal marsh accumulation rates at other marsh locations, and to come to a more thorough validation of the model.

For the Notelaar marsh, the main processes that caused changes in tidal marsh inundation, and consequently in suspended sediment supply and deposition, are the vertical rise of the marsh surface and the rising mean high water level. Other processes like subsidence or tectonic uplift were not incorporated in the model, since they are negligible compared with the above mentioned processes, at least for the Notelaar marsh. However, in other marsh areas in the world, subsidence or tectonic uplift may impact tidal

marsh accumulation (e.g., Sherrod, 2001) as a consequence of increased or decreased marsh inundation, sediment supply, and deposition.

The incorporation of the positive relationship between ISSC and inundation height has important consequences for the existing simulation models and the conclusions resulting from their implementation. The existing models of Krone (1987), Allen (1990; 1995; 1997) and French (1993) were specifically used to study the long-term vertical rise of tidal marshes when sea-level is rising. Figure 5.11 illustrates how the long-term simulation of tidal marsh accumulation under a future scenario of accelerated sea-level rise is influenced by the use of a constant  $C(0)$  or a  $C(0)$  as a function of inundation height (see also Table 5.1, model runs 5 and 6). Several studies, like the modelling study of French (1993) for the salt marshes along the coast of north-Norfolk (U.K.), indicate that marsh accumulation rates may not be enough to keep pace with future accelerated sea-level rise. The simulations of French (1993) showed that, under the most extreme sea-level rise scenarios, this will result in ‘drowning’ of tidal marsh vegetation and degradation to bare tidal flats. Our simulation model, however,

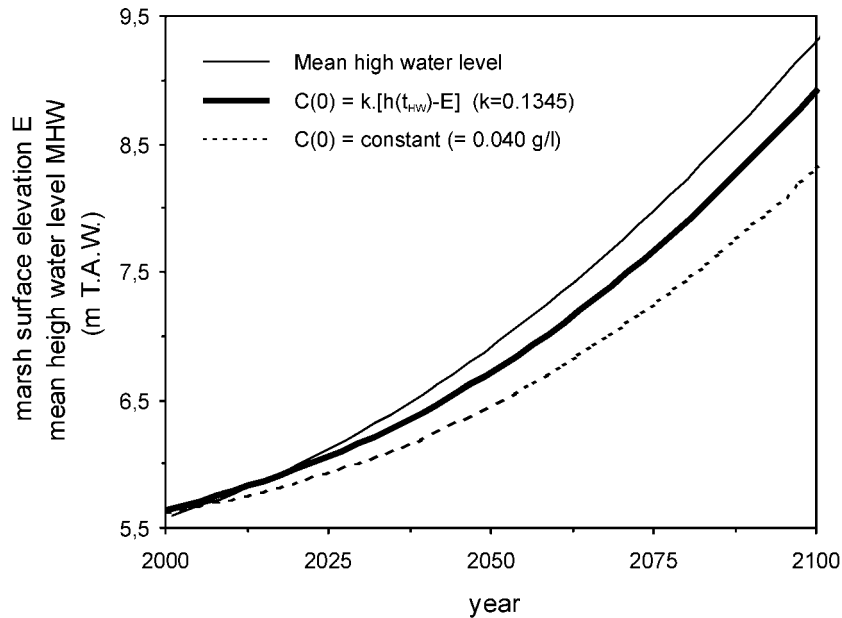


FIGURE 5.11. Simulation of vertical marsh accumulation for the next 100 years, starting from the observed 2000 elevation of the young marsh of the Notelaar, under a scenario of exponential rise of mean high water level (thin solid line), and using a constant  $C(0)$  ( $=0.040$  g/l) (thin broken line) or  $C(0)=k.[h(t_{HW})-E]$  ( $k=0.1345$ ) (thick solid line).

illustrates that, even under an extremely accelerated exponential MHWL rise, degradation of tidal marsh vegetation at the Notelaar marsh will be much longer delayed when the positive correlation between  $C(0)$  and inundation height is taken into account (Fig. 5.11). This correlation is responsible for a strong feedback mechanism through which higher and more frequent marsh inundation results in much higher sedimentation rates. Model simulations, which are based on a constant  $C(0)$ , result in underestimated sedimentation rates and exaggerated fast predictions of tidal marsh degradation. It can therefore be concluded that the long-term over-marsh suspended sediment regime has an important influence on long-term vertical marsh accumulation and that it is extremely important to incorporate the positive correlation between SSC and marsh inundation to model successfully the long-term behaviour of tidal marsh platforms.

### 5.6. Conclusions

- (1) The long-term vertical accumulation of freshwater tidal marshes in the Scheldt estuary is characterised by an asymptotic growth curve. Once a bare tidal flat is colonised by plants, the sediment surface rises rapidly due to sedimentation, until a certain level is attained, which is nearly equal to mean high water level. After that, the accumulation rate quickly decreases and the marsh surface is slowly built up to an equilibrium level, which is only one to two decimetres higher than mean high water level. This sedimentation pattern is in accordance with long-term accretionary mechanisms, reported from more marine salt marsh environments.
- (2) Intensive short-term field measurements showed that the initial suspended sediment concentration, in the water that floods the marsh surface at the beginning of an inundation cycle, increases linearly with maximum inundation height, at high tide. In addition this increase is much greater during the winter than during the summer period.
- (3) A 0-dimensional time-stepping model successfully simulates the observed long-term historical accumulation of the Notelaar marsh, using short-term empirical values for the input variables and incorporating the above-mentioned relationship between sediment concentration and inundation height. Application of the existing models of Krone (1987) and French (1993), without considering this relationship, leads to a strong underestimation of the observed historical accumulation and leads to biased predictions of vertical marsh accumulation under future scenarios of sea-level rise. Therefore the observed relationship between sediment concentration and inundation height has to be incorporated to fully explain and successfully simulate the long-term vertical accumulation of tidal marshes.

## Chapter 6

# Simulating the long-term development of levee-basin topography on tidal marshes \*

---

### 6.1. Introduction

The geomorphology of tidal marshes consist of a rather flat vegetated marsh surface dissected by a dendritic network of tidal creeks. However, the apparently flat surface of high, well-developed marshes is typified by a micro-relief of natural levees bordering the tidal creeks, and lower inner marsh basins located at larger distances from the creeks. This differentiation between levees and basins gives rise to one of the most important geomorphic gradients that determine hydrological, biogeochemical and ecological processes in tidal marshes (e.g. Covi and Kneib, 1995; Zedler *et al.*, 1999; Bockelmann *et al.*, 2002; Kostka *et al.*, 2002).

Analogous to the formation of natural levees along alluvial river channels, it is assumed that levees in tidal marshes arise from the progressive settling of suspended sediments as a consequence of decreasing flow velocities as the rising tide floods the marsh surface and flows through the marsh vegetation,

---

\* Based on: Temmerman, S., Govers, G., Meire, P. and Wartel, S., submitted. Simulating the long-term development of levee-basin topography on tidal marshes. submitted to *Geomorphology*.

starting from the creek margins into the inner marsh. Over recent years, various field studies have shown that at the time scale of individual inundation events the amounts of deposited sediment decrease with increasing distance from stream channels, both in alluvial floodplains (e.g. Walling *et al.*, 1996; Middelkoop and Asselman, 1998) and in tidal marshes (e.g. French *et al.*, 1995; Leonard *et al.*, 1995a; Reed *et al.*, 1999; Temmerman *et al.*, 2003b, see chapter 5). This lateral sedimentation gradient is also reported from a few numerical modelling studies of advective and diffusive sediment transport along transects perpendicular to stream channels of alluvial rivers (James, 1985; Pizzuto, 1987) and perpendicular to tidal creeks in tidal marshes (Woolnough *et al.*, 1995).

Until present the long-term evolution of tidal marsh surfaces has been studied using point data (e.g. Cundy and Croudace, 1996; Roman *et al.*, 1997) and 0-dimensional models simulating marsh accumulation with time at one point in space (Krone, 1987; Allen, 1990; French and Spencer, 1993; Allen, 1995; 1997; Day *et al.*, 1999; Van Wijnen and Bakker, 2001; Pont *et al.*, 2002; Rybczyk and Cahoon, 2002; Temmerman *et al.*, 2003a). These point approaches allow to investigate the overall response of tidal marshes to changing factors, such as changing sea level rise and changes in incoming sediment concentration (e.g. Allen, 1990; French and Spencer, 1993; Temmerman *et al.*, 2003a), but does not allow to understand the implications of the spatial variations in sedimentation rates on the development of geomorphic gradients *within* marshes. Up to now, we have a very little understanding of the long-term development of natural levees and of the factors controlling the height difference between levees and adjacent basins.

This paper aims to get a better insight in the long-term evolution of the surface elevation of tidal marsh levees and basins, by applying a 0-dimensional model using spatially differentiated parameter values for levee and adjacent basin locations. First, the model is calibrated using field data on short-term (<1 year) temporal variations in sedimentation rates measured along a series of levee-basin transects. Second, the ability of the model to predict the long-term (10-100 years) elevation change of levees and inner marsh basins is evaluated by comparing predicted elevations with the present-day observed topography along the studied levee-basin transects. Finally, additional model simulations are carried out to determine the dominant factors that control the height difference between tidal marsh levees and basins and to simulate the long-term response of levees and basins to different scenarios of changing sea-level and incoming sediment concentrations.

## 6.2. Study area

The numerical model was applied to four levee-basin transects situated within three tidal marshes along the Scheldt estuary: the Paulina marsh, a salt marsh near the mouth of the Western Scheldt, the Kruispolder marsh, a brackish marsh in the eastern part of the Western Scheldt, and the Notelaar marsh, a freshwater marsh along the Sea Scheldt (see Fig. 1.2 in chapter 1). All transects were established in high marshes with a well-developed levee-basin geomorphology and perpendicular to a similar first order marsh creek (with depth=1.5-2 m and width=5-8 m). A first transect was established in the salt Paulina marsh, within typical halophytic vegetation of high salt marshes (Fig. 6.1). A second transect is located within the brackish marsh vegetation of the Kruispolder marsh (Fig. 6.1). Finally, in the freshwater Notelaar marsh two transects were established in the two contrasting vegetation types that dominate the freshwater tidal marshes, *Phragmites australis* and *Salix* (Fig. 6.1). The vegetation, geomorphological and sedimentological characteristics of the four transects are shown in Figure 6.1.

## 6.3. Methods

### 6.3.1. The numerical model

The model used in this study is based on the 0-dimensional time-stepping model approach of Temmerman *et al.* (2003a) (chapter 5), simulating the elevation change  $dE/dt$  at a certain point of the marsh surface as:

$$dE/dt = dS_{\min}/dt + dS_{\text{org}}/dt + dP/dt \quad (6.1)$$

where  $dS_{\min}/dt$  is the rate of mineral sediment deposition,  $dS_{\text{org}}/dt$  the rate of organic sediment deposition and  $dP/dt$  is the rate of compaction of the deposited sediment, after dewatering, under younger sediment load. All terms are in  $\text{m a}^{-1}$ . According to Temmerman *et al.* (2003a) and to similar model approaches of Allen (1990) and French (1993),  $dS_{\text{org}}/dt$  can be considered as constant and  $dP/dt$  as negligible.  $dP/dt$  is therefore set to zero. The mineral sediment deposition term  $dS_{\min}/dt$  is further specified as:

$$dS_{\min}/dt = \int_{\text{year}} \int_T \frac{w_s \cdot C(t) \cdot dt}{\rho} \quad (6.2)$$

where  $w_s$  is the settling velocity (in  $\text{m s}^{-1}$ ),  $C$  the depth-averaged concentration (in  $\text{g l}^{-1}$  or  $\text{kg m}^{-3}$ ) of the suspended sediment above the marsh

surface, and  $\rho$  the dry bulk density (in  $\text{kg m}^{-3}$ ) of the inorganic surface sediment, after dewatering over spring-neap and seasonal time-scales. Eq. 6.2 calculates the sedimentation rate  $dS_{\text{min}}/dt$  over the total duration  $T$  of a tidal inundation cycle and then over all inundation cycles during a year.

The temporal variation in suspended sediment concentration  $C(t)$  during a tidal inundation cycle is further modelled using the following mass balance equation:

$$\frac{d[h(t) - E] \cdot C(t)}{dt} = -w_s \cdot C(t) + C(0) \cdot \frac{dh}{dt} \quad (6.3)$$

This equation describes the change in suspended sediment mass, during a tidal inundation cycle with a time-varying water surface elevation  $h(t)$  above a unit area of marsh surface with elevation  $E$  (first term), as the result of the vertical settling of suspended sediment (second term) and lateral flux of water with a suspended sediment concentration  $C(0)$  (third term).  $h(t)$  and  $E$  are expressed in m relative to a fixed datum.  $C(0)$  will have a specific value during flood tide (when  $dh/dt > 0$ ), while during ebb tide (when  $dh/dt < 0$ )  $C(0)$  is set to equal  $C(t)$ . Furthermore Temmerman *et al.* (2003a) empirically found that the incoming sediment concentration  $C(0)$  during flood tide can be written as a positive linear function of inundation height at high tide:

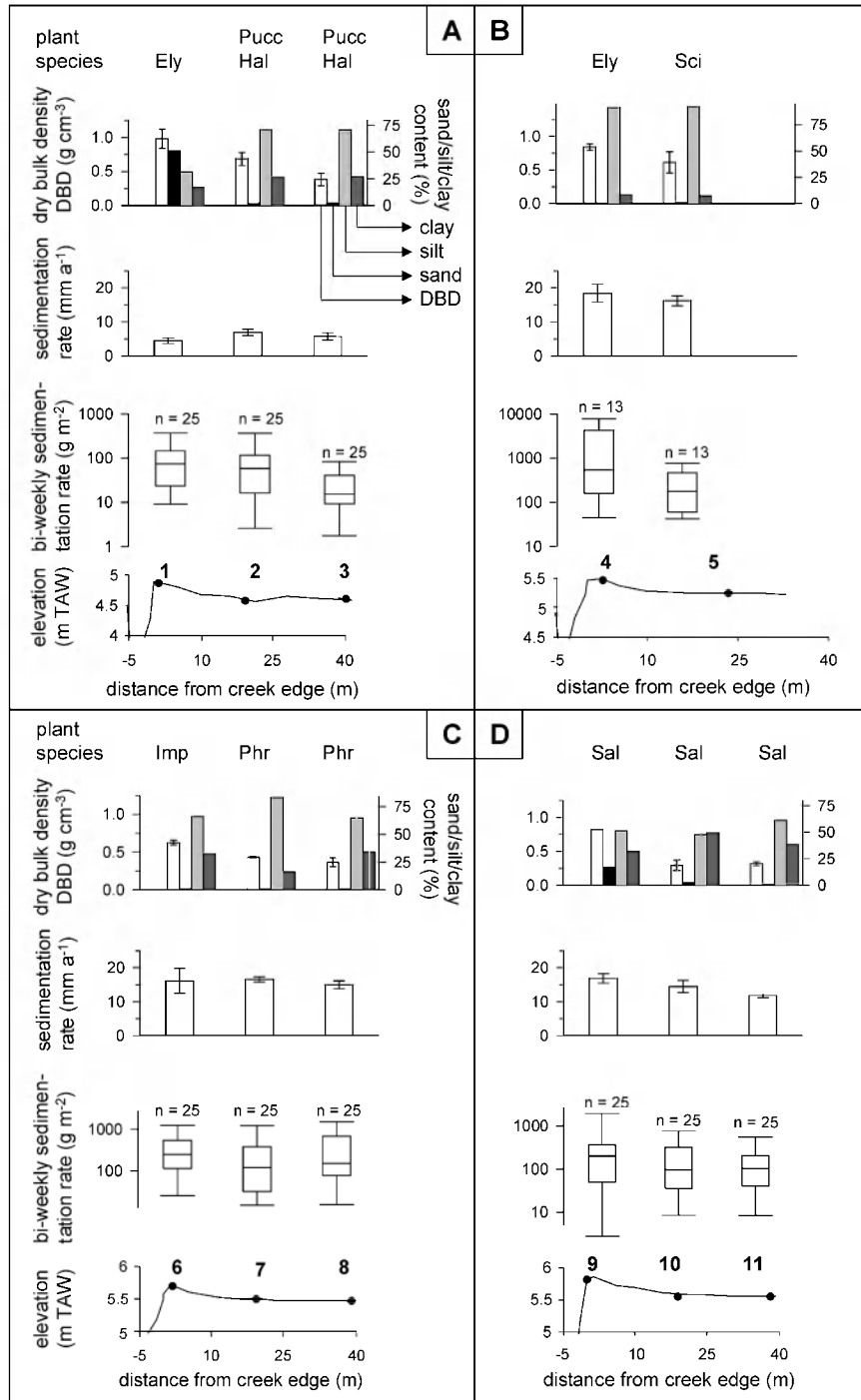
$$C(0) = k \cdot [h(t_{\text{HW}}) - E] \quad (6.4)$$

where  $k$  is an empirical constant and  $h(t_{\text{HW}})$  is the water level at high tide (relative to the fixed datum).

The model was programmed in Matlab, solving eqs. 6.3 and 6.2 in time steps of 300 s and eq. 6.1 in time steps of 1 year.

---

FIGURE 6.1. Description of the four levee-basin transects used in this study: (panel A) the salt Paulina marsh, (B) the brackish Kruispolder marsh, (C) the freshwater Notelaar Phragmites marsh, (D) the freshwater Notelaar Salix marsh. For each transect the following field data are presented (from foot to top in each panel): (1) topographic cross-section with location and numbering of the measuring sites; (2) Whisker boxplots of bi-weekly sedimentation rates (in  $\text{g m}^{-2}$ ) with indication of the number of measurements for each measuring site; (3) solid bars indicating the mean and error bars indicating the standard deviation of 6 measurements of sedimentation rates (in  $\text{mm a}^{-1}$ ) above feldspar marker horizons; (4) dry bulk density DBD (in  $\text{g cm}^{-3}$ ), clay ( $< 2 \mu\text{m}$ ), silt ( $2-63 \mu\text{m}$ ) and sand ( $> 63 \mu\text{m}$ ) content (in %) of surface sediment; for DBD: solid bars indicate the mean and error bars the standard deviation of measurements on 3 replicate samples on each measuring site; (5) dominant plant species: Ely=Elymus pycnanthus, Pucc=Puccinellia maritima, Hal=Halimione portulacoides, Sci=Scirpus maritimus, Imp=Impatiens glandulifera, Phr=Phragmites australis, Sal=Salix sp.



### 6.3.2. Model calibration

Along the four levee-basin transects that are used in this modelling study, bi-weekly measurements of sedimentation rates were carried out during a 1-year period using plastic sediment traps, which were placed on the marsh surface and replaced every two weeks (at neap tide after each spring-neap cycle). For each transect, measurements were carried out on the natural levee, at a distance of 2 m from the creek edge, and in the adjacent basin, 20 and 40 m from the creek edge (Fig. 6.1). This dataset of bi-weekly sedimentation rates was published in Temmerman *et al.* (2003b) (see chapter 2 of this thesis) and is used here for calibration of the model. For all model parameters representative input values could be derived from the field data, except for the parameters  $k$  en  $w_s$ , for which suitable values were obtained by model calibration.

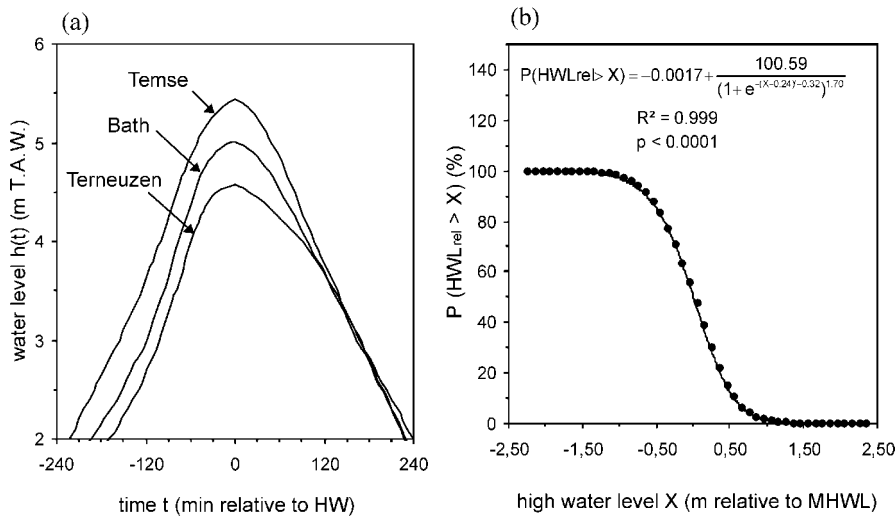


FIGURE 6.2. (a) Mean tidal curves for the period 1981-1990, used as input for the model parameter  $h(t)$  (see text), at the tide-gauge station of Terneuzen (used for sites 1 to 3 at the Paulina marsh), Bath (used for sites 4 and 5 at the Kruispolder marsh) and Temse (used for sites 6 to 11 at the Notelaar marsh). For the location of tide-gauge stations and marshes, see Fig. 1.2 in chapter 1. (b) Observed (dots) and modelled (line) high-water frequency distribution at Antwerp for the period 1981-1990 with indication of the regression equation and  $R^2$  and  $p$ -values. All tidal data after Claessens and Meyvis (1994).

For the model parameter  $[h(t_{HW})-E]$  (in eq. 6.4), which is the inundation height at high tide during a certain inundation cycle, we used data on inundation height that were automatically measured with an ISCO flowmeter for every inundation cycle during the 1-year measuring period and at each measuring transect. The function  $h(t)$  (in eq. 6.3), describing the temporal variation of the water level within one tidal inundation cycle, is modelled using the average tidal curve for the nearest tide-gauge station (Fig. 6.2a). For tidal inundation cycles with different inundation heights  $[h(t_{HW})-E]$ ,  $h(t)$  is simulated by shifting up or down this average tidal curve.

The model parameter  $k$  (in eq. 6.4), describing the relationship between incoming sediment concentration  $C(0)$  and inundation height at high tide  $[h(t_{HW})-E]$ , and the settling velocity  $w_s$  (in eqs. 6.3 and 6.2) of the suspended sediment, were directly derived from suspended sediment concentration measurements at the basin site 3 on the salt marsh and the basin site 8 on the freshwater marsh (Temmerman *et al.*, 2003a; 2003b) (see chapters 2 and 5). For both locations, a value for  $k$  was empirically determined by linear regression between incoming suspended sediment concentrations  $C(0)$ , measured above the marsh surface at the beginning of a large series of inundation events, and the inundation heights  $[h(t_{HW})-E]$ , measured during these events (Temmerman *et al.*, 2003b). Since  $C(0)$  values were found to be significantly higher during the winter (October-March) than during the summer period (April-September) for a same inundation height, higher  $k$  values were determined for the winter than for the summer (Table 6.1). The settling velocity  $w_s$  was calculated from the decrease in suspended sediment concentrations during a large series of inundation events and was estimated to be  $10^{-4}$  m s<sup>-1</sup> (Temmerman *et al.*, 2003a) (see chapter 5).

However, for all levee and basin sites other than sites 3 and 8, no such detailed data on suspended sediment concentrations are available to determine empirical values for  $k$  and  $w_s$ , but only bi-weekly sedimentation rates were measured. For each levee and basin site,  $k$  and  $w_s$  were calibrated using these datasets of bi-weekly sedimentation rates. As for all basin sites significantly higher sedimentation rates were measured during winter than during summer for a same inundation time (see Table 2.2 in chapter 2), calibration was done separately for the winter and summer dataset. For the levee sites no significant difference between winter and summer datasets was observed (see Table 2.2 in chapter 2) and therefore one calibration dataset was used, containing all sedimentation rates measured during the 1-year period.

For each levee or basin dataset, sedimentation rates (in g m<sup>-2</sup>) were calculated with the model for each bi-weekly spring-neap cycle, by solving eqs. 6.4, 6.3 and 6.2 in time steps of 300 s for each individual inundation event during the spring-neap cycle, and cumulating the total sedimentation rate over all inundations that occurred during that spring-neap cycle.

TABLE 6.1. Summary of model calibration results. Column (1) =  $D_{50}$  = median particle diameter (in  $\mu\text{m}$ ) of surface sediment; column (2) = settling velocity  $w_s$  (in  $\text{m s}^{-1}$ ) calculated from  $D_{50}$  and Stokes' formula (eq. 6.6); column (3) = optimal value for the model parameter  $k$  resulting from calibration; column (4) =  $ME$  = model efficiency; column (5) = settling velocity  $w_s$  (in  $\text{m s}^{-1}$ ) based on field measurements; column (6) =  $k$  values obtained from field measurements. Field data in column 5 and 6 are based on Temmerman et al., 2003a; 2003b (chapters 5 and 2).

location	(1)	(2)	(3) (4)		(5) (6)		
	$D_{50}$ ( $\mu\text{m}$ )	$w_s$ ( $10^{-4} \text{ m s}^{-1}$ )	model calibration		field measurements		
			$k$	$ME$	$w_s$ ( $10^{-4} \text{ m s}^{-1}$ )	$k$	
1	59	35.1	0.100	0.88			summer+winter
3	10	1.0	0.050			0.0585	mean
			0.025	0.35		0.026	summer
			0.075	0.78		0.091	winter
4	50	25.2	1.750	0.97			summer+winter
5	12	1.5	0.263				mean
			0.200	0.98			summer
			0.325	0.89			winter
6	14	2.0	0.450	0.92			summer+winter
8	10	1.0	0.150		1.0	0.1345	mean
			0.025	0.20		0.075	summer
			0.275	0.74		0.194	winter
9	43	18.4	0.675	0.93			summer+winter
11	12	1.5	0.100				mean
			0.025	0.29			summer
			0.175	0.67			winter

Sedimentation rates were calculated using  $k$  values ranging from 0.025 to 1.5 in steps of 0.025 and  $w_s$  values ranging from 1 to 10.  $10^{-4} \text{ m s}^{-1}$  in steps of  $10^{-4} \text{ m s}^{-1}$ . For each combination of a  $k$  and  $w_s$  value, the calculated sedimentation rates were compared with the measured rates. The model efficiency coefficient ( $ME$ ), as proposed by Nash and Sutcliffe (1970), was used as a measure of likelihood:

$$ME = 1 - \frac{\sum (SR_{obs} - SR_{pred})^2}{\sum (SR_{obs} - SR_{mean})^2} \quad (6.5)$$

where  $SR_{obs}$  is the observed sedimentation rate,  $SR_{pred}$  is the predicted sedimentation rate, and  $SR_{mean}$  is the mean of the observed sedimentation rate dataset. Values for  $ME$  range from  $-\infty$  to 1. The closer  $ME$  approximates 1, the better the model predicts individual sedimentation rates.

The calibrated values for  $k$  and  $w_s$  are compared with the values that were independently obtained from the suspended sediment concentration measurements at sites 3 and 8. In addition, the  $w_s$  values are compared with values calculated using Stokes' formula:

$$w_s = \frac{g \cdot d^2 \cdot (\rho_s - \rho_w)}{18\mu} \quad (6.6)$$

where  $g$  is the gravity acceleration ( $=9.81 \text{ m.s}^{-2}$ ),  $d$  is the median particle diameter of the surface sediment (m),  $\rho_s$  is the particle density (a value of  $2650 \text{ kg.m}^{-3}$  is used),  $\rho_w$  is the density of the water (a value of  $1000 \text{ kg.m}^{-3}$  is used), and  $\mu$  is the viscosity of the water (a value of  $0.000891 \text{ N.s.m}^{-2}$  at 298K is used). Grain size analyses were carried out on surface sediments, which were sampled with metal rings (0.05 m in diameter and height), using the standard sieve-pipette method after pre-treatment with  $\text{H}_2\text{O}_2$ , HCl and  $\text{Na}_2\text{C}_2\text{O}_4$ .

### 6.3.3. Model implementation

After calibration the model was used to simulate the long-term vertical rise of the marsh surface at the selected levee and basin locations, starting from a historical marsh surface elevation  $E(0)$  in a certain year  $T(0)$ . For sites 8 and 11 on the Notelaar marsh, historical marsh surface elevations were determined by dating of sediment cores, as presented in Temmerman *et al.* (2003a) (see chapter 5). Based on these field data representative  $E(0)$  and  $T(0)$  values were chosen for site 8 and 11 (see Table 6.2). For the adjacent levee locations along these two transects, no such detailed data on historical marsh surface elevations are available. For simplicity, the simulation is started from a planar marsh surface, taking the same  $E(0)$  and  $T(0)$  values along the whole transect (Table 6.2). This allows to investigate whether the simulation model can predict the formation of levees and basins starting from a planar marsh surface, and whether the model is able to reproduce the present-day levee-basin topography. The present-day topography was surveyed along each transect relative to Belgian Ordnance Level (TAW) using an electronic total station (Sokkia SET5F) (Fig. 6.1). For the transects on the Paulina and Kruispolder marsh, a similar methodology was used, starting the simulation from a planar marsh surface with an elevation  $E(0)$  in year  $T(0)$ . For these marshes historical data on  $E(0)$  and  $T(0)$  are available from old topographic surveys that were carried out by the Meetkundige

Dienst of Rijkswaterstaat, with a vertical accuracy of 0.1 m. The  $E(0)$  and  $T(0)$  values, as well as the input values for all other model parameters that were used for the implementation and validation of the model, are listed in Table 6.2.

Simulated deposition rates were also compared with accumulation rates that were measured over the last 3 years (Marsh 2000 - Marsh 2003) on each of the measuring sites using white feldspar marker horizons of 60 by 60 cm. The thickness of sediment deposits above these marker horizons was estimated by the mean and standard deviation of 6 measurements, carried out after three years above each marker horizon using a small gouge.

As already mentioned in section 3.2., the model parameter  $h(t)$  was determined from field data while  $k$  and  $w_s$  were derived by model calibration (Table 6.2). The mineral sedimentation rate  $dS_{min}/dt$  can then be calculated for any tidal inundation cycle with a high-water level  $h(t_{HW})$ , using eqs. 6.4, 6.3 and 6.2. However, to calculate  $dS_{min}/dt$  over a whole year, we further need to model the frequency with which high-water levels  $h(t_{HW})$  occur during every year of the simulation period. To do this, we used on the one hand the evolution of yearly mean high-water level (MHWL), which was interpolated for each of the studied marsh sites based on the yearly MHWL recorded at the nearest up- and downstream tide-gauge station: Vlissingen and Terneuzen for the Paulina marsh, Hansweert and Bath for the Kruispolder marsh, and Schelle and Temse for the Notelaar marsh (see Fig. 1.2 in chapter 1 for the location of these tide-gauge stations). On the other hand, the frequency distribution of all high water levels occurring during a year was then modelled based on this yearly MHWL and on the yearly-averaged frequency distribution of high-water levels around MHWL at Antwerp, which is considered representative for the whole estuary. Figure 6.2b shows how this frequency distribution is modelled using a regression model, based on tidal data from Claessens and Meyvis (1994).

The dry bulk density  $\rho$  (in eq. 6.2) of the deposited sediment was estimated from surface sediments sampled on each measuring site with metal rings (0.05 m in diameter and height).  $\rho$  was rather low in the basins (300-685 kg m<sup>-3</sup>) and up to two times larger on the natural levees (600-1000 kg m<sup>-3</sup>) (Fig. 6.1 and Table 6.2).

Finally, the deposition rate of organic matter  $dS_{org}/dt$  (in eq. 6.1) is estimated for each measuring location, based on organic matter content of the sediment and recent marsh accumulation rates measured above the marker horizons. The estimated  $dS_{org}/dt$  values, listed in Table 6.2, are very small compared to simulated values of  $dS_{min}/dt$  and will therefore have a negligible influence on the rate of marsh elevation change  $dE/dt$ .

TABLE 6.2. Summary of model parameter values used for model calibration and long-term model application for each of the levee and basin locations.

location	parameters model calibration				parameters long-term model application			
	$h(t)$	$h(t_{HW})-E$ (m TAW)	$w_s$ ( $10^{-4}$ m s $^{-1}$ )	$k$	$\rho$ (kg m $^{-3}$ )	$dS_{org}/dt$ (m a $^{-1}$ )	$E(0)$ (m TAW)	$T(0)$ (year)
1	*	**	35.1	0.1000	982	$2 \cdot 10^{-4}$	4.30	1931
3	*	**	1.0	0.0500	685	$4 \cdot 10^{-4}$	4.30	1931
4	*	**	1.0	1.7500	837	$1 \cdot 10^{-4}$	4.00	1931
5	*	**	1.5	0.2625	613	$7 \cdot 10^{-4}$	4.00	1931
6	*	**	2.0	0.4500	627	$9 \cdot 10^{-4}$	4.35	1947
8	*	**	1.0	0.1500	363	$9 \cdot 10^{-4}$	4.35	1947
9	*	**	18.4	0.6750	822	$9 \cdot 10^{-4}$	5.20	1958
11	*	**	1.5	0.1000	319	$9 \cdot 10^{-4}$	5.20	1958

$dP/dt = 0$  for every location

\*  $h(t)$  = mean tidal curve at Terneuzen (for locations 1, 3), at Bath (locations 4, 5) and Temse (locations 6, 8, 9, 11) (see Fig. 6.2a)

\*\*  $h(t_{HW})-E$  = for model calibration: maximum inundation height measured for each inundation cycle using ISCO equipment

= for model application: inundation heights modelled based on the evolution of yearly mean high water level (MHWL) at Paulina marsh (for locations 1, 2, 3), at Kruispolder marsh (locations 5, 6) and Notelaar marsh (locations 6 to 11), and based on the frequency distribution of high water levels around MHWL at Antwerp (see Fig. 6.2b; data after Claessens & Meyvis, 1994).

## 6.4. Results

### 6.4.1. Model calibration

The results of the model calibration are presented in Figures 6.3 and Table 6.1. Figure 6.3 shows the model efficiencies ( $ME$ ) obtained by model simulations using different combinations for  $k$  and  $w_s$ , for a typical levee and basin situation. For the parameter  $k$ , the calibration curve shows a rather well defined top from which an optimal value for  $k$  can be derived. However, for the parameter  $w_s$ , no clear top in the calibration curve can be defined. For a same  $k$  value, different  $w_s$  values ranging from 1 to  $10 \cdot 10^{-4}$  m s $^{-1}$  only have a very small influence on  $ME$ . This indicates that the model results are not very sensitive to the input value for the settling velocity  $w_s$  of the suspended sediment.

For the basin site 8 at the Notelaar marsh, the average settling velocity  $w_s$  was estimated to be  $10^{-4} \text{ m s}^{-1}$  based on field measurements (Temmerman *et al.*, 2003a) (see chapter 5). When using this value for  $w_s$ , model calibration results in a very well defined optimal  $k$  value of 0.025 for the summer dataset and 0.275 for the winter dataset, or a whole-year average value of 0.150 (Fig. 6.3 and Table 6.1). These  $k$  values obtained from model calibration using the sedimentation rate dataset compare well with the  $k$  values that were obtained from independent direct field measurements of incoming sediment concentrations on site 8 (see chapter 2, Fig. 2.6): based on regression analysis between the measured incoming sediment concentrations and inundation heights, a  $k$  value of 0.075 was derived for the summer, 0.194 for the winter and 0.1345 for the whole year (Table 6.1).

Initial model calibrations show then that the settling velocity  $w_s$  is not a very sensitive model parameter and that for all sites good simulation results can be obtained using a wide range of  $w_s$  values (Fig. 6.3). The basic reason for this is that sedimentation rates are primarily determined by incoming sediment concentrations: over each inundation cycle most of the incoming sediment that is initially present in the water column settles out. Thus, although the estimation of  $w_s$  would be a rough approximation, this will not have an important effect on the simulated sedimentation rates. Therefore,  $w_s$  was no longer determined by calibration, but a fixed value for  $w_s$  was used and only the parameter  $k$  was calibrated.

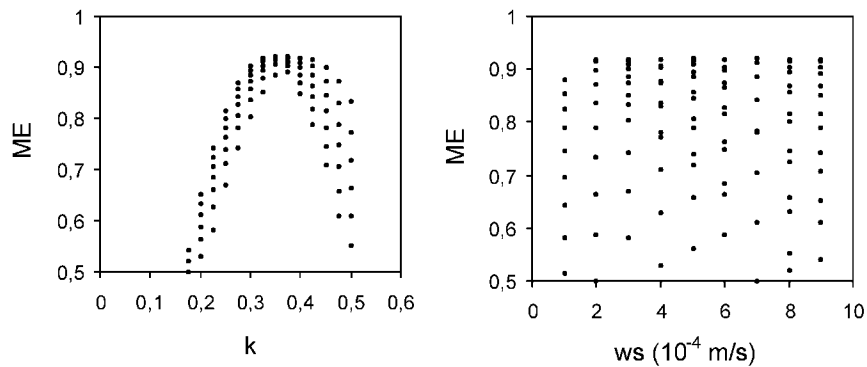


FIGURE 6.3. Results of model calibration using a combination of input values for the model parameters  $k$  and  $w_s$  (in  $10^{-4} \text{ m/s}$ ). ME = model efficiency (see text). Example for location 6.

For all basin sites, a  $w_s$  value of  $1.10^{-4}$  m s<sup>-1</sup> was used in the model calibration, since the median particle size of the surface sediment is for all basin sites very comparable to the median particle size at site 8, where a  $w_s$  value of  $1.10^{-4}$  m s<sup>-1</sup> was empirically derived from the detailed sediment concentration measurements. The resulting optimal  $k$  values are listed in Table 6.1 (column 3). For site 3, the calibrated  $k$  values are in good agreement with the  $k$  values obtained independently from field measurements of incoming sediment concentrations (column 6). For all basin sites high model efficiencies were found for the winter datasets (ranging from 0.67 to 0.89), while generally much lower  $ME$  values are obtained for the summer datasets (column 4). This is probably due to the very low sedimentation rates measured during the summer period and consequently the higher relative errors on the sedimentation rate measurements during the summer period. As can be expected, optimal  $k$  values are systematically lower for the summer datasets than for the winter datasets (column 3).

For the levee sites, the median grain size diameter of the surface sediments is generally coarser (Table 6.1 column 1). Calibration of  $k$ , using  $w_s$  values estimated from these median particle sizes using Stokes law, results in optimal  $k$  values which are systematically higher for the levees than for the adjacent basins (column 3). This suggests that the incoming water contains much higher sediment concentrations on the levees than in the basins. The obtained model efficiency values are all very high for the levee sites (0.88 to 0.98; column 4).

#### 6.4.2. Model validation

The model was then applied to simulate the long-term vertical rise of the marsh surface along each of the levee-basin transects during the last decades using the input parameter values listed in Table 6.2. Since sedimentation rates were calculated on a yearly basis in this long-term simulation, a single  $k$  value was used, which was calculated for the basin sites as the average of the winter and summer  $k$  values obtained by calibration (Table 6.1 and 6.2).

Figure 6.4 shows that the present-day observed levee-basin topography is very well predicted by the model for each of the four studied transects. Although we supposed a planar marsh surface for each transect at the beginning of the simulation period, the model correctly predicts that after 10-50 years natural levees are formed, which raise up to an elevation of 0.2 to 0.3 m above the adjacent inner marsh basins. Once this elevation difference is attained, the levees and basins further raise at a similar rate, which is in equilibrium with the rate of mean high water level rise (Fig. 6.4). Thus, the model simulations show that the originally flat marsh surface evolves within a period of only a few decades to a sedimentological-geomorphological equilibrium condition with levees, next to tidal creeks, which are 0.2 to 0.3 m higher than the inner marshes some 20 to 40 m away from the tidal creeks.

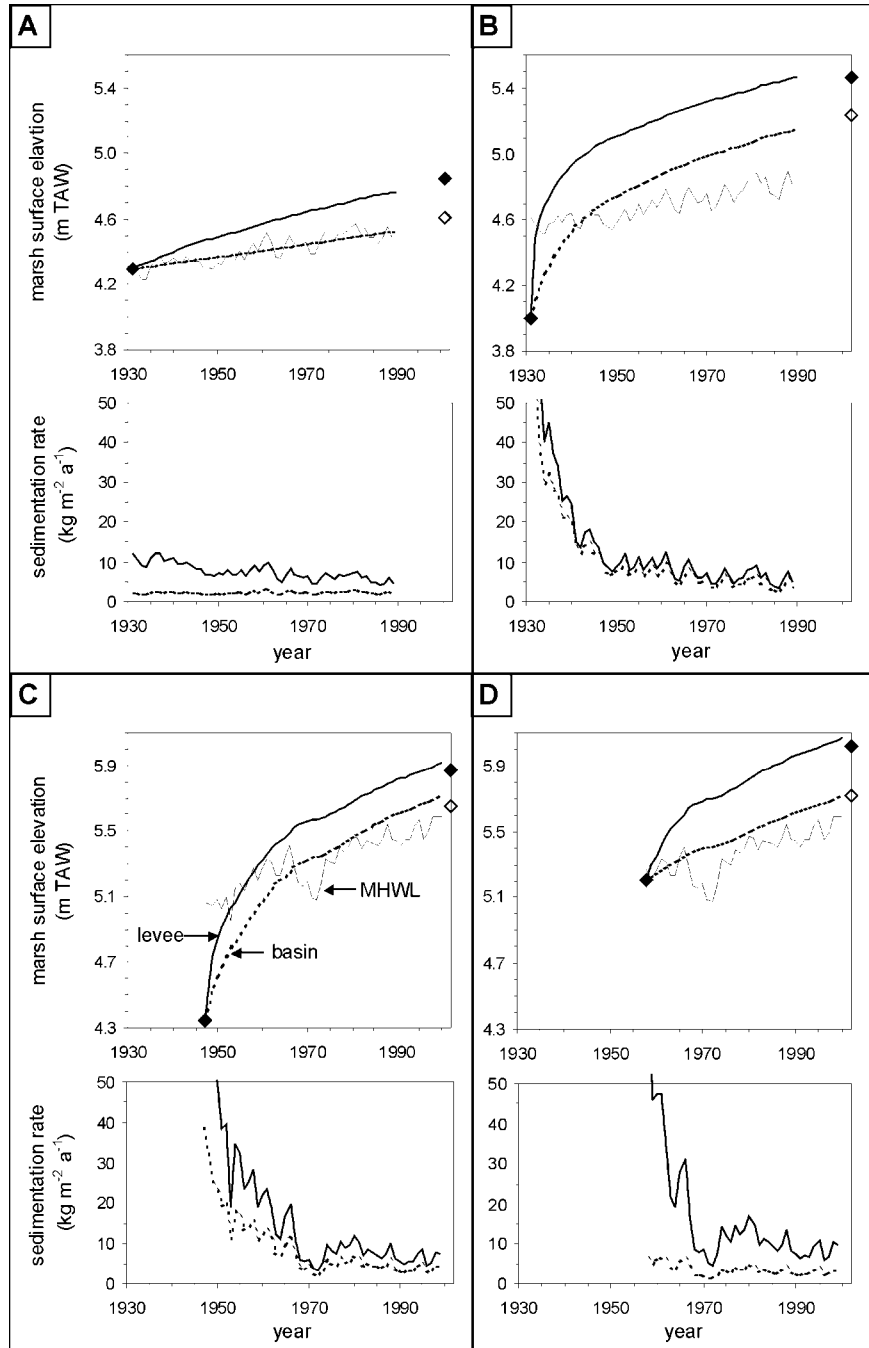
This is in agreement with the field observations (Fig. 6.4): even for transect 6-7-8, which was established on a young marsh surface that originated around 1950 from a bare tidal flat, the present-day morphology is characterised by a well-developed levee-basin morphology.

Starting from a flat marsh surface, the model simulates that the incoming sediment concentration  $C(0)$  is higher on the levees than in the inner basins, as  $k$  values are much higher for levee sites (Table 6.2). As a consequence, the predicted sedimentation rates  $dS_{min}/dt$  and rates of elevation change  $dE/dt$  are higher on the levees than in the basins (Fig. 6.4). This is in agreement with the widely reported finding that sedimentation rates in tidal marshes decrease with increasing distance from tidal creeks, as a result of progressive sediment trapping (e.g. French *et al.*, 1995; Leonard *et al.*, 1995a; Reed *et al.*, 1999; Temmerman *et al.*, 2003b). However, after a period of time the levees become higher than the basins so that the frequency and height of tidal inundations become considerably lower on the levees than in the basins. Since the incoming sediment concentration  $C(0)$  is related to inundation height (see eq. 6.4), the  $C(0)$  values that are simulated on the levees will decrease, which results in reduced rates of sedimentation and elevation change (Fig. 6.4). Thus, the positive influence of the proximity of the tidal creek on the sedimentation rate on the levee is progressively compensated by the negative influence of the higher surface elevation on the sedimentation rate. Both effects will compensate each other once an equilibrium in the elevation difference between levees and adjacent basins is attained. From that moment both levees and basins will accumulate at a similar rate. This mechanism would only work if inner marsh basins are submerged also by relatively low tides that do not overtop the higher natural levees. This is indeed typical for tidal marshes, where small shallow creeks that break through the natural levees, bordering the larger creeks, penetrate into the inner basins and supply water and suspended sediments even during relatively low tides that do not or only slightly overtop the higher levees.

The model simulations suggest that for all studied transects the geomorphic equilibrium condition, with levees that are 0.2 to 0.3 m higher than the basins, is met at present. However, the present-day short-term sedimentation rates (in  $\text{g m}^{-2}$  /spring-neap cycle) that were measured along these transects, are still up to two times larger on the levees than in the basins (Fig. 6.1). This

---

FIGURE 6.4. Comparison of observed (in symbols) and predicted (in thick lines) long-term change of marsh surface elevation (in m TAW) with time (graphs at the top of each panel) and change in sedimentation rate (in  $\text{kg m}^{-2} \text{a}^{-1}$ ) with time (graphs at the foot of each panel) on the levees (thick solid lines) and in the adjacent basins (thick broken lines) for each of the four studied transects: (panel A) Paulina marsh, (B) Kruispolder marsh, (C) Notelaar Phragmites marsh, (D) Notelaar Salix marsh. In the graphs at the top of each panel, the evolution of local mean high water level (MHWL) is plotted in thin solid lines.



is due to the difference in dry bulk density of the deposited sediments, which is up to two times larger on the levees than in the basins (Fig. 6.1). On its turn, this difference in bulk density can be explained by the higher sand content of the deposited sediments on the levees (Fig. 6.1), and the better drainage and compaction of the surface sediments during low tides on the levees, because of the proximity of a tidal creek. On the contrary, basins are rather enclosed and farther away from creeks, so that subsurface drainage and compaction is much less in basins. As a consequence, the volumetric accumulation rates (in  $\text{m a}^{-1}$ ), which were measured over a 3-year period above the feldspar marker horizons, are comparable on the levees and in the basins (Fig. 6.1). This is in agreement with the model simulations, which show that present-day simulated sedimentation rates  $dS_{\text{min}}/dt$  (in  $\text{kg m}^{-2} \text{a}^{-1}$ ) are indeed up to two times larger for levee than for basin sites, while the present-day simulated rates of elevation change  $dE/dt$  are comparable for levees and basins (Fig. 6.4).

#### 6.4.3. Factors influencing the long-term evolution of levees and basins

Model simulations of the vertical rise of a marsh surface, starting from different surface elevations  $E(0)$ , show that a marsh surface always tend to an equilibrium level  $E(eq)$  relative to the mean high water level (MHWL). Furthermore, this equilibrium level  $E(eq)$  is only marginally affected by the assumed initial marsh elevation  $E(0)$  (Fig. 6.5). Below we will further investigate how the different model parameters influence the precise elevation of this equilibrium level  $E(eq)$ , the time  $T(eq)$  (in years) necessary to reach  $E(eq)$  and especially the difference in equilibrium level  $\Delta E(eq)$  between levees and adjacent basins. In our simulations, the following criterion is used to define that an equilibrium elevation  $E(eq)$  is reached in the year  $T(eq)$ , which is the first year since the beginning of the simulation period for which:

$$(E - \text{MHWL})_{T(eq)} - (E - \text{MHWL})_{T(eq-1)} < 0.0002 \text{ m a}^{-1} \quad (6.7)$$

where  $(E - \text{MHWL})_{T(eq)}$  is the difference between the marsh surface elevation  $E$  and MHWL in the year  $T(eq)$  and  $(E - \text{MHWL})_{T(eq-1)}$  the difference between  $E$  and MHWL in the previous year  $T(eq-1)$ .

On the one hand,  $E(eq)$  is strongly dependent on the rate of MHWL rise (Fig. 6.6): the higher the rate of MHWL rise, the lower  $E(eq)$  will be, but also the faster this equilibrium elevation will be reached. On the other hand, the incoming sediment concentration  $C(0)$  also has a considerable influence. This is simulated by using different values for the model parameter  $k$  in eq. 6.4, describing the relationship between incoming sediment concentration  $C(0)$  and inundation height at high tide  $[h(t_{\text{HW}}) - E]$ . Model simulations using

higher  $k$  values result in higher equilibrium elevations  $E(eq)$  and show that this equilibrium elevation is obtained faster (Fig. 6.6). The influence of the settling velocity  $w_s$  and dry bulk density  $\rho$  is rather low compared to the influence of MHWL rise and  $k$ . Changing the input value for  $w_s$  or  $\rho$  with a factor 2 or 3 causes a change in  $E(eq)$  of only a few centimetres.

Thus, MHWL rise and incoming sediment concentration are the dominant parameters influencing the equilibrium elevation of marshes. However, changes in these parameters result in changes in equilibrium elevation, which are different for levees and basins. Figure 6.7a shows that the difference in equilibrium elevation  $\Delta E(eq)$  between a levee and an adjacent basin increases with an increasing rate of MHWL rise. A rising MHWL will result in more marsh inundations with higher inundation heights, and therefore in higher incoming sediment concentrations  $C(0)$  (see eq. 6.4) and higher sedimentation rates  $dS_{min}/dt$  (eq. 6.2). However, since  $k$  values are higher for levees than for basins, the difference in  $C(0)$  and  $dS_{min}/dt$  between levees and basins will become higher as the height of marsh inundations increase. As a result  $\Delta E(eq)$  increases when MHWL rises faster. Under a scenario of descending MHWL, the elevation difference between levees and basins decreases after a period of time (Fig. 6.7a).

The incoming sediment concentration will also have an effect on the difference in equilibrium elevation  $\Delta E(eq)$  between levees and adjacent

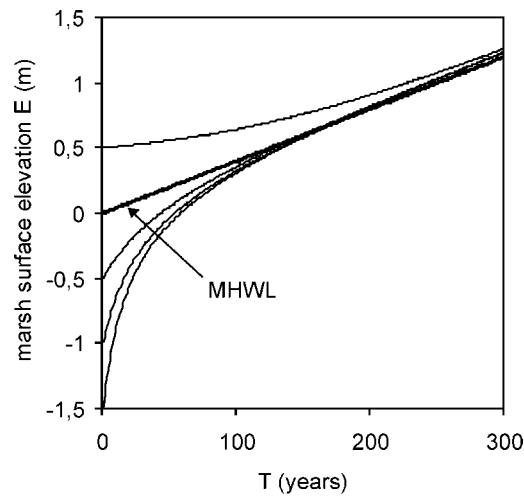


FIGURE 6.5. Model simulations starting from different initial marsh surface elevations  $E(0)$  show that marsh surfaces tend to a certain equilibrium elevation relative to mean high water level (MHWL) independent from  $E(0)$ . For these simulations:  $k = 0.0575$ ;  $w_s = 0.0001 \text{ m s}^{-1}$ ;  $h(t)$  = mean tidal curve at Terneuzen;  $\rho = 650 \text{ kg m}^{-3}$ ; MHWL rise =  $4 \text{ mm a}^{-1}$ ;  $dS_{org}/dt = 0.4 \text{ mm a}^{-1}$ .

basins. On the one hand, higher incoming sediment concentrations, which are simulated by multiplying the parameter  $k$  with the same factor for both the levee and basin (Fig. 6.7b), result in a much faster achievement of an equilibrium in  $\Delta E(eq)$  between levees and basins. However, changing the input  $k$  values for the levee and basin with a factor 2, results in a lowering of  $\Delta E(eq)$  of only a few centimetres (Fig. 6.7b). On the other hand, if the ratio  $k_{levee}/k_{basin}$  (the  $k$  value used for the levee and for the basin, respectively) increases, the difference in equilibrium elevation  $\Delta E(eq)$  between levees and basins increases considerably.

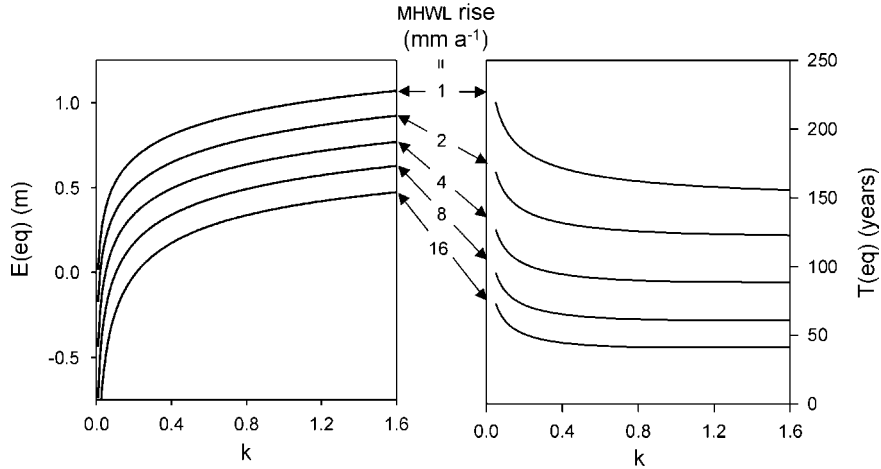
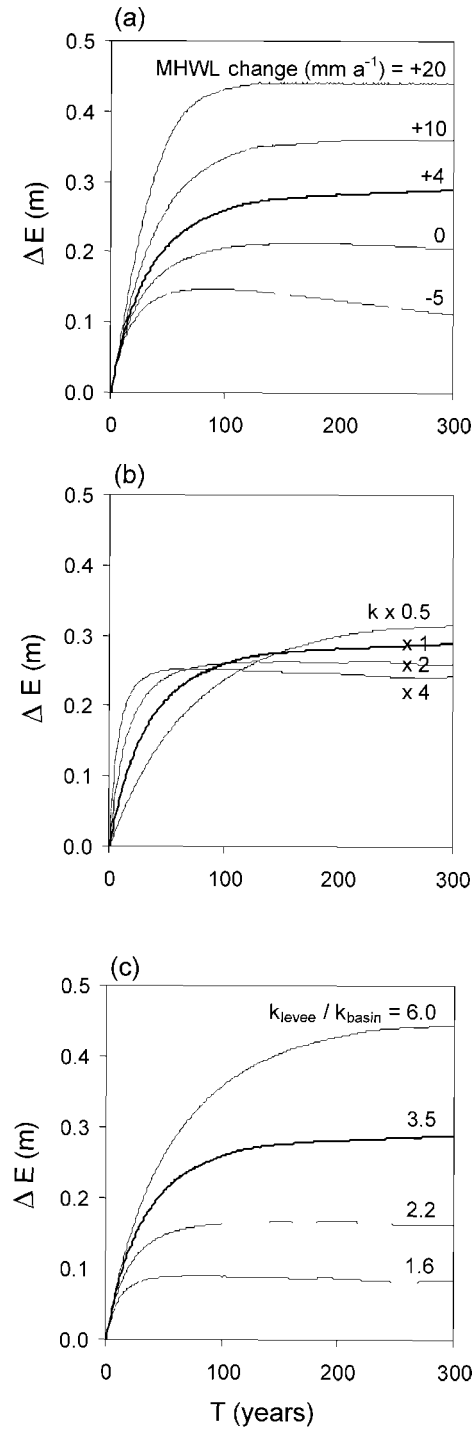


FIGURE 6.6. Results of model simulations showing the influence of the model parameter  $k$  (proportional to incoming sediment concentration) and the influence of mean high water level (MHWL) rise on the equilibrium elevation  $E(eq)$  of marsh surfaces relative to MHWL and the time  $T(eq)$  (in years) necessary to reach  $E(eq)$ . Simulations started from an initial marsh surface elevation  $E(0) = -0.7$  m relative to MHWL. Equation 6.7 was used to define  $E(eq)$  and  $T(eq)$  (see text). For all simulations:  $w_s = 0.0001$  m s<sup>-1</sup>;  $h(t)$  = mean tidal curve at Terneuzen;  $\rho = 650$  kg m<sup>-3</sup>;  $dS_{org}/dt = 0.4$  mm a<sup>-1</sup>.

FIGURE 6.7. Model simulations showing the elevation difference  $\Delta E$  between a levee and adjacent basin as a function of time  $T$  (in years). The thick curves in each of the three graphs represent model results that are representative for the Paulina marsh, for which  $h(t)$  = mean tidal curve at Terneuzen; mean high water level (MHWL) rise = 4 mm a<sup>-1</sup>;  $k = 0.2$  for the levee and  $k = 0.0575$  for the basin;  $w_s = 0.0005$  m s<sup>-1</sup> for the levee and  $w_s = 0.0001$  m s<sup>-1</sup> for the basin;  $\rho = 1000$  kg m<sup>-3</sup> for the levee and  $\rho = 650$  kg m<sup>-3</sup> for the basin;  $dS_{org}/dt = 0.2$  mm a<sup>-1</sup> for the levee and  $dS_{org}/dt = 0.4$  mm a<sup>-1</sup> for the basin. For all other simulations the same parameter values were used, except for MHWL rise and  $k$ . Graph (a) shows how  $\Delta E$  is influenced by different scenarios of MHWL change, while graphs (b) and (c) show the influence of different incoming sediment concentrations. The latter is simulated in graph (b) by multiplying the  $k$  values mentioned above with a factor 0.5, 1, 2 and 4 for both the levee and basin and in graph (c) using different values for the ratio between  $k$  on the levee and  $k$  in the basin ( $k_{levee}/k_{basin}$ ).



## 6.5. Discussion

Despite the fact that the geomorphology of high old marsh surfaces is characterised by levees and basins connected to the dendritic network of tidal marsh creeks, detailed studies about the formation and long-term evolution of this levee-basin geomorphology are very sparse. It is assumed that levees are the long-term result of the decrease in sedimentation rates with increasing distance from tidal creeks, as observed over short-term time-intervals (e.g. French and Spencer, 1993; Leonard *et al.*, 1995a; Reed *et al.*, 1999; Temmerman *et al.*, 2003b; see chapter 2). However, if this would be the only mechanism, levees would continuously grow higher above the adjacent basins.

This modelling study showed that levees will not grow higher than a certain equilibrium elevation. If levees would grow higher, a second mechanism that controls marsh accumulation would become more dominant: sedimentation rates decrease with increasing marsh elevation, because of decreasing inundation frequencies and heights (e.g. Stoddart *et al.*, 1989; French and Spencer, 1993; Cahoon and Reed, 1995; Temmerman *et al.*, 2003b; see chapter 2), and therefore after some time the higher levees will receive less sediment than the lower inner basins. These two mechanisms (the influence of distance to creeks and the influence of surface elevation) are just in balance when an equilibrium in the elevation difference between levees and basins is reached. From then on both levees and basins accumulate at the same rate.

For the studied marshes in the Scheldt estuary, the equilibrium condition is reached once the levees accumulated up to 0.2-0.3 m above the adjacent basins. Maximum elevation differences between levees and adjacent basins, reported from other tidal marshes in the world, are generally in the order of 0.3-0.4 m (e.g. Redfield, 1972; Christiansen *et al.*, 2000), suggesting that the existence of an equilibrium condition between levees and basins, and the model structure presented here to simulate this equilibrium condition, generally apply to tidal marshes. Our model simulations indicate that larger height differences between levees and basins would require higher rates of sea-level rise (or MHWL rise) and/or higher ratios between incoming sediment concentrations (or  $k$  values) on levees and in basins (Fig. 6.7).

In former numerical modelling studies the long-term response of tidal marshes to different scenarios of sea-level rise and/or incoming sediment concentrations were studied based on a 0-dimensional time-stepping point approach, without considering spatial variations within marshes (Krone, 1987; Allen, 1990; French, 1993; Van Wijnen and Bakker, 2001; Rybczyk and Cahoon, 2002; Temmerman *et al.*, 2003a). However, this model study demonstrates that the response of marsh surfaces cannot be considered to be uniform in space, but that at short distances levees and basins will react in a different way. The incorporation of this spatial variability in sediment

accretion within tidal marshes will be of great importance when evaluating changes in tidal marsh dynamics, including vegetation patterns and other ecological processes, in response to changing sea-level and incoming sediment concentrations. In this regard it is important to extend 0-dimensional approaches to 2-dimensional spatially distributed models that are able to simulate the long-term evolution of 2D marsh topographies under changing sea-level and incoming sediment concentrations.

## 6.6. Conclusions

(1) A 0-dimensional time-stepping model was successfully calibrated and validated to simulate the long-term elevation changes of levees and adjacent basins along four levee-basin transects in tidal marshes of the Scheldt estuary.

(2) The model results show that the elevation difference between levees and basins tend to a geomorphic equilibrium. For the studied marshes in the Scheldt estuary, this equilibrium is obtained within 10-50 years when the elevation difference between levees and adjacent basins is 0.2-0.3 m. From that moment, the levees and basins further raise at a similar rate, which is in equilibrium with the rate of mean high water level (MHWL) rise.

(3) Model simulations show that the equilibrium in elevation difference between levees and basins is dependent on mean high water level (MHWL) rise and incoming sediment concentration. A faster MHWL rise results in more pronounced elevation differences between levees and basins. Higher incoming sediment concentrations, when simulated by multiplying them with a factor 2 to 4 both for levees and basins, have a negligible effect on the equilibrium in elevation difference between levees and basins. Significantly larger elevation differences between levees and basins are only obtained when larger differences in incoming sediment concentrations between levees and basins are simulated. This study demonstrates then that the long-term response of tidal marsh surfaces to different scenarios of changing sea-level and incoming sediment concentrations is not uniform in space, but that natural levees and inner basins will react in a different way.



## Chapter 7

### Long-term tidal marsh accumulation along the estuarine gradient of the Scheldt estuary: evidence from field data and numerical modelling

---

#### 7.1. Introduction

The quantification of long-term (10-10<sup>2</sup> years) vertical accumulation rates in tidal marshes has been a major issue in research on tidal marsh morphodynamics for many years. Much attention has been paid to the question whether or not the studied marshes are able to accumulate as fast as local mean sea-level rise. The balance between accumulation rate and sea-level rise ultimately determines whether tidal marsh ecosystems will be sustainable in the long-term or will be increasingly inundated and degrade to bare tidal flats.

A large range of measuring techniques has been used to quantify long-term accumulation rates in tidal marshes, including radiometric dating of sediment cores (e.g. Armentano and Woodwell, 1975; DeLaune *et al.*, 1978; Roman *et al.*, 1997), geo-chemical dating based on historical inputs of pollutants (e.g. Allen and Rae, 1988; Cundy *et al.*, 1997), paleo-environmental dating based on historically known changes in vegetation cover or landuse (e.g. French and Spencer, 1993; Van Wijnen and Bakker, 2001; Temmerman *et al.*, 2003a), and repeated levelling of the marsh surface (e.g. Esselink *et al.*,

1998). Such studies reported strongly varying rates of long-term tidal marsh accumulation, ranging from 1 to several tens of  $\text{mm a}^{-1}$ , in a wide range of tidal marsh settings.

Although several studies focussed on the assessment of long-term accumulation rates in comparison to local sea-level rise, only relatively few studies examined the fundamental principles of long-term tidal marsh accumulation. Pethick (1981) showed that the long-term vertical accumulation of tidal marshes is mainly determined by a decrease in accumulation rate with increasing elevation of the marsh surface. Later field studies confirmed the importance of this negative feedback mechanism between long-term accumulation rates and marsh surface elevation (e.g. Allen and Rae, 1988; Allen, 1990; French, 1996).

In accordance with this, numerical simulations, using a physically-based mass-balance approach, showed that when a marsh surface rises higher within the tidal frame, the vertical accumulation rate decreases as a consequence of the decreasing frequency and period of tidal inundation and finally the marsh surface tends to an equilibrium level high in the tidal frame (Allen, 1990; French, 1993; Temmerman *et al.*, 2003a). However, as indicated by Allen (2000), these model simulations were used to examine the long-term behaviour of tidal marshes in a qualitative way, but they were not quantitatively validated against field data on long-term accumulation rates in tidal marshes.

Besides physically-based models, empirical models were also used to simulate the long-term accumulation of tidal marshes. In such models marsh accumulation is defined as an empirical function of surface elevation or inundation frequency (Day *et al.*, 1999; Van Wijnen and Bakker, 2001; Pont *et al.*, 2002; Rybczyk and Cahoon, 2002). These models were typically calibrated using short-term (1-10 years) measurements of surface elevation change and were subsequently used to simulate long-term ( $10\text{-}10^2$  years) marsh accumulation under the influence of future sea-level rise scenarios. However, until now very little attention was paid to the validation of long-term predictions of tidal marsh accumulation against field data on long-term accumulation rates.

The aim of this study is to validate the 0-dimensional physically-based model, presented in Temmerman *et al.* (2003a) (see chapter 5), for a large number of marsh sites along the estuarine gradient of the Scheldt estuary. First, data on long-term tidal marsh accumulation were collected for marsh sites with different rates of mean high water level rise and incoming suspended sediment concentrations. Next, these data were used to validate the model. Finally, the impact of potential changes in future mean high water level rise and changes in suspended sediment concentrations on tidal marsh accumulation was evaluated using the simulation model.

## 7.2. Study area

Along the 160 km length of the Scheldt estuary, large gradients in environmental conditions exist, which are expected to have their impact on tidal marsh sedimentation rates.

First, the semi-diurnal tidal regime strongly varies in magnitude along the estuary. During spring and neap tides, respectively, the mean tidal range increases from 4.46 m and 2.97 m at the mouth of the estuary up to 5.93 m and 4.49 m at Schelle (Fig. 7.1). Farther inland, these values again decrease to 2.24 m and 1.84 m at the most inland part of the estuary. In correspondence with this variation in mean tidal range, the mean high water level (MHWL) increases from 4.35 m TAW (i.e., Belgian ordnance level) at the mouth to 5.53 m TAW at Driegoten and then decreases again to 5.00 m TAW at the inland border of the estuary (Claessens and Meyvis, 1994). Furthermore, the MHWL has risen during the past century at rates that strongly vary along the estuary from 0.32 cm a<sup>-1</sup> at the mouth up to 1.50 cm a<sup>-1</sup> at Driegoten in the inner estuary.

Secondly, a strong gradient in suspended sediment concentration (SSC) exists along the estuary. The time-averaged longitudinal variation is characterised by low SSC values of 30-60 mg l<sup>-1</sup> in the Western Scheldt. A turbidity maximum with mean concentrations of 100-200 mg l<sup>-1</sup> is situated between the Dutch-Belgian border and Temse. Farther upstream the SSC again slightly decreases to 50-100 mg l<sup>-1</sup> (Van Damme *et al.*, 2001).

Thirdly, a full salinity gradient from salt to fresh water exists along the Scheldt estuary. As a consequence, a distinction can be made between salt, brackish and freshwater tidal marshes in the estuary. The vegetation structure on these marsh types is highly different, ranging from low plant species (0.2-0.8 m in height) on the salt and brackish marshes (e.g., *Spartina anglica*, *Puccinellia maritima*, *Halimione portulacoides*, *Aster tripolium*, *Scirpus maritimus*) up to vegetation canopies of 3 m and higher on the freshwater tidal marshes (e.g., *Phragmites australis*, *Impatiens glandulifera*, *Salix* sp.) (Van den Bergh *et al.*, 2001).

The above-described gradients make the Scheldt estuary then an excellent study area where the long-term vertical accumulation of tidal marshes can be studied under the influence of different environmental conditions that are thought to control tidal marsh sedimentation.

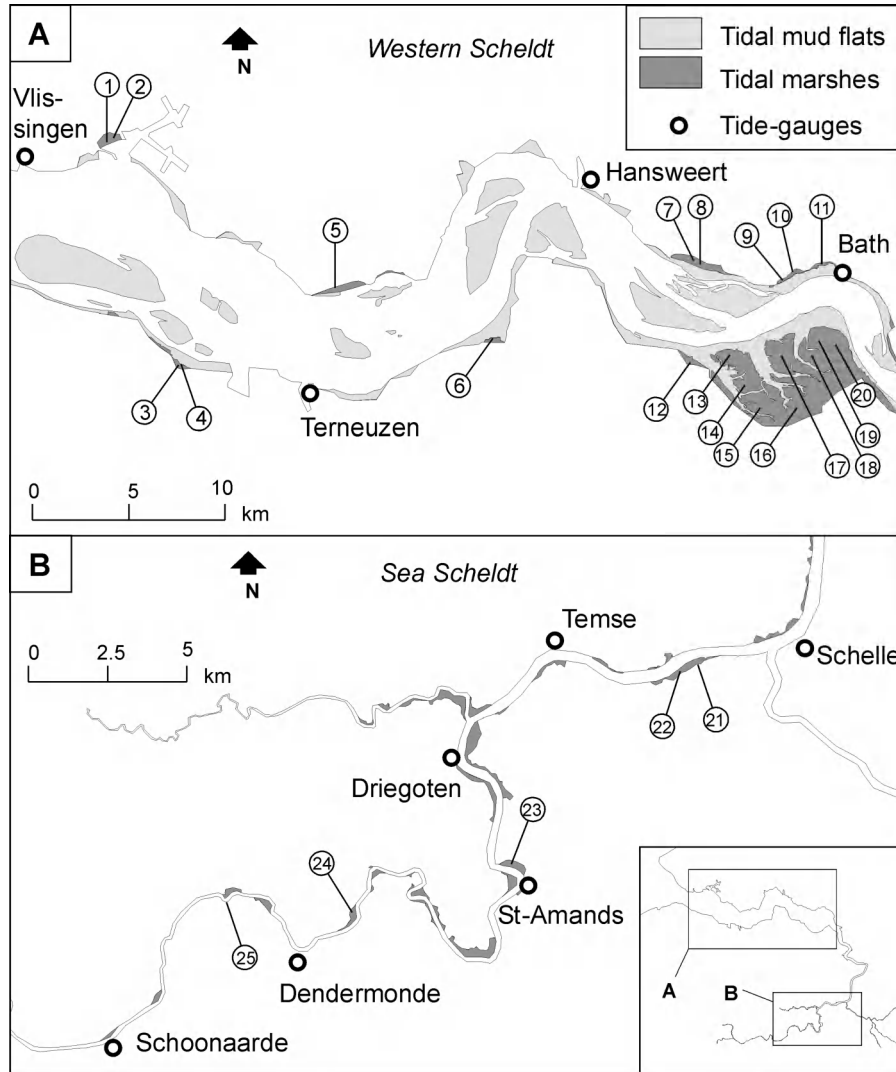


FIGURE 7.1. Map of the study area: (A) the Western Scheldt; (B) the Sea Scheldt. The studied marsh sites are indicated with numbers, the names of the marsh sites corresponding to these numbers are listed in Table 7.1.

TABLE 7.1. Overview of the different marsh sites and the different methods that were used to determine historic marsh elevations and accumulation rates: topo = analysis of old and recent topographic data;  $^{137}\text{Cs}$  = radiometric dating of sediment cores; paleo = paleo-environmental dating of sediment cores. The location of the marsh sites is indicated on Figure 7.1.

nr	marsh site	age	method	years of determined historic marsh elevation
1	Sloehaven	old	$^{137}\text{Cs}^*$	1986, 1999
2	Sloehaven	young	$^{137}\text{Cs}^*$	1963, 1986, 1999
3	Paulina	old	topo	1931, 1955, 1968, 2001
4	Paulina	young	paleo $^{137}\text{Cs}^\ddagger$	1982, 2002 1986, 2002
5	Zuidgors	young	topo $^{137}\text{Cs}^*$ $^{137}\text{Cs}^*$	1931, 1955, 1968, 2001 1963, 1986, 1999 1963, 1986, 1999
6	Hellegat	old	topo	1931, 1968, 2001
7	Waarde	old	topo	1931, 1955, 2001
8	Waarde	young	topo paleo $^{137}\text{Cs}^\ddagger$	1931, 1955, 2001 1940, 2002 1963, 1987
9	Bath west	old	topo	1955, 2001
10	Bath mid	young	topo	1931, 1955, 2001
11	Bath east	old	topo	1931, 1955, 2001
12	Kruispolder	young	topo	1931, 1961, 1992, 2001
13	Konijnenschor	young	topo $^{137}\text{Cs}^\ddagger$	1931, 1961, 1992, 2001 1963, 1987
14	Grauwse Plaat	old	topo	1931, 1961, 1992, 2001
15	Heuvel	old	topo	1931, 1961, 1992, 2001
16	Weideschor	old	topo	1931, 1961, 1992, 2001
17	Marlemontse Plaat	young	topo	1931, 1961, 1992, 2001
18	Rotte Putten	young	topo	1931, 1961, 1992, 2001
19	Blauwe Plaat	young	topo	1931, 1961, 1992, 2001
20	Noord	old	topo	1931, 1961, 1992, 2001
21	Notelaar	old	paleo	1958, 2002
22	Notelaar	young	paleo $^{137}\text{Cs}^\ddagger$	1947, 1958, 2002 1963, 1986, 2002
23	Mariekerke	young	paleo	1968, 2002
24	Grembergen	old	$^{137}\text{Cs}^\ddagger$	1963, 1986, 2002
25	Appels	young	paleo	1982, 2002

\* after Dyer et al. (2002)

† after Zwolsman et al. (1993)

‡ own Cs-137 analysis

### 7.3. Methods

#### 7.3.1. *Estimating long-term tidal marsh accumulation*

In order to collect field data on tidal marsh accumulation during the past century, a number of different methods were used depending on the available data: (1) analysis of old and recent topographic data; (2) radiometric dating of sediment cores; and (3) paleo-environmental dating of sediment cores. Based on these three methods, historic marsh surface elevations and long-term accumulation rates could be determined for 25 marsh sites scattered along the Scheldt estuary (Fig. 7.1 and Table 7.1). For a number of marsh sites (see Table 7.1: sites 4, 5, 8, 13, 22) a combination of these three methods was used, in order to compare the results and correspondence between the different methods.

##### 7.3.1.1. Analysis of old and recent topographic data

Since 1931 until present the tidal marshes of the Western Scheldt were surveyed at three or in some cases at four points in time by the Dutch Rijkswaterstaat Meetkundige Dienst (see Table 7.1 for the exact years). In general, these elevation surveys were carried out along transects with a spacing of about 50 m between elevation points surveyed along the transects and a spacing of about 150 m between the transects. Elevations were mapped to the nearest 0.10 m in m NAP (= Dutch ordnance level; elevations in m NAP are 2.33 m lower than elevations in m TAW, the Belgian ordnance level). These old elevation data points were imported in a Geographical Information System (GIS) relative to the Dutch xy coordinate system and these data were processed by Rijkswaterstaat to Digital Elevation Models (DEM) with a resolution of 20 by 20 m.

Apart from these old topographic surveys, recent elevation data (2001) are available from airborne laser altimetry or LiDAR (light-induced direction and ranging) measurements carried out by Rijkswaterstaat Meetkundige Dienst. These LiDAR measurements resulted in data sets of elevation points with a resolution of 3 by 3 m and a vertical and horizontal accuracy of 0.20 and 0.30 m respectively (Van Heerd and Van 't Zand, 1999). These data points are also in Dutch xy coordinates and the elevation is in m NAP. We used these data to generate DEMs with a resolution of 20 by 20 m for all tidal marshes in the Western Scheldt (e.g., Fig. 7.2).

These DEMs were used then to calculate marsh surface elevations at different points in time and long-term accumulation rates. In order to reduce the vertical inaccuracy of the DEM data, the average of all DEM pixels was calculated for a whole marsh or marsh part with a same accumulation history. The standard deviation was calculated as a measure of the error on the estimation of the average marsh surface elevation.

In order to define marsh parts with a same accumulation history, the following GIS procedure was used. As we already showed in the previous chapters, old marshes, which already existed since at least 100 years ago, and young marshes, which formed more recently, accumulate in a different way (see chapter 5). Furthermore, spatial variations within old or young marshes, such as between levees and inner basins, are important, but in the long-term the elevation difference between levees and basins tend to be in equilibrium (see chapter 6). Therefore, on the one hand, it is important to distinguish between old and young marshes, but on the other hand, it is acceptable to calculate mean surface elevations for a whole old or young marsh surface that formed at a certain point in time.

In order to distinguish between marsh parts of different age, old and recent aerial photograph series were used. Based on these photos, changes in surface area since 1935 were mapped in detail for all tidal marshes along the Western Scheldt by Rijkswaterstaat (Huijs, 1995; Van der Pluijm and De Jong, 1998). The digitised marsh edge polygons (in Dutch xy coordinates), resulting from this study, were placed at our disposal and were used as a basis to select old and young marsh surfaces for which mean elevations could be calculated from the DEMs.

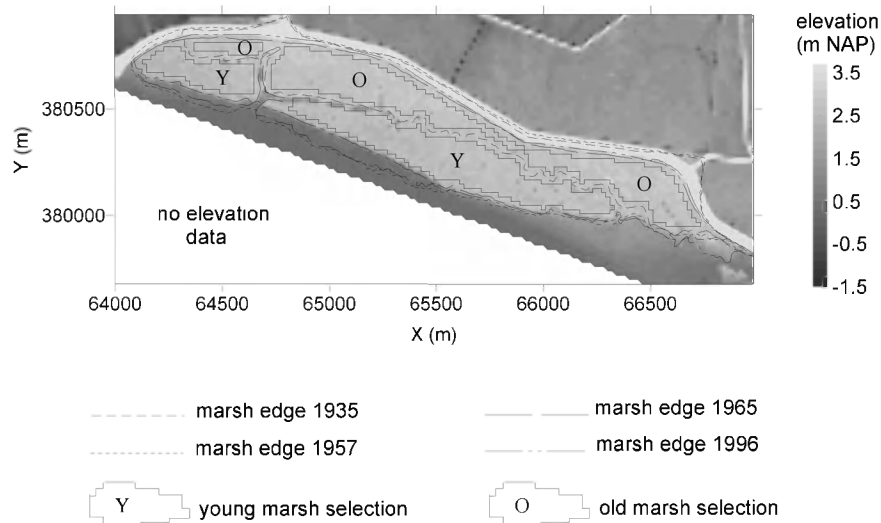


FIGURE 7.2. Illustration of how young and old marsh surfaces were determined. Example for the old and young marsh of Waarde (sites 7 and 8). The figure shows in background the DEM (Digital Elevation Model) for 2001 (based on LiDAR data of Rijkswaterstaat Meetkundige Dienst); the marsh edge polygons determined from aerial photographs (based on Van der Pluijm and De Jong, 1998); and the old and young marsh polygons calculated by overlay procedures in a GIS.

Old marsh surfaces were defined as marshes that were already present on the oldest aerial photograph series of 1935. On the aerial photographs, they can be recognised by the dense vegetation cover and the well-developed network of tidal creeks and associated levee-basin system. On the contrary, young marshes, which were not yet present on the photos of 1935, appear on later photos as initially less dense vegetated areas (with the vegetation often growing in concentric patches) and without a well-developed creek and levee-basin system. Since their first appearance on the aerial photograph series, several of these old and young marshes have decreased in surface area on later photos, either due to lateral erosion at the marsh edge or partial embankment during the past decades (Huijs, 1995; Van der Pluijm and De Jong, 1998).

Therefore, the old and young marsh surfaces that are still present today were selected from the digitised marsh edge polygons of Rijkswaterstaat by overlay techniques in a GIS. This GIS procedure is illustrated in Figure 7.2. The smallest enclosed polygon, at a distance of 20 m from the enclosing marsh edges, was calculated. This buffer of 20 m was used in order to exclude erroneous elevation data that can be present in the DEMs near marsh edges as a consequence of the spatial interpolation process during generation of the 20 by 20 m DEMs. From that part of the DEM situated within this calculated smallest polygon, the mean surface elevation and standard deviation of surface elevations was calculated. An algorithm was written so that these GIS analyses could be performed in a uniform and automated way for each marsh site in the Western Scheldt.

For the Sea Scheldt no such old and recent elevation data are available and therefore other methods need to be used.

#### 7.3.1.2. Radiometric dating of sediment cores

Radiometric dating of sediment cores, based on the determination of  $^{210}\text{Pb}$  and  $^{137}\text{Cs}$  activity profiles, is probably the most widely used technique to estimate accumulation rates in tidal marshes on the time-scale of the last 10-100 years (e.g. Armentano and Woodwell, 1975; DeLaune *et al.*, 1978; Cundy and Croudace, 1996; Roman *et al.*, 1997).  $^{210}\text{Pb}$  is a natural radionuclide in the  $^{238}\text{U}$  decay series. It originates from radioactive decay of  $^{226}\text{Ra}$  via the gaseous intermediate nuclide  $^{222}\text{Rn}$  that is released from land into the atmosphere. After decay of  $^{222}\text{Rn}$  to  $^{210}\text{Pb}$ , the latter is removed from the atmosphere by wet and dry fallout processes and accumulates in sedimentary environments like tidal marshes. Once buried, the so-called 'excess' or 'unsupported'  $^{210}\text{Pb}$ , which is in excess of radioactive secular equilibrium with  $^{226}\text{Ra}$  present in the sediment, decays with a half-life of 22.3 years. This results in a typical exponential decrease in  $^{210}\text{Pb}$  activity with increasing depth. Based on this  $^{210}\text{Pb}$  activity profile and under certain assumptions of constant sedimentation rate and/or constant rate of  $^{210}\text{Pb}$

supply, the age of the sediment since deposition can be calculated (see e.g. Appleby and Oldfield (1984) for more details). However, this method was not successful for the Scheldt estuary, as explained below.

The  $^{137}\text{Cs}$  method is based on the atmospheric fallout of the artificial radionuclide  $^{137}\text{Cs}$  that was first released into the atmosphere by nuclear weapon tests that started in the 1950s. A maximum in  $^{137}\text{Cs}$  fallout occurred in 1963-1964, after which the International Test Ban Treaty stopped large-scale atmospheric nuclear testing, and a second maximum occurred with the Chernobyl accident in 1986. In principle, both maxima in  $^{137}\text{Cs}$  fallout can be recognised in sedimentary records as horizons with peak  $^{137}\text{Cs}$  activity. Although vertical post-depositional migration of  $^{137}\text{Cs}$  may occur under certain conditions (e.g. Comans *et al.*, 1989; Appleby *et al.*, 1991), the fallout from nuclear weapon testing contained also other artificial radionuclides, such as  $^{241}\text{Am}$ , that are much less mobile in sediments and that can be used to verify the position of the  $^{137}\text{Cs}$  peaks (Appleby *et al.*, 1991).

Zwolsman *et al.* (1993) and Dyer *et al.* (2002) determined accumulation rates based on  $^{210}\text{Pb}$ ,  $^{137}\text{Cs}$  and  $^{241}\text{Am}$  activity in sediment cores collected on five marsh sites along the Western Scheldt (see Table 7.1: sites 1, 2, 5, 8, 13). These data, in combination with elevation data of the boring locations provided by personal communication with both authors, were used to determine historic marsh surface elevations. However, again, no data exist for the Sea Scheldt. To overcome this lack in data, we collected sediment cores on 15 marsh sites along the whole Scheldt estuary and initially applied the  $^{210}\text{Pb}$  method to determine accumulation rates \*. However, it was found that the  $^{210}\text{Pb}$  profiles in the Scheldt estuary systematically deviate from the theoretical exponential decrease of  $^{210}\text{Pb}$  activity with increasing depth, which made it impossible to use the  $^{210}\text{Pb}$  method to calculate marsh accumulation rates. This was also noticed by Dyer *et al.* (2002). This phenomenon of aberrant  $^{210}\text{Pb}$  activity profiles in the Scheldt estuary was not further elaborated in this thesis, but instead 3 of the 15 cores were dated using  $^{137}\text{Cs}$  and  $^{241}\text{Am}$  analyses (see Table 7.1: sites 4, 22, 24).

The sediment cores were sampled in the field using cylindrical pvc tubes (diameter = 9.7 cm). Compaction as a consequence of the boring process was limited for all cores (<7 %). For some locations with very soft and water saturated bottom sediments (sites 8, 21, 22, 23, 25 in Table 7.1), sediment cores were collected with a “Beeker-sampler”, a piston corer (diameter = 5.7 cm) with an inflatable valve at the bottom, so that disturbance, compaction and loss of sediment is minimized. The elevation of the boring locations was surveyed with an electronic total station relative to local benchmarks in m NAP or m TAW. In the lab, the cores were cut into slices of 2 cm, which were oven-dried at 105° C for 48 hours to determine the dry bulk density (in

---

\* The radiometric analyses were carried out by Dr. S. Wartel and Dr. P. Van Den Winkel at the CYCLOTRON unit of the VUB.

$\text{g cm}^{-3}$ ; corrected for compaction as a consequence of the boring process). For a series of sub-samples, one half of the sample was compressed to tablets after mixing the sediment sample with a cellulose binding agent in proportion 2 to 1. These tablets were analysed for  $^{137}\text{Cs}$  and  $^{241}\text{Am}$  activity, using a Silicon detector and a Germanium detector, respectively, connected to a multichannel analyser (Canberra Series 35 PLUS). On the other half of these sub-samples, grain size analyses were carried out using the standard sieve-pipette method after pre-treatment with  $\text{H}_2\text{O}_2$ ,  $\text{HCl}$  and  $\text{Na}_2\text{C}_2\text{O}_4$ .

#### 7.3.1.3. Paleo-environmental dating of sediment cores \*

As shown in Temmerman *et al.* (2003a) (chapter 5), marked vegetation cover changes in tidal marshes can be used to determine historic marsh surface elevations: these vegetation cover changes are reflected in sediment cores as changes in plant debris preserved at different depths, on the one hand, and the vegetation cover changes can be dated using aerial photographs of different age, on the other hand. This simple method was successfully used for the old and young marshes of the Notelaar (see chapter 5). For this study, the same method was applied for four other young marshes (sites 4, 8, 23, 25 in Table 7.1). For these young marshes, the moment of marsh formation, at which the initially bare tidal flat was colonized by marsh plants, could be determined from aerial photographs of different age. The marsh surface elevation at the moment of marsh formation was determined in sediment cores as the contact level between the marsh sediments, which are rich in plant debris, and the underlying tidal flat sediments, which contain no plant material. The sediment cores were collected with a “Beeker-sampler” (see above) and cut into 2 cm slices, for which the presence and type of plant debris was determined in the lab. For every marsh site, three to five replicate cores were collected and analysed (see Table 7.5). The error on the determination of the contact elevation between sediment layers containing different types of plant debris was estimated by the standard deviation, as determined from these replicate cores.

---

\* This work was done as part of the master thesis of Tom De Bruyn (2003)

### 7.3.2. Modelling long-term tidal marsh accumulation

In chapter 5, we developed a 0-dimensional time-stepping model that incorporates the main factors that control long-term ( $10\text{-}10^2$  years) tidal marsh accumulation (Temmerman *et al.*, 2003a). These factors are the tidal inundation regime, the concentration  $C(0)$  and settling velocity  $w_s$  of the suspended sediments in the water that floods the marsh surface, the dry bulk density  $\rho$  of the deposited sediment, the rate of sediment compaction  $dP/dt$  due to burying under younger sediments, and the rate of organic matter deposition  $dS_{org}/dt$ . For the description of the model, we refer to chapter 5.

In order to investigate to what extent the model is able to explain the observed large-scale variability in tidal marsh accumulation along the estuarine gradient of the Scheldt estuary, the model was applied for 13 of the 25 marsh sites mentioned above (see Table 7.2 for these marsh sites). Field data on all model variables could be determined for these 13 sites. For the other marsh sites (especially sites 13 to 20 situated in the large and quite remote Saefinghe marsh), field data on some model variables were not collected and therefore the model could not be applied.

#### 7.3.2.1. Tidal inundation data

In the model, the tidal inundation regime is incorporated on two time-scales. First, the temporal variation of the water level  $h(t)$  during one semi-diurnal tidal cycle is modelled based on the average tidal curve recorded in the nearest tide-gauge station (Claessens and Meyvis, 1994) (Fig. 7.1 and Table 7.2). In order to simulate semi-diurnal cycles with different high water levels  $h(t_{HW})$ , this tidal curve  $h(t)$  is shifted up or down, which is an acceptable approach since only the top of the tidal curve floods the marsh surface.

Secondly, the frequency of high water levels  $h(t_{HW})$  with which the marsh surface is flooded is simulated for every year in the simulation period. This is done using data on the local evolution of yearly mean high water level (MHWL) and the yearly-averaged frequency distribution of high water levels around this MHWL. These data are well documented for the Scheldt estuary thanks to a dense network of *ca.* 20 tide-gauge stations, operated since the end of the 19<sup>th</sup> century by Rijkswaterstaat for the Dutch part of the estuary and by the Flemish Administratie Waterwegen en Zeewezen for the Belgian part of the estuary (Claessens and Meyvis, 1994). For each marsh site, the evolution of yearly MHWL was calculated by linear distance interpolation of the yearly MHWL recorded at the nearest up- and downstream tide-gauge stations (see Fig. 7.1 and Table 7.2). All MHWL data were recalculated to m TAW. In order to simulate the frequency distribution of all high water levels occurring in each year, we used data on the yearly-averaged frequency distribution of high-water levels around MHWL at Antwerp, which is assumed to be representative for the whole estuary.

TABLE 7.2. Summary of input values for all model variables, which were determined from field data for 13 marsh sites (see locations on Fig. 7.1). All input values are representative for basin locations.

site nr	$T(0)$ (year)	$E(0)$ (m TAW)	tidal data*	$k$	$w_s$ ( $10^{-4}$ m s $^{-1}$ )	$\rho$ (kg m $^{-3}$ )	$dP/dt$ (mm a $^{-1}$ )	$dS_{org}/dt$ (mm a $^{-1}$ )
1	1963	4.24	A/B	0.0451	0.7	397	2.12	0.64
2	1963	3.99	A/B	0.0451	1.1	448	3.11	0.79
3	1931	4.25	A/B	0.0585	1.0	260	3.09	0.41
4	1982	3.45	A/B	0.0585	1.7	500	22.13	0.94
5	1931	3.81	B	0.0614	3.4	685	3.65	0.55
6	1931	4.38	B/C	0.0552	1.2	478	3.65	0.64
8	1931	4.05	C/D	0.0606	1.1	560	0.00	2.19
12	1931	3.84	C/D	0.0606	1.5	492	0.00	0.83
21	1958	5.20	E/F	0.1345	1.0	350	0.00	0.90
22	1947	4.38	E/F	0.1345	1.0	350	0.00	0.90
23	1968	4.87	G	0.1958	1.3	434	9.62	1.55
24	1963	4.90	G/H	0.1610	1.0	389	1.57	0.69
25	1982	4.87	H/I	0.1555	3.6	610	4.01	1.79

\* Tidal data (on the mean tidal curve  $h(t)$  and the evolution of yearly mean high water level  $h(t_{HW})$ ) were obtained by linear interpolation of tidal data recorded at the nearest upstream and downstream tide-gauge stations: A=Vlissingen; B=Terneuzen; C=Hansweert; D=Bath; E=Schelle; F=Temse; G=St-Amands; H=Dendermonde; I=Schoonaarde (see Fig. 7.1 for locations; tidal data after Claessens and Meyvis, 1994).

### 7.3.2.2. Suspended sediment concentration and settling velocity

In chapter 5, we showed that the variation in incoming suspended sediment concentration  $C(0)$  (in g l $^{-1}$ ) between different semi-diurnal tidal cycles with high water level  $h(t_{HW})$  (in m TAW), needs to be modelled as a linear positive relationship between  $C(0)$  and  $h(t_{HW})$  (Temmerman *et al.*, 2003a):

$$C(0) = k \cdot [h(t_{HW}) - E] \quad (7.1)$$

where  $E$  = the marsh surface elevation (in m TAW). For the Notelaar and Paulina marshes, the  $k$  factor, describing this relationship, could be quantified based on intensive field measurements (Temmerman *et al.*, 2003b) (see chapter 2). For all other marsh sites that are considered in this study, no such detailed field data are available.

In order to obtain a best estimate of the  $k$  factor for each marsh site, existing data were used on variations in suspended sediment concentrations (SSC) along the Scheldt estuary. From January 1996 to January 2002, water

samples were taken every month in the main stream channel at 29 locations scattered along the estuary and the SSC of these water samples was determined (Van Damme *et al.*, 2001). However, during each monthly sampling campaign, the water samples were taken at the different sampling locations at different stages of the tidal cycle. This makes it difficult to compare the SSC between the sampling locations, since large temporal variations in SSC occur over the time-span of a tidal cycle (e.g., Fettweis *et al.*, 1998; Francken and Wartel, 2001). However, the dataset of Van Damme *et al.* (2001) is the only dataset that covers the whole length of the estuary and gives at least the best estimate of time-averaged SSC values along the Scheldt estuary.

For this long-term model application, these time-averaged SSC values were used to estimate the  $k$  factor in eq. 7.1 for each marsh site, using the following method. In order to reduce the large temporal variability in the SSC data of Van Damme *et al.* (2001), the time-averaged SSC was calculated for each sampling location in the dataset. As a measure of this temporal variability, the 10<sup>th</sup> and 90<sup>th</sup> percentiles of the SSC distributions

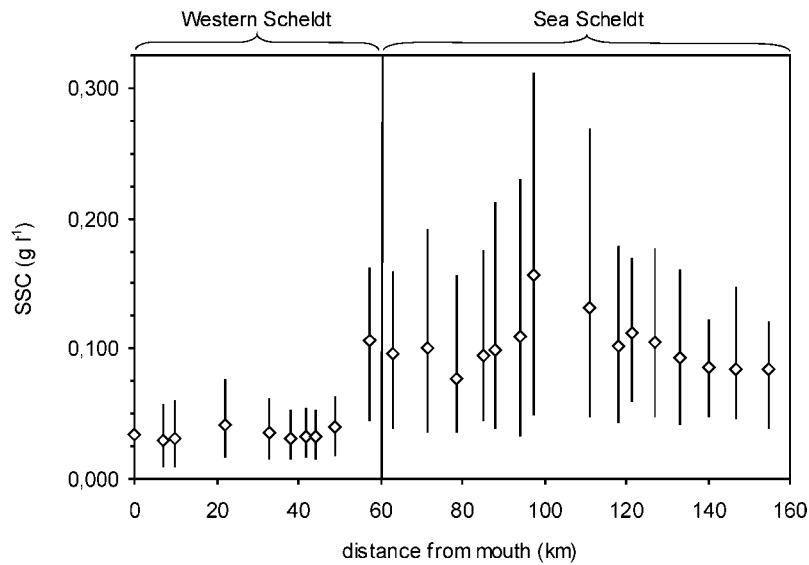


FIGURE 7.3. Time-averaged longitudinal variation in suspended sediment concentration (SSC) along the Scheldt estuary, calculated from monthly monitoring data for the period of January 1996 to January 2002 (no data for the Sea Scheldt for the period of August 1998 to July 2000; based on data of Van Damme *et al.* (2001)). Error bars indicate 10<sup>th</sup> and 90<sup>th</sup> percentiles of the distributions of all SSC measurements at each measuring location. This figure has to be interpreted with caution, since large temporal variations in SSC occur over semi-diurnal, spring-neap and seasonal time-scales (e.g. Fettweis *et al.*, 1998; Francken and Wartel, 2001).

were calculated for each sampling location (Figure 7.3). At the Paulina marsh, the average SSC in the adjacent stream channel is rather low ( $0.033 \text{ g l}^{-1}$ ), while at the Notelaar marsh this is much higher ( $0.109 \text{ g l}^{-1}$ ). This is in accordance with the SSC measurements on both marsh sites, which showed that incoming SSC values are generally higher at the Notelaar marsh (ranging from  $0.01$  to  $0.32 \text{ g l}^{-1}$ ) than at the Paulina marsh ( $0.01$  to  $0.11 \text{ g l}^{-1}$ ) (see Fig. 2.6 in chapter 2). The yearly averaged  $k$  factor, determined from these incoming SSC measurements, is also considerably higher for the Notelaar marsh ( $k=0.1345$ ) than for the Paulina marsh ( $k=0.0585$ ). The ratio between  $k$  determined on the marsh and average SSC in the adjacent stream channel is very comparable for both marsh sites ( $12 \cdot 10^{-6}$  for the Notelaar and  $17 \cdot 10^{-6}$  for the Paulina marsh). Based on a mean ratio of  $14.5 \cdot 10^{-6}$ , the  $k$  factor can then be estimated for every marsh site as:

$$k = 14.5 \cdot 10^{-6} \cdot \text{SSC} \quad (7.2)$$

Since the ratio of  $14.5 \cdot 10^{-6}$  is representative for basin locations (the measurements at the Notelaar and Paulina marshes were carried out in basins; see chapter 2), the so-calculated  $k$  values are also representative for basin locations for each marsh site in Table 7.2. The average SSC in the stream channel was calculated for every marsh site by linear distance interpolation of the data of Van Damme *et al.* (2001). Thus, using this procedure we assume that, for a given inundation height, the incoming sediment concentration in the marsh basins is proportional to the average sediment concentration in the stream channel of the Scheldt.

Apart from the concentration, also a characteristic settling velocity  $w_s$  of the incoming suspended sediment needs to be specified in the model. As already discussed in chapter 5, it is very difficult to obtain accurate field data on in situ settling velocities. However, in chapter 6 we showed that the model predictions are not very sensitive to the model parameter  $w_s$ . Therefore, as in chapter 6, we made a rough approximate estimation of  $w_s$  based on the median particle diameter ( $D_{50}$ ) of surface sediments and Stokes' formula for settling velocities of spherical particles. On each of the 13 marsh sites in Table 7.2, four replicate samples of surface sediments were taken on a basin location using metal rings (0.05 m in diameter and height). On these samples grain size analyses were performed using the standard sieve-pipette method after pre-treatment with  $\text{H}_2\text{O}_2$ ,  $\text{HCl}$  and  $\text{Na}_2\text{C}_2\text{O}_4$ . For comparison, also 5 litre water samples were collected on five sites during two inundation events to determine the median grain size of the sediment in suspension (see Table 7.3). Since the mass of sediment in the water samples is typically very low ( $< 1 \text{ g}$ ), grain size analyses of the undispersed sediment were carried out here using a laser diffraction particle size analyser (Beckman Coulter LS 13 320). All results are presented in Table 7.3.

TABLE 7.3. Median grain size ( $D_{50}$ ) determined for each marsh site from deposited sediments (4 replicate samples of top 5 cm layer) and from suspended sediment samples (5 litre water samples collected during two inundation events). Mean values, calculated from the replicate samples, are presented. Settling velocities ( $w_s$ ) were calculated from  $D_{50}$  using Stokes' formula.

site nr	$D_{50}$ deposited ( $\mu\text{m}$ ) n=4	$w_s$ deposited ( $10^{-4} \text{ m s}^{-1}$ ) n=4	$D_{50}$ suspended ( $\mu\text{m}$ ) n=2	$w_s$ suspended ( $10^{-4} \text{ m s}^{-1}$ ) n=2
1	8.5	0.7		
2	10.3	1.1		
3	9.8	1.0		
4	13.2	1.7	10.0	1.0
5	18.3	3.4		
6	10.9	1.2		
8	10.2	1.1	7.8	0.5
12	12.1	1.5		
21	11.9	1.5		
22	9.5	0.9		
23	11.2	1.3	11.1	1.2
24	9.8	1.0		
25	19.0	3.6	17.2*	2.7*

\* For Appels (site 25) suspended sediment samples could be collected for only one of the two inundation events.

### 7.3.2.3. Compaction and organic matter deposition

The same surface sediment samples, which were taken on each of the 13 marsh sites using the metal rings, were used to determine the dry bulk density  $\rho$  (in  $\text{g cm}^{-3}$ ) of the deposited sediment, after dewatering and consolidation over spring-neap and seasonal time-scales (Table 7.2). In addition, sediment cores were taken on each marsh site, using either pvc tubes or the Beeker-sampler, as explained above. These cores were cut into 2 cm slices for which the dry bulk density and the organic matter content was determined (the latter by loss on ignition). For a number of subsamples, also grain size analysis were performed using the sieve-pipette method after pre-treatment with  $\text{H}_2\text{O}_2$ ,  $\text{HCl}$  and  $\text{Na}_2\text{C}_2\text{O}_4$ . These data were used to estimate values for the model variable  $dP/dt$ , which is the rate of sediment compaction under younger sediment deposits, and  $dS_{org}/dt$ , which is the rate of organic matter deposition.

The depth profiles of dry bulk density were used as a measure of sediment compaction. For a number of marsh sites, the density does not vary significantly with depth (e.g., Fig. 7.4b). For these sites  $dP/dt$  was set to zero

(see Table 7.2). For the other marsh sites, a linear increase in dry bulk density with depth was observed (e.g., Fig. 7.4a). Since the grain size distribution in the sediment cores does not change significantly with depth, the increase in dry bulk density with depth can be attributed to compaction with burying and aging of the sediments. For these sediment cores, the compaction rate  $dP/dt$  was estimated as follows.

The thickness  $P$  (in m) after compaction of a sediment layer with an initial thickness  $P_0$  at deposition is:

$$P = P_0 \frac{\rho_0}{\rho} \quad (7.3)$$

where  $\rho_0$  and  $\rho$  are, respectively, the initial and final dry bulk densities (in  $\text{g cm}^{-3}$ ) of that sediment layer. The compaction rate  $\Delta P/\Delta t$  (in  $\text{m a}^{-1}$ ) can be written as:

$$\frac{\Delta P}{\Delta t} = \frac{P \left( 1 - \frac{\rho}{\rho_0} \right)}{\Delta t} \quad (7.4)$$

Based on eq. 7.4, the average compaction rate for the sediment column of thickness  $P$  (in m), deposited over the time period  $\Delta t$  (in years), was calculated using for  $\rho_0$  the dry bulk density determined from the surface sediment samples (see above) and for  $\rho$  the average dry bulk density of the compacted sediment column with thickness  $P$ . Data on  $P$  and  $\Delta t$  were provided by the determination of historic marsh surface elevations as described above. Using this approach, we assume that the compaction rate is constant in time, which simplifies model calculations: this assumption is reasonable considering the relatively short time period over which marsh accumulation is simulated ( $< 70$  years). However, it is clear that over longer time periods the compaction rate cannot remain constant and a different formulation should be used. The calculated  $\Delta P/\Delta t$  values are presented for all marsh sites in Table 7.2.

Finally, the deposition rate of organic matter  $dS_{\text{org}}/dt$  is estimated for each marsh site, based on the average organic matter content measured in the sediment cores and based on the long-term accumulation rates determined for each site. The estimated  $dS_{\text{org}}/dt$  values are listed in Table 7.2.

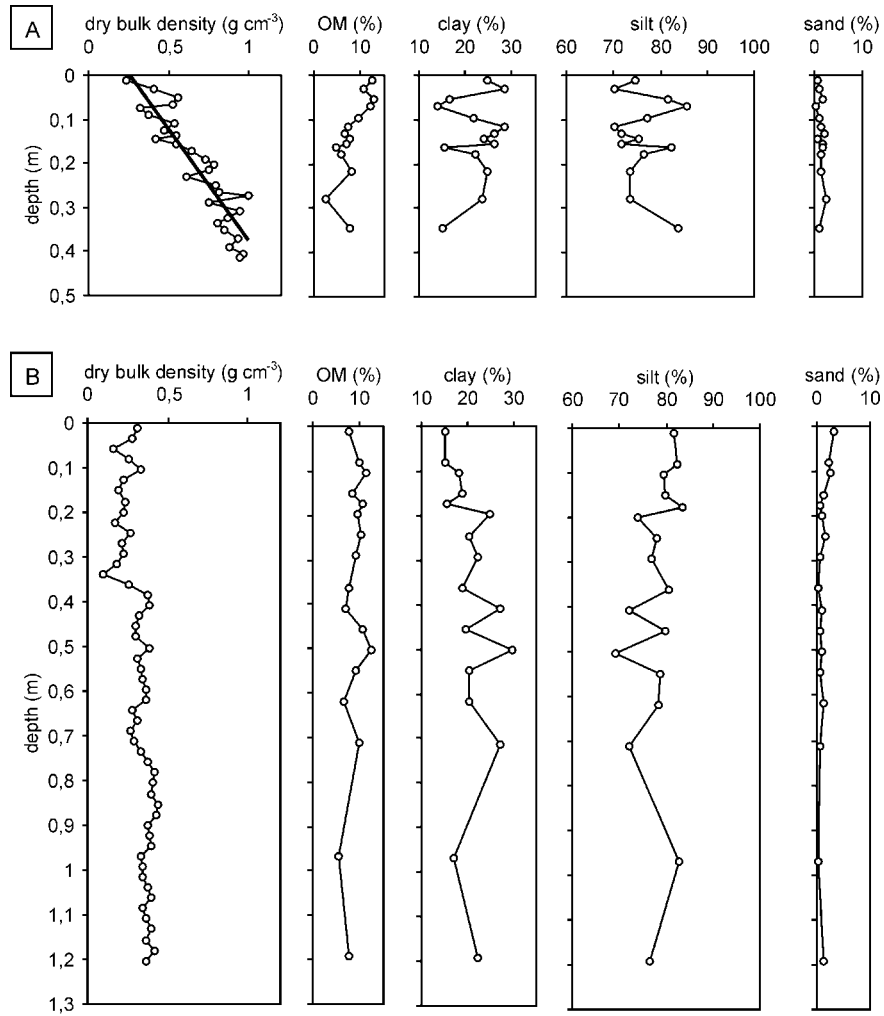


FIGURE 7.4. Two examples of depth profiles of dry bulk density, organic matter content (OM), clay (<2  $\mu\text{m}$ ), silt (2-63  $\mu\text{m}$ ) and sand (>63  $\mu\text{m}$ ) content determined from sediment cores: (A) for the old Paulina marsh (site 3), which is an example of linear increase of dry bulk density with depth; (B) for the young Notelaar marsh (site 22), which is an example of constant dry bulk density with depth.

## 7.4. Results

### 7.4.1. Long-term tidal marsh accumulation

The surface elevations that were calculated based on old and recent topographic data of the Western Scheldt marshes are presented in Table 7.4. In all, 17 marsh sites with a different accumulation history could be identified along the Western Scheldt using the above-described GIS analysis. Table 7.4 shows that the standard deviations on the mean elevations that were calculated for each marsh site are rather low (0.21 m on average). This indicates that within each marsh site spatial variability in marsh surface elevation and in vertical accumulation is rather limited. Yet some higher standard deviations (up to 0.55 m) were calculated from the 1931 data for some marsh sites (Table 7.4). This may be attributed partially to the lower quality of these old elevation data and partially to the fact that on young marsh surfaces the spatial variability in elevation is higher than on old marsh surfaces.

The results of the radiometric dating of the sediment cores are presented in Figure 7.5. For all three sites, for which  $^{137}\text{Cs}$  and  $^{241}\text{Am}$  analyses were carried out, peaks in the  $^{137}\text{Cs}$  profiles could be identified and attributed to the  $^{137}\text{Cs}$  fallout maxima of 1963 and 1986. Overall there is a good correspondence between the levels at which increased  $^{137}\text{Cs}$  and increased  $^{241}\text{Am}$  activity was observed in the cores, which confirms the reliability of the datings. Furthermore, for sites 4 and 22 a good agreement was found between the radiometric dating and paleo-environmental dating based on the preservation of different types of plant debris in the cores (Fig. 7.5). The results of all paleo-environmental datings are listed in Table 7.5.

Figure 7.6 presents all historic marsh surface elevations, which could be determined, as a function of time. For sites 4, 5, 8, 13 and 22, for which a combination of two or three of the above-described methods was used, a good correspondence between the different methods was obtained. A clear distinction can be made between the vertical accumulation of young and old marsh surfaces. The surface elevation of old marshes is at any time very close to mean high water level (MHWL) and the accumulation rate of old marshes is very similar to or slightly in excess of the rate of MHWL rise. On the contrary, young marshes have an initial elevation that is considerably lower than the elevation of adjacent high marshes. Once the young marshes are formed they quickly accumulate up to the level of MHWL. From then on, they actually can be considered as old marsh surfaces, which are in equilibrium with MHWL and which maintain this relative equilibrium elevation by accumulating at a similar rate as MHWL rises. This mechanism, which was first observed for the young and old marsh of the Notelaar (Temmerman *et al.*, 2003a; see chapter 5), seems then to be the general mechanism controlling the long-term accumulation of tidal marshes along the whole Scheldt estuary.

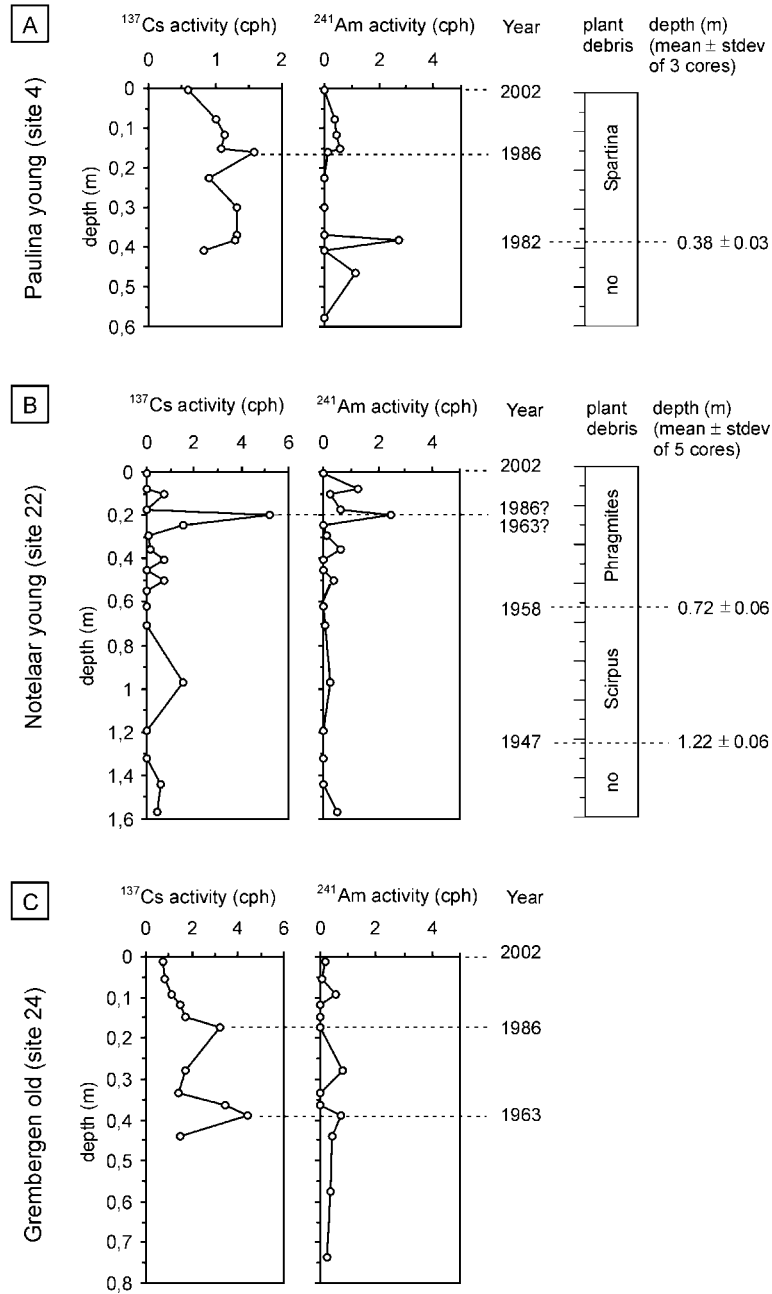


FIGURE 7.5. Results of radiometric dating ( $^{137}\text{Cs}$  and  $^{241}\text{Am}$  activity in cph = counts per hour) and paleo-environmental dating (based on type of plant debris) of sediment cores collected at (A) the young Paulina marsh (site 4), (B) the young Notelaar marsh (site 22) and (C) the old Grembergen marsh (site 24).

TABLE 7.4. Summary of marsh surface elevations (in m TAW) calculated for all marshes in the Western Scheldt based on old and recent topographic data of Rijkswaterstaat. Mean elevations and standard deviations (between brackets) were calculated (see text).

site nr	1931	1955/61*	1968/92†	2001
3	4.25 (0.55)	4.52 (0.14)	4.54 (0.12)	4.70 (0.18)
5	3.81 (0.36)	4.38 (0.24)	4.39 (0.24)	4.70 (0.18)
6	4.38 (0.23)		4.57 (0.10)	4.84 (0.09)
7	4.71 (0.31)	4.86 (0.16)		5.06 (0.17)
8	4.05 (0.17)	4.76 (0.09)		4.92 (0.20)
9		4.88 (0.31)		5.17 (0.19)
10	3.77 (0.17)	4.15 (0.20)		4.83 (0.21)
11	4.50 (0.31)	4.93 (0.17)		5.34 (0.12)
12	3.84 (0.29)	4.60 (0.21)	5.11 (0.18)	5.19 (0.10)
13	3.51 (0.49)	4.58 (0.17)	4.93 (0.16)	5.19 (0.25)
14	4.61 (0.41)	4.89 (0.16)	5.03 (0.18)	5.09 (0.20)
15	4.34 (0.44)	4.86 (0.17)	5.15 (0.13)	5.22 (0.19)
16	4.70 (0.19)	4.99 (0.15)	5.17 (0.15)	5.32 (0.12)
17	3.87 (0.21)	4.75 (0.11)	5.07 (0.16)	5.13 (0.16)
18	3.81 (0.21)	4.78 (0.12)	5.08 (0.34)	5.19 (0.25)
19	4.15 (0.25)	4.69 (0.27)	5.07 (0.19)	5.15 (0.17)
20	4.78 (0.21)	4.97 (0.15)	5.24 (0.23)	5.28 (0.26)

\* data are of 1955 for sites 3 to 11 and of 1961 for sites 12 to 20.

† data are of 1968 for sites 3 to 6 and of 1992 for sites 12 to 20.

TABLE 7.5. Summary of historic marsh surface elevations determined from paleo-environmental dating of sediment cores. The error on the year (between brackets) is determined by the time interval between successive aerial photos before and after vegetation cover change. The error on the elevation (between brackets) at which the type of plant debris in sediment cores changes is estimated as the standard deviation of three replicate cores for sites 4, 8, 23 and 24, and five replicate cores for sites 21 and 22.

site nr	year	elevation (m TAW)
4	1982 (±5)	3.45 (±0.03)
8	1940 (±4)	3.91 (±0.01)
21	1958 (±6)	5.20 (±0.03)
22	1947 (±3)	4.38 (±0.06)
23	1968 (±7)	4.87 (±0.06)
25	1982 (±5)	4.87 (±0.01)

7.4.2. Implementation and validation of the model

The 0-dimensional time-stepping model was then applied to simulate the observed large-scale variability of tidal marsh accumulation along the Scheldt estuary. The input values for the model variables, which were determined from field data as explained above, are listed in Table 7.2 for the 13 marsh sites, for which the model was applied. The results of the model simulations are shown in Figure 7.6. The model simulates that, on the one hand, old marshes, which were already at their equilibrium level around local MHWL at the beginning of the simulation period, accumulated quasi linearly with time in equilibrium with local MHWL rise. On the other hand, the model simulates that young marshes accumulated asymptotically up to their equilibrium level around local MHWL.

For all marsh sites the simulated versus observed marsh surface elevations are plotted in Figure 7.7a. Both the historic and present-day elevations, which could be determined, are plotted. The simulated and observed elevations correspond extremely well ( $R^2=0.95$ ). The model overestimated the observed elevations by only 0.20 m at most, which is acceptable. For 4 of the 32 observations the model underestimated the observed elevation by more than 0.20 m and up to 0.27 m in the most extreme case. This difference between observed and simulated elevation is already considerable given the simulated period of 70 years of sediment accumulation. In this respect, it is important to look also at the simulated accumulation rates. Figure 7.7b shows that the observed and simulated accumulation rates correspond fairly well ( $R^2=0.64$ ). For only 2 of the 32 observations, the model simulations underestimated or overestimated the observed accumulation rates by a factor two to three.

---

FIGURE 7.6. Observed (in symbols) and simulated (in thick lines) marsh elevation change with time for 25 marsh sites along the Scheldt estuary (see Fig. 7.1 and Table 7.1 for locations and names of marsh sites). Old marshes are indicated in black symbols and black thick lines, young marshes are indicated in grey symbols and grey thick lines. The time evolution of local mean high water level (MHWL) is indicated in thin black lines. For clarity, standard deviations on the estimated elevations were not indicated on this figure but are listed in Table 7.4 and 7.5.

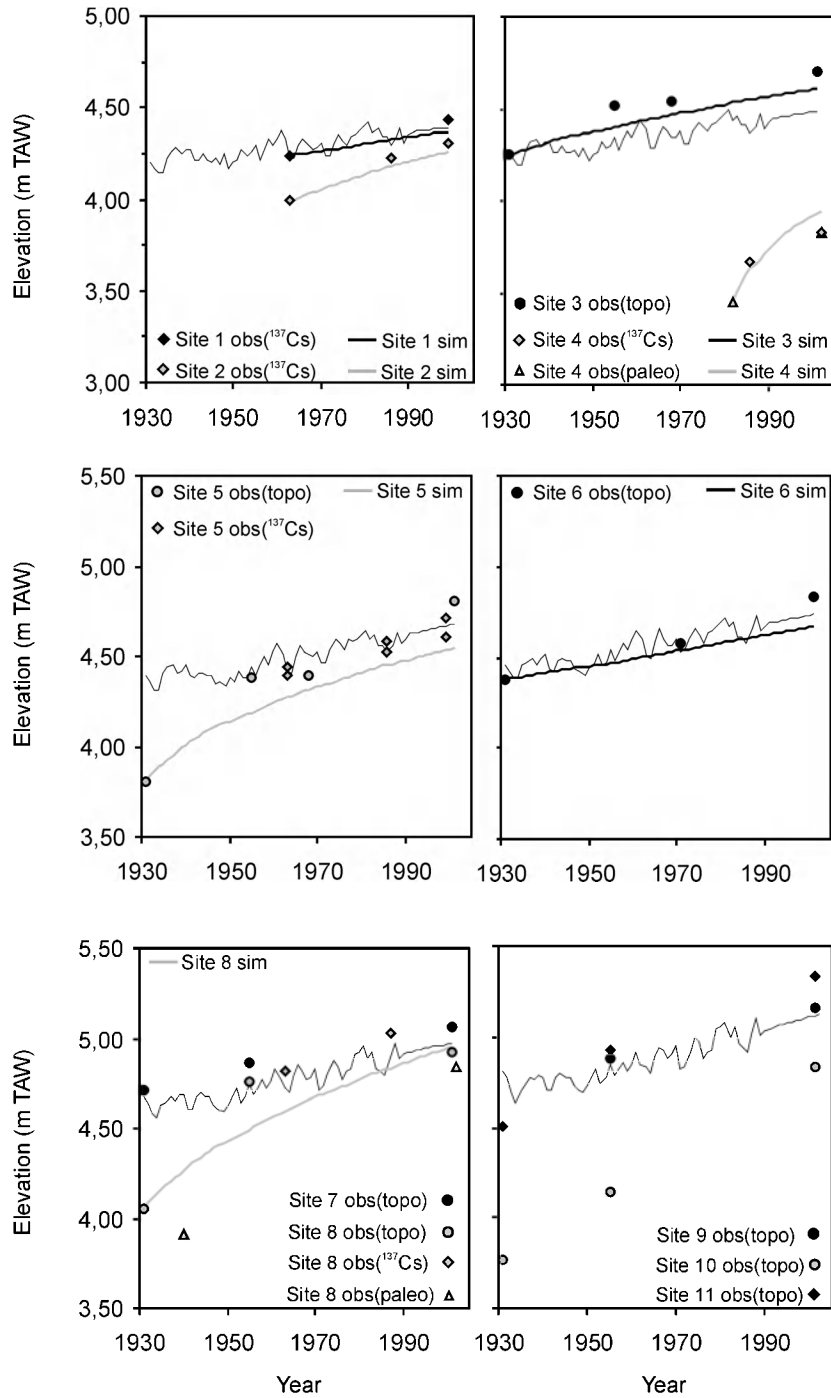


FIGURE 7.6 (to be continued)

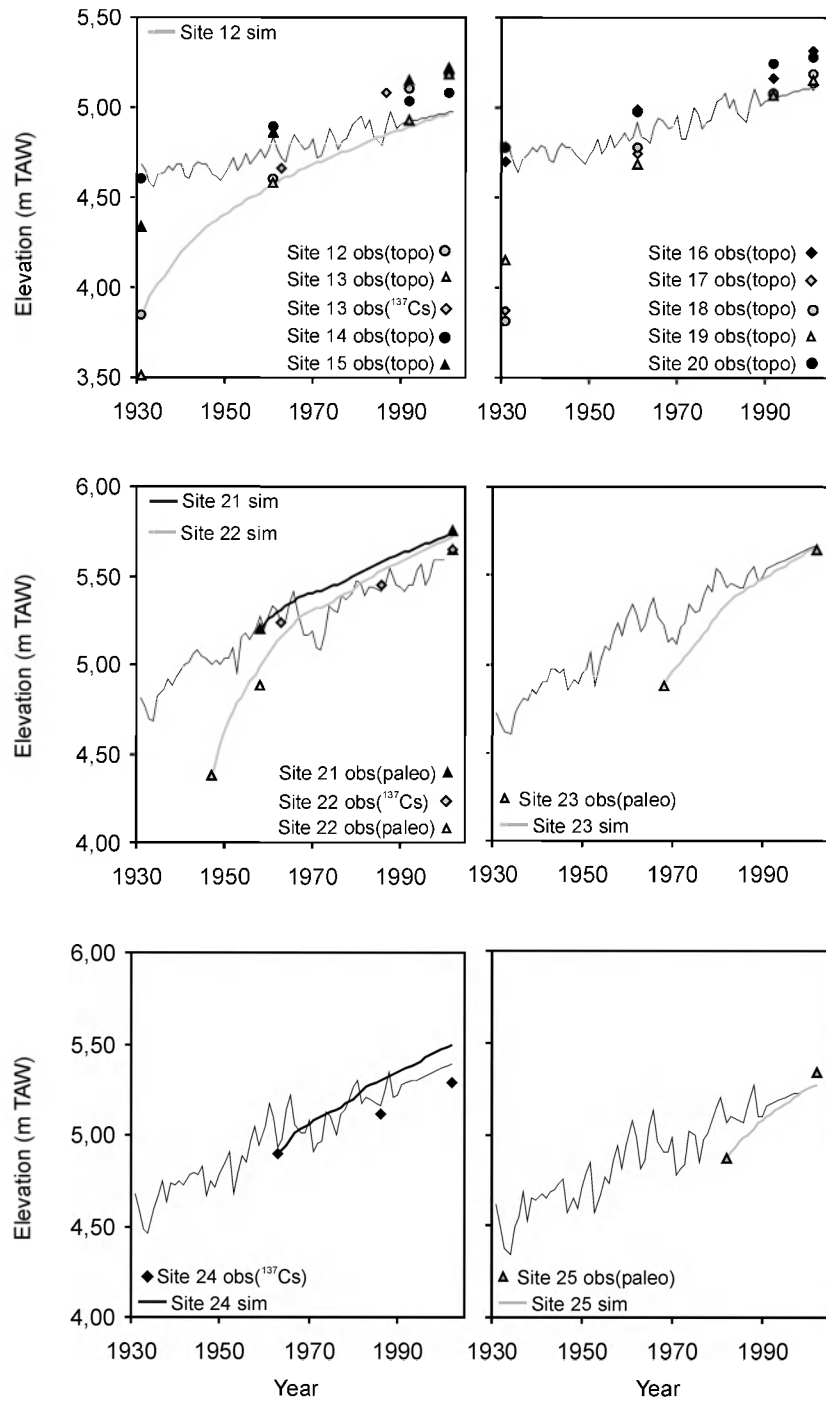


FIGURE 7.6

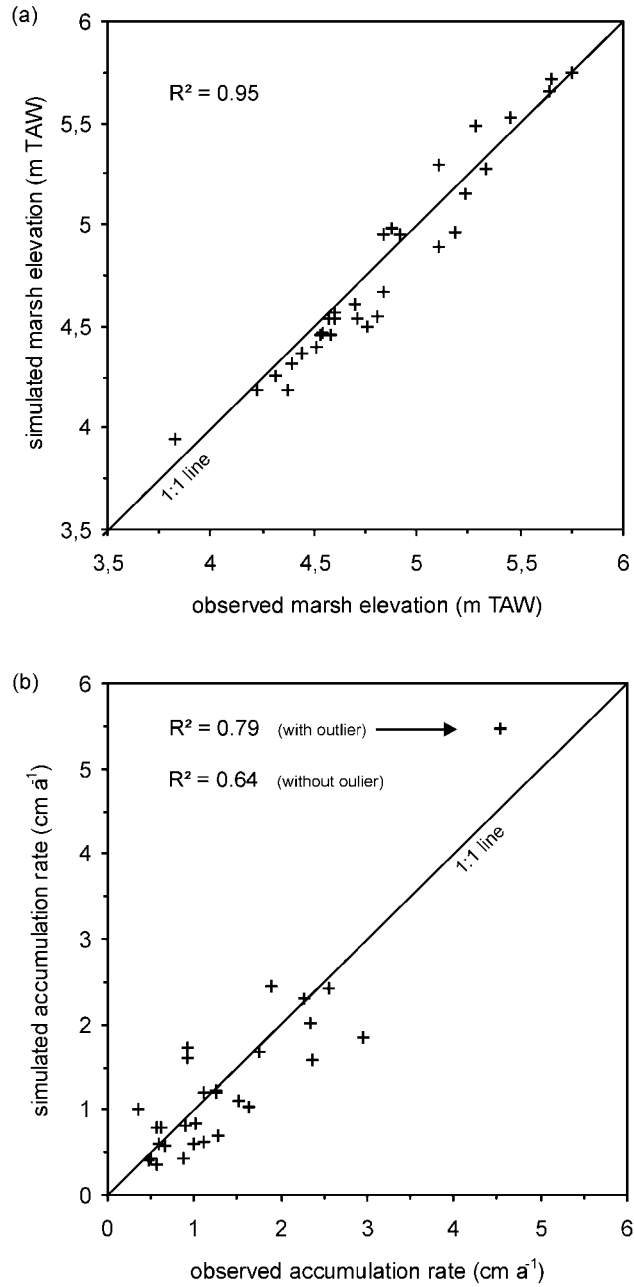


FIGURE 7.7: (a) Observed versus simulated marsh surface elevations. Data are plotted for both the historic and present-day elevations, which could be determined. (b) Observed versus simulated accumulation rates.

## 7.5. Discussion

### 7.5.1. Factors controlling estuarine variations in marsh accumulation

The field data showed that the asymptotic rise of young marshes up to MHWL and the steady rise of old marshes with MHWL rise is a general mechanism controlling the long-term accumulation of tidal marshes in the Scheldt estuary (Fig. 7.6). As a result, the large-scale estuarine variation in marsh elevations and accumulation rates is strongly controlled by estuarine variations in MHWL and MHWL rise. Figures 7.7 and 7.8 illustrate that at places where MHWL and MHWL rise is highest, the highest marsh surface elevations and accumulation rates are observed.

MHWL and MHWL rise are lowest in the Western Scheldt (Fig. 7.8 and 7.9). For this part of the estuary, we can say that an important phase of young marsh formation and of fast accumulation of these young marshes occurred between 1931 and 1955. During this period, young marshes started to grow at an elevation of 1.10 to 0.55 m below local MHWL (Fig. 7.8) and they accumulated at rates of 1.58 to 3.22 cm a<sup>-1</sup> (Fig. 7.9). Compared to the MHWL rise of 0.32 to 0.58 cm a<sup>-1</sup> in the Western Scheldt, these accumulation rates are high. The old marshes in the Western Scheldt accumulated at lower rates of 0.48 to 1.73 cm a<sup>-1</sup> during the period 1931-1955 (Fig. 7.9). By 1955 most young marshes attained their equilibrium elevation around local MHWL (Fig. 7.8). Consequently, during the subsequent period of 1955 up to present, the young and old marshes accumulated at comparable rates of 0.43 to 1.84 cm a<sup>-1</sup> (Fig. 7.9).

A factor that is often assumed to influence the accumulation rates on the tidal marshes in the Western Scheldt, is the dredging of the main stream channel of the Western Scheldt. The hypothesis is then that dredging and dumping of the dredged sediments at locations near tidal marshes leads to increased suspended sediment concentrations in the water that floods the marshes and consequently to increased sediment accumulation rates (e.g. Stikvoort *et al.*, 2003). However, the necessary data, especially on marsh accumulation rates for the period before dredging was widespread in the Western Scheldt, are often lacking to prove these hypotheses. In this respect, it can not be proved from the data presented here that dredging leads to increased marsh sedimentation: since the 1970's dredging activities increased considerably (e.g., Liek, 2001), while marsh accumulation rates were higher during the period 1931-1955 (before the increased dredging) than during the period 1955-2002 (Figure 7.9).

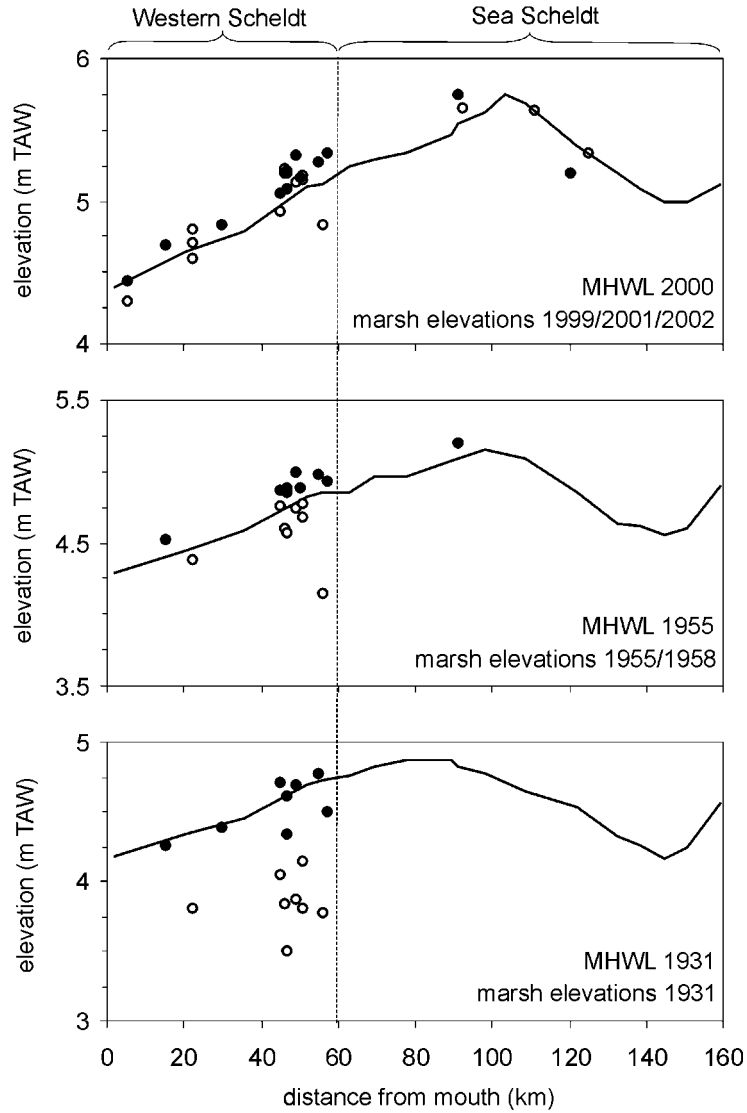


FIGURE 7.8. Observed historic and present-day marsh surface elevations and mean high water level (MHWL) as a function of distance from the mouth of the Scheldt estuary, for three points in time (1931; 1955/1958; 1999/2001/2002). Old marsh surfaces are indicated in black symbols, young marsh surfaces are indicated in white symbols. For clarity, standard deviations on the estimated marsh elevations were not indicated on this figure but are listed in Table 7.4 and 7.5.

For the Sea Scheldt no data on tidal marsh accumulation are available for the period 1931-1955. However, from old aerial photographs and topographic maps, we know that no important marsh formation occurred in the Sea Scheldt as this was the case in the Western Scheldt (Hoffmann, 1993). For the period 1955 up to present accumulation rates were generally higher in the Sea Scheldt than in the Western Scheldt (Fig. 7.9). This is partly due to the much faster MHWL rise in the Sea Scheldt than in the Western Scheldt, which causes more frequent and higher marsh inundations and consequently higher accumulation rates. Furthermore, time-averaged suspended sediment concentrations in the main stream channel are two to three times higher in the Sea Scheldt than in the Western Scheldt, which also explains the higher marsh accumulation rates in the Sea Scheldt.

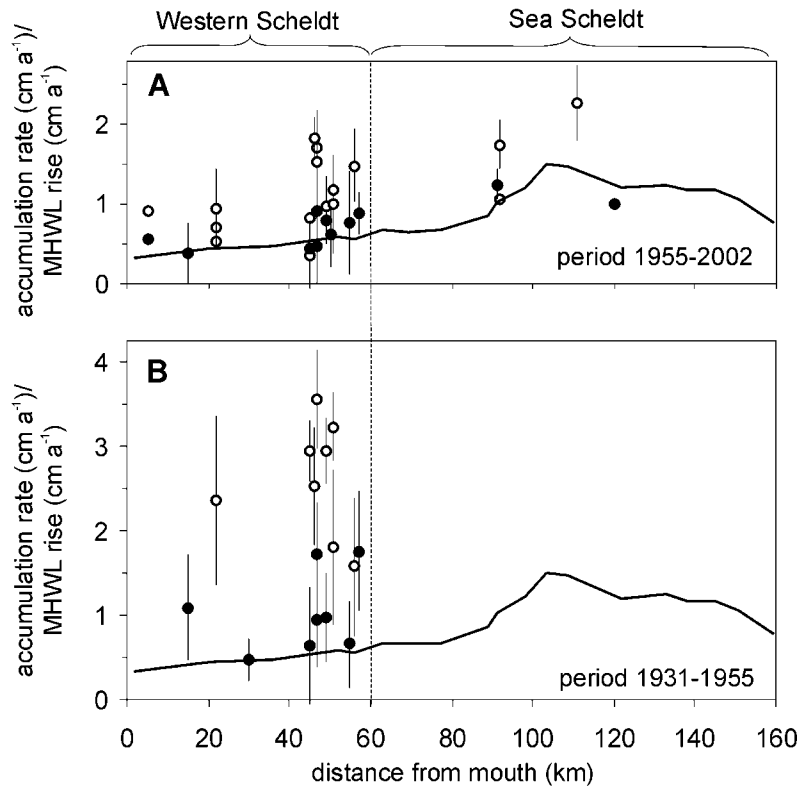


FIGURE 7.9: Observed accumulation rates of tidal marshes (mean values in symbols and standard deviations in error bars) in relation to mean high water level (MHWL) rise (in black line) along the Scheldt estuary: (A) accumulation rates calculated for the period 1955-2002 and (B) for the period 1931-1955. For both figures MHWL rise is calculated for the period 1931-1990, since MHWL rise was rather constant during this whole period (see Fig. 7.6). Old marsh surfaces are indicated in black symbols, young marsh surfaces are indicated in white symbols.

### 7.5.2. Model performance

It was shown from former field and modelling studies that young low marshes are characterised by a quick asymptotic vertical rise and that marsh surfaces finally tend to an equilibrium elevation high in the tidal frame (Pethick, 1981; Allen, 1990; French, 1993). However, although we may say that these existing models are qualitatively valid, until now very little work was done on the *quantitative* validation of long-term model predictions against observed accumulation rates.

In this respect, this study showed that the 0-dimensional time-stepping model, presented in Temmerman *et al.* (2003a), is capable to simulate quite well the observed long-term accumulation of tidal marshes under varying environmental conditions. Important to notice, is that the model correctly predicted the varying rates at which young marshes accumulate asymptotically up to their equilibrium level around MHWL. In the Western Scheldt this equilibrium level is reached relatively slower than in the Sea Scheldt (Fig. 7.6), which may be attributed to the lower suspended sediment concentrations in the Western Scheldt than in the Sea Scheldt (Fig. 7.3). For example, for the young Paulina marsh (site 4), situated in the Western Scheldt, the model simulated correctly that, 20 years after the marsh was formed, the present marsh surface is not yet in equilibrium with MHWL (Fig. 7.6). On the contrary, for the young Notelaar marsh (site 22), which is an example for the Sea Scheldt, the model simulated, in correspondence with the field data, that the equilibrium level around MHWL was already attained 15 years after the marsh was formed (Fig. 7.6). After this, the young Notelaar marsh accumulated at a much slower rate similar to the rate of MHWL rise, which was correctly simulated. Also for all other young marshes the model simulated the asymptotic rise of the marsh surface with time in accordance with the field data.

The ability of the model to simulate this large-scale estuarine variability in tidal marsh accumulation supports the potential of the model to be used as a tool to predict the evolution of young marshes that originated either spontaneously or by human intervention in the framework of nature development plans. However, apart from the vertical accumulation of tidal marshes, also the lateral changes in marsh surface area need to be considered in this respect: on the one hand, the formation of new young marshes, by lateral extension of marsh vegetation over adjacent tidal flats, and on the other hand, the lateral erosion of marsh edges. The field data gathered in this study indicated that the formation of new young marshes started at an elevation of about 0.55 to 1.10 m below MHWL in the Western Scheldt and 0.30 to 0.70 m below MHWL in the Sea Scheldt. However, apart from the elevation relative to the tidal frame, also other factors may exert an important control on the colonisation of bare tidal flats by marsh vegetation, such as sediment quality, tidal currents and wind-wave activity, which can cause episodic erosion events that prevent the germination and growth of marsh

plants. Further research is needed to fully incorporate these processes of lateral extension and shrinkage of tidal marshes.

7.5.3. Marsh accumulation in response to MHWL rise and incoming SSC

Former field studies indicated that in certain areas tidal marshes are not able to keep up with the rising sea-level (Reed, 1995; Ward *et al.*, 1998), resulting in submergence and major losses of tidal marsh areas (e.g., Baumann *et al.*, 1984; Walker *et al.*, 1987). However, this study showed that in the Scheldt estuary all marshes are able to maintain their equilibrium level, which is around local MHWL. This may be surprising, because MHWL is rising at highly varying rates along the estuary, ranging from 0.32 up to 1.5 cm a<sup>-1</sup> (Fig. 7.9). Former simulations using the presented model showed that, when MHWL rises faster, higher incoming SSC values are needed to maintain the same equilibrium elevation relative to MHWL (see Fig. 6.6 in chapter 6). Indeed, in the Sea Scheldt, where MHWL rise is highest (Fig. 7.9), also the highest SSC values are observed (Fig. 7.3) and thus the highest *k* values were used as input for the model simulations (Table 7.2). Model simulations for the Sea Scheldt marshes (sites 21 up to 25), using a lower *k* value of 0.05 which is representative for the Western Scheldt, resulted in predicted present-day (2002) elevations that are 0.20 to 0.30 m lower than the elevations predicted using the *k* values originally determined for the Sea Scheldt (Table 7.6). Thus, if sediment concentrations in the Sea Scheldt had been lower, the marsh surfaces would have experienced increased flooding and might have degraded to bare tidal flats. This suggests that a delicate balance exists between the variation in MHWL rise and in SSC along the estuary, which causes the tidal marshes to maintain their equilibrium elevation around MHWL along the whole Scheldt estuary. This is an intriguing conclusion. Nevertheless, the question remains whether this

TABLE 7.6. Predicted present-day (2002) surface elevations (in m TAW) for the Sea Scheldt marshes (sites 21 up to 25), (1) using a *k* value of 0.05, which is representative for the Western Scheldt, and (2) using the original *k* values determined from field data on suspended sediment concentrations (see Table 7.2).

site nr	(1)	(2)	(2)-(1)
21	5.54	5.75	0.20
22	5.42	5.65	0.30
23	5.22	5.64	0.24
24	5.21	5.29	0.28
25	5.04	5.34	0.23

balance between the estuarine variation in MHWL rise and in SSC is just a matter of coincidence or whether a causal relationship has to be sought between MHWL rise and SSC.

Additional model runs were carried out to simulate the impact of future MHWL rise and changes in SSC on tidal marsh accumulation along the Scheldt estuary. Simulations were carried out starting from the present-day observed marsh elevations and simulating marsh accumulation for the next 100 years under two scenarios of MHWL rise: first, by extrapolating the 'current' rate of MHWL rise (observed at every marsh site during the last 70 years), and secondly, using this current rate of MHWL rise multiplied by a factor 1.5. For both MHWL rise scenarios, three model runs were carried out using (1) the present-day  $k$  values (determined from the SSC field data; see Table 7.2), (2) these  $k$  values multiplied by a factor 0.5 and (3) these  $k$  values multiplied by a factor 2. In this way, the impact of changes in SSC in the Scheldt estuary was simulated.

Figure 7.10 shows that under the current trend of MHWL rise and SSC all marshes will be able to maintain an elevation around MHWL during the next 100 years. Even if MHWL rise would increase with a factor 1.5, no considerable changes in marsh surface elevation relative to MHWL would occur by 2100, given the present-day SSC values observed along the Scheldt estuary. However, a decrease in SSC values by a factor 0.5 would result in 2100 in marsh surface elevations up to 0.27 m below local MHWL, under the current trend of MHWL rise, and up to 0.38 m below MHWL, under the increased trend of MHWL rise (Fig. 7.10). These changes in marsh surface elevation are considerable and would result in increased tidal flooding and consequently in significant changes in marsh vegetation and other ecologic processes. On the contrary, an increase in SSC values by a factor 2 would result in increased marsh elevations up to 0.31 and 0.25 m above local MHWL, under the current and increased trend of MHWL rise, respectively (Fig. 7.10).

Although it may be difficult to estimate accurately how MHWL rise and SSC will evolve in the Scheldt estuary during this century, the model simulations suggest that the tidal marshes in the Scheldt estuary will sustain their present-day elevation relative to MHWL, if MHWL rise and SSC would not change drastically. However, management options that would lead to increased MHWL rise, such as intensive dredging, and other measures that would result in a decrease in SSC, such as the planning of water purification plants and soil erosion control measures in the Scheldt basin, could potentially lead to the failure of tidal marshes to keep up with the rising MHWL and finally result in drastic ecological changes.

Apart from vertical accumulation, tidal marshes can also be subject to lateral erosion at the marsh edge. Thus, in the case that tidal marshes are able to accumulate vertically with the rising mean high water level, this does not exclude that tidal marsh area can be lost due to lateral erosion of the marsh

edge. On the contrary, due to the vertical rise of the marsh surface, the slope between the marsh edge and the low water line will increase in steepness and this will potentially decrease the stability of this slope. As a result, this could lead to increased lateral erosion of the marsh edge. However, the possible feedback mechanisms between vertical rise and lateral erosion of marshes was not studied here and needs more research.

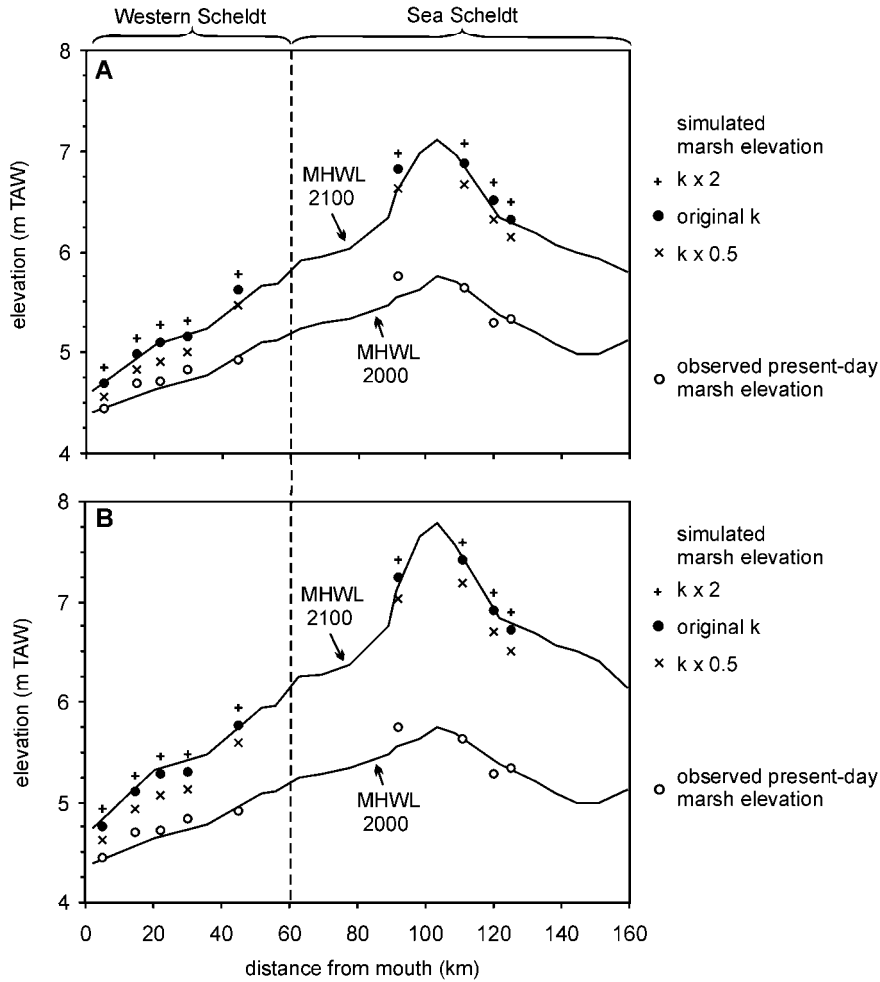


FIGURE 7.10. Simulation of marsh accumulation along the Scheldt estuary for the next 100 years under different scenarios of mean high water level (MHWL) rise and suspended sediment concentrations (SSC): (A) extrapolation of the 'current' rate of MHWL rise; (B) 1.5 times the 'current' rate of MHWL rise. For both MHWL rise scenarios, three scenarios of SSC were simulated, using in eq. 7.1 (1) the original present-day  $k$  values, (2) these  $k$  values multiplied by 0.5 and (3) these  $k$  values multiplied by 2.

## 7.6. Conclusions

(1) The quick asymptotic vertical rise of young low marsh surfaces up to an equilibrium level around MHWL, is a general mechanism that controls the long-term ( $10$ - $10^2$  years) vertical accumulation of tidal marshes in the Scheldt estuary. Once this equilibrium level is attained, high old marshes accumulate much slower at rates that are comparable to local MHWL rise. Furthermore, the rate at which young marshes attain their equilibrium level is higher in the inner part (the Sea Scheldt) than in the outer part of the estuary (the Western Scheldt). This difference can be attributed to the higher suspended sediment concentrations that are present in the inner estuary.

(2) A 0-dimensional physically-based time-stepping model for long-term vertical marsh accumulation was validated against the field data on long-term accumulation rates. The model was able to simulate very well the observed large-scale variability in accumulation rates along the Scheldt estuary. The model simulations showed that a delicate balance between the estuarine variation in MHWL rise and SSC offers the ability to the tidal marshes to maintain their equilibrium elevation around MHWL, although MHWL is rising at highly varying rates along the estuary. Finally, model simulations suggest that the tidal marshes have the potential to keep up with the rising MHWL during the next 100 years, unless MHWL rise would increase and suspended sediment concentrations would decrease importantly in the Scheldt estuary.

## Chapter 8

### General discussion and conclusions

---

Given the growing attention that is paid to the sustainable management of coastal and estuarine ecosystems such as tidal marshes, there is an increasing demand for scientific knowledge and predictive simulation models with regard to the response of tidal marshes on changing environmental conditions such as sea-level rise. In this respect, knowledge of sedimentation and elevation changes in tidal marshes is crucial, since these are the major factors controlling ecological changes in tidal marshes. Although numerous field studies concentrated on the study of tidal marsh sedimentation, many aspects are still poorly understood: as a consequence, predictive simulation models are in a very rudimentary stage of development and were to a very limited degree validated against field data (see e.g. Allen (2000) for an extensive review). The aim of this work was to contribute to a better understanding of tidal marsh sedimentation processes, using a combined approach of field measurements and the development, application and testing of numerical simulation models.

### 8.1. Short-term sedimentation patterns

Former field studies showed that short-term temporal variations in sedimentation rates are mainly controlled by either variations in tidal inundation (e.g., Allen and Duffy, 1998a; Christiansen *et al.*, 2000), wind-wave activity (e.g., Reed, 1989; Leonard *et al.*, 1995a; Van Proosdij *et al.*, 2000) or seasonal variations in biological activity (e.g., Hutchinson *et al.*, 1995; Leonard, 1997; Pasternack and Brush, 2001). Spatial sedimentation patterns were found to be related to the marsh surface elevation (e.g., Stoddart *et al.*, 1989; Cahoon and Reed, 1995), the distance to tidal creeks (e.g., French and Spencer, 1993; Leonard, 1997; Reed *et al.*, 1999), or differences in vegetation structure (e.g., Boorman *et al.*, 1998).

Apart from sedimentation on tidal marshes, the deposition of suspended sediments on alluvial floodplains during overbank flows is recently increasingly being studied (e.g., Anderson *et al.*, 1996). While in tidal marshes sedimentation takes place during regularly occurring but rather shallow inundation events controlled by the tide, alluvial floodplain sedimentation occurs during events of high river discharge that are less frequent but that generally result in higher inundation heights. Given this analogy between alluvial floodplains and tidal marshes, the findings of studies on floodplain sedimentation can potentially contribute to the understanding of tidal marsh sedimentation and vice versa.

It is widely reported from field studies that spatial variations in sedimentation rates on alluvial floodplains are mainly related to the distance from the river channel: the farther away from the channel, the less suspended sediment reaches the floodplain and is deposited (e.g., Asselman and Middelkoop, 1995; Walling *et al.*, 1996; 1999). In the long term, this leads to the formation of raised natural levees along alluvial river channels and lower lying inner basins at farther distances from the channel. This spatial sedimentation pattern clearly corresponds with the decrease of sedimentation rates with increasing distance from tidal creeks and the formation of levees next to creeks, which is observed in tidal marshes (e.g., French and Spencer, 1993; Leonard, 1997; Reed *et al.*, 1999; see also chapters 2 and 6 of this thesis). Apart from the influence of the distance to a stream channel, also variations in the elevation of an alluvial floodplain or a tidal marsh exerts a strong control on variations in the sedimentation rate. Lower lying floodplains or tidal marshes are characterised by higher sedimentation rates because they are inundated more frequently, higher and longer (e.g., Asselman and Middelkoop, 1998). As a consequence, the higher a floodplain accumulates the less frequent it is inundated and the lower the sedimentation rates become (e.g., Moody and Troutman, 2000). This corresponds with our finding that young low marshes are characterised by an initially fast sedimentation rate, which progressively decreases when the marsh surface accumulates higher within the tidal frame (see chapters 5 and 7).

Recently attempts were made to model the 2-dimensional spatial patterns of sediment deposition on tidal marshes. The starting point to model the detailed spatial sedimentation pattern is that it is ultimately the result of the transport pathways of water and suspended sediment during overbank flow over the complex micro-topography of floodplains (Walling *et al.*, 1996; Middelkoop and Asselman, 1998). In order to model these transport pathways, either complex hydrodynamic models were used, based on the solution of the Navier-Stokes equations (e.g., Bates *et al.*, 1996; Hardy *et al.*, 2000) or simplified hydraulic modelling schemes (e.g., Nicholas and Walling, 1997; Middelkoop and Van der Perk, 1998). However, until now no such models were applied and evaluated to simulate the 2-dimensional spatio-temporal sedimentation patterns on tidal marshes.

Up to now, the relative importance and interactions between the different variables thought to control temporal and spatial variations in marsh sedimentation rates are poorly understood. As a consequence, the prediction of the overall variations in sedimentation rates was found to be difficult. In part I of this thesis (chapters 2, 3 and 4) special attention was given to (1) the identification of the relative importance of the different factors controlling short-term temporal and spatial patterns of tidal marsh sedimentation based on field measurements, and (2) the simulation of 2-dimensional spatio-temporal sedimentation patterns using an empirical and physically-based modelling approach.

#### *8.1.1. Temporal patterns*

Chapter 2 reported the results of a 1-year measuring campaign during which the temporal and spatial variations in suspended sediment concentration (SSC) and deposition were studied within a salt and freshwater tidal marsh in the Scheldt estuary. Large temporal variations in sedimentation rates were measured, ranging in the order of 1 to  $10^3$  g.m<sup>-2</sup> per bi-weekly spring-neap cycle. These temporal variations in sedimentation rates were found to be controlled by the tidal inundation regime, while the influence of wind-wave action was negligible. It was shown that the incoming SSC, measured above the marsh surface at the beginning of tidal inundation cycles, is linearly increasing with the maximum inundation height, occurring during these inundation cycles (Fig. 2.6). In accordance with this, an exponential relationship was observed between inundation time and sedimentation rate. Further in the thesis (chapter 5), it was shown that this relationship between incoming SSC and inundation height is crucial to successfully simulate the long-term vertical rise of marsh surfaces (see below). In addition to this tidal control on sediment supply and deposition, a seasonal control was observed: both SSC and sedimentation rates were higher during winter than during summer for a same inundation height or time.

### 8.1.2. *Spatial patterns*

Spatial variations in sedimentation rates were shown to be large within the studied salt and freshwater marsh: time-averaged sedimentation rates ranged from 40 to 1650  $\text{g}\cdot\text{m}^{-2}$  per bi-weekly spring-neap cycle (chapter 2), and from 1.5 to 140  $\text{g}\cdot\text{m}^{-2}$  per single semi-diurnal cycle (chapter 3). Analysis of these spatial variations showed that they are strongly related to the marsh surface topography. On the one hand, sedimentation rates decrease with increasing marsh surface elevation, since high marsh surfaces are inundated less frequent, lower and shorter than low marsh surfaces (Fig. 2.8a). On the other hand, sedimentation rates decrease with increasing distance from tidal marsh creeks and increasing distance from the marsh edge, measured along the creeks system (Fig. 2.8b and c). This is explained by progressive sediment trapping along flow paths from the marsh edge via the creeks system over the marsh platform.

More detailed measurements of the suspended sediment transport and deposition within a tidal creek catchment during single tidal cycles were presented in chapter 3. These measurements showed that the tidal creeks system serves as the major transport pathway of water and sediment to and from the surrounding marsh surface. Both the water volumes and sediment masses that were discharged through the creek system, accounted for a significant proportion of the total water volumes stored above the marsh surface at high tide and the total sediment mass deposited over a tidal cycle. However, the supply of water over the marsh edge, rather than through the creeks system, becomes more and more important with increasing high water level of the tidal cycles (Fig. 3.12).

### 8.1.3. *Spatial modelling*

In order to model the observed spatial sedimentation patterns, first a rather simple empirical multiple regression model was proposed, predicting the spatial variations in sedimentation rates based on the three topographic parameters mentioned above: (1) surface elevation, (2) distance to the nearest tidal creek, and (3) distance to the marsh edge, measured along the nearest tidal creek (chapters 2 and 3). Implementation of this model in a raster-based Geographical Information System (GIS) resulted in predicted sedimentation rates that are in good agreement with observed sedimentation rates (Fig. 2.10 and Fig. 3.6). However, more detailed field data on the spatial sedimentation pattern in chapter 3 showed that on low young marsh surfaces, where a dense tidal creek system had not yet developed, sedimentation rates need to be modelled based on surface elevation alone.

An important conclusion is that the same model successfully predicted the spatial sedimentation pattern on a salt and freshwater marsh, only based on the three topographic parameters explained above. This suggests that,

although spatial differences in vegetation characteristics are large between and within the studied salt and freshwater marsh, they do not have a significant effect on the spatial sedimentation pattern.

Although the topography-based model proved to be able to simulate the spatial sedimentation patterns in the studied tidal marshes, it may be questioned to what extent such an empirical model approach is also applicable to other tidal marshes. Furthermore, the topography-based approach does not allow to predict the impact of changing environmental conditions, such as changes in incoming sediment concentrations. In this respect, a more physically-based approach offers perspectives.

In chapter 4, a physically-based hydrodynamic and sediment transport model, Delft3D, was implemented and evaluated for its ability to simulate the 2-dimensional spatial sedimentation pattern in tidal marshes. The Delft3D model is based on a 3-dimensional finite difference solution of the Navier-Stokes equations, which allows the simulation of free surface water flows over complex topographies. Furthermore, additional formulations were recently incorporated to account for the effect of vegetation on friction and turbulence.

The Delft3D model was implemented, calibrated and validated using the measured spatial sedimentation pattern in the salt marsh creek catchment, studied in chapter 3. The simulated spatial variations in sedimentation rates were shown to correspond quite well with observed spatial variations (Fig. 4.8; and compare Fig. 4.9 and Fig. 3.5). However, a more detailed analysis of the simulated flow paths showed that the model underestimated the role of the tidal creek system in transporting water and sediment to and from the surrounding marsh platform. Instead, the model simulated that this transport mainly takes place through the marsh edge, which is in contradiction with the field measurements discussed above. This leads to the conclusion that hydrodynamic models offer clear potential for use as a predictive tool, but need to be applied with caution, and that further work is needed to enhance model representation of tidal marsh processes.

Additional model simulations allowed to get some insight in the sensitiveness of the simulated spatial sedimentation pattern on changes in model variables, which are generally thought to control marsh sedimentation. First, higher concentrations and settling velocities of the incoming suspended sediment resulted in higher sedimentation rates, without any systematic change in the spatial sedimentation pattern. Secondly, during tidal inundation cycles with higher high water levels, sedimentation rates are higher and the sediment is transported relatively higher on the marsh and farther away from the marsh edge before it is deposited. Finally, model simulations showed that large differences in vegetation structure have no significant effect on the spatial sedimentation pattern. Even the presence or absence of a vegetation cover makes no significant difference for the simulated spatial sedimentation

pattern. This is a quite remarkable conclusion, since it is often assumed in the literature that the presence of vegetation is crucial to promote sediment deposition on tidal marshes. However, the model simulations seem to suggest that not the vegetation cover but the topography of tidal marshes is the main factor controlling the spatial sedimentation pattern. A possible explanation for this is that, due to the high elevation within the intertidal zone and the flat topography of tidal marshes, flow velocities are very low on tidal marshes even without a vegetation cover. As a consequence of these low flow velocities, the interactions between the flow and the vegetation cover are rather limited, which possibly explains that the relative influence of the vegetation cover on flow hydrodynamics and on the spatial sedimentation pattern is negligible compared to the influence of the topography of tidal marshes. However, further experimental research, both in the field and in the laboratory, is needed to confirm or refine these findings that resulted from numerical modelling.

## 8.2. Long-term tidal marsh accumulation

Former field studies especially focussed on long-term ( $10^1$ - $10^2$  years) tidal marsh accumulation in response to sea-level rise. In this respect, the quick asymptotic rise of young low marsh surfaces up to an equilibrium level high in the tidal frame is widely considered as a general mechanism controlling long-term tidal marsh accumulation (e.g., Pethick, 1981; Allen, 1990; Allen, 2000). Recently, a number of model approaches, either physically-based or empirical, have been used to simulate this pattern of long-term tidal marsh accumulation, and especially to evaluate the expected response of tidal marsh surfaces to future sea-level rise scenarios (Krone, 1987; Allen, 1990; 1995; 1997; French, 1993; Callaway *et al.*, 1996; Day *et al.*, 1999; Van Wijnen and Bakker, 2001; Pont *et al.*, 2002; Rybczyk and Cahoon, 2002). Although we may say that these models are qualitatively valid, until now very little attention was paid to the quantitative validation of model predictions against field data on long-term marsh accumulation rates. Furthermore, existing models are all 0-dimensional time-stepping models, simulating vertical elevation changes with time for one point in space and thus neglecting spatial variations in long-term elevation changes.

Elaborating on part I of this thesis, related to short-term sedimentation processes, we studied in part II: (1) how young and old marshes, with a different surface elevation, accumulate in the long-term (chapter 5); (2) to what extent the decrease in short-term sedimentation rates with increasing distance from tidal creeks will result in the formation of natural levees, next to tidal creeks, and inner basins, farther away from creeks (chapter 6); and (3) how estuarine gradients in mean high water level rise and suspended

sediment concentrations will impact the long-term accumulation of tidal marshes along the whole Scheldt estuary (chapter 7). Special attention was paid to the development and validation of a model approach that allows to simulate the long-term vertical rise of tidal marshes at all three scales mentioned above.

### *8.2.1. Young versus old marsh surfaces*

In chapter 5, we developed a physically-based 0-dimensional time-stepping model to simulate long-term tidal marsh accumulation, based on the mass balance approach of Krone (1987). In order to evaluate the model, field data were collected on the historical accumulation of a young and old marsh surface within a freshwater marsh in the Scheldt estuary, based on aerial photographs and sediment cores. These data showed that the young marsh was formed 55 years ago by plant colonisation of a bare tidal flat at an elevation of *ca.* 0.7 m below local mean high water level (MHWL). Since then it accumulated very quickly and asymptotically up to an equilibrium level around MHWL. On the contrary, the old marsh was 55 years ago already at its equilibrium level around MHWL and since then accumulated as fast as MHWL raised (Fig. 5.3). This pattern of long-term tidal marsh accumulation, which was observed for a freshwater marsh, is in accordance with the asymptotic rise reported from salt marshes (e.g., Pethick, 1981).

Next, the model was implemented using field data on the evolution of the tidal regime and on the present-day suspended sediment regime as input for the model. The field data on long-term accumulation rates were used as an independent data set for model evaluation. The application of the existing model approach of Krone (1987), which assumes a constant incoming suspended sediment concentration (SSC), leads to an underestimation of the observed accumulation rate of the young and old marsh surface. However, in chapter 2 we showed that the incoming SSC, in the water that floods the marsh surface at the beginning of an inundation cycle, is not constant but increases linearly with maximum inundation height, at high tide. This relationship between incoming SSC and inundation height was used then in the model to simulate the long-term change in incoming SSC, as the tidal inundation regime is changing due to changes in marsh elevation relative to the tidal frame. After incorporation of this relationship, the model successfully simulated the observed marsh accumulation (Fig. 5.10). This leads to the conclusion that not only the decrease in tidal inundation, but also the decrease in SSC with decreasing marsh inundation height, is of great importance to fully explain and successfully simulate the asymptotic vertical rise of tidal marshes.

### 8.2.2. *Levees versus basins*

Natural levees, next to tidal creeks, and lower lying basins, some 10 to 20 m farther away from creeks, are a typical geomorphic feature within tidal marshes. In chapter 6, the formation and long-term evolution of levees and basins was studied by applying the 0-dimensional model, described in chapter 5, using spatially differentiated model parameter values for levees and basins. First, the model was calibrated using field data on short-term spatio-temporal variations in sedimentation rates that were collected for four levee-basin transects (see chapter 2). Next, the long-term elevation changes of the levees and basins were simulated, starting from a historically known marsh elevation. The model simulated correctly that the elevation difference between levees and basins tends to an equilibrium (Fig. 6.4). Once levees grow 20 to 30 cm higher than the adjacent basins, the positive influence of the proximity of a tidal creek on the sedimentation rate on the levees is compensated by the negative influence of the higher surface elevation of the levees. Once this sedimentological-geomorphic equilibrium condition is attained, both levees and basins accumulate at the same rate, which is in equilibrium with the rate of MHWL rise.

Additional simulations showed that this equilibrium in the elevation difference between levees and adjacent basins is controlled by the rate of MHWL rise and the incoming SSC (Fig. 6.7). A faster MHWL rise results not only in a generally lower equilibrium elevation of the marsh surface relative to MHWL, but also in a more pronounced elevation difference between levees and adjacent basins. On the other hand, higher incoming SSC values resulted in higher equilibrium elevations. However, significantly larger elevation differences between levees and basins were only obtained for increased differences in incoming sediment concentrations between levees and basins. Thus, this study demonstrated that the long-term response of tidal marsh surfaces to different scenarios of changing sea-level and incoming sediment concentrations is not uniform in space, but that spatial variability in tidal marsh morphodynamics is important and that natural levees and inner basins will react in a different way.

### 8.2.3. *Large-scale estuarine variability*

Along the Scheldt estuary, large gradients exist in MHWL rise and SSC (Fig. 7.9 and Fig. 7.3). Based on the insights acquired in chapters 5 and 6, we may expect that these gradients will have a strong influence on large-scale variations in marsh accumulation rates along the Scheldt estuary. Therefore, in chapter 7, field data on long-term accumulation rates were collected for 25 marsh sites scattered along the Scheldt estuary. The observed accumulation rates highly ranged from 0.35 to 4.55 cm a<sup>-1</sup>. The field data showed that the quick asymptotic rise of young low marshes up to an equilibrium level

around MHWL is a general mechanism that controls the long-term accumulation of tidal marshes in the Scheldt estuary (Fig. 7.6). Once this equilibrium level is attained, high old marshes accumulate much slower at rates that are comparable to local MHWL rise. However, young marshes attain their equilibrium level faster in the Sea Scheldt than in the Western Scheldt, which is attributed to the higher suspended sediment concentrations that are present in the Sea Scheldt.

The model, presented in chapters 5 and 6, was evaluated for its ability to simulate this observed large-scale estuarine variability in tidal marsh accumulation. For 13 of the 25 marsh sites, values for the model input variables could be determined from field data. It was shown that the model was able to simulate quite well the observed variability in long-term accumulation rates (Fig. 7.7). Furthermore, the model simulations showed that a delicate balance exists between the estuarine variation in MHWL rise and SSC, so that the tidal marshes can maintain an equilibrium elevation around MHWL along the whole estuary: in the Sea Scheldt, where MHWL rise is highest along the estuary, also the highest SSC values are observed, while in the Western Scheldt both MHWL rise and SSC are lower. The model simulations indicated that, if SSC had been lower in the Sea Scheldt, the tidal marshes would not have been able to keep up with the quickly rising MHWL.

Finally, it was demonstrated that the model can be used to evaluate the impact of changing environmental conditions on tidal marsh accumulation. In this respect, model simulations indicated that the tidal marshes in the Scheldt estuary have the potential to keep up with the rising MHWL during the next 100 years, unless MHWL rise would increase and suspended sediment concentrations would decrease drastically in the Scheldt estuary.

### 8.3. Possible applications and prospects for further research

In the framework of the ecological management of tidal marshes, it is of great importance to have a profound knowledge of tidal marsh morphodynamics, since these will largely determine the ecological functioning of tidal marshes. Especially with regard to future accelerated sea-level rise and – in particular for the Scheldt estuary – human interventions that may change mean high water level rise (e.g., dredging) and/or suspended sediment concentrations in the estuary (e.g., waste water purification, soil erosion control measures), it is important to be able to estimate the response of tidal marshes to these changing environmental conditions. In this respect, this thesis demonstrated the potential of numerical modelling to be used as a tool to predict tidal marsh sedimentation in response to future changes in environmental conditions such as mean high water level rise or suspended sediment concentrations.

Furthermore, the importance of geomorphic knowledge also applies to projects for marsh restoration or creation, such as are currently carried out along the Sea Scheldt by the Flemish government. A specific example is the digging off and lowering of marshes that were formerly raised by dumping of dredged or waste material, such as was recently done for the marsh of the Ketenisepolder (*ca.* 30 ha). Similar projects of digging off raised marshes to create low, young marshes are also proposed for other locations along the Sea Scheldt (see e.g. Van den Bergh *et al.*, 1998). Based on the findings from this thesis, we may expect that once marsh vegetation starts to grow on these lowered locations, the newly formed marsh will accumulate relatively quickly up to an equilibrium level around mean high water level. In this respect, the long-term model presented in this thesis can be used to calculate expected accumulation rates and to simulate the effect of different options for the elevation to which the marsh will be dug off.

Other projects that will be carried out along the Sea Scheldt, include the creation of tidal marshes in controlled inundation areas. In the framework of the accomplishment of the Sigmaphan, which was set up to protect the Flemish Sea Scheldt basin from estuarine flooding during storm surges, the construction of so-called controlled inundation areas is planned, e.g. in the polders of Kruibeke, Bazel and Rupelmonde (*ca.* 580 ha). This controlled inundation area is also reserved for nature development: a marsh area of *ca.* 300 ha will be created in the polders through the introduction of a controlled reduced tide by use of sluices in the embankment surrounding the polders (e.g., Meire *et al.*, 1997; Van den Bergh *et al.*, 1999). A similar project is planned as a preparatory study on a smaller scale in the Lippensbroek (*ca.* 8 ha). It is clear that such projects will result in the deposition of sediments in the controlled inundation area and that the resulting elevation changes will strongly determine the ecological processes and will reduce the water storage capacity of the controlled inundation area. However, it is unknown how fast

this process of sediment infilling will happen and to what extent spatial variations in sediment deposition and elevation will lead to spatial variations in habitats. Based on the findings from this thesis, we may say that much will depend on the magnitude of the tidal inundation regime that will be introduced in the polders and on the development of a tidal creek network. The models presented in this thesis offer a first approach to evaluate the impact of different inundation regimes on the rates of sediment accumulation that may be expected.

Although this thesis clearly contributed to the understanding of tidal marsh morphodynamics, until now our understanding is far from complete. As illustrated below, numerous aspects of tidal marsh morphodynamics may be identified that need further research.

First, this thesis showed that sediment deposition in tidal marshes takes place according to specific spatial and temporal patterns. However, we are not yet so far that the long-term effects of sediment deposition and elevation changes can be simulated and predicted in a fully 2-dimensional way. This thesis showed that complex hydrodynamic models, such as the Delft3D model, offer clear potential. Nevertheless, further work is needed to enhance the representation of tidal marsh processes, such as the simulation of flow paths via the creek system over the marsh platform. Furthermore, the applicability of such hydrodynamic models for long-term simulations is limited, given the numerical complexity and large computation times needed. In this regard, short-term hydrodynamic simulations need to be simplified and updated at relatively coarse time intervals to allow simulations over time-scales of  $10^1$ - $10^2$  years. One possible approach could be the extension of the 0-dimensional point model, presented in this thesis, to two dimensions, combined with flow paths simulated based on hydrodynamic modelling. The main challenge here is to retain model representation of only those short-term sedimentation processes that are relevant to the long-term changes in marsh elevation.

Secondly, when trying to understand the fully 2-dimensional morphodynamics of tidal marshes, it is not longer possible to consider only vertical accumulation of tidal marsh platforms, but also lateral changes in the geomorphology of tidal marshes need to be considered: (1) the lateral erosion of the seaward marsh edge; (2) the formation of new young marshes, by lateral extension of marsh vegetation over adjacent tidal flats; (3) the lateral movement of tidal marsh creeks and elongation, extension or reduction of the tidal creeks system. Although it is clear that these processes will affect the long-term geomorphic evolution of tidal marshes, until now little attention has been paid to the study of these lateral morphodynamic processes in comparison to the study of vertical accumulation. Furthermore, in order to fully understand the processes of lateral extension and erosion of tidal marshes, it will also be necessary to extend the research field to the adjacent tidal flats and especially to the interaction between tidal flats and marshes.

Finally, the work presented in this thesis offers new perspectives to link geomorphic processes to ecological processes in tidal marshes. In order to assess the impact of changing environmental factors, such as sea-level rise, on the ecological processes within tidal marshes, such as changes in vegetation, it is crucial to consider to what extent tidal marshes are able to maintain their elevation relative to the rising sea-level by the accumulation of sediments. In this respect, the integration of simulation models for sediment accumulation and vegetation succession would allow the prediction of long-term changes in tidal marsh vegetation in response to changing environmental factors such as sea-level rise.

## References

---

- Allen, J.R.L., 1989. Evolution of salt-marsh cliffs in muddy and sandy systems: a qualitative comparison of British West-coast estuaries. *Earth Surface Processes and Landforms*, 14: 85-92.
- Allen, J.R.L., 1990. Salt-marsh growth and stratification: a numerical model with special reference to the Severn Estuary, southwest Britain. *Marine Geology*, 95: 77-96.
- Allen, J.R.L., 1994. A continuity-based sedimentological model for temperate-zone tidal salt marshes. *Journal of the Geological Society*, 151: 41-49.
- Allen, J.R.L., 1995. Salt-marsh growth and fluctuating sea level: implications of a simulation model for Flandrian coastal stratigraphy and peat-based sea-level curves. *Sedimentary Geology*, 100: 21-45.
- Allen, J.R.L., 1997. Simulation models of salt-marsh morphodynamics: some implications for high-intertidal sediment couplets related to sea-level change. *Sedimentary Geology*, 113: 211-223.
- Allen, J.R.L., 1999. Geological impacts on coastal wetland landscapes: some general effects of sediment autocompaction in the Holocene of northwest Europe. *Holocene*, 9: 1-12.
- Allen, J.R.L., 2000. Morphodynamics of Holocene salt marshes: a review sketch from the Atlantic and Southern North Sea coasts of Europe. *Quaternary Science Reviews*, 19(12): 1155-1231.

## References

---

- Allen, J.R.L. and Duffy, M.J., 1998a. Medium-term sedimentation on high intertidal mudflats and salt marshes in the Severn Estuary, SW Britain: the role of wind and tide. *Marine Geology*, 150(1-4): 1-27.
- Allen, J.R.L. and Duffy, M.J., 1998b. Temporal and spatial depositional patterns in the Severn Estuary, southwestern Britain: intertidal studies at spring-neap and seasonal scales, 1991-1993. *Marine Geology*, 146(1-4): 147-171.
- Allen, J.R.L. and Pye, K., 1992. Coastal saltmarshes: their nature and importance. In: J.R.L. Allen and K. Pye (Editors), *Saltmarshes: morphodynamics, conservation and engineering significance*. Cambridge University Press, Cambridge, pp. 1-18.
- Allen, J.R.L. and Rae, J.E., 1988. Vertical salt-marsh accretion since the Roman Period in the Severn Estuary, southwest Britain. *Marine Geology*, 83: 225-235.
- Anderson, M.G., Walling, D.E. and Bates, P.D., 1996. *Floodplain processes*. Wiley, Chichester.
- Appleby, P.G. and Oldfield, F., 1984. The assessment of  $^{210}\text{Pb}$  data from sites with varying sediment accumulation rates. *Hydrobiologia*, 103: 29-35.
- Appleby, P.G., Richardson, N. and Nolan, P.J., 1991.  $^{241}\text{Am}$  dating of lake sediments. *Hydrobiologia*, 214: 35-42.
- Armentano, T.V. and Woodwell, G.M., 1975. Sedimentation rates in a Long Island marsh determined by Pb-210 dating. *Limnology and Oceanography*, 20: 452-456.
- Asselman, N.E.M. and Middelkoop, H., 1995. Floodplain sedimentation - Quantities, patterns and processes. *Earth Surface Processes and Landforms*, 20(6): 481-499.
- Baeyens, W., Van Eck, B., Lambert, C., Wollast, R. and Goeyens, L., 1998. General description of the Scheldt estuary. *Hydrobiologia*, 366: 1-14.
- Baltsavias, E.P., 1999. Airborne laser scanning: basic relations and formulas. *ISPRS Journal of Photogrammetry and Remote Sensing*, 54: 199-214.
- Baptist, M.J., 2003. A flume experiment on sediment transport with flexible, submerged vegetation, International workshop on riparian forest vegetated channels: hydraulic, morphological and ecological aspects, Trento, Italy.
- Bates, P.D., Anderson, M.G., Price, D.A., Hardy, R.J. and Smith, C.N., 1996. Analysis and development of hydraulic models for floodplain flows. In: M.G. Anderson, D.E. Walling and P.D. Bates (Editors), *Floodplain Processes*. Wiley, Chichester, pp. 215-254.
- Bates, P.D., Baird, L., Anderson, M.G., Walling, D.E. and Simm, D., 1992. Modelling floodplain flows using a two-dimensional finite element model. *Earth Surface Processes and Landforms*, 217(6): 575-588.
- Bates, P.D., Horrit, M. and Hervouet, J.-M., 1998. Investigating two-dimensional finite element predictions of floodplain inundation using fractal generated topography. *Hydrological Processes*, 12(8): 1257-1278.
- Baumann, R.H., Day, J.W. and Miller, C.A., 1984. Mississippi deltaic wetland survival: sedimentation versus coastal submergence. *Science*, 224: 1093-1095.
- Bayliss-Smith, T.P., Healey, R., Lailey, R., Spencer, T. and Stoddart, D.R., 1979. Tidal flow in salt marsh creeks. *Estuarine Coastal and Marine Science*, 9: 235-255.
- Bockelmann, A.C., Bakker, J.P., Neuhaus, R. and Lage, J., 2002. The relation between vegetation zonation, elevation and inundation frequency in a Wadden Sea salt marsh. *Aquatic Botany*, 73(3): 211-221.

- Booker, D.J., Sear, D.A. and Payne, A.J., 2001. Modelling three-dimensional flow structures patterns of boundary shear stress in a natural pool-riffle sequence. *Earth Surface Processes and Landforms*, 26: 553-576.
- Boon, J.D., 1978. Suspended solids transport in a salt marsh creek: an analysis of errors. In: B.J. Kjerfve (Editor), *Estuarine Transport Processes*. University of South Carolina Press, Columbia, pp. 147-159.
- Boorman, L.A., Garbutt, A. and Barratt, D., 1998. The role of vegetation in determining patterns of the accretion of salt marsh sediment. In: K.S. Black, D.M. Paterson and A. Cramp (Editors), *Sedimentary Processes in the Intertidal Zone*, pp. 389-399.
- Bouma, T.J., De Vries, M.B., Low, E., Kusters, L., Herman, P.M.J., Tanczos, I.C., Hesselink, A., Temmerman, S., Meire, P. and Van Regenmortel, S., submitted. Hydrodynamic measurements on a mudflat and in salt marsh vegetation: identifying general relationships for habitat characterisations. *Hydrobiologia*.
- Cahoon, D.R., French, J.R., Spencer, T., Reed, D. and Möller, I., 2000a. Vertical accretion versus elevational adjustment in UK saltmarshes: an evaluation of alternative methodologies. In: K. Pye and J.R.L. Allen (Editors), *Coastal and estuarine environments: sedimentology, geomorphology and geoarchaeology*. The Geological Society, London, pp. 223-238.
- Cahoon, D.R., Marin, P.E., Black, B.K. and Lynch, J.C., 2000b. A method for measuring vertical accretion, elevation, and compaction of soft, shallow-water sediments. *Journal of Sedimentary Research*, 70(5): 1250-1253.
- Cahoon, D.R. and Reed, D.J., 1995. Relationships among marsh surface topography, hydroperiod, and soil accretion in a deteriorating Louisiana salt marsh. *Journal of coastal research*, 11(2): 357-369.
- Callaway, J.C., Nyman, J.A. and Delaune, R.D., 1996. Sediment accretion in coastal wetlands: a review and simulation model of processes. *Current Topics in Wetland Bio-geochemistry*, 2(2-23).
- Christiansen, T., Wiberg, P.L. and Milligan, T.G., 2000. Flow and sediment transport on a tidal salt marsh surface. *Estuarine Coastal and Shelf Science*, 50(3): 315-331.
- Claessens, J., 1988. Het hydraulisch regime van de Schelde. *Water*, 43: 163-169.
- Claessens, J. and Meyvis, L., 1994. Overzicht van de tijwaarnemingen in het Zeescheldebekken gedurende het decennium 1981-1990, Ministerie van de Vlaamse Gemeenschap AWZ Afdeling Maritieme Schelde, Antwerpen.
- Comans, R.N.J., Middelburg, J.J., Zonderhuis, J., Woittiez, J.R.W., De Lange, G.J., Das, H.A. and Van der Weijden, C.H., 1989. Mobilization of radiocesium in pore water of lake-sediments. *Nature*, 339(6223): 367-369.
- Covi, M.P. and Kneib, R.T., 1995. Intertidal distribution, population dynamics and production of the amphipod *Ehlorchestia spartinophila* in a Georgia, USA, salt-marsh. *Marine Biology*, 121(3): 447-455.
- Criel, B., Muylaert, W., Hoffmann, M., De Loose, L. and Meire, P., 1999. Vegetatiemodellering van de buitendijkse gebieden langs de Zeeschelde. Rapport OMES DS7.2, Instituut voor Natuurbehoud, Brussel.
- Cundy, A.B. and Croudace, I.W., 1996. Sediment accretion and recent sea-level rise in the Solent, southern England: Inferences from radiometric and geochemical studies. *Estuarine Coastal and Shelf Science*, 43(4): 449-467.

## References

---

- Cundy, A.B., Croudace, I.W., Thomson, J. and Lewis, J.T., 1997. Reliability of salt marshes as "geochemical recorders" of pollution input: A case study from contrasting estuaries in southern England. *Environmental Science and Technology*, 31: 1093-1101.
- Dankers, N., Binsberger, M., Zegers, K., Laane, R. and Van de Loeff, M.R., 1985. Transport of water, particulate and dissolved organic and inorganic matter between a salt marsh and the Ems-Dollard Estuary, The Netherlands. *Estuarine Coastal and Shelf Science*, 19: 143-165.
- Davidson-Arnott, R.G.D., Van Proosdij, D., Ollerhead, J. and Schostak, L., 2002. Hydrodynamics and sedimentation in salt marshes: examples from a macrotidal marsh, Bay of Fundy. *Geomorphology*, 48(1-3): 209-231.
- Day, J.W., Rybczyk, J., Scarton, F., Rismondo, A., Are, D. and Cecconi, G., 1999. Soil accretionary dynamics, sea-level rise and the survival of wetlands in Venice Lagoon: A field and modelling approach. *Estuarine Coastal and Shelf Science*, 49: 607-628.
- De Bruyn, T., 2003. Opslibbing van recent gevormde schorren in het Schelde-estuarium: een terreinstudie en modevaluatie. Licentiaatsverhandeling, Katholieke Universiteit Leuven, Leuven, 132 pp.
- De Ferraris, J., 1774-1777. Kabinetskaart van de Oostenrijkse Nederlanden. reprint Gemeentekrediet, Brussels.
- DeLaune, R.D., Patrick Jr, W.H. and Buresh, R.J., 1978. Sedimentation rates determined by <sup>137</sup>Cs in a rapidly accreting salt marsh. *Nature*, 275: 532-533.
- Durinck, P., 1981. Het getijdenrivierengebied in ons land. *Natuurreservaten*, 4bis: 60-68.
- Dyer, F.M., Thomson, J., Croudace, I.W., Cox, R. and Wadsworth, R.A., 2002. Records of change in salt marshes: A radiochronological study of three Westerschelde (SW Netherlands) marshes. *Environmental Science & Technology*, 36(5): 854-861.
- Eastman, R., 1994. IDRISI for Windows 2.0 Users Guide. Clark University, Worcester Mass.
- Eisma, D., Dyer, K.R. and Van Leussen, W., 1997. The in-situ determination of the settling velocities of suspended fine-grained sediment - a review. In: N. Burt, R. Parker and J. Watts (Editors), *Cohesive Sediments*. Wiley, Chichester, pp. 17-44.
- Esselink, P., Dijkema, K.S., Reents, S. and Hageman, G., 1998. Vertical accretion and profile changes in abandoned man-made tidal marshes in the Dollard estuary, the Netherlands. *Journal of Coastal Research*, 14(2): 570-582.
- Fettweis, M., Sas, M. and Monbaliu, J., 1998. Seasonal, neap-spring and tidal variation of cohesive sediment concentration in the Scheldt Estuary, Belgium. *Estuarine Coastal and Shelf Science*, 47(1): 21-36.
- Francken, F. and Wartel, S., 2001. Studie van de langdurige meetreeksen in de Beneden-Zeeschelde. Ministerie van de Vlaamse Gemeenschap, Departement Leefmilieu en Infrastructuur, Administratie Waterwegen en Zeewezen, Afdeling Maritieme Schelde, Antwerpen.
- French, J.R., 1993. Numerical simulation of vertical marsh growth and adjustment to accelerated sea-level rise, north Norfolk, U.K. *Earth Surface Processes and Landforms*, 18(1): 63-81.
- French, J.R. and Clifford, N.J., 2000. Hydrodynamic modelling as a basis for explaining estuarine environmental dynamics: some computational and methodological issues. *Hydrological Processes*, 14(11-12): 2089-2108.

- French, J.R. and Spencer, T., 1993. Dynamics of sedimentation in a tide-dominated backbarrier salt marsh, Norfolk, U.K. *Marine Geology*, 110(3-4): 315-331.
- French, J.R., Spencer, T., Murray, A.L. and Arnold, N.S., 1995. Geostatistical analysis of sediment deposition in two small tidal wetlands, Norfolk, United Kingdom. *Journal of Coastal Research*, 11(2): 308-321.
- French, J.R. and Stoddart, D.R., 1992. Hydrodynamics of salt marsh creek systems: implications for marsh morphological development and material exchange. *Earth Surface Processes and Landforms*, 17: 235-252.
- French, P.W., 1996. Implications of a saltmarsh chronology for the Severn Estuary based on independent lines of dating evidence. *Marine Geology*, 135: 115-125.
- Frey, R.W. and Basan, P.B., 1985. Coastal salt marshes. In: R.A. Davis Jr. (Editor), *Coastal Sedimentary Environments* (2nd edn). Springer Verlag, New York, pp. 225-301.
- Gabet, E.J., 1998. Lateral migration and bank erosion in a saltmarsh tidal channel in San Francisco Bay, California. *Estuaries*, 21: 745-753.
- Gee, D.M., Anderson, M.G. and Baird, L., 1990. Large-scale floodplain modelling. *Earth Surface Processes and Landforms*, 15: 513-523.
- Hardy, R.J., Bates, P.D. and Anderson, M.G., 2000. Modelling suspended sediment deposition on a fluvial floodplain using a two-dimensional dynamic finite element model. *Journal of Hydrology*, 229(3-4): 202-218.
- Healey, R.G., Pye, K., Stoddart, D.R. and Bayliss-Smith, T.P., 1981. Velocity variations in saltmarsh creeks, Norfolk, England. *Estuarine Coastal and Shelf Science*, 13: 535-545.
- Hervouet, J.-M. and Van Haren, L., 1996. Recent advances in numerical methods for fluid flows. In: M.G. Anderson, D.E. Walling and P.D. Bates (Editors), *Floodplain processes*. Wiley, Chichester, pp. 183-214.
- Hoffmann, M., 1993. Vegetatiekundig-ecologisch onderzoek van de buitendijkse gebieden langs de Zeeschelde met vegetatiekartering. University of Ghent, Ghent.
- Hoffmann, M., Graré, W. and Meire, P., 1997. De oevers langs de Zeeschelde: van uniformiteit naar structuurdiversiteit. *Water*, 95: 131-137.
- Houtekamer, N.K., 1996. De schorren van de Westerschelde 1990/1993, overzichtskaarten van de vegetatie met begeleidende rapportage. MD-GAT 9623, Rijkswaterstaat Meetkundige Dienst, Delft.
- Houwing, E.J., Tánčzos, I.C., Kroon, A. and De Vries, M.B., 2000. Interaction of submerged vegetation, hydrodynamics and turbidity: analysis of field and laboratory studies, INTERCOH 2000.
- Huijs, S.W.E., 1995. Geomorfologische ontwikkelingen van het intergetijdegebied in de Westerschelde 1935-1989. R 95-3, Institute for Marine and atmospheric Research Utrecht and Rijkswaterstaat Rijksinstituut voor Kust en Zee, Utrecht /Middelburg.
- Hutchinson, S.E., Sklar, F.H. and Roberts, C., 1995. Short term sediment dynamics in a Southeastern USA *Spartina* marsh. *Journal of Coastal Research*, 11(2): 370-380.
- James, C.S., 1985. Sediment transfer to overbank section. *Journal of Hydraulic Research*, 23: 435-452.

## References

---

- Kearney, M.S. and Stevenson, J.C., 1991. Island land loss and marsh vertical accretion rate evidence for historical sea-level changes in Chesapeake Bay. *Journal of Coastal Research*, 7: 403-415.
- Koppejan, H., 2000. Toelichting bij de vegetatiekartering Westerschelde 1998, Rijkswaterstaat, Meetkundige Dienst, Delft.
- Kostka, J.E., Roychoudhury, A. and Van Cappellen, P., 2002. Rates and controls of anaerobic microbial respiration across spatial and temporal gradients in saltmarsh sediments. *Biogeochemistry*, 60(1): 49-76.
- Krone, R.B., 1962. Flume studies of the transport of sediment in estuarial shoaling processes, University of California, Hydraulic Engineering Laboratory and Sanitary Engineering Research Laboratory, Berkeley.
- Krone, R.B., 1987. A method for simulating historic marsh elevations. In: N.C. Kraus (Editor), *Coastal sediments '87*. American Society of Civil Engineers, New York, pp. 316-323.
- Lane, S.N., 1998. Hydraulic modelling in hydrology and geomorphology: A review of high resolution approaches. *Hydrological Processes*, 12(8): 1131-1150.
- Lane, S.N. and Richards, K.S., 1998. High resolution, two-dimensional spatial modelling of flow processes in a multi-thread channel. *Hydrological Processes*, 12: 1279-1298.
- Lauwaet, D., 2003. Ruimtelijke analyse van de sedimentatie op een zout schor. Licentiaatsverhandeling, Katholieke Universiteit Leuven, Leuven, 77 pp.
- Leendertse, P.C., Roozen, A.J.M. and Rozema, J., 1997. Long-term changes (1953-1990) in the salt marsh vegetation at the Boschplaat on Terschelling in relation to sedimentation and flooding. *Plant Ecology*, 132(1): 49-58.
- Leonard, L.A., 1997. Controls of sediment transport and deposition in an incised mainland marsh basin, southeastern North Carolina. *Wetlands*, 17(2): 263-274.
- Leonard, L.A., Hine, A.C. and Luther, M.E., 1995a. Surficial sediment transport and deposition processes in a *Juncus-Roemerianus* marsh, west-central Florida. *Journal of Coastal Research*, 11(2): 322-336.
- Leonard, L.A., Hine, A.C., Luther, M.E., Stumpf, R.P. and Weight, E.E., 1995b. Sediment transport processes in a west-central Florida open marine marsh tidal creek - the role of tides and extra-tropical storms. *Estuarine Coastal and Shelf Science*, 41(2): 225-248.
- Leonard, L.A. and Luther, M.E., 1995. Flow hydrodynamics in tidal marsh canopies. *Limnology and Oceanography*, 40(8): 1474-1484.
- Leonard, L.A., Wren, P.A. and Beavers, R.L., 2002. Flow dynamics and sedimentation in *Spartina alterniflora* and *Phragmites australis* marshes of the Chesapeake Bay. *Wetlands*, 22(2): 415-424.
- Letsch, W.S. and Frey, R.W., 1980. Deposition and erosion in a Holocene salt marsh, Sapelo Island, Georgia. *Journal of Sedimentary Petrology*, 50: 529-542.
- Liek, G.-J., 2001. Monitoring van de effecten van de verruiming 48'-43'. MOVE-rapport 5: Beschrijving van de fysische toestand van de Westerschelde t/m 2000. Rapport RIKZ/2001.023, Rijkswaterstaat Rijksinstituut voor Kust en Zee, Middelburg.
- Measures, R.M., 1991. *Laser Remote Sensing: Fundamentals and Applications*. Krieger Publishing, Melbourne.

- Meire, P., Rossaert, G., De Regge, N., Ysebaert, T. and Kuijken, E., 1992. Het Schelde-estuarium: ecologische beschrijving en een visie op de toekomst, Instituut voor Natuurbehoud, Hasselt.
- Meire, P., Starink, M. and Hoffmann, M., 1997. Integratie van ecologie en waterbouwkunde in de Zeeschelde: aanleiding tot en situering van het Onderzoek Milieu-Effecten Sigmaplan (OMES). *Water*, 95: 147-165.
- Middelkoop, H. and Asselman, N.E.M., 1998. Spatial variability of floodplain sedimentation at the event scale in the Rhine-Meuse delta, the Netherlands. *Earth Surface Processes and Landforms*, 23: 561-573.
- Mol, A.C.S., 2003. Wave attenuation by vegetation, WL | Delft Hydraulics, Delft, The Netherlands.
- Möller, I., Spencer, T., French, J.R., Leggett, D.J. and Dixon, M., 1999. Wave transformation over salt marshes: A field and numerical modelling study from north Norfolk, England. *Estuarine Coastal and Shelf Science*, 49(3): 411-426.
- Möller, I., Spencer, T., French, J.R., Leggett, D.J. and Dixon, M., 2001. The sea-defence value of salt marshes: Field evidence from north Norfolk. *Journal of the Chartered Institution of Water and Environmental Management*, 15(2): 109-116.
- Moody, J.A. and Troutman, B.M., 2000. Quantitative model of the growth of floodplains by vertical accretion. *Earth Surface Processes and Landforms*, 25: 115-133.
- Nash, J.E. and Sutcliffe, J.V., 1970. River flow forecasting through conceptual models. Part I. A discussion of principles. *Journal of Hydrology*, 10: 282-290.
- Neubauer, S.C., Anderson, I.C., Constantine, J.A. and Kuehl, S.A., 2002. Sediment deposition and accretion in a mid-Atlantic (USA) tidal freshwater marsh. *Estuarine Coastal and Shelf Science*, 54(4): 713-727.
- Nicholas, A.P. and Walling, D.E., 1997. Investigating spatial patterns of medium-term overbank sedimentation on floodplains: A combined numerical modelling and radiocaesium-based approach. *Geomorphology*, 19: 133-150.
- Oenema, O. and DeLaune, R.D., 1988. Accretion rates in salt marshes in the eastern Scheldt, southwest Netherlands. *Estuarine Coastal and Shelf Science*, 26: 379-394.
- Olf, H., De Leeuw, J., Bakker, J.P., Platerink, R.J., Van Wijnen, H.J. and De Munck, W., 1997. Vegetation succession and herbivory in a salt marsh: changes induced by sea level rise and silt deposition along an elevational gradient. *Journal of Ecology*, 85(6): 799-814.
- Orson, R.A., Simpson, R.L. and Good, R.E., 1990. Rates of sediment accumulation in a tidal freshwater marsh. *Journal of Sedimentary Petrology*, 60: 859-869.
- Orson, R.A., Warren, R.S. and Niering, W.A., 1998. Interpreting sea level rise and rates of vertical marsh accretion in a southern New England tidal salt marsh. *Estuarine Coastal and Shelf Science*, 47: 419-429.
- Partheniades, E., 1965. Erosion and deposition of cohesive soils. *Journal of the Hydraulic Division, ASCE*, 91(HY1).
- Pasternack, G.B. and Brush, G.S., 2001. Seasonal variations in sedimentation and organic content in five plant associations on a Chesapeake Bay tidal freshwater delta. *Estuarine Coastal and Shelf Science*, 53(1): 93-106.
- Pethick, J., 2002. Estuarine and tidal wetland restoration in the United Kingdom: Policy versus practice. *Restoration Ecology*, 10(3): 431-437.

## References

---

- Pethick, J.S., 1980. Velocity surges and asymmetry in tidal channels. *Estuarine Coastal Shelf Science*, 11: 331-345.
- Pethick, J.S., 1981. Long-term accretion rates on tidal salt marshes. *Journal of Sedimentary Petrology*, 51: 571-577.
- Pethick, J.S., 1992. Saltmarsh geomorphology. In: J.R.L. Allen and K. Pye (Editors), *Saltmarshes: morphodynamics, conservation and engineering significance*. Cambridge University Press, Cambridge, pp. 41-62.
- Pethick, J.S., Leggett, D. and Husain, L., 1990. Boundary layers under salt marsh vegetation developed in tidal currents. In: J.B. Thomes (Editor), *Vegetation and erosion*. John Wiley & Sons, Chichester, pp. 113-124.
- Philips, N.A., 1957. A co-ordinate system having some special advantages for numerical forecasting. *Journal of Meteorology*, 14.
- Pizzuto, J.E., 1987. Sediment diffusion during overbank flow. *Sedimentology*, 34: 301-317.
- Pizzuto, J.E. and Schwendt, A.E., 1997. Mathematical modeling of autocompaction of a Holocene transgressive valley-fill deposit, Wolfe Glade, Delaware. *Geology*, 25(1): 57-60.
- Pont, D., Day, J.W., Hensel, P., Franquet, E., Torre, F., Rioual, P., Ibanez, C. and Coulet, E., 2002. Response scenarios for the deltaic plain of the Rhone in the face of an acceleration in the rate of sea-level rise with special attention to *Salicornia*-type environments. *Estuaries*, 25(3): 337-358.
- Pye, K. and French, P.W., 1993. *Erosion and accretion processes on British salt marshes*, Vol 5, *Management of salt marshes in the context of flood defence and coastal protection*. Cambridge Environmental Research Consultants, Cambridge.
- Redfield, A.C., 1972. Development of a New England saltmarsh. *Ecological Monograph*, 42: 201-237.
- Reed, D.J., 1987. Temporal sampling and discharge asymmetry in salt marsh creeks. *Estuarine Coastal and Shelf Science*, 25: 459-466.
- Reed, D.J., 1988. Sediment dynamics and deposition in a retreating coastal salt marsh. *Estuarine Coastal and Shelf Science*, 26(1): 67-79.
- Reed, D.J., 1989. Patterns of sediment deposition in subsiding coastal marshes, Terrebonne Bay, Louisiana: the role of winter storms. *Estuaries*, 12(4): 222-227.
- Reed, D.J., 1993. Hydrology of temperate wetlands. *Progress in Physical Geography*, 17(1): 20-31.
- Reed, D.J., 1995. The response of coastal marshes to sea-level rise: survival or submergence? *Earth Surface Processes and Landforms*, 20(1): 39-48.
- Reed, D.J., Spencer, T., Murray, A.L., French, J.R. and Leonard, L., 1999. Marsh surface sediment deposition and the role of tidal creeks: implications for created and managed coastal marshes. *Journal of Coastal Conservation*, 5: 81-90.
- Reed, D.J., Stoddart, D.R. and Bayliss-Smith, T.P., 1985. Tidal flows and sediment budgets for a salt-marsh system, Essex, England. *Vegetatio*, 62: 375-380.
- Roman, C.T., Peck, J.A., Allen, J.R., King, J.W. and Appleby, P.G., 1997. Accretion of a New England (U.S.A.) salt marsh in response to inlet migration, storms, and sea-level rise. *Estuarine Coastal and Shelf Science*, 45(6): 717-727.

- Rybczyk, J.M. and Cahoon, D.R., 2002. Estimating the potential for submergence for two wetlands in the Mississippi River Delta. *Estuaries*, 25(5): 985-998.
- SAS Institute Inc., 1989. SAS/STAT User's Guide, Version 6, Fourth Edition, Volume 1. SAS Institute Inc., Cary, NC, 943 pp.
- Schwimmer, R.A., 2001. Rates and processes of marsh shoreline erosion in Rehoboth Bay, Delaware, USA. *Journal of Coastal Research*, 17(3): 672-683.
- Settlemyre, J.L. and Gardner, L.R., 1977. Suspended sediment flux through a salt marsh drainage basin. *Estuarine Coastal and Shelf Science*, 5: 653-663.
- Shaw, J. and Ceman, J., 1999. Salt-marsh aggradation in response to late-Holocene sea-level rise at Amherst Point, Nova Scotia, Canada. *Holocene*, 9: 439-451.
- Sherrod, B.L., 2001. Evidence for earthquake-induced subsidence about 1100 yr ago in coastal marshes of southern Puget Sound, Washington. *Geological Society of America Bulletin*, 113(10): 1299-1311.
- Shi, Z., 1993. Recent saltmarsh accretion and sea level fluctuations in the Dyfi Estuary, central Cardigan Bay, Wales, UK. *Geo-Marine Letters*, 13: 182-188.
- Shi, Z., Hamilton, L.J. and Wolanski, E., 2000. Near-bed currents and suspended sediment transport in saltmarsh canopies. *Journal of Coastal Research*, 16(3): 909-914.
- Shi, Z., Pethick, J.S., Burd, F. and Murphy, B., 1996. Velocity profiles in a salt marsh canopy. *Geo-Marine Letters*, 16: 319-323.
- Shi, Z., Pethick, J.S. and Pye, K., 1995. Flow structure in and above the various heights of a saltmarsh canopy: a laboratory flume study. *Journal of Coastal Research*, 11: 1204-1209.
- Stapel, J. and De Jong, D., 1998. Sedimentatiemetingen op het schor bij Waarde en het Verdrongen Land van Saeftinge, Westerschelde (ZW Nederland). RIKZ-98.022, Rijkswaterstaat Rijksinstituut voor Kust en Zee, Middelburg.
- Steers, J.A., 1977. Physiography. In: V.J. Chapman (Editor), *Wet Coastal Ecosystems*. Elsevier Science, Amsterdam, pp. 31-60.
- Stelling, G.S. and Van Kester, J.A.T.M., 1994. On the approximation of horizontal gradients in sigma coordinates for bathymetry with steep bottom slopes. *International Journal for Numerical Methods in Fluids*, 18: 915-955.
- Stikvoort, E., Berrevoets, C., Kuijper, M., Lefèvre, F., Liek, G.-J., Lievaart, M., Van Maldegem, D., Meininger, P., Peters, B., Pouwer, A., Schippers, H. and Wijsman, J., 2003. Monitoring van de effecten van de verruiming 48'-43'. MOVE-rapport 7: MOVE Hypothesendocument 2003. Onderliggende rapportage bij MOVE-rapport 8 (deel A en B) Evaluatierapport 2003. Rapport RIKZ/2003.009, Rijkswaterstaat Rijksinstituut voor Kust en Zee, Middelburg.
- Stoddart, D.R., Reed, D.J. and French, J.R., 1989. Understanding salt marsh accretion, Scolt Head Island, north Norfolk, England. *Estuaries*, 12(4): 228-236.
- Stumpf, R.P., 1983. The process of sedimentation on the surface of a salt marsh. *Estuarine Coastal and Shelf Science*, 17: 495-508.
- Swart, J.P., 1987. Onderzoek verhouding marien-fluviatiel slib in de Westerschelde. Nota GWAO-91.081, Rijkswaterstaat, Directie Zeeland, Middelburg.

## References

---

- Taverniers, E., 2000. Zeescheldebekken: de afvoer van de Schelde in 1999. Verslag AMS-2000.03, Ministerie van de Vlaamse Gemeenschap AWZ Afdeling Maritieme Schelde, Antwerpen.
- Teeter, A.M., 2001. Clay-silt sediment modeling using multiple grain classes. Part I: Settling and deposition. In: W.H. McAnally and A.J. Mehta (Editors), Coastal and Estuarine Fine Sediment Processes. Elsevier Science, Amsterdam, pp. 157-171.
- Temmerman, S., Govers, G., Meire, P. and Wartel, S., 2003a. Modelling long-term tidal marsh growth under changing tidal conditions and suspended sediment concentrations, Scheldt estuary, Belgium. *Marine Geology*, 193(1-2): 151-169.
- Temmerman, S., Govers, G., Wartel, S. and Meire, P., 2003b. Spatial and temporal factors controlling short-term sedimentation in a salt and freshwater tidal marsh, Scheldt estuary, Belgium, SW Netherlands. *Earth Surface Processes and Landforms*, 28(7): 739-755.
- Temmerman, S., Govers, G., Meire, P. and Wartel, S., submitted. Simulating the long-term development of levee-basin topography on tidal marshes. *Geomorphology*.
- Uittenbogaard, 2003. Modelling turbulence in vegetated aquatic flows, International workshop on riparian forest vegetated channels: hydraulic, morphological and ecological aspects, Trento, Italy.
- Van Damme, S., De Winder, B., Ysebaert, T. and Meire, P., 2001. Het 'bijzondere' van de Schelde: de abiotiek van het Schelde-estuarium. *De Levende Natuur*, 102(2): 37-39.
- Van Damme, S., Ysebaert, T., Meire, P. and Van den Bergh, E., 1999. Habitatstructuren, waterkwaliteit, en leefgemeenschappen in het Schelde-estuarium. Rapport 99/24, Instituut voor Natuurbehoud, Brussel.
- Van den Bergh, E., Huiskes, A., Criel, B., Hoffmann, M. and Meire, P., 2001. Biodiversiteit op de Scheldeschorren. *De Levende Natuur*, 102(2): 62-66.
- Van den Bergh, E., Meire, P., Hoffmann, M. and Ysebaert, T., 1999. Natuurherstelplan Zeeschelde: drie mogelijke inrichtingsvarianten. Rapport IN 99/18, Instituut voor Natuurbehoud, Brussel.
- Van der Pluijm, A.M. and De Jong, D.J., 1998. Historisch overzicht schorareaal in Zuid-West Nederland. Werkdocument RIKZ/OS-98.860 x, Rijkswaterstaat - Rijksinstituut voor Kust en Zee, Middelburg.
- Van Eck, G.T.M., De Pauw, N., Van Langenbergh, M. and Verreet, G., 1991. Emissies, gehalten, gedrag en effecten van (micro)verontreinigingen in het stroomgebied van de Schelde en het Schelde-estuarium. *Water*, 60: 84-99.
- Van Eerd, M.M., 1985. Salt marsh cliff stability in the Oosterschelde. *Earth Surface Processes and Landforms*, 10: 95-106.
- Van Heerd, R.M. and Van 't Zand, R.J., 1999. Productspecificatie Actueel Hoogtebestand Nederland, Rijkswaterstaat Meetkundige Dienst, Delft.
- Van Leussen, W., 1988. Aggregation of particles, settling velocity of mud flocs - a review. In: J. Dronkers and W. Van Leussen (Editors), *Physical Processes in Estuaries*. Springer, Berlin, pp. 347-403.
- Van Proosdij, D., Ollerhead, J. and Davidson-Arnott, R.G.D., 2000. Controls on suspended sediment deposition over single tidal cycles in a macrotidal saltmarsh, Bay of Fundy, Canada. In: K. Pye and J.R.L. Allen (Editors), *Coastal and estuarine environments: sedimentology, geomorphology and geoarchaeology*. Geological Society, London, pp. 43-57.

- Van Wijnen, H.J. and Bakker, J.P., 2001. Long-term surface elevation change in salt marshes: a prediction of marsh response to future sea-level rise. *Estuarine Coastal and Shelf Science*, 52(3): 381-390.
- Vandermaelen, P., 1846-1854. Carte topographique de la Belgique. l' Etablissement Géographique de Bruxelles, Bruxelles.
- Walker, H.J., Coleman, J.M., Roberts, H.H. and Tye, R.S., 1987. Wetland loss in Louisiana. *Geografiska Annaler*, 69A: 189-200.
- Walling, D.E., He, Q. and Nicholas, A.P., 1996. Floodplains as suspended sediment sinks. In: M.G. Anderson, D.E. Walling and P.D. Bates (Editors), *Floodplain Processes*. Wiley, Chichester, pp. 399-440.
- Walling, D.E., Owens, P.N. and Leeks, G.J.L., 1999. Rates of contemporary overbank sedimentation and sediment storage on the floodplains of the main channel systems of the Yorkshire Ouse and River Tweed, UK. *Hydrological Processes*, 13: 993-1009.
- Wang, F.C., Lu, T.S. and Sikora, W.B., 1993. Intertidal marsh suspended sediment transport processes, Terrebonne Bay, Louisiana, U.S.A. *Journal of Coastal Research*, 9(1): 209-220.
- Ward, L.G., 1981. Suspended-material transport in marsh tidal channels, Kiawah Island, South Carolina. *Marine Geology*, 40: 139-154.
- Ward, L.G., Kearney, M.S. and Stevenson, J.C., 1998. Variations in sedimentary environments and accretionary patterns in estuarine marshes undergoing rapid submergence, Chesapeake Bay. *Marine Geology*, 151: 111-134.
- Wartel, S., 1973. Variations in concentration of suspended matter in the Scheldt estuary. *Bulletin of the Royal Belgian Institute for Natural Sciences*, 49(2): 1-11.
- Wartel, S., 1977. Composition, transport and origin of sediments in the Schelde estuary. *Geologie en Mijnbouw*, 56(3): 219-233.
- Wartel, S. and Chen, M.S., 1998. Bepaling van de verhouding marien-fluviatiel slib in de Beneden Zeeschelde in het voorjaar van 1998, Ministerie van de Vlaamse Gemeenschap, Departement Leefmilieu en Infrastructuur, Bestuur Waterwegen en Zeewezen, Afdeling Maritieme Schelde, Brussel.
- Wartel, S. and Van Eck, G.T.M., 2000. Slibhuishouding van het Schelde-estuarium, Koninklijk Belgisch Instituut voor Natuurwetenschappen en Rijksinstituut der Kust en Zee, Brussel/Middelburg.
- Winterwerp, J.C. and Uittenbogaard, R.E., 1997. Sediment transport and fluid mud flow. Z2005, WL|Delft Hydraulics, Delft.
- WL | Delft Hydraulics, 2003. User Manual Delft3D-FLOW. WL | Delft Hydraulics, Delft, The Netherlands.
- Woolnough, S.J., Allen, J.R.L. and Wood, W.L., 1995. An exploratory numerical model of sediment deposition over tidal marshes. *Estuarine Coastal and Shelf Science*, 41(5): 515-543.
- Yang, S.L., 1998. The role of Scirpus marsh in attenuation of hydrodynamics and retention of fine sediment in the Yangtze Estuary. *Estuarine Coastal and Shelf Science*, 47: 227-233.
- Yang, S.L., 1999. Tidal wetland sedimentation in the Yangtze Delta. *Journal of Coastal Research*, 15: 1091-1099.

## References

---

- Zanting, H.A. and Ten Thij, F., 2001. Langetermijnvisie Schelde-estuarium, projectbureau LTV p.a., Delft.
- Zedler, J.B., Callaway, J.C., Desmond, J.S., Vivian-Smith, G., Williams, G.D., Sullivan, G., Brewster, A.E. and Bradshaw, B.K., 1999. Californian salt-marsh vegetation: An improved model of spatial pattern. *Ecosystems*, 2(1): 19-35.
- Zwolsman, J.J.G., Berger, G.W. and Vaneck, G.T.M., 1993. Sediment accumulation rates, historical input, postdepositional mobility and retention of major elements and trace-metals in salt-marsh sediments of the Scheldt estuary, SW Netherlands. *Marine Chemistry*, 44(1): 73-94.

## List of symbols and abbreviations

---

### Symbols

$a, b, c$	regression parameters	
$A(h)$	wet cross-section of tidal creek	(m <sup>2</sup> )
$C$	suspended sediment concentration	(kg m <sup>-3</sup> or g l <sup>-1</sup> )
$C_b$	suspended sediment concentration in the near bottom computational layer	(kg m <sup>-3</sup> )
$C(t)$	suspended sediment concentration at time-step $t$	(kg m <sup>-3</sup> )
$C(0)$	initial suspended sediment concentration in the water that floods the marsh surface	(kg m <sup>-3</sup> )
$d$	median particle diameter	(m)
$DBD$	dry bulk density of surface sediment	(g cm <sup>-3</sup> )
$D_c$	distance to the nearest creek or marsh edge	(m)
$D_e$	distance to the marsh edge, measured along the nearest creek	(m)
$dE/dt$	rate of marsh surface elevation change	(m a <sup>-1</sup> )
$dh/dt$	rate of water level change	(m s <sup>-1</sup> )

## List of symbols and abbreviations

---

$dP/dt$	rate of compaction of the deposited sediment, after dewatering, under younger sediment load	(m a <sup>-1</sup> )
$dS_{min}/dt$	rate of mineral sediment deposition	(m a <sup>-1</sup> )
$dS_{org}/dt$	rate of organic sediment deposition	(m a <sup>-1</sup> )
$D_{50}$	median particle diameter	( $\mu\text{m}$ )
$E$	marsh surface elevation	(m NAP or TAW)
$E(eq)$	equilibrium level of a marsh surface relative to local mean high water level	(m)
$E(0)$	initial marsh surface elevation (at the beginning of a model simulation)	(m NAP or TAW)
$g$	gravity acceleration	(m s <sup>-2</sup> )
$H$	marsh surface elevation	(m NAP or TAW)
$h$	water level	(m NAP or TAW)
$h(t)$	water level at time-step $t$	(m NAP or TAW)
$h(t_{HW})$	high water level during a random tidal cycle	(m NAP or TAW)
$h(t_{HW})-E$	maximum inundation height (at high tide) above the marsh surface	(m)
$h(t_{MHW})$	mean high water level	(m NAP or TAW)
$HWL_{rel}$	high water level during a random tidal cycle relative to mean high water level	(m)
$I_h$	inundation height above the marsh surface at high tide	(m)
$I_t$	cumulative inundation time	(minutes)
$k, l, m, n$	regression parameters (in chapters 2, 3, 4)	
$k$	calibration parameter (in chapters 5, 6, 7)	
$k_{basin}$	calibration parameter $k$ used for a basin site	
$k_{levee}$	calibration parameter $k$ used for a levee site	
$\log SR$	log-transformed sedimentation rate data	
$m, n, \sigma$	grid co-ordinates in lateral directions ( $m$ and $n$ ) and vertical direction ( $\sigma$ )	
$ME$	model efficiency coefficient	
$P$	thickness of a sediment layer after compaction	(m)
$P_0$	initial thickness of a sediment layer before compaction	(m)
$SR$	sedimentation rate	(kg m <sup>-2</sup> per time unit)
$SR_{Delft3D}$	sedimentation rate simulated with Delft3D	(kg m <sup>-2</sup> per time unit)
$SR_{mean}$	mean of the observed sedimentation rates	(kg m <sup>-2</sup> per time unit)

$SR_{obs}$	observed sedimentation rate	(kg m <sup>-2</sup> per time unit)
$SR_{pred}$	predicted sedimentation rate	(kg m <sup>-2</sup> per time unit)
$t$	time	(s)
$T$	total duration of one tidal inundation	(s)
$T(eq)$	time needed to reach the equilibrium level of a marsh surface relative to the local mean high water level	(years)
$TSS_{dep}$	total suspended sediment mass deposited on the marsh surface	(tonnes)
$TSS_E$	total suspended sediment mass transported through the creeks system during ebb (negative)	(tonnes)
$TSS_F$	total suspended sediment mass transported through the creeks system during flood (positive)	(tonnes)
$TSS_{net}$	net import (positive) or export (negative) of suspended sediment over one semi-diurnal tidal cycle	(tonnes)
$T(0)$	initial year from which a model simulation is started	
$u$	flow velocity	(m s <sup>-1</sup> )
$u, v, w$	flow velocity components in $x, y$ and $z$ directions	(m s <sup>-1</sup> )
$V_E$	total water volume discharged through the creeks system during ebb	(m <sup>3</sup> )
$V_F$	total water volume discharged through the creeks system during flood	(m <sup>3</sup> )
$V_{HW}$	total water volume stored above the marsh surface at high tide	(m <sup>3</sup> )
$W_d$	daily mean wind velocity	(m s <sup>-1</sup> )
$W_{sn}$	daily mean wind velocity averaged over the 14-days period of a spring-neap cycle	(m s <sup>-1</sup> )
$w_s$	settling velocity of suspended sediment	(m s <sup>-1</sup> )
$x, y, z$	dimensions	
$X_0, Y_0$	regression parameters	
$z_{LiDAR}$	elevation determined by generation of a digital elevation model based on LiDAR data	(m NAP)
$z_{survey}$	elevation determined by field surveying using a total station	(m NAP)
$\Delta E(eq)$	difference between the equilibrium level of a levee and the adjacent basin	(m)
$\epsilon_{s,x}, \epsilon_{s,y}, \epsilon_{s,z}$	eddy diffusivities in $x, y$ and $z$ directions	(m <sup>2</sup> s <sup>-1</sup> )
$\mu$	viscosity of the water	(N s m <sup>-2</sup> )
$\rho$	dry bulk density of sediment	(kg m <sup>-3</sup> )
$\rho_s$	particle density	(kg m <sup>-3</sup> )
$\rho_w$	density of water	(kg m <sup>-3</sup> )
$\rho_0$	initial dry bulk density of a sediment layer before compaction	(kg m <sup>-3</sup> )
$\tau$	bed shear stress	(N m <sup>-2</sup> )
$\tau_{cr,d}$	critical shear stress for sediment deposition	(N m <sup>-2</sup> )

## Abbreviations

ANOVA	analysis of variance
CFD	computational fluid dynamics
cph	counts per hour
DEM	digital elevation model
EMF	electro-magnetic flow meter
FTU	formazine turbidity units
GIS	geographical information system
HW	high water level
HHW	highest high water level
ISSC	initial suspended sediment concentration, measured at the beginning of flooding of the marsh surface, i.e. when the water level exceeds a height of 0.15 m above the marsh surface
LiDAR	light-induced direction and ranging
LUCC	land use or vegetation cover change
m NAP	elevation (in m) relative to the Dutch reference level NAP = Nieuw Amsterdams Peil $\approx$ mean sea level at the Dutch coast
m TAW	elevation (in m) relative to the Belgian reference level TAW = Tweede Algemene Waterpassing = -2.33 m NAP $\approx$ 2.3 m below mean sea level at the Belgian coast
MHWL	mean high water level
MHWLN	mean high water level at neap tide
MHWLS	mean high water level at spring tide
MLWLN	mean low water level at neap tide
MLWLS	mean low water level at spring tide
OBS	optical back scatter
SSC	suspended sediment concentration

## List of publications

---

### 1. International SCI journals

- Temmerman, S., Govers, G., Meire, P. and Wartel, S., 2003. Modelling long-term tidal marsh growth under changing tidal conditions and suspended sediment concentrations, Scheldt estuary, Belgium. *Marine Geology*, 193(1-2): 151-169.
- Temmerman, S., Govers, G., Wartel, S. and Meire, P., 2003. Spatial and temporal factors controlling short-term sedimentation in a salt and freshwater tidal marsh, Scheldt estuary, Belgium - SW Netherlands. *Earth Surface Processes and Landforms*, 28(7): 739-755.
- Temmerman, S., Govers, G., Meire, P., and Wartel, S., submitted. Simulating the long-term development of levee-basin topography on tidal marshes. Submitted to *Geomorphology*.

## 2. International conferences

- Temmerman, S., Govers, G., Wartel, S. and Meire, P., 2001. Tidal marsh sedimentation in the Scheldt estuary (Belgium, SW Netherlands): Short-term measurements and their implications for long-term modeling. 16<sup>th</sup> Biennial Conference of the Estuarine Research Federation, St-Pete Beach, Florida, USA, 4-8/11/2001. *Oral presentation.*
- Temmerman, S., Govers, G., Wartel, S. and Meire, P., 2002. Sediment dynamics and geomorphic changes in tidal marshes. ECSA-symposium "Ecological structures and functions in the Scheldt Estuary: from past to future", Antwerp, Belgium, 7-10/10/02. *Invited oral presentation.*
- Temmerman, S., Govers, G., Wartel, S. and Meire, P., 2002. Small-scale sediment transport and deposition patterns within a salt-marsh basin, Paulinaschor, Western Scheldt. ECSA-symposium "Ecological structures and functions in the Scheldt Estuary: from past to future", Antwerp, Belgium, 7- 10/10/02. *Poster presentation.*
- Temmerman, S., Govers, G., Meire, P. and Wartel, S., 2003. Simulating sediment deposition and elevation changes in tidal marshes using a 2-dimensional spatially distributed modelling approach. 17<sup>th</sup> Biennial Conference of the Estuarine Research Federation, Seattle, USA, 14-18/09/2003. *Poster presentation.*

## 3. National meetings

- Temmerman, S., Govers, G., Wartel, S. and Meire, P., 2001. Tidal Marsh sedimentation in the Scheldt Estuary: A Field and Modelling Approach. VLIZ Young Scientists's Day, Brugge, 23/02/2001.
- Temmerman, S. and Govers, G., 2001. Tidal Marsh Sedimentation in the Scheldt Estuary: A Field and Modelling Approach on different scales. ICG symposium "Scale Issues in Geo-ecological Research", Utrecht, 20/03/2001.
- Temmerman, S., Govers, G., Wartel, S. and Meire, P., 2001. Small-scale temporal and spatial variations in tidal marsh sedimentation in the Scheldt estuary. Workshop "Ecologisch Onderzoek in het Scheldebekken", Brussel, 29-30/03/2001.
- Temmerman, S. and Govers, G., 2001. Overstromingen en sedimentatie in natuurlijke oeverzones: een kwestie van evenwicht. Studiedag "Natuurlijke oeverzones en bufferstroken Theorie en praktijk van een multifunctioneel beekbeheer", Instituut voor Natuurbehoud en AMINAL afdeling Water, Brussel, 12/10/2001.
- Temmerman, S. and Govers, G., 2001. Tidal Marsh sedimentation in the Scheldt Estuary: A Field and Modelling Approach. Symposium of the Belgian Soil Science Society, Leuven, 14/11/01.

Nederlandse samenvatting

Sedimentatie op schorren in het Schelde-estuarium:  
een studie op basis van veldmetingen  
en numerieke modellering

---

**1. Inleiding en doelstellingen**

Schorren zijn estuariene en kustgebonden milieus die bij hoge waterstanden (springtij) overstromen, waarbij er gesuspendeerde sedimenten (slib en fijn zand) in het overstromende water worden aangevoerd en gedeeltelijk worden afgezet op het schoroppervlak. Op langere termijn leidt dit tot ophoging van schorren. Deze sedimentatie en hoogteveranderingen zijn bepalend voor voortdurende veranderingen in het ecologisch functioneren van schorren, zoals bijvoorbeeld de successie van planten die zijn aangepast aan een verschillende graad van overspoeling door het getij. Bovendien resulteert sedimentatie in een afnemende capaciteit van schorren om water te bergen tijdens extreem hoge waterstanden, wat kan leiden tot meer kans op overstromingen langs bewoonde estuaria en kustgebieden. In het kader van het duurzame beheer en herstel van schorregebieden, zowel omwille van hun ecologische waarde en om veiligheidsredenen, is er dan ook een groeiende

vraag naar wetenschappelijke kennis omtrent sedimentatie en geomorfologische processen in schorren.

Gedurende de laatste decennia werd een groot aantal studies verricht naar het kwantificeren van sedimentatiesnelheden op schorren, op tijdsschalen gaande van één halfdagelijkse getijcyclus tot de laatste 100 tot 1000 jaar. Hierbij werd ruime aandacht besteed aan de snelheid waarmee schorren zich ophogen in verhouding tot de lokale snelheid van zeespiegelstijging; in sommige gebieden werd vastgesteld dat schorren in staat zijn zich sneller of tenminste even snel op te hogen dan de zeespiegelstijging, terwijl in andere gebieden grote arealen aan schorren als het ware verdrinken en verloren gaan.

Naast deze talrijke studies die zich richtten op het kwantificeren van sedimentatiesnelheden, werd er heel wat minder *proces-gebaseerd* onderzoek verricht, met als doel inzicht te verkrijgen in de fundamentele processen van sedimentatie en hoogteveranderingen binnen schorren. Hoewel het belang van controlerende factoren zoals variaties in getijregime, sedimentkarakteristieken en de topografie van schorren werd aangetoond, blijft het erg moeilijk om temporele en ruimtelijke variaties in sedimentatie in schorren te voorspellen. Tot nu toe werd heel weinig aandacht besteed aan de ontwikkeling en het testen van numerieke modellen die toelaten temporele en ruimtelijke variaties in schorresedimentatie te simuleren. Nochtans is het van bijzonder belang om in het kader van de evaluatie van beheers- en herstelmaatregelen voor schorren te kunnen beschikken over simulatie modellen die grondig werden getest op hun voorspellende waarde.

Met dit werk willen we een bijdrage leveren tot een beter inzicht in de controlerende factoren voor temporele en ruimtelijke variaties in schorresedimentatie. Hierbij werd enerzijds uitgegaan van veldmetingen en anderzijds de ontwikkeling, toepassing en evaluatie van numerieke modellen die moeten toelaten om veranderingen in schorresedimentatie te voorspellen bij veranderende omstandigheden. Als studiegebied werden de schorren van het Schelde-estuarium gekozen. In een eerste deel van de thesis (hoofdstukken 2, 3 en 4) werden korte-termijn variaties in sedimentatie bestudeerd, op een tijdsschaal van één halfdagelijkse getijcyclus tot 1 jaar. Een tweede deel (hoofdstukken 5, 6 en 7) handelt over de ophoging van schorren op lange termijn (10-100 jaar).

## 2. Korte-termijn sedimentatie

### 2.1. Ruimtelijke en temporele factoren die korte-termijn sedimentatie bepalen in een zout- en zoetwaterschorre

In hoofdstuk 2 worden de resultaten gepresenteerd van een intensieve meetcampagne van de ruimtelijke en temporele variaties in korte-termijn (< 1 jaar) sedimentatie in twee contrasterende schorretypes in het Schelde-estuarium, een zout- en zoetwaterschorre. De meetresultaten werden in dit hoofdstuk ten eerste geanalyseerd om na te gaan wat het relatieve belang is van verschillende factoren in de determinatie van ruimtelijke en temporele variaties in schorresedimentatie. Ten tweede werd onderzocht in welke mate zowel ruimtelijke als temporele variaties kunnen voorspeld worden aan de hand van een relatief eenvoudig topografisch gebaseerd model dat het effect van de verschillende determinerende factoren integreert. Tenslotte werd nagegaan in hoeverre sedimentatiepatronen verschillend zijn in de bestudeerde zout- en zoetwaterschorre.

Als gevolg van de estuariene zout-zoet gradiënt komen langsheen het Schelde-estuarium zowel zout-, brak- als zoetwaterschorren voor, welke onderling sterk verschillen in vegetatiestructuur (Fig. 1.2). Als studiegebieden werd gekozen voor een zoutwaterschorre (het Paulinaschor) en zoetwaterschorre (de Notelaar). In elk gebied werden gedurende een jaar lang (april 2000 tot mei 2001) enerzijds metingen uitgevoerd van temporele variaties in sedimentconcentratie (in g/l) in het water dat het schoroppervlak overspoelt. Hierbij werd gebruik gemaakt van een geautomatiseerde meetopstelling centraal opgesteld in elk studiegebied, om waterpeilfluctuaties onder invloed van het getij te meten en waterstalen te nemen. Anderzijds werd de sedimentatiesnelheid (in g/m<sup>2</sup> per 14-daagse springtij-doodtij cyclus) gemeten met zogenaamde 'sediment traps' voor 25 springtij-doodtij cycli gedurende het ganse jaar en op 17 locaties verspreid over beide studiegebieden.

De resultaten van deze metingen toonden aan dat temporele variaties in sedimentatiesnelheden erg groot zijn, met waarden in de orde van 1 tot 1000 g/m<sup>2</sup> per 14-daagse springtij-doodtij cyclus. Temporele variaties in sedimentconcentratie en sedimentatiesnelheden worden hoofdzakelijk bepaald door variaties in overstroming van het schoroppervlak door het getij, terwijl de invloed van golfwerking door wind verwaarloosbaar is. De inkomende sedimentconcentratie, in het water dat het schoroppervlak overspoelt bij het begin van een overstroming, neemt lineair toe met de maximale hoogte waarmee het schoroppervlak wordt overstromd tijdens een halfdagelijkse getijcyclus (Fig. 2.6). In overeenstemming hiermee, werd een exponentieel verband waargenomen tussen overstromingsduur en sedimentatiesnelheid. Naast deze invloed van het getij, werd ook een seizoenale invloed vastgesteld: zowel sedimentconcentraties als

sedimentatiesnelheden zijn hoger tijdens de winterperiode dan tijdens de zomerperiode voor een zelfde overstromingshoogte of –duur.

De tijdsgemiddelde sedimentatiesnelheden variëren ruimtelijk tussen de verschillende meetlocaties van 40 tot 1650 g/m<sup>2</sup> per springtij-doodtijcyclus. Deze ruimtelijke variaties zijn sterk gerelateerd aan de schorretopografie. Ten eerste nemen sedimentatiesnelheden af met toenemende hoogteligging van het schoroppervlak, aangezien hogere schorren minder vaak, minder hoog en minder lang worden overstroomd door het getij dan lager gelegen schorren. Ten tweede nemen sedimentatiesnelheden af met toenemende afstand van de geulen die het schoroppervlak versnijden en ten derde met toenemende afstand van de schorrand gemeten langsheen de dichtstbijzijnde geul. Dit wordt verklaard door de progressieve sedimentatie van suspensiemateriaal uit het water dat vanaf de schorrand doorheen het geulensysteem en tenslotte vanuit de geulen over het schoroppervlak stroomt.

Vervolgens werd nagegaan in hoeverre de waargenomen temporele en ruimtelijke variaties in sedimentatiesnelheid kunnen verklaard worden door een meervoudig regressiemodel op basis van de drie topografische parameters: hoogteligging, afstand tot geul en afstand tot schorrand. De toepassing van dit model in een raster-gebaseerd Geografisch Informatie Systeem resulteerde in voorspelde sedimentatiesnelheden die in goede overeenstemming zijn met de waargenomen variaties in sedimentatiesnelheden (Fig. 2.9 en 2.10). Een opmerkelijke bevinding is dat dit topografisch gebaseerd model in staat is om de waargenomen variaties in sedimentatiesnelheden te simuleren zowel voor de bestudeerde zout- als zoetwaterschorre. Ondanks dat de dichtheid en hoogte van de vegetatie sterk verschilt tussen beide schorretypes, kunnen we besluiten dat de verschillen in vegetatie geen significante invloed hebben op het ruimtelijke sedimentatiepatroon binnen schorren.

## *2.2. Ruimtelijke patronen van sedimenttransport en sedimentatie tijdens individuele getijcycli in een klein geulbekken*

De aanvoer, ruimtelijke verspreiding en afzetting van sediment over schorren wordt uiteindelijk bepaald door de stromingspatronen die optreden tijdens individuele getijcycli over de complexe topografie van schorren en door de schorrevegetatie. Recent werden er veldstudies verricht om deze kleinschalige gedetailleerde stromingspatronen en sedimenttransport in schorren te karakteriseren. De ruimtelijke resolutie waarmee dergelijke veldmetingen kunnen worden uitgevoerd is echter erg beperkt. In dit opzicht bieden hydrodynamische modellen nieuwe mogelijkheden. Dergelijke modellen worden recent meer en meer toegepast om stromingspatronen en sedimenttransport over complexe topografieën te simuleren met een hoge temporele en ruimtelijke resolutie. Tot nu toe werden echter geen

hydrodynamische modellen toegepast en geëvalueerd om 2-dimensionale ruimtelijke stromingspatronen en patronen van sedimenttransport en sedimentatie in schorren te simuleren.

In hoofdstuk 3 worden de resultaten gepresenteerd van een veldmeetcampagne, die werd uitgevoerd om de noodzakelijke data aan te leveren voor input, kalibratie en validatie van een hydrodynamisch model. De eigenlijke toepassing van het model wordt beschreven in hoofdstuk 4. De metingen werden uitgevoerd binnen een 5.6 ha groot stroomgebied van één dendritisch geulensysteem in het Paulinaschor. Enerzijds werd het ruimtelijke sedimentatie patroon binnen het studiegebied opgemeten aan de hand van ‘sediment traps’ die werden opgesteld op 50 locaties en tijdens vier individuele halfdagelijkse getijcycli en twee 14-daagse springtij-doodtij cycli. Anderzijds werd tijdens dezelfde meetperiodes het sedimenttransport doorheen het geulensysteem geregistreerd aan de hand van twee geautomatiseerde meetframes, waarmee stroomsnelheden, stroomrichtingen, turbiditeit en sedimentconcentraties werden gemeten.

De resultaten van de metingen van de ruimtelijke variaties in sedimentatiesnelheden zijn grotendeels in overeenstemming met onze bevindingen uit hoofdstuk 2: de sedimentatiesnelheden nemen af met toenemende hoogteligging van het schoroppervlak en met toenemende afstand tot de dichtstbijzijnde geul en tot de schorrand. Op basis van deze drie topografische variabelen kan met het topografisch gebaseerde model, dat werd gepresenteerd in hoofdstuk 2, het waargenomen ruimtelijke sedimentatiepatroon vrij goed voorspeld worden (Fig. 3.6). Voor jonge, laag gelegen schorren, waar nog geen dicht geulensysteem aanwezig is, worden ruimtelijke variaties in sedimentatiesnelheden echter in hoofdzaak bepaald door hoogteverschillen, terwijl de invloed van geulen en de schorrand hier eerder verwaarloosbaar is.

De hydrodynamische metingen in de geul toonden aan dat de getijdestroming doorheen het geulensysteem wordt gekenmerkt door een uitgesproken vloed-eb asymmetrie en het optreden van stroomsnelheidspulsen op het moment van overstroming (tijdens vloed) en weer droogvallen (tijdens eb) van het omringende schoroppervlak. Aan de schorrand werden dergelijke stroomsnelheidspulsen niet waargenomen, aangezien er hier geen duidelijke geul aanwezig is.

Ondanks dat er geen directe metingen van het gedetailleerde ruimtelijke stromingspatroon werden uitgevoerd, biedt de berekening en analyse van de water- en sedimentbalansen voor de meetperiodes meer inzicht in de transportpaden die het water en sediment volgen doorheen het schor. Voor het laag gelegen schorgedeelte dichtbij de schorrand, vindt de aanvoer en afvoer van water en sediment plaats doorheen de ganse lengte van de schorrand, aangezien op het lage, jonge schor geen dicht geulensysteem aanwezig is. Op het hoge schor heeft zich een dicht geulensysteem ontwikkeld en deze geulen spelen een cruciale rol in de aanvoer en afvoer

van water en sediment naar het omringende schoroppervlak. Voor getijcycli waarbij het schoroppervlak met meer dan 0.2 m wordt overstroomt, zien we echter dat de directe aanvoer van water via de schorrand en over het schoroppervlak heen in belang toeneemt met toenemende hoogwaterpeil tijdens deze getijcycli.

### *2.3. Hydrodynamische modellering van het ruimtelijke patroon van sedimenttransport en sedimentatie*

In hoofdstuk 4 werd een fysisch-gebaseerd hydrodynamisch en sedimenttransport model, Delft3D, toegepast en geëvalueerd om na te gaan in hoeverre een dergelijke modelbenadering in staat is het 2-dimensionale ruimtelijke sedimentatie patroon in schorren te simuleren. Het Delft3D model laat toe om stromingspatronen te berekenen over complexe oppervlakken op basis van een 3-dimensionale oplossing van de Navier-Stokes vergelijkingen. Bovendien werd het Delft3D model recent uitgebreid om het effect van vegetatie op wrijving en turbulentie te incorporeren.

Het Delft3D model werd toegepast, gekalibreerd en gevalideerd aan de hand van de velddata die in hoofdstuk 3 werden verzameld. Hierbij werd aangetoond dat het model vrij goed in staat is om de waargenomen ruimtelijke variaties in sedimentatiesnelheden te simuleren (Fig. 4.8 en vergelijk Fig. 4.9 en Fig. 3.5). Uit een meer gedetailleerde analyse van het gesimuleerde stromingspatroon bleek echter dat het belang van het geulensysteem voor de aan- en afvoer van water en sediment naar en van het omringende hoog gelegen schoroppervlak wordt onderschat door het model. Het model simuleert dat de aan- en afvoer van water en sediment vooral plaats vindt via de schorrand en over het schoroppervlak heen, terwijl uit de veldmetingen is gebleken dat transport naar en van het hoge schor vooral plaats vindt via het geulensysteem. Deze studie toont dus aan dat een hydrodynamische modelbenadering mogelijkheden biedt om het complexe sedimentatiepatroon binnen schorren te voorspellen, maar dat modelsimulaties met de nodige voorzichtigheid dienen geïnterpreteerd te worden.

Aanvullende modelsimulaties lieten ons toe om enig inzicht te verkrijgen in de gevoeligheid van het gesimuleerde sedimentatiepatroon voor de input waarden die worden gebruikt voor model variabelen, waarvan algemeen wordt aangenomen dat zij schorresedimentatie beïnvloeden. Ten eerste resulteerden hogere concentraties en valsnelheden van het inkomende gesuspendeerde sediment in hogere absolute sedimentatiesnelheden, zonder enige systematische verandering in de relatieve ruimtelijke verschillende in sedimentatiesnelheden. Ten tweede simuleert het model dat tijdens getijcycli met hogere hoogwaterpeilen hogere sedimentatiesnelheden optreden en dat het sediment hoger en verder over het schoroppervlak wordt getransporteerd vooraleer het wordt afgezet. Tenslotte toonden modelsimulaties aan dat grote

verschillen in vegetatie structuur geen significante invloed hebben op het ruimtelijke sedimentatiepatroon. Zelfs de aan- of afwezigheid van vegetatie maakt geen verschil uit voor het gesimuleerde ruimtelijke sedimentatiepatroon. Dit is een opmerkelijke vaststelling, aangezien in de literatuur vaak wordt aangenomen dat de aanwezigheid van vegetatie een cruciale rol speelt in het bevorderen van sedimentatie in schorren. In overeenstemming met onze velddata, geven de modelsimulaties aan dat de topografie van schorren de belangrijkste factor is die het ruimtelijke sedimentatiepatroon in schorren bepaalt, terwijl de relatieve invloed van vegetatie op het ruimtelijke sedimentatiepatroon verwaarloosbaar is.

### 3. Lange-termijn ophoging

#### *3.1. Modellering van lange-termijn ophoging van schorren onder invloed van veranderingen in getijregime en sedimentconcentraties*

Uit eerder onderzoek weten we dat de lange-termijn (10-100 jaar) ophoging van schorren wordt bepaald door een negatieve feedback tussen de hoogteligging van schorren en de overspoeling door het getij, waardoor jonge, laag gelegen schorren zich aanvankelijk snel gaan ophogen en waardoor sedimentatiesnelheden afnemen naarmate schorren hoger komen te liggen in de intergetijdenzone. Op basis van dit mechanisme werden empirische en fysisch-gebaseerde modellen ontwikkeld om de lange-termijn invloed van toekomstige zeespiegelstijging op schorresedimentatie te simuleren. Hoewel we kunnen stellen dat deze modelbenaderingen kwalitatief geldig zijn, werd tot nu toe zeer weinig aandacht besteed aan de kwantitatieve validatie van modelvoorspellingen ten opzichte van gemeten sedimentatiesnelheden op lange termijn (10-100 jaar).

In hoofdstuk 5 ontwikkelden we een fysisch-gebaseerd model om de lange-termijn ophoging van schorren te simuleren. Het model is 0-dimensionaal, wat wil zeggen dat schorreophoging wordt gesimuleerd in functie van de tijd en voor één punt in de ruimte. Het model is gebaseerd op de simulatie van lange-termijn veranderingen in het overstromingsregime van schorren onder invloed van het getij en de simulatie van sedimentatie over elk van deze overstromingen op basis van een massabalans benadering, zoals voorgesteld door Krone (1987) en French (1993).

Om het model te evalueren, werden veldgegevens verzameld over de historische ophoging van de jonge en oude schorre van de Notelaar, op basis van oude luchtfoto's en boommonsters. Deze veldgegevens toonden aan dat de jonge schorre ongeveer 55 jaar geleden werd gevormd door de kolonisatie van planten op een oorspronkelijk onbegroeide slikke met een hoogteligging van ongeveer 0.7 m onder het toenmalige gemiddelde hoogwaterpeil (GHW).

Sindsdien hoogde de jonge schorre zich zeer snel op en bereikte na ongeveer 15 jaar een evenwichtsniveau rond GHW. De oude schorre daarentegen bevond zich 55 jaar geleden reeds op dit evenwichtsniveau rond GHW en hoogde zich even snel op als de snelheid waarmee GHW is gestegen gedurende de laatste 55 jaar (Fig. 5.3)

Het model werd vervolgens toegepast voor de jonge en oude schorre van de Notelaar. Als input data voor het model werd enerzijds gebruik gemaakt van historische gegevens over de evolutie van GHW. Anderzijds dient de inkomende sedimentconcentratie, in het water dat het schoroppervlak overspoelt, te worden gespecificeerd in het model. Voor dit laatste werd gebruik gemaakt van de veldmetingen van temporele variaties in sedimentconcentraties, die werden gepresenteerd in hoofdstuk 2. De toepassing van de bestaande modelbenadering van Krone (1987) en French (1993), waarbij wordt uitgegaan van een constante inkomende sedimentconcentratie, resulteerde in een aanzienlijke onderschatting van de waargenomen accumulatiesnelheid van het oude en jonge schoroppervlak. In hoofdstuk 2 toonden we echter aan dat de inkomende sedimentconcentratie niet constant is over verschillende getijcycli maar lineair toeneemt met de maximale hoogte waarmee het schoroppervlak wordt overstroomd tijdens getijcycli. Deze relatie tussen inkomende sedimentconcentratie en overstromingshoogte werd vervolgens gebruikt in het model om lange-termijn veranderingen in inkomende sedimentconcentratie te simuleren onder invloed van veranderingen in het overstromingsregime wanneer het schoroppervlak zich ophoogt binnen de intergetijdenzone. Na incorporatie van deze relatie is het model goed in staat om de waargenomen ophoging van de jonge en oude schorre van de Notelaar te simuleren (Fig. 5.10). Aanvullende modelsimulaties toonden tenslotte aan dat de incorporatie van deze relatie tussen inkomende sedimentconcentratie en overstromingshoogte van groot belang is wanneer men de reactie van een schoroppervlak op toekomstige zeespiegelstijging wil simuleren. Deze studie toonde aan dat niet alleen veranderingen in overstromingsregime, maar ook veranderingen in inkomende sedimentconcentraties als gevolg van veranderingen in overstromingshoogte, van cruciaal belang zijn om de lange-termijn ophoging van schorren te verklaren en voorspellen.

### *3.2. Simulatie van de lange-termijn ontwikkeling van oeverwallen en kommen in schorren*

De geomorfologie van oude schorren wordt typisch gekenmerkt door een micro-topografie van oeverwallen, vlak naast geulen, en lager gelegen kommen, verder verwijderd van geulen. Deze oeverwal-kom topografie is sterk bepalend voor gradiënten in hydrologische, biogeochemische en ecologische processen in schorren. Desondanks werden lange-termijn veranderingen in de hoogteligging van schorren tot nu toe bestudeerd uitgaande van een puntbenadering, zonder daarbij rekening te houden met ruimtelijke variaties en het ontstaan van geomorfologische gradiënten binnen schorren.

In hoofdstuk 6 werd de vorming en lange-termijn evolutie van oeverwallen en kommen in schorren bestudeerd aan de hand van modelsimulaties. Hierbij maakten we gebruik van het model dat werd voorgesteld in hoofdstuk 5 en van ruimtelijk gedifferentieerde input waarden voor de modelvariabelen. Het model werd gekalibreerd aan de hand van korte-termijn (< 1 jaar) metingen van ruimtelijke en temporele variaties in sedimentatiesnelheden, gemeten langsheen vier oeverwal-kom transecten. Vervolgens werden de lange-termijn veranderingen in de hoogteligging van de oeverwallen en kommen gesimuleerd, vertrekkend van een historisch gekende hoogteligging. In overeenstemming met de huidige geobserveerde oeverwal-kom topografie, simuleert het model dat het hoogteverschil tussen oeverwallen en kommen toeneemt tot een bepaald evenwicht is bereikt (Fig. 6.4): eenmaal oeverwallen 20 tot 30 cm hoger zijn dan de aangrenzende kommen, wordt het belang van de nabijheid van de geul als aanvoer weg voor sediment gecompenseerd door het belang van de hoogteligging als bepalende factor voor variaties in overstromingsfrequentie, -hoogte en -duur. Van zodra deze sedimentologisch-geomorfologische evenwichtstoestand is bereikt, hogen oeverwallen en kommen zich op met een zelfde snelheid, welke in evenwicht is met de stijging van het gemiddelde hoogwaterpeil (GHW).

Aanvullende modelsimulaties toonden aan dat dit evenwicht in het hoogteverschil tussen oeverwallen en kommen wordt bepaald door de snelheid van GHW stijging en de inkomende sedimentconcentratie (Fig. 6.7). Een snellere GHW stijging resulteert niet alleen in een algemeen lager evenwichtsniveau van schorren ten opzichte van GHW, maar ook in een groter hoogteverschil tussen oeverwallen en aangrenzende kommen. Anderzijds leiden hogere inkomende sedimentconcentraties tot een hoger evenwichtsniveau van schorren ten opzichte van GHW. De modelsimulaties toonden echter aan dat significant grotere of kleinere hoogteverschillen tussen oeverwallen en kommen pas ontstaan wanneer ook de relatieve verschillen in inkomende sedimentconcentratie tussen oeverwallen en kommen groter of kleiner worden.

Deze studie toont dus aan dat de lange-termijn reactie van schorren op verschillende scenario's voor veranderingen in zeespiegelstijging of in

inkomende sedimentconcentraties niet uniform is in de ruimte. Er is echter een belangrijke ruimtelijke variabiliteit in sedimentatie en ophoging binnen schorren, waardoor oeverwallen en kommen op een verschillende manier zullen reageren op deze veranderingen in zeespiegelstijging en in inkomende sedimentconcentraties.

### *3.3. Lange-termijn ophoging van schorren langsheen de estuariene gradiënt van het Schelde-estuarium: veldgegevens en modellering*

Langsheen het Schelde-estuarium komen belangrijke gradiënten voor in GHW stijging en in gemiddelde sedimentconcentraties in de waterkolom (Fig. 7.9 en 7.3). Op basis van de inzichten die werden verworven in de hoofdstukken 5 en 6, mogen we verwachten dat deze gradiënten een belangrijke invloed zullen hebben op grootschalige variaties in lange-termijn sedimentatiesnelheden op de schorren langs het Schelde-estuarium. Om dit nader te onderzoeken, werden in hoofdstuk 7 veldgegevens verzameld over lange-termijn sedimentatiesnelheden voor 25 schorren verspreid langs de Schelde. Vervolgens werd het model, dat eerder werd gebruikt in hoofdstukken 5 en 6, toegepast en geëvalueerd in hoeverre het in staat is de geobserveerde grootschalige estuariene variabiliteit in schorresedimentatie te verklaren en voorspellen.

De geobserveerde sedimentatiesnelheden variëren sterk van 0.35 tot 4.55 cm/jaar. Uit de veldgegevens blijkt dat de snelle asymptotische ophoging van jonge, lage schorren tot op een evenwichtsniveau rond GHW, een algemeen mechanisme is voor de lange-termijn ophoging van schorren in het Schelde-estuarium (Fig. 7.6). Eenmaal dit evenwichtsniveau is bereikt hogen oude, hoge schorren zich veel trager op aan een snelheid die vergelijkbaar is met de snelheid van GHW stijging. Jonge schorren bereiken hun evenwichtsniveau echter sneller in de Zeeschelde dan in de Westerschelde, wat te wijten is aan de hogere sedimentconcentraties die aanwezig zijn in de Zeeschelde.

Voor de toepassing van het model konden input waarden voor de modelvariabelen bepaald worden aan de hand van terreingegevens voor 13 van de 25 onderzochte schorren. Toepassing en evaluatie van het model toonden aan dat het model goed in staat is de waargenomen variaties in lange-termijn ophoging te simuleren (Fig. 7.7). Bovendien bleek uit de modelsimulaties dat er een delicaat evenwicht bestaat tussen de estuariene variaties in de stijging van GHW en in sedimentconcentraties, zodanig dat de schorren overal langsheen het Schelde-estuarium in staat zijn hun evenwichtsniveau rond GHW te behouden: in de Zeeschelde, waar de GHW stijging het snelst is in het estuarium, worden ook de hoogste sedimentconcentraties waargenomen, terwijl in de Westerschelde de stijging van GHW trager gaat en sedimentconcentraties lager zijn. De modelsimulaties geven aan dat; wanneer in de Zeeschelde sedimentconcentraties lager zouden zijn, de schorren niet in staat zouden zijn

om hun hoogteligging door sedimentatie te behouden ten opzichte van het snel stijgende GHW.

Tenslotte werd aangetoond dat het model kan gebruikt worden om de impact van veranderende milieuecondities op schorresedimentatie te evalueren. In dit kader gaven modelsimulaties aan dat de schorren in het Schelde-estuarium ruimschoots de mogelijkheid hebben om zich op te hogen gedurende de volgende 100 jaar en hun evenwichtsniveau te behouden ten opzichte van GHW, indien de huidige omstandigheden van GHW stijging en sedimentconcentraties zich voortzetten. Een versnelde GHW stijging en/of drastische vermindering van sedimentconcentraties, hetzij door min of meer natuurlijke evoluties (bv. zeespiegelstijging) hetzij door menselijke ingrepen (bv. baggeren, waterzuivering, maatregelen tegen bodemerosie), kunnen echter leiden tot een tekort aan sedimentatie en verdrinking en degradatie van schorren in het Schelde-estuarium.

#### 4. Conclusies

In dit werk werden terreingegevens verzameld en modellen ontwikkeld en toegepast die toelaten om de sedimentatie en ophoging van schorren op verschillende tijd- en ruimteschalen te verklaren en te voorspellen. Op een tijdsschaal van een getijcyclus tot 1 jaar, werd aangetoond dat temporele variaties hoofdzakelijk worden bepaald door variaties in overstromingsregime onder invloed van het getij. Ruimtelijke variaties in sedimentatiesnelheden worden dan weer bepaald door topografische parameters: (1) de hoogteligging, (2) afstand tot geulen en (3) afstand tot de schorrand. Zowel een eenvoudig empirisch topografisch gebaseerd model als een complex fysisch-gebaseerd hydrodynamisch model (Delft3D) werd met succes toegepast om ruimtelijke sedimentatiepatronen in schorren te simuleren. Hierbij werden de voor- en nadelen van beide modelbenaderingen onderzocht. Zowel de veldgegevens als modelsimulaties geven aan dat verschillen in schorrevegetatie weinig invloed hebben op de afzetting van sedimenten.

Op een tijdsschaal van 10 tot 100 jaar werd aangetoond dat de ophoging van schorren wordt gekenmerkt door een snelle asymptotische opbouw van lage schorren tot op een evenwichtsniveau rond gemiddeld hoogwaterpeil. In dit werk werd een fysisch-gebaseerd model ontwikkeld om deze lange-termijn ophoging van schorren te kunnen simuleren en voorspellen. Het model bleek goed in staat te zijn om variaties in sedimentatiesnelheden te voorspellen, en dit op verschillende ruimteschalen: (1) variaties tussen jonge, laag gelegen schorren en oude, hoog gelegen schorren; (2) het ontstaan en de lange-termijn evolutie van oeverwallen en kommen binnen schorren; en (3) de grootschalige variatie in sedimentatiesnelheden langsheen de estuariene

gradiënt van het ganse Schelde-estuarium. Met dit model is het verder mogelijk om veranderingen in sedimentatie en hoogteligging van schorren te simuleren als reactie op veranderende milieucondities zoals zeespiegelstijging en veranderende sedimentconcentraties. Dergelijke modellen zijn van bijzonder belang ter ondersteuning van beleidsopties en projecten voor het beheer en herstel van schorregebieden.